UNIVERSITÉ DE PARIS

ÉCOLE DOCTORALE MÉDICAMENT, TOXICOLOGIE, CHIMIE, IMAGERIES

DOCTORAT

Champ Disciplinaire: **Sciences et Technologie**

Specialité: **Interface Chimie-Biologie**

Fernanda Custódio de MORAES

Development of polysaccharide-based nanoparticles for miRNA delivery

---

Directeur de Thèse : Dr. Didier LETOURNEUR

Co-Directeur de Thèse : Pr. Frédéric CHAUBET

Soutenue publiquement le 2 mars 2021

Devant le jury composé de :

Docteur Juergen SIEPMANN	Rapporteur
Professeur Chantal PICHON	Rapporteur
Docteur Ruxandra GREF	Examinateur
Docteur Didier LETOURNEUR	Directeur de thèse
Professeur Frédéric CHAUBET	Co-directeur de thèse

Laboratory for Vascular Translational Science (LVTS) – INSERM U1148

Hôpital Bichât – Claude Bernard, Paris, France

ACKNOWLEDGEMENTS

This thesis is the result of the support of several people to whom I am extremely grateful.

First, I would like to express my deepest gratitude to all my supervisors. Didier Letourneur and Frédéric Chaubet thanks for giving me such a good opportunity to become part of your prestigious laboratory team. Your support through all these years was essential for the success of this work. Thank you so much for guiding me on this journey. You provided me the tools that I needed to follow the right direction.

I owe my heartfelt gratitude also to Joana Antunes. I am grateful for all the time she spent training and guiding me. I would like to thank her for being a consistent source of support and advice. I´m eternally grateful for her teachings.

Then, I would like to thanks Juergen Siepmann and Chantal Pichon for accepting to evaluate my manuscript as well as Ruxandra Gref for accepting to judge my work. Thank you in advance for helping me strengthen my thesis.

Thanks also to all the members of my team for their friendship and for the moments shared in the day-to-day work. Huge thanks to Laura, Rachida, Teresa, Camille and Paola for the many advices, thank you for sharing your experience with me. Thanks to the others PhD students and lab mates, Soraya, Alina, Abbas, Lucie, Elnaz, Jérôme, Xavier, Louise, Chau, Alessandra and Rodolphe for the mutual support. Many thanks to Cédric for all his teachings and advices. Thanks to Murielle, for all the help and technical support. I would like to extend my sincere thanks to all the other members of the LVTS who were somehow involved in this work. Without all of you, this job would not be the same.

Thanks to my parents, Claudio and Rosana, and my brother, Leandro, for their unconditional love, their encouragement, and support that they give me every day. Thank you for giving me the best foundation. You taught me so much. This work would not have been possible without your love beyond limits. Thanks for believing in me.

Thanks to my husband, William, for your love, understanding and daily support. You have been patient and you are there whenever I need you. Thank you for giving me the driving forces through these years. I am truly thankful for having you in my life.

Finally, thanks to Conselho Nacional de Desenvolvimento Científico e Tecnológico (CNPq) from Brazil for the funding to perform my PhD.

"*A person who never made a mistake, never tried anything new.*"

ALBERT EINSTEIN

RÉSUMÉ

Les maladies du système cardiovasculaire restent une cause majeure de morbidité et de mortalité dans le monde, soulignant la nécessité de développer de nouvelles thérapies. La thérapie génique est une approche prometteuse pour traiter de nombreuses maladies. Alors que la délivrance d'acides nucléiques reste un défi, de nouveaux systèmes sont introduits et testés en continu. La clé du succès de la thérapie génique repose sur le développement de véhicules de délivrance de gènes sûrs et efficaces. L'objectif de ce projet de doctorat est la synthèse de dérivés cationiques de pullulane pour le développement de nanoparticules polysaccharides injectables, bon marché et biocompatibles pour la délivrance de miARN. Les nanoparticules ont été synthétisées en utilisant l'approche de complexation des polyélectrolytes, une méthodologie simple et versatile pour la production de nanoparticules de polysaccharides. Les dérivés cationiques du pullulane ont été capables de compacter et de délivrer des miARN *in vitro* à de faibles rapports N/P. Cependant, les nanoparticules formées uniquement par des interactions électrostatiques sont connues pour avoir une mauvaise stabilité en sérum. Pour résoudre le problème de stabilité des nanoparticules, nous avons ainsi développé des complexes de polyélectrolytes réticulés, appelés "*nanogels*", par un procédé écologique et innovant. Les *nanogels* pourraient se lier *in vitro* à la P-sélectine dans des conditions de flux artériel en raison de leur fonctionnalisation avec le fucoïdane. La nature biocompatible et biodégradable, ainsi que la stabilité colloïdale élevée des nanogels préparés, en font des candidats attractifs à des fins d'administration de médicaments, en particulier dans le domaine cardiovasculaire grâce à la possibilité de cibler la P-sélectine, un indicateur fort des maladies liées à l'athérothrombose.

Mots-clés: nanomédecine, maladies cardiovasculaires, miARN, polysaccharides, pullulane, fucoïdane

ABSTRACT

Diseases of the cardiovascular system remain a major cause of morbidity and mortality worldwide, underscoring the need for the development of new therapies. Gene therapy is a promising approach for treating many diseases. While the delivery of nucleic acids remains a challenge, new carriers are introduced and tested continuously. The key to the success of gene therapy relies on the development of safe and efficient gene delivery vehicles. The aim of this doctoral project was the synthesis of cationic pullulan derivatives for the development of injectable, low-cost and biocompatible polysaccharide-based nanoparticles focused on miRNA delivery. Nanoparticles were synthetized using the polyelectrolyte complex approach, an easy and versatile methodology for the production of polysaccharide nanoparticles. Cationic pullulan derivatives were able to compact and deliver miRNA *in vitro* at low N/P ratios. However, nanoparticles formed only by electrostatic interactions are known to have poor serum stability. To address nanoparticle stability issues, we further developed crosslinked polyelectrolyte complexes, called "nanogels", by an eco-friendly and innovative process. Nanogels could bind *in vitro* to P-selectin in arterial flow conditions due to their functionalization with fucoidan. The biocompatible and biodegradable nature, as well as the high colloidal stability of the prepared nanogels, make them attractive candidates for drug delivery purposes, especially in the cardiovascular field thanks to the possibility of targeting P-selectin, a strong indicator of atherothrombotic-related diseases.

Keywords: nanomedicine, cardiovascular diseases, miRNA, polysaccharides, pullulan, fucoidan

GENERAL CONTENTS

RÉSUMÉ ..... **VII**

ABSTRACT ..... **IX**

LIST OF FIGURES ..... **XIII**

LIST OF TABLES ..... **XXI**

ABBREVIATIONS ..... **XXIII**

1. GENERAL INTRODUCTION **1**

2. BIBLIOGRAPHIC REVIEW **7**

2.1 Cardiovascular diseases 9

2.2 Nanomedicine and drug delivery systems 14

2.3 Pharmaceutical development of nanomedicines 18

2.4 Polymeric nanoparticles 22

2.4.1 Polysaccharides – an overview 22

2.4.2 Preparation approaches of polysaccharide-based nanoparticles 25

2.5 The emergence of miRNA-based therapeutics 30

2.5.1 miRNA delivery vehicles 33

2.5.1.1 Inorganic nanoparticles 33

2.5.1.2 Lipid-based nanoparticles 35

2.5.1.3 Polymeric nanoparticles 36

2.5.2 Challenges in the delivery of small RNAs 41

3. EXPERIMENTAL WORK **43**

3.1 CHAPTER I 45

Synthesis of cationic pullulan derivatives for miRNA delivery

3.2 CHAPTER II 95

Biospecific polysaccharide-based nanogels crosslinked with genipin for miRNA delivery

4. GENERAL DISCUSSION **133**

5. GENERAL CONCLUSION **141**

6. REFERENCES **145**

7. ANNEXES **171**

Annex 1: Environmental scanning electron microscopy images 173

Annex 2: Synthesis and characterization of pullulan methacrylate 174

Annex 3: Synthesis and characterization of pullulan with primary amines and quaternary ammonium groups 178

Annex 4: Flow cytometry analysis of FAM-miRNA delivery 181

Annex 5: Reconstructed 3D images of FAM-miRNA delivery in HUVECs 185

Annex 6: Publications 186

LIST OF FIGURES

Figure 1. Progression of atherosclerosis from earliest fatty streaks to complicate lesion [9]. 10
Figure 2. MicroRNA biogenesis and mechanism of action. miRNA genes are transcribed to produce primary miRNA (pri-miRNA) by RNA polymerase II and cleaved into precursor miRNA transcript (pre-miRNA) by the microprocessor complex Drosha-DGCR8 in the nucleus. Pre-miRNA moves into the cytoplasm via Exportin-5, where it is further processed by Dicer and TRBP, producing a double-stranded miRNA duplex. The functional strand of mature miRNA is loaded onto the RNA-induced silencing complex (RISC) and negatively regulates gene expression resulting in either target mRNA degradation or translation repression, while the passenger strand is degraded [20]..... 12
Figure 3. Schematic model of Nrf2/ARE pathway activation by redox stress and potential regulation by miRNAs [25]. 13
Figure 4. SPECT/CT scans of an ischemia-reperfusion rat model. From left to right: 3D view, sagittal, coronal, and axial planes. The white arrow indicates the diseased heart area where the 99mTc labeled fucoidan has accumulated [35]..... 14
Figure 5. Different types of nanocarriers used in drug delivery systems and their morphological features [51]. 16
Figure 6. Design parameters of nanoparticles according to the composition, size, shape and surface properties of NPs. Adapted from M.A., Dobrovolskaia and S.E., McNeil 2007 [75]. 20
Figure 7. Chemical structures of commonly used natural polysaccharides [96]..... 23
Figure 8. Schematic illustration of different intra- and intermolecular forces in polysaccharide systems. A) Covalent crosslinking. B) Ionic crosslinking. C) Electrostatic interactions. D) Hydrophobic interactions [101]. 26
Figure 9. (a) Gardenia jasminoides Ellis and (b) chemical structure of genipin. 27
Figure 10. Structural representation of sodium tripolyphosphate (TPP). 28
Figure 11. (a) Schematic representation of polyplexes formation between polycations and DNA; and (b) Transmission electron micrograph of polyplexes (scale bar 200 nm) [166]. 32

Figure 12. Main types of polymeric delivery vehicles employed for miRNA delivery: (a) polyplexes, (b) PLGA NPs and (c) dendrimers. Therapeutic miRNA is depicted in black [21]. 36
Figure 13. Chemical structure of (a) linear (lPEI) and (b) branched PEI (bPEI). 37
Figure 14. Schematic illustration of the barriers for a successful gene delivery to target cells [171]. 42
Figure 15. Schematic representation of synthesis route for alkylation of pullulan using glycidyltrimethylammonium chloride (GTMAC). 57
Figure 16. FTIR spectra of (a) non-modified pullulan and (b) QA-pullulan. 59
Figure 17. 1H-NMR spectra of (a) non-modified pullulan and (b) QA-pullulan in D2O. 1A, 1B, 1C signals depicted anomeric H from maltotriose base unit of pullulan. Numbers 2-6 corresponded to H on anydroglucose unit. H from GTMAC substituent (b) were depicted with numbers from 7 to 10. 59
Figure 18. Cytocompatibility of (a) non-modified pullulan and (b) QA-pullulan towards HUVECs at 200, 500 and 1000 µg/mL after 24, 48 and 72h of incubation. Results are shown as mean ± SD from 3 independent experiments with no statistical differences detected using the Wilcoxon matched-pairs signed rank test. 60
Figure 19. Schematic representation of preparation of QA-pullulan/miRNA polyplexes by electrostatic interactions. 61
Figure 20. Physico-chemical characterization of QA-pullulan/miRNA polyplexes: (a) Size distribution from Light Scattering (LS) expressed by intensity and number percentages; (b) Morphology of polyplexes obtained by TEM microscopy; (c) Size (nm), PdI, attenuator and count rate values measured by LS and zeta potential (mV) measured by Doppler laser electrophoresis. Results are shown as mean ± standard deviation of 3 different samples. 62
Figure 21. miRNA presence onto polyplexes: (a) miRNA presence onto polyplexes after miRNA desorption confirmed by agarose gel electrophoresis using an Ultra-Low Range GeneRuler DNA Ladder (10-300 bp) as control and RNA amount (ng) quantified by the intensity of the band when compared to miRNA alone (0.04 mg/mL, 9 µL) using ImageJ software; (b) RNA amount (ng/µL) quantified by UV absorbance (n=3). 63
Figure 22. Stability of QA-pullulan/miRNA polyplexes evaluated by size (left) and PdI evolution (right) measured by Light Scattering as function of time of incubation in water at 4°C (mean ± SD, n=3). 64

Figure 23. Cytocompatibility of complexes. (a) Cytocompatibility of complexes towards HUVECs exposed to increasing concentrations of QA-pullulan/miRNA polyplexes measured by resazurin conversion after 1 day of incubation. Results are shown as mean ± SD from 3 independent experiments with no statistical differences detected using the Wilcoxon matched-pairs signed rank test. (b) Optical images of confluent cells without polyplexes and with 100 µg/mL and 200 µg/mL of polyplexes. Scale bar corresponds to 200 µm. 65
Figure 24. FAM-miRNA delivery. Fluorescence microscopy images of HUVECs evidencing miRNA delivery. Left column: cells' nuclei stained with DAPI (depicted in blue); middle column: FAM labelled miRNA (depicted in green); right column: merged images. (A) Without treatment, (B) cells treated with FAM-labelled miRNA, (C) cells treated with FAM-labelled miRNA in presence of unmodified pullulan; (D) cells treated with polyplexes formed by FAM-labelled miRNA and QA-pullulan including Z-stack-assembled fluorescence images (zoom). Treatments were performed for 30 min at 37°C. Scale bar: 20 µm. 66
Figure 25. Synthesis route for amination of pullulan grafted with 2-chloro-N, N-diethyl ethylamine hydrochloride. 73
Figure 26. Cytocompatibility of non-modified pullulan, DEAE-pullulan and QA-pullulan towards HUVECs at 200, 500 and 1000 µg/mL after 24h of incubation. Results are shown as mean ± SD from 3 independent experiments with no statistical differences detected using the Wilcoxon matched-pairs signed rank test. 74
Figure 27. Scheme of polyplexes production. All the solutions were filtered (0.2 µm) before use. 75
Figure 28. Physico-chemical characterization of polyplexes: Size distribution of (A) DEAE-pullulan/miRNA and (B) QA-pullulan/miRNA polyplexes from Light Scattering (LS) expressed by intensity percentages; (C) Size (nm) and PdI values measured by LS and zeta potential (mV) measured by Doppler laser electrophoresis. (D) miRNA presence onto polyplexes after miRNA desorption confirmed by agarose gel electrophoresis using an Ultra-Low Range GeneRuler DNA Ladder (10–300 bp) as control and RNA amount (ng) quantified by the intensity of the band when compared to miRNA alone (0.04 mg/mL, 9 µL) using ImageJ software; Results are shown as mean ± standard deviation of 3 different samples. 76

Figure 29. Size distribution from Light Scattering (LS) expressed by intensity percentages of DEAE-pullulan/miRNA polyplexes dissolved in 0.9% NaCl. Data was acquired in triplicate. 77
Figure 30. Scheme to produce polyelectrolyte complexes between QA-pullulan and fucoidan. All the solutions were filtered (0.2 µm) before use. 78
Figure 31. Visual turbidity for PECs with different polyelectrolyte concentrations (0.08, 0.2, 0.5 and 1.0 mg/mL). 79
Figure 32. Characterization QA-pullulan/fucoidan PECs prepared at equally PEs concentration of 0.008% (w/v): (A) Size distribution measured from Light Scattering (LS) expressed by intensity percentages and (B) Size (nm) and PdI values measured by LS and zeta potential (mV) measured by Doppler laser electrophoresis. Results are shown as mean ± standard deviation of 3 different samples. 80
Figure 33. Scheme to produce polyelectrolyte complexes between QA-pullulan and fucoidan loaded with miRNA. 81
Figure 34. Physico-chemical characterization of loaded PECs: (A) Size distribution from Light Scattering (LS) expressed by intensity percentages; (B) Size (nm) and PdI values measured by LS and zeta potential (mV) measured by Doppler laser electrophoresis. (C) miRNA presence onto PECs after miRNA desorption confirmed by agarose gel electrophoresis using an Ultra-Low Range GeneRuler DNA Ladder (10–300 bp) as control and RNA amount (ng) quantified by the intensity of the band when compared to miRNA alone (0.04 mg/mL, 9 µL). Results are shown as mean ± standard deviation of 3 different samples. 82
Figure 35. Stability of PECs QA-pullulan/fucoidan loaded with miRNA evaluated by size (left) and PdI (right) measured by Light Scattering as function of time of incubation in water at 4°C (mean ± SD, n = 3). 82
Figure 36. Size distribution from Light Scattering (LS) expressed by intensity percentages of PECs dissolved after 1h incubation in 0.9% NaCl. Data was acquired in triplicate. 83
Figure 37. Cytocompatibility of polyplexes, unloaded PECs and loaded miRNA PECs towards HUVECs at 100 and 200 µg/mL after 24h of incubation. Results are shown as mean ± SD from 3 independent experiments with no statistical differences detected using the Wilcoxon matched-pairs signed rank test. 84
Figure 38. Polyelectrolyte complexes nanoparticles of EA-pullulan and fucoidan: (A) before crosslinking, (B) after crosslinking with genipin and (C) schematic representation of crosslinking bridges between genipin and primary amine groups of EA-pullulan. 113

Figure 39. Absorption spectra of free genipin and genipin crosslinked PECs (G-PECs) at different temperatures (room temperature, 37°C and 50°C) over time (0h, 8h, 24h, 48h). 114
Figure 40. Physico-chemical characterization of crosslinked nanoparticles: (A) Dynamic diffusion of light measured in intensity. (B) Images obtained by transmission electron microscopy (upper image) and environmental scanning electron microscopy (bottom image). (C) Size (nm), polydispersion index and zeta potential (mV) measured by Zetasizer Nano-ZS. The percent of fucoidan by weight of the total nanoparticle weight was determined by elemental analysis. 115
Figure 41. Stability of G-PECs in water (▫) and NaCl 0.9% (▪) after preparation (day 0), and after 1, 7, 14, 21 and 28 days of storage at 4°C. (A) NP size (nm) and (B) PdI were measured by DLS; (C) ζ potential values (mV) by ELS; (D) Effect of the addition of a cryoprotectant on nanoparticles size before and after freeze-drying. Results are shown as mean ± SD from three independent experiments. 116
Figure 42. (A) Cytocompatibility of G-PECs towards HUVECs exposed to increasing concentrations of G-PECs measured by resazurin conversion after 1 day of incubation. Results are shown as mean ± SD from 3 independent experiments with no statistical differences detected using the Wilcoxon matched-pairs signed rank test. (B) Optical and (C) fluorescence images of confluent cells without G-PECs and with 250, 500 and 1000 µg/mL of G-PECs, respectively. Scale bar corresponds to 200 µm (top image) and 20 µm (bottom image)..... 117
Figure 43. Blood hemolysis percentage of human blood from healthy donors after incubation with increasing concentrations of 250,500 and 1000 µg/mL of G-PECs nanogels. Water and PBS were used as positive and negative control, respectively. Results are shown as mean ± SD from three independent experiments. 118
Figure 44. Confocal microscopy images of HUVECs treated without G-PECs and with G-PECs produced using fluorescent labelled EA-pullulan (RBITC-EA-pullulan). G-PECs were incubated with HUVECs for 24h at 37˚C. HUVECs were then washed, fixed, and observed under fluorescence microscopy. Red, G-PECs; green, phalloidin; blue, cell nuclei. Scale bars, 20 µm. 119
Figure 45. Evaluation of G-PECs binding on activated platelets under arterial flow conditions. Particles and platelets aggregates co-localization was evaluated by merged fluorescence microscopy images (right). G-PECs without fucoidan were used as control. Scale bars corresponds to 50 µm. 120

Figure 46. miRNA loading and release. (A) Zeta potential (mV) measured by the Zetasizer Nano-ZS at pH 3 and pH 7 before and after miRNA loading. (B) Loading efficiency of miRNA at pH 3 and 7 and (C) miRNA release from G-PECs nanogels at 37°C in PBS. Results are shown as mean ± SD from three independent experiments. 121
Figure 47. FAM-miRNA delivery. (A) Fluorescence microscopy images of HUVECs evidencing miRNA delivery. Left column: cells' nuclei stained with DAPI (depicted in blue); middle column: FAM labelled miRNA (depicted in green); right column: merged images for cells treated with naked FAM-labelled miRNA and cells treated with G-PECs nanogels loaded with FAM-labelled miRNA; Treatments were performed for 2h at 37°C. Scale bar: 20 µm. (B) Mean fluorescence intensity (MFI) of fluorescein amidite (FAM) measured by flow cytometry analysis. Results are shown as mean ± SD from three experiments..... 122
Figure 48. Synthesis route for amination of pullulan grafted with 2-chloroethylamine hydrochloride. 124
Figure 49. 1H NMR spectrum at 400 Mhz of 2-chloro-ethylamine hydrochloride in D2O. 125
Figure 50. 1H NMR spectra at 400 Mhz of (A) non-modified pullulan and (B) EA-pullulan in D2O. 1A, 1B, 1C signals depicted anomeric H from maltotriose base unit of pullulan. Numbers 2–6 corresponded to H on anydroglucose unit. H from ethylamine (B) were depicted with numbers 7 and 8..... 126
Figure 51. Cytocompatibility of EA-pullulan derivatives. (A) Cytocompatibility of EA-pullulan (1.6%N) measured by resazurin assay after 1-day exposure to increasing concentrations ranging from 10-1000 µg/mL compared to unmodified pullulan. (B) Cytocompatibility of EA-pullulan with different N contents (0.7, 1.6 and 2.0 %N) after 1-day exposure to increasing concentrations ranging from 200-1000 µg/mL of EA-pullulan compared to unmodified pullulan. Results are shown as mean ± SD from 3 independent experiments. *$p < 0.05$ using the Wilcoxon matched-pairs signed rank test. 127
Figure 52. Zeta potential (mV) curve of EA-pullulan solution at 2.5 mg/mL at different pH values (mean ± SD, n = 3). 127
Figure 53. FTIR spectra of unmodified pullulan, EA-pullulan, fucoidan, PECs and G-PECs. 128
Figure 54. Histograms of particle size distribution at different genipin concentrations from Light Scattering (LS) expressed by intensity percentages (mean ± SD, n=3). 129

Figure 55. TEM pictures of polyelectrolyte complexes (A) before and (B) after crosslinking. Scale bars represents 500 nm. 129
Figure 56. Reconstructed 3D images of G-PECs internalization in HUVECs using the Imaris® software. Scale bars corresponds to 10µm. 130
Figure 57. (A) Size (nm) and (B) polydispersity index measured by the Zetasizer Nano-ZS at pH 3 and pH 7 before and after miRNA loading. Results are shown as mean ± SD from three independent experiments. 130
Figure 58. Agarose gel electrophoresis of unloaded G-PECs, loaded G-PECs before ultracentrifugation (bUC) and after ultracentrifugation (aUC) and supernatant for miRNA loading performed at (A) acid pH (pH 3) and (B) neutral pH (pH 7). An ultra-low weight GeneRuler (10–300 base pairs) was used as a control and the amount of RNA incorporated was compared to miRNA alone at the same concentration used for loading (0.04 mg/mL, 9 µL). 131
Figure 59. Environmental scanning electron microscopy images of polyelectrolyte complexes EA-pullulan and fucoidan. 173
Figure 60. Environmental scanning electron microscopy images of crosslinked polyelectrolyte complexes EA-pullulan and fucoidan with genipin. 173
Figure 61. Synthesis of pullulan methacrylate. Pullulan were reacted with glycidyl methacrylate (GMA) during 24h at room temperature. 174
Figure 62. 1H NMR spectra at 400 Mhz of non-modified pullulan (top) and pullulan methacrylate (bottom) in D2O. 176
Figure 63. Crosslinked Pull-MA hydrogels after 4h exposed to UV irradiation in the absence of photoinitiators. 177
Figure 64. Chemical structure of cationic pullulan derivative with primary amines and quaternary ammonium groups. 179
Figure 65. 1H NMR spectra at 400 Mhz of (a) non-modified pullulan, (b) QA-pullulan (0.25%N) and (c) QA-pullulan-PA (1.24%N) in D2O. 180
Figure 66. Reconstructed 3D images of FAM-miRNA delivery in HUVECs using the Imaris® software. Cells'nuclei were stained with DAPI (blue); Phalloidin were stained with Alexa Fluor 633 (red); miRNA was labelled with FAM (green); Scale bars corresponds to 20µm (top) and 10 µm (bottom). 185

LIST OF TABLES

Table 1. Impediments faced by native drug are surpassed by drug in nanoformulations leading to optimum therapeutic efficiency [32]. 17
Table 2. Techniques for physicochemical characterization of nanoparticles. 19
Table 3. Representative research on miRNA therapeutics based on polymeric delivery systems. 40
Table 4. Characterization of pullulan and cationic pullulan derivatives. 58
Table 5. Elemental analysis of pullulan and cationic pullulan derivatives. 58
Table 6. Characterization of pullulan and cationic pullulan derivatives. 73
Table 7. Characterization of LMWF by elemental analysis. 77
Table 8. Size (nm) and polydispersity index for QA-pullulan/fucoidan PECs at different polyelectrolyte concentrations and volumes. 78
Table 9. Size (nm) and polydispersity index for QA-pullulan/fucoidan PECs at different polyelectrolyte concentrations and volume ratios. 79
Table 10. Size (nm) and Polydispersity Index for QA-pullulan/fucoidan PECs at different polyelectrolyte concentrations and weight ratios. 80
Table 11. Characterization of cationic pullulan derivative with primary amine groups. 110
Table 12. Effect of pH on PECs formation by mixing EA-pullulan (0.2 mg/mL) and fucoidan (0.2 mg/mL). Results are expressed as mean ± SD (n=3). 111
Table 13. Effect of EA-pullulan/fucoidan mass ratio on PECs formation. Results are expressed as mean ± SD (n=3). 112
Table 14. Characterization of cationic pullulan derivatives with primary amine groups performed in one-step of synthesis. 124
Table 15. Characterization of cationic pullulan derivatives with primary amine groups performed in two steps of synthesis during 3h at 55°C each step. 125
Table 16. Nanoparticles concentration before and after purification by ultracentrifugation (UC). 130
Table 17. Characterization of cationic pullulan derivatives with quaternary ammonium and primary amines. 179

ABBREVIATIONS

AGU	Anhydroglucose unit
aUC	After ultracentrifugation
bUC	Before ultracentrifugation
D	Diameter
Da	Dalton
DAPI	4′,6-Diamidino-2-phenylindole
DEAE	Diethylaminoethyl
DLS	Dynamic light scattering
DMSO	Dimethyl sulfoxide
D_2O	Deuterium Oxide
DS	Degree of substitution
C	Carbon
EA	Ethylamine
ELS	Electrophoretic light scattering
Eq	Equivalent
ESEM	Environmental scanning electron microscopy
FAM	Fluorescein amidite
FBS	Fetal bovine serum
FDA	Food & drug administration
FTIR	Fourier-transform infrared spectroscopy
GMP	Good manufacturing practices
GTMAC	Glycidyltrimethylammonium chloride

H	Hydrogen
^{1}H NMR	Proton nuclear magnetic resonance
HUVECs	Human umbilical vein endothelial cells
K	Kilo
KBr	Potassium bromide
M	Molar
MALLS	Multiangle laser light scattering
mg	Milligrams
MHz	Megahertz
miRNA	MicroRNA
miR	Mature miRNA
mL	Milliliters
Mn	Number average molecular weight
mV	Millivolts
Mw	Weight average molecular weight
N	Nitrogen
nm	Nanometer
NP	Nanoparticle
O	Oxygen
PA	Propylamine
PBS	Phosphate buffered saline
PdI	Polydispersity index
PE	Polyelectrolytes
PEC	Polyelectrolyte complexe

PEG	Polyethylene glycol
ppm	parts-per-million
QA	Quaternized ammonium
RBC	Red blood cells
RBITC	Rhodamine B isothiocyanate
RNA	Ribonucleic acid
RT	Room temperature
S	Sulfur
SEC	Size exclusion chromatography
TEM	Transmission electron microscopy
TLC	Thin layer chromatography
TRPS	Tunable resistive pulse sensing
UV	Ultraviolet light
µg	Microgram
µL	Microliters

1. GENERAL INTRODUCTION

As we develop new drug delivery systems, we should focus on choosing diseases that have high need for new therapies. Diseases of the cardiovascular system represent the first cause of morbidity and mortality worldwide, underscoring the need for the development of innovative therapies. Among the many strategies explored, the use of microRNA (miRNA) associated with a suitable vector is one of the most promising.

miRNAs are small non-coding nucleic acids that are expressed instantaneously in the cytoplasm without the risk of genomic integration. The most recent works evidenced that these molecules could fulfill relatively generic functions in cells being implicated in the control of many fundamental cellular and physiological processes such as cellular differentiation, metabolism, proliferation, cell cycle control, migration and apoptosis.

However, in order to advance miRNAs into clinical settings, the delivery of miRNA therapeutics remains a major challenge. Combining the use of miRNAs with nanotechnology is a promising strategy for the development of clinically viable therapeutic options.

Within the different classes of biomaterials used for biomedical applications (polymers, metals, ceramics and composites), polymers represent the largest percentage. In particular, the use of polysaccharides is of great interest thanks to their good biocompatibility as well as that of their degradation products. Besides, polysaccharides can be easily modified with different chemical groups to confer them, as an exemple, the capacity to interact with anionic molecules by introducing cationic substituents. Owing to their unique potentials, polysaccharides have thus received considerable attention for a long time to build drug delivery systems.

In this work, we developed a strategy based on the formation of polyelectrolyte complexes (PECs) between cationic pullulan derivatives and a miRNA able to trigger specific modifications of cellular pathways implicated in the development of vascular diseases. Pullulan, a polysaccharide extracted from a yeast, is widely used by the pharmaceutical industry. Although there are still no pullulan-based nanotherapeutics in current clinical use, numerous works have already evidenced this potential.

Eventually, PECs were endowed with biospecificity for the pathological vascular wall by combining them with fucoidan, a sulfated polysaccharide capable of specifically target P-selectin expressed on activated platelets and on inflamed endothelium. With this project, we hope to contribute for the development of new safe polysaccharide-based delivery

systems for miRNA therapeutics as a potential strategy in particular for the treatment of atherosclerosis and its complications.

The manuscript is divided in two main parts:

The **bibliographic review** is divided in three main topics. In the first topic, we briefly discuss about the pathogenic mechanism of atherosclerosis that leads to myocardial infarction and the interest in using miRNAs as therapeutic alternative to treat cardiovascular diseases. Due to the serum instability of miRNA, its hydrophilic nature, negative charge and high molecular weight, the delivery is a key point to consider when using miRNA in therapeutics. The second topic focus on polysaccharide-based drug delivery systems. In the third part, we present an overview of the main delivery nanosystems (inorganic nanoparticles, lipid-based nanoparticles and polymer-based nanoparticles) that have been employed for miRNA delivery and the challenges that need to be adressed to design efficient miRNA delivery systems.

In the **experimental part**, the results are presented under two main chapters written in the form of publication. Each chapter is preceded by an introduction, which situates the developed strategy in the context of the project.

In the 1st chapter, we developed pullulan-based nanoparticles via the polyelectrolyte complexation approach using cationic pullulan derivatives and miRNA, which were characterized by physical and chemical techniques. Cationic pullulan derivatives modified with quaternary ammonium groups showed to exhibit high biocompatibility and were able to delivery miRNA *in vitro*. These data were published in International Journal of Pharmaceutics. Some complementary works that were not published, are presented and discussed after the published part.

In the 2nd chapter, crosslinked PECs associated with fucoidan are developed using a natural crosslinking agent. The particles are produced using a green synthesis methodology without the use of any toxic solvent. Their ability to target P-selectin and to deliver miRNA is investigated *in vitro* with human endothelial cells. The high stability of the nanoparticles in physiological conditions and the potential for their long-term storage endows their potential as miRNA delivery systems. These data were also published in International Journal of Pharmaceutics.

A **general discussion** confronting our results to the literature and developing some perspectives is followed by a **general conclusion**, which closes the presentation of this work.

2. BIBLIOGRAPHIC REVIEW

2.1 Cardiovascular diseases

Cardiovascular diseases (CVDs) are the leading cause of morbidity and mortality worldwide, being responsible for 31% of all global deaths, and their incidence are in constant increase due to the progressive aging of population along with enhanced risk factors for atherosclerosis [1]. These factors most frequently include hypertension, tobacco smoking, diabetes mellitus, obesity, as well as genetic predisposition [2]. Heart failure (HF) associated to an ischemic coronary artery disease is currently the most common cardiac disorder being considered as a major public health issue, and correlates with the worse prognosis [3].

The coronary artery disease starts due to the accumulation of lipoproteins in the intima of the coronary vessels. Oxidized or modified low-density lipoprotein (LDL) then attract leukocytes into the intima of the coronary vessels, which can be scavenged by macrophages, leading to the formation of foamy cells. An imbalance in cholesterol metabolism and a maladaptive immune response progress the formation of an atherosclerotic plaque (Figure 1) [4,5]. Eventually, plaque rupture can occur, and the contact of blood with the exposed sub endothelial matrix and plaque content cause the formation of an occlusive thrombus. The complete occlusion of coronary vessels impedes a sufficient oxygen supply to the heart muscle throughout the anatomic region supplied by this artery resulting in acute myocardial infarction (MI). After 20-40 min of sustained severe ischemia an irreversible damage is produced, the heart progressively loses its contractility, ultimately leading to HF [6–8].

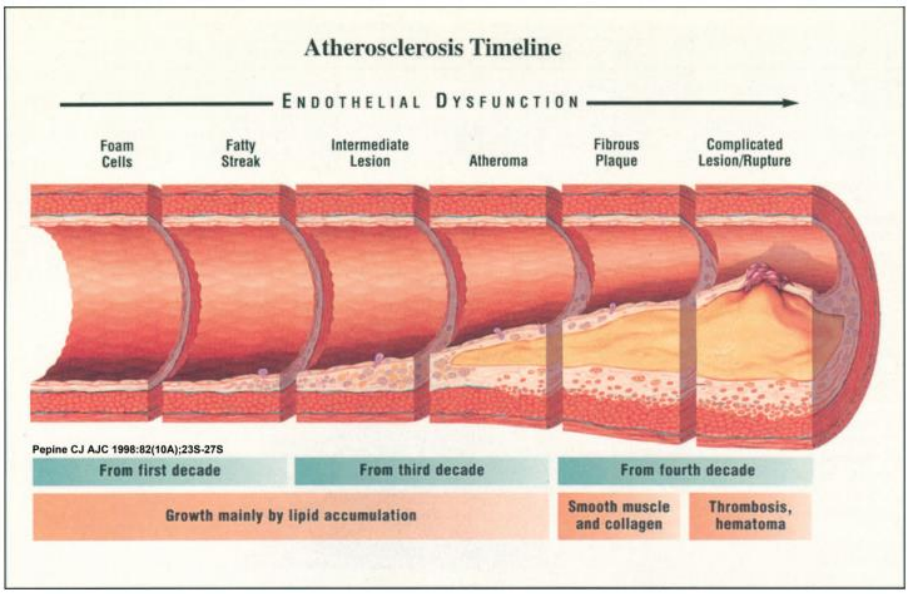

Figure 1. Progression of atherosclerosis from earliest fatty streaks to complicate lesion [9].

Current post-MI therapy options, including pharmacological treatments (e.g., antiplatelet therapy [10], beta-blockers [11]) and surgical interventions (e.g., coronary angioplasty and stenting), are limited to mitigating symptoms and do not induce tissue repair [12]. Hence, none of the current treatments available to data is sufficient to surpass a sustained severe ischemia and prevent patient's death. Nowadays, the only efficient long-term treatment is through heart transplantation, yet limited by the lack of heart donors and the problems linked with the risk of immunorejection [13,14]. As such, there is a need to develop alternative strategies to repair hearts with infarction in order to ameliorate both patient prognosis and life quality.

Despite the rapid restoration of coronary blood flow in response to an ischemic event be the standard care to minimize the infarct size, the restoration of blood flow itself leads to further irreversible myocardial damage in a process known as ischemia/reperfusion injury [8,14]. The reperfusion of cardiac muscle result in a burst of reactive oxygen species (ROS). The excessive production of ROS and inability of the anti-oxidant system to neutralize them results in oxidative stress which causes further cardiac injury reducing the beneficial effects of myocardial reperfusion. ROS have been identified as major contributors of the pathogenesis of cardiac remodeling which leads to cardiac insufficiency and heart failure [7,15,16].

Besides the use of standard pharmacological approaches, miRNA-based therapies offer new challenging avenues to ameliorate or reverse the progression of heart failure. MicroRNAs (miRNAs) are short (~ 21-23 nucleotides), non-coding endogenous RNA molecules that modulate gene expression at the post-transcriptional level via the endogenous RNA interference machinery of the cell. In mammals, miRNAs originate from a primary transcript, named as primary miRNAs (pri-miRNAs), which are transcribed in the nucleus by the action of RNA polymerase II. Pri-miRNAs are processed within a microprocessor complex, consisting of a ribonuclease III, DROSHA and its associated cofactor DiGeorge critical region 8 gene (DGCR8) to generate a hairpin shaped pre-miRNA (pre-miRNA) with ~ 70 nucleotides in lenght. These intermediates are then exported to the cytoplasm via the nuclear export factor Exportin- 5 and further processed by the RNAse Dicer and transactivation response element RNA-binding protein (TRBP) into ~ 22 nucleotides double-stranded miRNA duplexes [17–20].

The gene regulation process is mediated by the load of mature miRNAs strand into a protein complex present in the cell cytoplasm called RNA-induced silencing complex (RISC), which serves as a guide for the recognition of targeted messenger (mRNAs). Their binding potency to the 3′-untranslated region (3'-UTR) of mRNAs determines their mode of action. A perfect complementarity with targeted mRNA induces the endonuclease activity of Argonaute (Ago) protein resulting in mRNA degradation. In a different way, a partially complementary base pairing between targeted mRNA and miRNA is not able to activated Ago of the miRISC complex and the silencing of mRNA targets occurs by translational repression (Figure 2) [19,21–23].

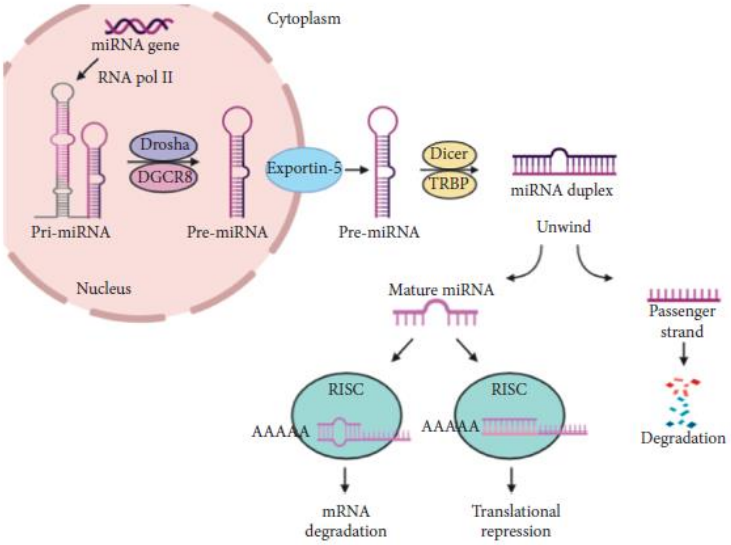

Figure 2. MicroRNA biogenesis and mechanism of action. miRNA genes are transcribed to produce primary miRNA (pri-miRNA) by RNA polymerase II and cleaved into precursor miRNA transcript (pre-miRNA) by the microprocessor complex Drosha-DGCR8 in the nucleus. Pre-miRNA moves into the cytoplasm via Exportin-5, where it is further processed by Dicer and TRBP, producing a double-stranded miRNA duplex. The functional strand of mature miRNA is loaded onto the RNA-induced silencing complex (RISC) and negatively regulates gene expression resulting in either target mRNA degradation or translation repression, while the passenger strand is degraded [20].

Different miRNAs were described to modulate the oxidative stress in the cardiovascular system by targeting ROS generators [24], antioxidant signaling pathways [25,26], and antioxidant effectors [4,27]. Among them, Nrf2 (nuclear factor erythroid 2-related factor 2) is a potent transcriptional activator with a central, and well-established, role in the inducible expression of several cytoprotective genes in response to oxidative and electrophilic stresses. Under normal conditions, the activity of the Nrf2-mediated transcription is low, as most of Nrf2 protein is sequestrated to an inhibitory protein, Kelch-like ECH associated protein-1 (Keap1), and degraded in the proteasome. Under stressed conditions, Nrf2 is translocated to the nucleus, where it binds to the antioxidant response element (ARE), resulting in the upregulation of targeted antioxidant enzymes such as glutathione S-transferase (GST), NAD(P)H:quinone oxidoreductase 1(NQO 1), S-superoxide dismutase 1 (SOD1), and heme oxygenase 1 (HO-1) (Figure 3) [4,28].

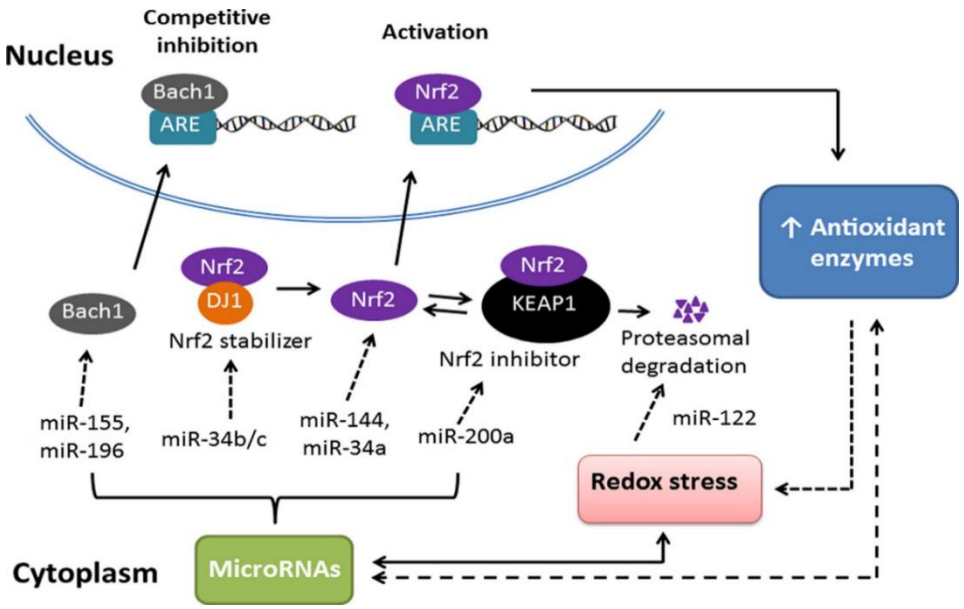

Figure 3. Schematic model of Nrf2/ARE pathway activation by redox stress and potential regulation by miRNAs [25].

miRNAs were reported to modulate the Nrf2 pathway by direct targeting Nrf2 [29] or its regulators [26,30]. Notably, miR-155-5p have been described to silence the messenger RNA (mRNA) of the transcription factor BACH1 *in vitro* in endothelial cells (ECs), resulting in enhanced production of heme oxygenase 1 (HO-1) and conferring protection against oxidative stress [26]. BACH 1 is a competitor in the run to bind to ARE, since BACH1 has a higher affinity with ARE than Nrf2. If BACH1 is targeted, more Nrf2 becomes activated and can bind to ARE [25]. Mice that suffered MI and had BACH1 deleted, had an infarct size of less 48.4% than the controls [31].

Unfortunately, following intravenous injection, unprotected miRNAs are quickly degraded by the presence of abundant nucleases in the extracellular and plasma environment and hence the construction of delivery systems is crucial toward achieving effective systemically administration of miRNA-based therapeutics. The ideal carrier should be able to protect miRNA during circulation avoiding biological barriers until it reaches its targeted tissues. For this purpose, nanotechnology has provided significant improvements on the delivery of molecules with short circulation life and unfavorable pharmacokinetics profiles. In addition, as miRNA's behavior is highly dependent on cell type and context, cell-type-specific delivery tools might need to be developed in order to only regulate the intended drug target in the diseased tissue in a way that off-target effects are avoided [18,32].

Concerning the targeted tissue, P-selectin, an adhesion molecule expressed at the surface of activated platelets and ECs upon activation, is a strong indicator of an atherothrombotic-related disease such as a MI. Sulfated polysaccharides have been described as P-selectin ligands due to the ability to bind their sugar recognition domains [5,33]. Fucoidan, for example, is a naturally occurring sulfated polysaccharide derived from brown algae, that presents a high affinity for P-selectin [34]. Single Photon Emission Computed Tomography coupled with Computed Tomography (SPECT/CT) scans images of an ischemia-reperfusion rat model acquired 2h after intravenous injection of GMP grade low molecular weight fucoidan (LMWF) labeled with ^{99m}Tc clearly indicate an uptake in the area of myocardial ischemia thanks to the presence of exposed P-selectin either by endothelium cells or by activated platelets in this region (Figure 4). Decorating NPs surface with fucoidan would therefore confer them the ability to target P-selectin in activated ECs, cells reachable through intravenous injection.

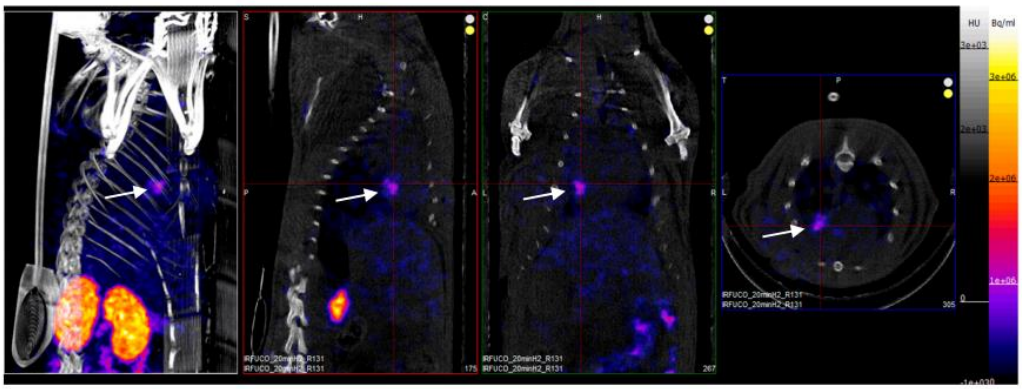

Figure 4. SPECT/CT scans of an ischemia-reperfusion rat model. From left to right: 3D view, sagittal, coronal, and axial planes. The white arrow indicates the diseased heart area where the 99mTc labeled fucoidan has accumulated [35].

2.2 Nanomedicine and drug delivery systems

Drug delivery is a challenging aspect of pharmaceutical sciences given that drug molecules face numerous barriers until reaching its targeted tissues, organs and cells before producing a desired pharmacological effect [36]. These barriers include immunological and renal clearance, enzymatic and mechanical degradation, vascular endothelium, the extracellular matrix, the cell membrane, the lysosome, and membrane pumps, resulting in suboptimal concentration of the administered free drug at the disease

site [36,37]. A drug delivery system (DDS) is defined as any formulation or device used to transport therapeutic drugs in the body in order to improve their action over time by maintaining therapeutic concentrations of the active ingredient in the site of action [38,39]. The modulation of the biopharmaceutical properties of the conventional drugs through their encapsulation in innovative drug delivery systems makes them more effective at lower dosages resulting in decreased side effects and providing optimum therapeutic efficacy in clinical setting [40].

In recent years, nanotechnology applied to the area of medicine (nanomedicine) has been increasing as a new independent field of life sciences that combines pharmaceutical and biomedical sciences, with the goal of developing drugs and imaging agents with higher efficacy and improved safety and toxicological profiles [41,42]. The Food and Drug Administration (FDA) defines nanomaterial as any material with at least one dimension smaller than 1000 nm and a nanoparticle as an object with all three external dimensions in the 1–100 nm size range. Nanosystems can be applied for drug delivery purposes (nanotherapeutics/ nanopharmaceutics) imaging and diagnosis (nanodiagnostics) and medical implants (nanobiomaterials). The European Medicines Agency (EMA) working group introduces the definition of nanomedicines as purposely designed nanosystems for clinical applications, with at least one component at the nanoscale, which can be used as drug nanocarriers exhibiting key differences when compared to bulk materials thanks to their small size and high surface/volume ratio [43–45].

Broadly, materials that have been employed to construct such nanoparticles, include polymers, micelles, dendrimers, liposomes, metals/metal oxides and other inorganic materials (Figure 5) [46,47]. Polymeric-based nanoparticles and liposomes have been the major component of nanomaterial based formulations in clinical translation with the highest number of FDA approved drugs [37,44,48]. It has been claimed that one of the ways to avoid the potential toxicity associated with the use of nanocarriers, a relevant issue preventing diverse clinical applications so far, could be overcome by using natural materials [49,50].

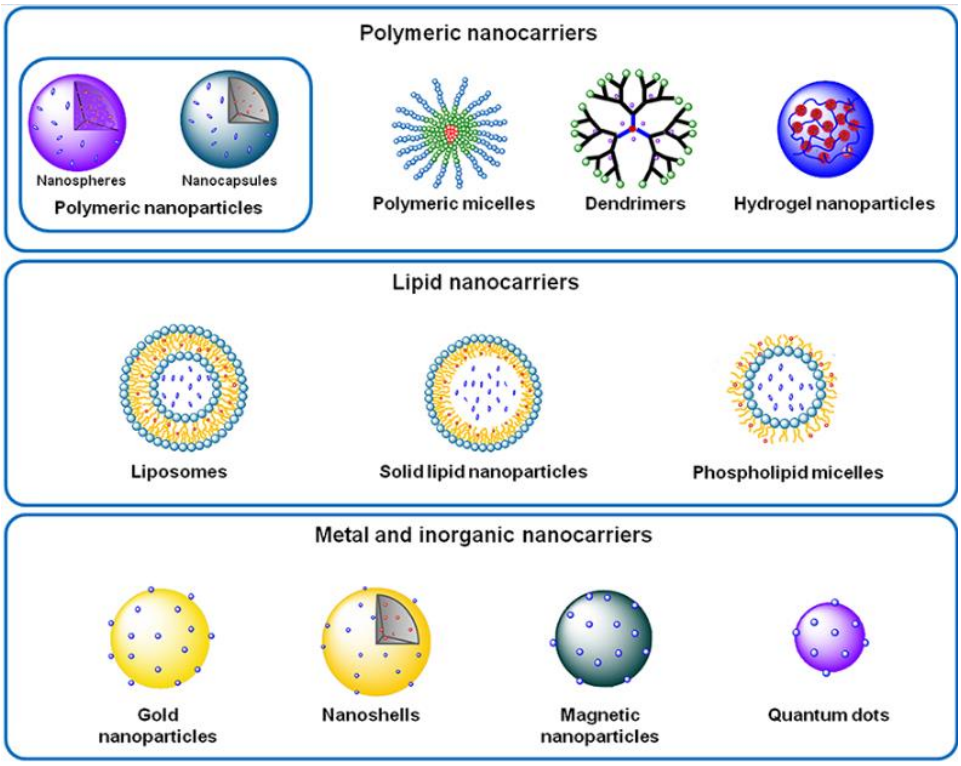

Figure 5. Different types of nanocarriers used in drug delivery systems and their morphological features [51].

There are several advantages of nanoparticular drug formulations such as the possibility to modify properties like solubility, diffusivity, bioavailability and immunogenicity which can lead to the improvement and development of convenient administration routes, lower toxicity, fewer side effects, improved biodistribution and extended drug life cycle (Table 1) [52]. The incorporation of targeted moieties can contribute to enhance the selective delivery of encapsulated drug towards the site of the action. Such biospecific nanosystems reduce off-target organ toxicities, and facilitate cellular uptake of therapeutics [40,41]. Besides conventional drugs, recombinant proteins, vaccines, and nucleic acids may also be effectively delivered by nanosystems [45,53].

Table 1. Impediments faced by native drug are surpassed by drug in nanoformulations leading to optimum therapeutic efficiency [36].

Native Drug	Nanoformulations
Biological barriers	Selective targeting
Decreased solubility	Sustained release
Drug resistance	Increased half-life
Enzymatic degradation	Optimum therapeutic use
Short plasma half-life	Less systemic toxicity
Systemic toxicity	

Nanosystems have been used in clinic since the early 1990's with Doxil® (doxorubicin hydrochloride, Janssen), a pegylated liposomal formulation of doxorubicin, being the first FDA-approved nanodrug (1995) indicated for AIDS-related Kaposi's sarcoma. Although equally effective, its main advantage in comparison to conventionally formulated free-doxorubicin is reduced cardiotoxicity, which improves patients therapy [37,54–56]. More than 20 years after its approval, Doxil® is still widely used for its original indication, as well as to treat recurrent ovarian cancer, metastatic breast cancer and multiple myeloma [36,56].

From 1995 to 2019, many other nanodrugs have been approved by the FDA or EMA for clinical use and even more are being evaluated in ongoing clinical trials for a wide range of indications such as cancer, neurological disorders, diabetes, infectious diseases, and allergy [37,57]. Anselmo and Mitragotri (2016) listed the main approved nanoparticles and their use, such as formulations that are currently being evaluated in clinical trials [58].

With the exception of nucleic acid–based nanotherapeutics, nanomedicinal products are typically reformulations of active pharmaceutical ingredients (API), which have already been approved for clinical use [59]. Soon after the initial approval of Doxil®, various other liposomal formulations were approved for: (i) cancer: DaunoXome® (daunorubicin liposomes) and Myocet® (non-PEGylated liposomal doxorubicin); (ii) vaccines: Epaxal® (liposome with hepatitis A virus) and Inflexal V® (liposome with trivalent-influenza); (iii) fungal infections: AmBisome® (liposomal amphotericin B); (iv) pain treatment: DepoDur® (liposomal morphine) [58,60]. In addition to lipid-based nanomedicines, another examples includes Abraxane®, an albumin nanoparticle

conjugated with paclitaxel indicated for metastatic breast cancer, and Copaxone® and Neulasta®, polymeric-based nanoformulations indicated for multiple sclerosis and chemotherapy-induced neutropenia, respectively [42,45].

Alongside this, inorganic nanoparticles have been used mainly for the treatment of anemia related to chronic kidney diseases (CKD) as iron replacement therapy with the goal to increase the levels of iron in the organism. Ferrlecit®, Venofer® and Dexferrum® are some examples of approved drugs. These nanosystems consist in an iron oxide core coated with a hydrophilic polymer, such as sucrose and dextran, in order to avoid toxicity issues associated with the injection of free iron [61,62]. Few iron-oxide nanoparticles have also been approved as contrast enhancement agents (Feridex®) for magnetic resonance imaging (MRI) due to its inherent physical properties, especially unique super paramagnetic behavior. MRI has been the preferred tool for imaging the brain and the central nervous system, for assessing cardiac function, and for detecting tumors [42,63].

Modern approaches in protein engineering, as well as advances in polymer and inorganic chemistry, have resulted in an expansion of novel nanomaterials allowing the design of systems with more complex functions such as controlled release and active targeting compared to the traditional goals of initial nanopharmaceutics (improved PK, efficacy and safety) [56]. New trends in nanomedicine includes the delivery of biotherapeutics (especially nucleic acids), multifunctional targeted nanocarriers, metal-based nanoparticles acting as therapeutic under an external stimulus, and the development of combined therapies, encompassing both imaging and therapeutic capabilities, or diagnosis and thermal ablation, which is defined as “theranostics” [45,64].

2.3 Pharmaceutical development of nanomedicines

Although the FDA and EMA approved a number of nanomedicine products, their clinical translation still remains challenging once there are no specific international regulation for the production, handling or labeling, testing toxicity and evaluating the environmental impact of nanoystems [41,65,66]. The current approval process for nanosystems in humans is regulated by the FDA, and is essentially the same as that for any other regulated drug, device or biologic, following the same steps of clinical trials [42,61]. As for any drug, the authorities evaluate the marketing application by the established principles of benefit/risk analysis, rather than solely based on the technology of the new product [44].

Designing efficient nanosystems requires a better understanding of how nanosized structure governs the interaction with the biological systems, and thus their mechanism of action and ability to cross biological barriers in order to successfully deliver a drug [47,67]. Due to its dimension and structural complexity, a comprehensive analysis of the physicochemical characteristics of nanomaterial is essential to achieve a consistent product with desired pharmacological profiles [41,42,68]. Their characterization should be carried out at different stages throughout their life cycle starting from the design of the nanomaterial until the evaluation of its *in vitro* and *in vivo* performance [43].

The Nanotechnology Characterization Laboratory (NCL) in the US and its European counterpart, European Nanomedicine Characterization Laboratory (EU-NCL), provide guidelines covering a large set of preclinical validated characterization assays to be assessed for every nanomaterial before being sent to clinical studies. Evaluation parameters listed in these guidelines includes nanoparticles size, size distribution, surface composition and charge, morphology, drug loading and release profile, concentration as well as *in vitro* stability (Table 2) [44,61,67].

Table 2. Techniques for physicochemical characterization of nanoparticles.

Parameter	**Characterization technique**
Particle size and size distribution	Non imaging technique: Dynamic light scattering (DLS)
	Imaging-based techniques: Transmission electron microscopy (TEM), Scanning electron microscopy (SEM), Atomic force microscopy (AFM)
Particle morphology	Transmission electron microscopy (TEM)
	Scanning electron microscopy (SEM)
	Atomic force microscopy (AFM)
Surface charge	Electrophoretic light scattering (ELS)
Surface chemistry	Fourier Transformed Infrared Spectroscopy (FTIR)
	Nuclear resonance magnetic (NMR)
	X-ray photoelectron spectroscopy (XPS)
	Raman spectroscopy

The appropriate characterization of intrinsic nanosystems properties is essential in order to better understand their behavior after *in vivo* administration [43,67]. Many NP

characteristics including size, shape, charge and surface functionality are known to influence their biodistribution, biological fate, clearance and toxicity (Figure 6). For example, nanosystems smaller than about 100 nm can be injected intravascularly and have the potential to permeate and traffic through different tissues, to bind to cell surface receptors and to be internalized by target cells for the intracellular delivery of therapeutics without risk of embolization [51,69,70]. Meanwhile, larger nanosystems are quickly sequestrated by the spleen, while those smaller than 10 nm are rapidly removed through extravasation and renal clearance [71]. Hence, preferred size range for nanoparticle drug delivery should be in the 10-100 nm range [61,66,72]. Besides size, nanosystems shape can also affect cellular uptake [73]. Li *et al.* suggested a higher and faster internalization rate of spherical nanosystems because they need to overcome a minimal membrane binding energy barrier compared with non-spherical ones [74].

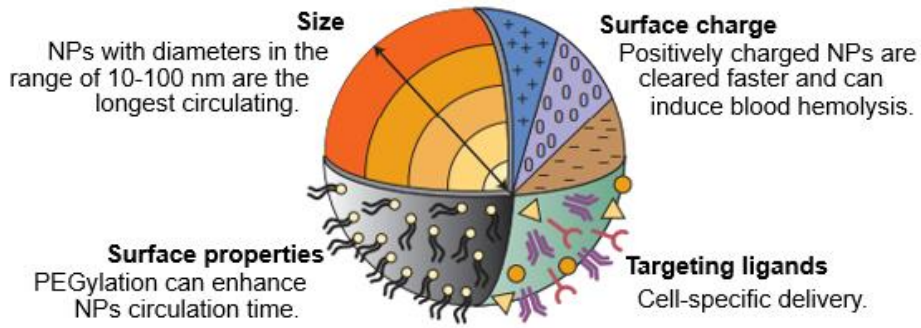

Figure 6. Design parameters of nanoparticles according to the composition, size, shape and surface properties of NPs. Adapted from M.A., Dobrovolskaia and S.E., McNeil 2007 [75].

Further, the surface charge, estimated by the zeta potential, can potentially affect receptor binding and physiological barrier penetration [44,76]. A positively charged nanosystem enhances cell association through the interaction with the negatively-charged phospholipid bilayer of cells which can result in enhanced internalization compared with neutral and negatively charged ones [47,53]. However, when injected in the bloodstream, positively charged NPs are cleared faster than negative or neutral NPs and are generally more toxic and may cause hemolysis [21]. Zeta potential also has an effect in the colloidal stability or aggregation of nanosystems. Those with a zeta potential above (+/-) 30 mV

are more stable in suspension, as the surface charge prevents the aggregation of the particles [77].

The surface chemistry also plays a significant role in the circulation time and cell internalization of nanomaterials. Once in the bloodstream, one of the major obstacles to achieve the required levels in the target tissue is their rapid clearance by the mononuclear phagocyte system (MPS) and reticuloendothelial system (RES) [78]. The liver, spleen and bone marrow are the major organs involved in nanoparticle clearance. The binding of plasma proteins (known as opsonization) is the primary mechanism for RES to recognize the circulating nanoparticles [79]. To overcome this issue and increase blood circulation time, nanoparticles are often coated with polyethylene glycol (PEG) [80,81]. The coating with PEG can dramatically reduce the protein opsonization on NPs surface and their subsequent recognition and sequestration by the immune system, thereby increasing their serum half-life. However, the PEGlyation of NPs can decrease their cellular uptake by target cells, reducing biological activity. Additional modifications, including NPs functionalization with targeting moieties are often necessary to direct nanoparticles towards the diseased tissue mediating cell specific binding and internalization [44,74].

Finally, to advance nanosystems as nanomedicines into the market, they must be amenable to industrial-scale development. The large-scale production and the reproducibility of manufacturing process of nanopharmaceutics are some of the most critical factors during pharmaceutical development [41]. A considerable number of nanosystems fail this requirement and, consequently, are not introduced on the pharmaceutical market [43]. A well-controlled robust manufacturing process including controlled batch-to-batch reproducibility that meets the good manufacturing practice (GMP) standards is fundamental to ensure the quality, safety and efficacy of the product [36,44]. By carefully addressing these challenges early in the development of new nanosystems together with the creation of harmonized guidelines for their characterization, evaluation and process, it may be possible to avoid major pitfalls and to contribute for the development of more efficient product pipelines [43,45].

2.4 Polymeric nanoparticles

Polymeric NPs are particles obtained from natural, semi-synthetic (artificial) or synthetic polymers. They have a size ranging from 10 nm to up to several 100 nm and are made up of polymers and copolymers protecting a drug, either embedded within particle or, adsorbed or chemically linked to the surface [60,82]. Depending on the type of polymer, different techniques, such as nanoprecipitation, mini and micro emulsion, emulsion-polymerization or ionotropic gelation allow to obtain nanoparticles [83,84].

Polymeric nanoparticles can be made from a large variety of natural polymers (chitosan, alginate, gelatin, collagen, dextran, heparin, and albumin) and synthetic polymers (polylactide–polyglycolide copolymers, polyacrylates and polycaprolactones (PCL), polylactic acid (PLA), poly (lactic-co-glycolic acid) (PLGA) [51]. Among natural polymers, chitosan is a biodegradable and biocompatible polymer largely studied for drug and gene delivery applications [85–87]. Among the synthetic polymers utilized to date, PLGA have received considerable attention due to their attractive characteristics such as low immunogenicity, nontoxicity, and biodegradability. The FDA approved PLGA for human use. However, poor hydrophilicity and low surface energy are some disadvantages of PLGA [48,88].

Tunable physicochemical properties and easy manipulation of polymers carriers have highlighted their use as drug delivery systems [51,89]. Biodegradable polymers are of particular interest because they can be fully metabolized and removed from the body, which is an important parameter to be considered for developing successful formulations. Despite some synthetic polymers are known to degrade *in vivo*, especially those belonging to the polyester family (PLGA, PCL,…), most of them are characterized by their low biodegradability [33,46,77]. In this manuscript, we have focused on the development of polymeric nanoparticles using polysaccharides due to unique features such as high abundance, renewability, nontoxicity, water solubility, biodegradability, and low cost processing [90,91].

2.4.1 Polysaccharides – an overview

Polysaccharides are a class of polymeric carbohydrate structures composed of repeating monosaccharide units adjoined by glycosidic bonds [92]. They are composed of a chain

of saccharide units, from a few (oligosaccharide) to several thousand monosaccharide units, the molecular weight of up to tens of thousands or millions Daltons [93]. They can be obtained from various natural and abundant resources, such as algae (e.g. alginate), plants (e.g. pectins, cellulose, cyclodextrins), microorganisms (e.g. dextran, pullulan) and animals (e.g. chitosan, hyaluronic acid) (Figure 7) [94]. They can be linear, for example chitosan and hyaluronic acid; branched as amylopectin or cyclic such as the cyclodextrins [95]. Polysaccharides may also be classified by their charge as cationic (chitosan), anionic (hyaluronic acid, heparin) and neutral (dextran, pullulan) [33].

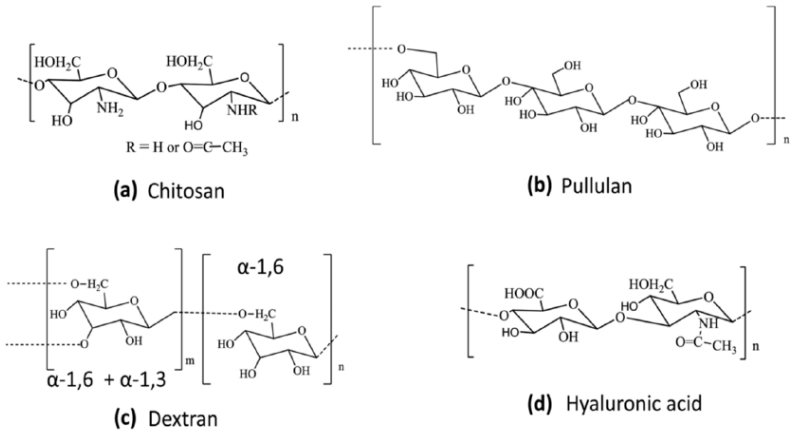

Figure 7. Chemical structures of commonly used natural polysaccharides [96].

Due to their diversity, carbohydrates are highly rich information molecules in the body and have many critical biological functions. They are source of cellular energy, the building blocks of nucleic acids and they have important structural functions since they are the primary constituents of eukaryotic cell surface and the extracellular environment [33,97]. The presence of several sugar units on the side chain of carbohydrate polymers makes them good candidates for targeted delivery by carbohydrate recognizing receptors found on the surface of several cells [49]. Most of the targeting strategies uses the highly specific interactions of carbohydrates to endogenous lectins, a large number of carbohydrate-binding proteins expressed on the surface of mammalian cells [98]. Additionally, the chemical groups bearing highly polarized hydrogens such as hydroxyl and amino groups allow the formation of hydrogen bonds with components of the biological tissues (mainly epithelia and mucous membranes). Some polysaccharides, as chitosan for example, exhibit high bioadhesive properties making them useful starting

materials for the design of oral drug delivery carriers with improved residence time and increased absorbance of loaded drugs by the intestinal epithelium [99,100].

Numerous polysaccharides have the "generally recognized as safe" status (GRAS) and are broadly used in the food industry as well as excipients for drug formulation, approved by regulatory authorities in different countries [101]. Carriers based on polysaccharides are expected to be easily eliminated from the organism, as these will be processed to result in small sugar units that integrate conventional metabolic processes, thereby permitting their elimination from the body or reabsorption [49]. Most of the naturally occurring polymers undergo enzymatic degradation [102]. Glycosidases are common enzymes present in the gastrointestinal tract that can readily catalyze the hydrolysis of many different glycosidic linkages present in the structure of complex sugars [103]. For example, lysozyme demonstrated to degrade chitosan and chitosan nanoparticles *in vitro* and *in vivo* [104–106].

In addition to the structural diversity, that allows the selection of the most suitable polysaccharide for each case, polysaccharides have a large number of reactive groups, including hydroxyl (-OH), amino (-NH_2), and carboxylic acid groups (-COOH), which can be easily derivable and contributes to their structural and functional diversity [90,100]. The use of semi-synthetic polymers benefits of tailor-able properties and predictable lot-to-lot uniformity avoiding drawbacks generally associate with the use of natural polysaccharides such as broad molecular weight distribution and batch to batch variability [107].

The simplest polysaccharide molecules consist of a monosaccharide repeating units with an abundance of reactive free hydroxyl groups as the only functional groups (cellulose, starch, pullulan, arabinogalactan) [108]. Chemical modifications of polysaccharides involve the use of chemical methods to modify some special structures or functional groups of polysaccharides on the main or side chains. Usual methods includes sulfation, phosphorylation, acetylation, carboxymethylation and so on [93,109].

Chemically modified natural polysaccharides have shown diverse potential due to their enhanced hydrophilic properties and their intrinsic polyelectrolyte character [110]. Charged polysaccharides can be obtained by derivatization of hydroxyl groups of neutral polysaccharides by using a negatively functional group, such as a sulfate, or a positively molecular entity, such as a quaternary ammonium salt [111]. Pullulan, a neutral

polysaccharide composed by α-1,6-linked maltotriose units (α-1,6-Glc-α-1,4-Glc-α-1,4-Glc-α-1,6) has been successful grafted with sulfate and ammonium groups generating anionic and cationic derivatives, respectively [112,113]. Combination of polysaccharides with opposite charges allows the formation of nanoparticles (polyelectrolyte complexes) via electrostatic interactions [111].

Chemical modifications can be performed also to modify the solubility of polysaccharides including cellulose, alginate and chitosan that typically show limited solubility in common organic solvents [114]. The water solubility of chitosan is improved for pH above 6 by adding glycidyltrimethylammonium chloride (GTMAC) on primary amino groups (in acidic condition of synthesis) or on hydroxyl groups (in alkaline condition of synthesis) widening the application of chitosan as bioactive matrix [87,115]. These derivatives are characterized by their permanent cationic charge improving their aqueous solubility over a wide range of pH as well as enhancing mucoadhesive properties which is essential for a better drug delivery through the epithelium [116].

Finally, the presence of functional groups allows for conjugation of therapeutic drugs to the main chain through functional linkers [117]. Polysaccharide conjugates have been used as attachment points for chemotherapeutics, imaging probes, and targeting agents using facile chemical modifications. The conjugation with hydrophilic polyethylene glycol (PEG), for example, is one of the most popular and most efficient structural modification strategy applied on polysaccharides to improve circulation time by avoiding the fast clearance [101,118]. Functional groups available on the drug and the polymer determine the best method of conjugation and sometimes the use of linkers is necessary to bridge together the polymer with the desired molecule (drugs or macromolecules) [119].

2.4.2 Preparation approaches of polysaccharide-based nanoparticles

Various procedures to prepare NPs that take advantage of the charge, solubility, and other intrinsic properties of polysaccharides have been used to produce polysaccharide NPs [117]. NPs synthesized from polysaccharides are mainly categorized according to the mechanism of their formation in four categories: chemically crosslinked nanoparticles, physically crosslinked nanoparticles, polyelectrolyte complex and self-assembled nanoparticles (Figure 8) [101,120]. The choice of the method is based on nanosystem

chemistry, desired particle size, polysaccharide chemistry and the intended application, although covalent protocols are generally preferred due to the considerably higher stabilities in physiological conditions [33].

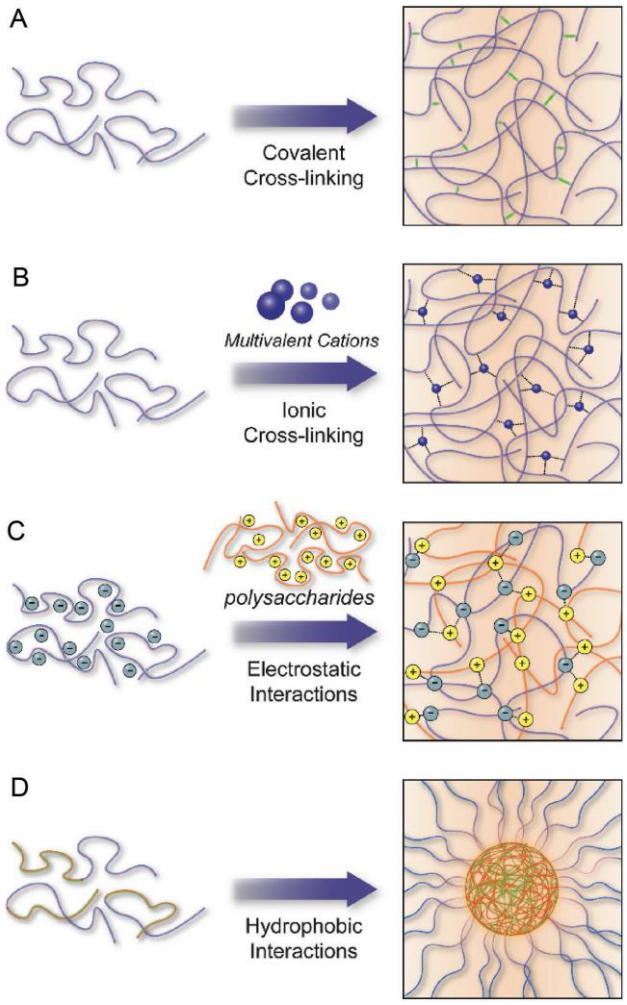

Figure 8. Schematic illustration of different intra- and intermolecular forces in polysaccharide systems. A) Covalent crosslinking. B) Ionic crosslinking. C) Electrostatic interactions. D) Hydrophobic interactions [101].

a) Polysaccharide nanoparticles by chemical crosslinking

The synthesis of polysaccharide NPs by crosslinking can be achieved by either covalent (chemical) or ionic (physical) crosslinking [120]. In chemical crosslinking, covalent bonds are established between functional groups of polymeric chains or are mediated by covalent crosslinking molecules with at least two active moieties leading to the formation of rigid networks. These networks allow the absorption of water and bioactive molecules without dissolution of the nanoparticles even with drastic changes in pH or ionic environment [101,120,121]. The most common covalent crosslinker used with

polysaccharides are dialdehydes such as glutaraldehyde, largely employed in the crosslinking of chitosan NPs [104,122].

However, due to the toxicity of glutaraldehyde, recently, biocompatible crosslinking agents have received much attention in the field of biomedical application [123]. The use of genipin, for example, is an interesting alternative to conventional toxic crosslinkers. It is a naturally occurring material isolated from the fruits of *Gardenia jasminoides* Ellis (Figure 9) and is commonly used in herbal medicine or functional food supplement in China being 5000 ~10,000 times less cytotoxic when compared to glutaraldehyde [109,121,124]. It can spontaneously react with primary amine groups to form stable networks via formation of heterocyclic amines [125,126]. Few studies used genipin to produced crosslinked chitosan micro/nanoparticles and improve their physical and chemical stability with good biocompatibility profile [127]. Genipin-crosslinked fucose conjugated chitosan/heparin NPs were also developed for controlled release of the antimicrobial agent amoxicillin [128].

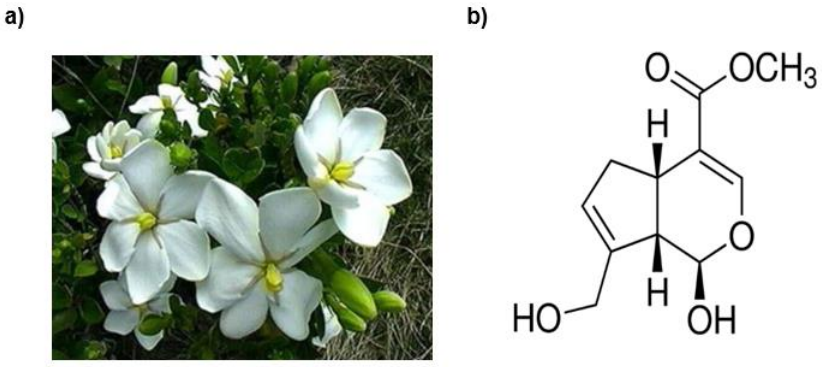

Figure 9. (a) *Gardenia jasminoides* Ellis and (b) chemical structure of genipin.

b) Polysaccharide nanoparticles by physical crosslinking

In contrast to chemical crosslinking that allows the formation of covalently crosslinked NPs, physical crosslinking yields suprarmolecular NPs formed by non-covalent interactions between polysaccharides and external ionic crosslinkers (magnesium sulfate, sodium sulfate, and sodium tripolyphosphate) [114]. The main interaction inside the network is ionic bonds that form bridges between the polysaccharide chains, although as with covalent crosslinking, additional interactions such as hydrogen bonds are also present [109]. This method produces NPs with reversibility and biocompatibility due to

the lack of harsh preparation conditions without the use of organic solvent or any toxic crosslinkers [97,120].

Because of the mild preparation conditions used to prepare NPs (no organic solvents or elevated temperatures are required), fragile biomacromolecular drugs such as peptides and proteins can be efficiently encapsulated without significant loss of activity [117]. Moreover, the use of ionic crosslinkers, such as sodium tripolyphosphate (TPP) is generally recognized as safe by the FDA for the preparation of food additives (Figure 10) [104]. TPP has also been used in the preparation of chitosan NPs with nucleic acids [129,130]. It can form a gel via reversible electrostatic interactions between positively charged protonated amino groups of chitosan and negatively charged counter ions of TPP in a pH dependent manner [104,131,132]. However, relatively weak interactions occur between chitosan and TPP at low and high pH values [131].

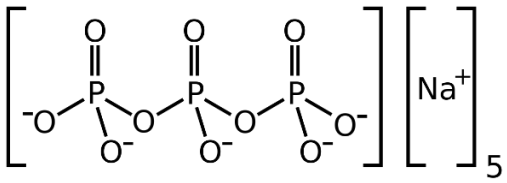

Figure 10. Structural representation of sodium tripolyphosphate (TPP).

c) Polysaccharide nanoparticles obtained by polyelectrolyte complexes

Polysaccharide-based polyelectrolyte complexes (PECs) are spontaneously formed in solution by the direct mixing of at least two oppositely charged polyelectrolytes due to an increase in the entropy of the system with the release of low-molecular weight counter ions which is able to produce nanosized structures [86,133]. Despite strong electrostatic interactions, inter-macromolecular forces are also involved in complex formation including hydrogen bonding, hydrophobic interactions and dipole interactions between polymeric chains leading to the formation of non permanent networks without the need to use chemical crosslinkers [134,135].

The formation and the thermodynamical stability of PECs is governed by many factors including the concentration of polyelectrolytes solutions, charge ratio, molecular weights of the components, presence of low molecular-weight ions, mismatch of charge densities,

pH (for weak polyelectrolytes), temperature, polymer chain rigidity and other controllable factors [136,137]. The most predominant method for complex formation is the polyelectrolyte or colloid titration (polyelectrolyte complexation), where a solution of one of the polyelectrolyte is gradually added drop by drop to a stirred solution of the oppositely charged polyelectrolyte [138].

The design of biocompatible PECs is a promising strategy for *in vivo* delivery of biological macromolecules such as proteins [139,140] and nucleic acids [141,142] since they are easily prepared and exhibit a wide range of colloidal properties with responsiveness to various stimuli [40,110,124,137,143]. Particularly, the condensation of nucleic acids, highly charged molecules (strong polyanions) due to the phosphate esters along their backbone, by polycations forming structures named "polyplexes" received considerable attention for potential use in gene delivery applications, where the development of safe and effective non-viral vectors remains a central challenge [143,144].

d) Polysaccharide nanoparticles by self-assembly

Hydrophobized polysaccharides can self-associate to form colloidal nanoparticles in aqueous environments with an inner hydrophobic core allowing the encapsulation of hydrophobic molecules such as insoluble drugs and proteins whereas the hydrophilic shell would adsorb hydrophilic molecules through non-covalent interactions [95,145]. The structure of such polymers greatly varies from block amphiphilic copolymers to grafted amphiphilic polymers [146].

The introduction of hydrophobic segments into polysaccharides is achieved by grafting hydrophobic groups (deoxycholic acid, cholesterol, carboxylic acids and hydrophobic polymers) onto hydroxyl, amino or carboxyl groups of the polysaccharide [120]. The spontaneous self-assembly of these macromolecules into polymeric nanostructures generally relies on different driving forces including hydrophobic-hydrophobic interactions, hydrogen bonding, electrostatic interactions, stereo complexation, π–π stacking, and host-guest interactions [69]. By modulating one or many types of these interactions, self-assemblies can be produced with a wide range of structures and different functions [147].

Pullulan may lead a self-associating drug carrier after hydrophobic modifications [145]. Alhaique *et al.* have reviewed pullulan-based nanostructures obtained by self-assembly

using various hydrophobization strategies [148]. A self-assembled polymeric system based on amphiphilic carboxymethyl-pullulans, varying in the substitution rate on grafted alkyl chains, have been proposed for the efficient dissolution of poorly water-soluble drugs [146]. Cholesterol-bearing pullulan (CHB) self-aggregates revealed very high colloidal stability and have since been investigated as a way of protecting proteins from the physiological environment [149]. Finally, a unique advantage of amphiphilic cationic copolymers is the possibility to co-deliver drug and gene: biodegradable cationic micelles were prepared from PDMAEMA–PCL–PDMAEMA triblock copolymers containing cationic poly (2-dimethylaminoethyl methacrylate) (PDMAEMA) blocks and applied for the combined delivery of siRNA and lipophilic paclitaxel into cancer cells [150].

2.5 The emergence of miRNA-based therapeutics

The idea behind gene therapy is that human disease can be treated by the transfer of genetic material into specific targeted cells rather than by conventional drugs [151]. Nowadays, there is a strong tendency in modern therapies in which several biological molecules including nucleic acids (plasmid DNA, antisense oligonucleotides, therapeutic RNAs, siRNAs, miRNAs, etc) and proteins (monoclonal antibodies, growth factors, hormones, therapeutic enzymes, synthetic oligopeptides, etc) are being used as highly specific pharmaceutical agents [87,152]. Gene therapy uses nucleic acids for the treatment, cure or prevention of human disorders and has gained considerable attention over the past three decades as it holds great promise for the treatment of many diseases such as cancers, genetic diseases, viral infections and cardiovascular disorders [151,153].

Specially, in the past few years, noncoding small interfering RNAs (siRNAs) and microRNAs (miRNAs) have emerged as key regulators of gene expression and are some of the most important biopharmaceuticals that are in commercial space as future medicines, due to their multiple unique features and advantages when compared to DNA-based therapy [154,155]. RNA therapeutics do not have the risk of genomic integration, do not need to cross the nucleus membrane to their function, and are expressed instantaneously [156,157]. Much evidence has suggested that small RNA molecules can fulfill relatively generic functions in cells being implicated in the control of many fundamental cellular and physiological processes such as cellular differentiation, metabolism, proliferation, cell cycle control, migration and apoptosis [158]. The first

therapeutic small interfering RNA was approved by the FDA in 2018, Onpattro® (patisiran), a lipid complex injection to treat hereditary polyneuropathy of hereditary transthyretin- mediated amyloidosis (hATTR) in adult patients [32].

Compared with siRNAs, miRNAs have a broader therapeutic application once they are able to affect multiple pathways/cellular processes rather than specific targets because miRNA recognition requires the binding to a much shorter seed sequence (2-8 nucleotides) instead the entire nucleotide sequence of a siRNA [19,22,89]. miRNAs modulate gene expression by imperfectly binding to targeted messenger RNAs (mRNA), which results in mRNA degradation or translational repression [159]. At the target, miRNAs can generate strong, sustained and comprehensive biological effects, through endogenous gene silencing with very low concentrations (at least 0.5 nM) [160,161].

Two different therapeutic approaches are generally used for miRNA-based therapeutics: miRNA inhibition and miRNA replacement. miRNA inhibition is used in situations when the target miRNA is overexpressed. It involves the use of synthetic single-stranded RNAs that are partially or completely complementary to the target miRNA and acts as miRNA antagonists (anti-miRNA) to inhibit the action of the target miRNA. On the other hand, miRNA mimics (replacement therapy) is employed when the target miRNA is down-regulated. In order to restore miRNA levels, synthetic double-stranded miRNAs are used to mimic the function of the target miRNAs and bind specifically to its target mRNA to produce post-transcriptional repression of the gene [73,162,163]. Despite the emergence of miRNA therapeutics, they have not been yet translated into FDA-approved drugs, but some candidates are in clinical development or in phase 1 and phase 2 clinical trials [164].

Currently, the main barrier to implementing miRNA-based therapies in clinical practice is the lack of an effective delivery system. Nucleic acids are far larger than conventional drugs since they cannot diffuse across lipid membranes into target cells and display very limited biological stability [133]. Hence, a major challenge of gene therapy is developing a delivery system that can efficiently deliver nucleic acids to the target cells, with minimal toxicity and high bioavailability during the delivery process [165]. Vectors employed for gene delivery purposes can be divided into two main groups: (a) viral carriers, where the DNA/RNA to be delivered is inserted into a virus, and (b) non-viral carries, including cationic molecular carriers such as lipids and polymers, which can form electrostatic interactions with DNA/RNA for delivering gene to cells [151].

The majority of approved vectors for gene therapy currently applied in clinical protocols are viral vectors due to their high transfection efficiency. Viruses such as retrovirus, lentivirus (for example, HIV), adenovirus and adeno-associated virus can be transformed in gene delivery systems by the replacement of part of viral genome for a therapeutic gene [166]. Viral vectors have the natural ability to enter the cells and express their own proteins which allows high transfection rate and a rapid transcription of the foreign material inserted in the viral genome [167]. However, limitations of virally mediated gene delivery such as immunogenic properties, toxicity, potential replication, cancer formation and high cost could limit their doses and frequency of treatment limiting their clinical application [96,151,168].

These limitations have prompted the development of non-viral gene carriers, in particular polymer-based carriers [89]. The first class of polymeric carries used for nucleic acid delivery was mainly represented by synthetic cationic polymers, including poly(ethylene)imine (PEI), poly(L-lysine) (PLL), and poly(-amino) esters. They can efficiently condense DNA/RNA into nanometer range complexes (~50-300 nm), formed by entropy-driven self-assembly between protonated amine groups present in polymers backbone and negatively-charged phosphate groups of nucleic acids (referred as the N/P ratio) (Figure 11) [169,170]. Different parameters control complexation and polyplexes formation influencing the particles size and stability and are dependent on several polymer characteristics, such as molecular weight, structure (e.g., linear vs branched), the number and the density of charges, in addition to the composition of the complexes, e.g. the ratio of polymer to DNA/RNA [86,171].

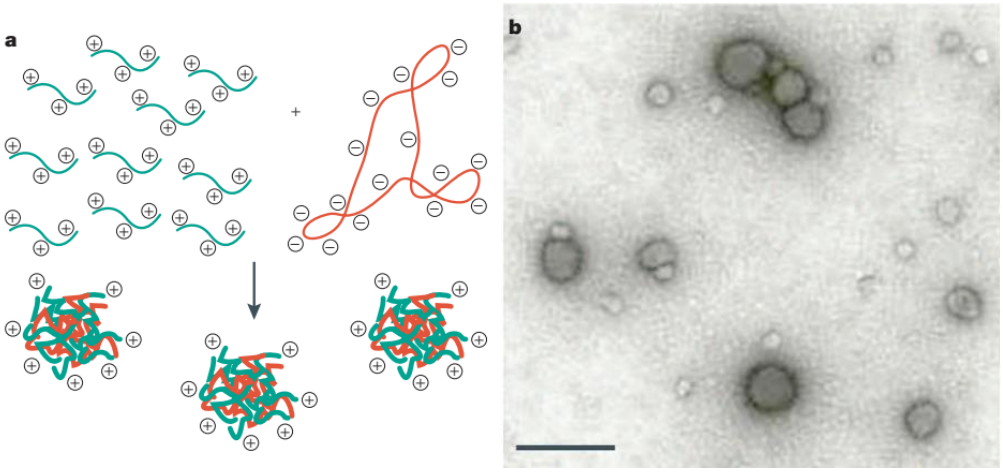

Figure 11. (a) Schematic representation of polyplexes formation between polycations and DNA; and (b) Transmission electron micrograph of polyplexes (scale bar 200 nm) [166].

The design of NPs with genetic cargo has primarily focused on DNA and siRNA, and only few have detailed work with miRNA. Despite the similar chemical structures of all nucleic acids differences arises in terms of size, structure and stability and must be considered during nanoparticles formulation [172]. Compared to DNA-based gene therapy, the delivery of small RNAs is more challenging and cationic carriers typically used may not form sufficiently strong interactions with small RNAs simply through electrostatic interactions because of their relatively small size (usually 21-23 base pairs) compared to pDNA (several kilo base pairs) [173,174]. Hence, most of the polymeric delivery strategies originally developed for plasmid DNA (pDNA), cannot be used for siRNA or miRNA delivery without formulation optimization [175].

In addition, the extra vulnerability of RNA to enzymatic degradation (hydrolyses) by serum nucleases due to an extra hydroxyl group in the 2′ position of pentose ring in ribose structure, instead of a hydrogen atom present in DNA structure, induces additional challenges to RNA delivery [176,177]. Common linker modifications can be performed to replace endogenous phosphodiester bonds with phosphorothioate or amide-based linkages improving the stability of nucleotides [54]. However, the use of nanosystems generally provides much better protection of small RNAs against serum degradation and is essential for systemic administration in order to allow them to cross cellular membranes [178].

2.5.1 miRNA delivery vehicles

2.5.1.1 Inorganic nanoparticles

Inorganic materials that have been studied for the intracellular delivery of miRNAs includes examples such as gold, silica and iron oxide [179,180]. Synthetic materials present important advantages as vehicles for miRNA delivery due to their simplified manufacturing procedures, and the possibility to produce structures with adjustable size and morphology and controlled composition [18,181]. Depending on the nature of the material core, different strategies can be used for nucleic acid incorporation: the absorption method is generally employed for mesoporous silica NPs and nanostructures bearing positively charged groups, while the covalent binding is preferred when the NP surface can be modulated by reactive groups [181].

In special, gold nanoparticles (AuNPs) have received great attention as non-viral gene delivery system [162]. AuNPs present mechanical and chemical stability and can easily be modified making them amenable for a large variety of binding reactions. They can be functionalized with thiol or amino groups to allow surface loading of negatively charged miRNAs through electrostatic interaction [182,183]. Sukumar *et al.* developed polyfunctional gold-iron oxide nanoparticle (polyGION) for intranasal delivery of antimiR-21 and miR-100. They functionalized the surface of polyGION NPs with chitosan cyclodextrin (CD-CS) hybrid polymers. Upon the inclusion of CD-CS coating, the surface potential of these NPs shifted from −15 mV to 39 mV owing to excess of positively charged free amine groups of chitosan. A loading efficiency of almost 80% of added miRNA was achieved [179]. Potential cytotoxicity of the NPs could limit their application in the clinics. For example, AuNPs measuring 5 nm were associated with cytotoxic effects disrupting the cytoskeletal organization of fibroblasts after 72h of exposition [184].

Silica has also been used for miRNA delivery because of its biodegradability and easily functionalization [162,185]. For example, Tivnan *et al.* developed a functionalized disialoganglioside GD2-antibody conjugated porous silica nanoparticles for the targeted delivery of miR-34a to neuroblastoma tumours. GD2 is a glycolipid overexpressed on the surfaces of neuroblastoma tumor cells. Nanoparticles encapsulating miR-34a resulted in significantly decreased tumor growth and increased apoptosis thanks to the antibody-mediated cell cytotoxicity [186]. Silica dioxide nanoparticles (SiO_2-NPs) were also effectively used for the delivery of miR-34a into normal and cancer epithelial cells grown in culture. miR-34a is part of a tumor-supressor miRNA family often down- regulated in cancers. The miRNA delivery using SiO_2-NPs leads to a reduction of mammary tumor growth. The delivery of miR34a by SiO_2-NPs was equally effective as by lipofection, with the additional advantage of being more applicable to clinical settings [187].

Inorganic nanoparticles with applications in MRI have also been studied and demonstrated extremely useful for both nucleic acid delivery and imaging of NPs. Leder *et al.* developed silica-based micron-sized iron oxide-containing particles (sMPIO) for the delivery of miRNA and MRI-based tracking of transplanted cells thanks to magnetic properties of the iron oxide core. The oligonucleotide was covalently immobilized on the NPs surface, assuring higher stability and efficient deliver [180]. Similarly, Yang *et al.* developed a poly(amidoamine) dendrimer-grafted gadolinium-functionalized

nanographene oxide (Gd-NGO) nanoparticles for combined miRNA delivery and MRI [188].

2.5.1.2 Lipid-based nanoparticles

Lipid-based nanoparticles (LNPs) represent one of the most widely used strategies for *in vivo* delivery of small interfering RNAs [189,190]. They are composed of a lipid bilayer that contains the miRNA encapsulated in the hydrophilic aqueous core or, complexed with the lipids on the surface [182,191]. In order to achieve high nucleic acid loading, cationic lipids are generally preferable because they can easily associate with negatively charged nucleic acids, with consequent formation of complexes, named lipoplexes [192]. Among such cationic lipids, quaternary amine based cationic lipids, such as N-[1-(2,3-dioleyloxy) propyl-N,N,N-trimethylammonium chloride (DOTMA) and 1,2-dioleoyl-3-trimethylammonium-propane (DOTAP), are currently used due to their permanent positive charge [193]. Lipoplexes prepared with cationic lipids containing LNPs, such as the lipofectamine reagent, have found considerable utility for *in vitro* transfection [194]. However, because most of permanently charged cationic lipids are highly toxic, their *in vivo* application can be limited.

In order to avoid the toxicity issues, LNPs have been developed from ionizable cationic lipids with primary, secondary, or tertiary amines in the headgroup and apparent pKa values below 7. These LNPs could be loaded with nucleic acid at pH values below the pKa of the ionizable lipid where it is positively charged while providing a LNP with relatively neutral exterior under physiological conditions [189,195–197]. Yung *et al.* prepared LNPs based on cationic lipids bearing tertiary and quaternary amine groups for therapeutic delivery of antimiR-21. The design combined the advantage of the high charge density provided by the permanent positive charge of ammonium groups and the pH responsiveness behavior of tertiary amines in order to achieve a balanced charge-vs-pH profile for optimal miRNA delivery [198].

Lipid nanoparticles may also have additional components in their formulation such as cholesterol (Chol) and dioleoylphosphatidyl ethanolamine (DOPE), known as “helper lipids” which contributes to increase nanoparticle stability and reduce their toxicity. Also the incorporation of PEG is frequently employed to reduce NPs aggregation in the presence of serum proteins and enhance circulation time [182,191]. In the study of

Campani *et al*. they investigated the use of different cationic lipids, neutral lipids, and PEGylated lipids in order to achieve the highest delivery of miRNA. By combining different lipids, they developed formulations with good technological characteristics and stable in serum with a low hemolytic activity. Moreover, the intracellular uptake studies on gliobastoma cell lines showed that the developed nanosystems allowed higher miRNA delivery when compared to comercial lipofectamine reagent [190].

Trang *et al.* explored the potential of a neutral lipid emulsion (NLE) for *in vivo* delivery of miR-34a mimics. They demonstrated efficient therapeutic delivery of miRNA formulations with reduction in tumor size. Particles formulated with neutral lipids are less prone to aggregation in biological fluids, to be filtered by the liver, or be taken up by scavenging macrophages [199]. In the work of Nogueira *et al.* they encapsulated siRNA in the aqueous core of DOPE-derived neutral PEGylated liposomes by the hydradation of the lipid film with a concentrated solution containing the payload prior to liposome formation. A loading efficiency around 100% was achieved using this strategy. The encapsulation of small RNAs inside the hydrophilic core of liposomes can avoid premature payload release in the presence of biological fluids [200].

2.5.1.3 Polymeric nanoparticles

Three main types of polymeric nanocarriers have been studied for miRNA delivery and are represented by polyplexes, PLGA NPs and dendrimers (Figure 12). The miRNA can be incorporated to the delivery systems by complexation (electrostatic interactions), conjugation (covalent linkers), or encapsulation [21,89].

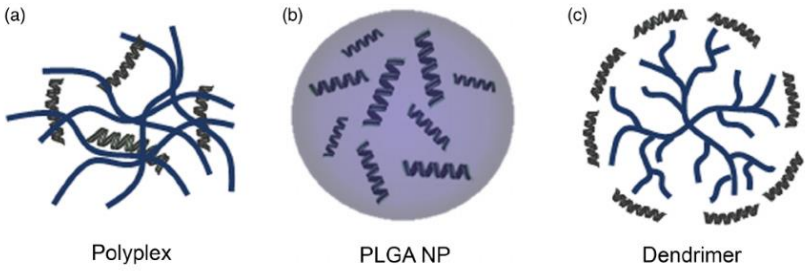

Figure 12. Main types of polymeric delivery vehicles employed for miRNA delivery: (a) polyplexes, (b) PLGA NPs and (c) dendrimers. Therapeutic miRNA is depicted in black [21].

Traditionally, PEI, a positively charged linear (lPEI) or branched polymer (bPEI) (Figure 13), is the most studied polymer being considered the "gold standard" for gene transfection protocols [155]. PEI consists of multiple positively charged amines (primary, secondary and tertiary amino groups) depending on the linear or branched structure of the polymer. Its advantages are its high cationic charge density and buffering capacity due to the protonation of primary amines that enables endosomal escape through the "proton sponge effect" in which a change in the osmolarity of the acidic vesicles results in endosomal swelling and rupture allowing nucleic acid release [89]. Radmanesh *et al.* used deoxycholic acid (DA) modified PEI for miR-210 delivery. They demonstrated an efficient balance between polyplexes stabilization and cargo release into the cytosol [201]. In the work of Gao *et al.*, a PEI-PLL derivative was successfully synthesized and confirmed to transfect plasmid and miRNA more effectively than PEI in MCF-7 cells (human breast cancer cells) [202]. Nevertheless, the lack of degradability of PEI with a risk to accumulate in the body, in particular after repeated administration, largely limited their use [203]. *In vivo* application of PEI was shown to be limited by a molecular weight-dependent cytotoxicity related with an excess of positive charges which leads to non-specific interactions and aggregation in the blood, while polymers based on amino acids such as poly(lysine) are immunogenic [151,204,205].

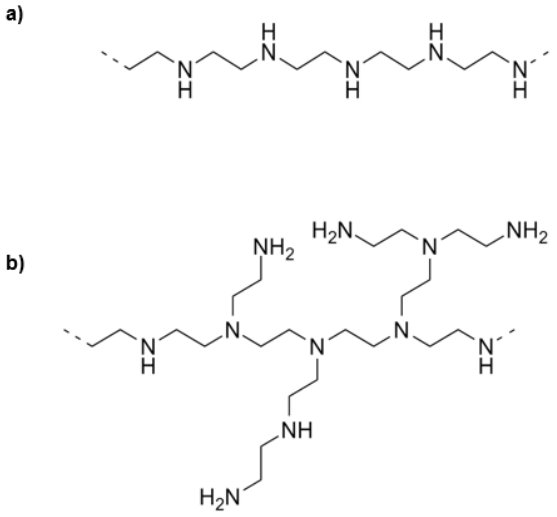

Figure 13. Chemical structure of (a) linear (lPEI) and (b) branched PEI (bPEI).

Alternatively, PLGA has been frequently investigated to formulate NPs for the delivery of miRNA [21,206,207]. The slow degradation profile of PLGA is ideal for the controlled

release of genes [208]. Although the biocompatibility of PLGA, its hydrophobicity and rapid opsonization in circulation are the main limitations for their use in miRNA delivery. To facilitate miRNA loading, many PLGA NPs are typically prepared with the incorporation of additional positively charged polymers. In the work of Kapadia *et al.*, they synthetized layer-by-layer assembled nanoparticles (LbL NPs) comprised of spherical biodegradable PLGA core surrounded by alternating layers of poly-L-lysine (PLL) and miR-34a. By combining both polymers, they reduced the risk of systemic toxicity. Moreover, LbL NPs prepared from PLGA cores offer the possibility for co-drug delivery by loading other therapeutic agents into the PLGA core [21]. For efficient encapsulation (~ 78%) of miR-150 mimics in PLGA nanoparticles, Singh *et al.*, incorporated PEI to the formulation of PLGA nanoparticles using double emulsion solvent evaporation method [207]. Devulapally *et al.* developed PLGA-b-PEG-NPs loaded with antisense-miRNAs using water-in-oil-in-water (w/o/w) double emulsion method for breast cancer therapy. The PEGylation of PLGA would increase the circulation time of NPs [206].

Another class that has been investigated for miRNA delivery are dendrimers. They are a class of synthetic macromolecules characterized by tree-like structures with a high density of cationic charges. The high structural flexibility of dendrimers allows a more efficient interaction with nucleic acids [209,210]. There are different types of dendrimers such as poly(propylene imine) (PPI) dendrimers, poly(l-lysine)dendrimers, polyamidoamine (PAMAM) dendrimers, etc. PAMAM, a highly branched spherical polymer, is the most widely studied. It is characterized by the presence of primary amine groups at the surface and tertiary amine groups in the interior and can thus promote miRNA intracellular release via the proton sponge effect [210,211]. Few works have used PAMAM for miRNA delivery. Sayed *et al.*, designed poly (amidoamine)-histidine (PAMAM-His) nanocarriers for the delivery of miRNA in injured cardiomyocytes. The conjugation of PAMAM with histidine resulted in the reduction of polymer cytotoxicity and increased buffering capacity. At the highest tested concentration (150 μg/mL), PAMAM-His showed approximately 80% cell viability while commercial lipofectamine treatment resulted in approximately 61% of cell viability. PAMAM-His NPs effectively delivered miRNAs to the cardiomyocytes and prevented the hypoxia/reperfusion-induced apoptosis after MIs [212]. In another study, PAMAM dendrimer was employed as a carrier to co-deliver anti-miR-21 and 5-fluorouracil (5-FU) to glioblastoma cells. PAMAM was simultaneously loaded with 5-FU and anti-miR-21, forming a complex

smaller than 100 nm in diameter. The unique structure of PAMAM allowed them to interact with miRNA through charge-based interactions and facilitated the entrapment of chemotherapeutics in the interior of PAMAM through hydrophobic interactions [213].

Besides the use of synthetic polymers, several natural carbohydrate polymers have been proposed due to their low toxicity, low immunogenicity and generally good hemocompatibility properties [107,168]. Chitosan is the only naturally existing cationic polysaccharide and has received the most attention as a nanoparticulate gene delivery vehicle due to its high positive charge density [96,129]. The glucosamine unit in chitosan backbone provides primary amine groups which is positive charged at acidic pH confering the ability to form complexes with polyanions [214]. Chitosan-based carriers have been largely used for the delivery of plasmid DNA (pDNA)[143,167], siRNA [81,215] and miRNA [216].

Santos-Carballal *et al.* studied the physicochemical and biological properties of chitosan polyplexes with miR-145. They found that ideal complexes were formed using chitosans with a molecular weight of ~40 kDa, and a N/P ratio of 1.5, resulting in transfection efficiencies similar to the commercial reagent used as positive control [217]. Kaban *et al.* used chitosan as carrier for the delivery of miRNA to breast cancer cell lines. Full complexation between chitosan and miRNA was obtained at a N/P ratio of 4 [218]. Cosco *et al.* developed nanocomplexes with a combination of chitosan and PLGA for miR-34a delivery. Chitosan was added in order to provide a positive surface charge onto PLGA nanoparticles allowing miRNA complexation. Polyplexes using chitosan allowed a high level of entrapment efficiency of the miR-34a along with a high degree of transfection and a significant *in vitro* antitumor effect against multiple myeloma cells [40]. However, in spite of its interesting profile, chitosan has its own drawbacks such as low water solubility at physiological pH because of partial protonation of primary amino groups, which can affects nucleic acid interactions, and stability of complexes in bloodstream [177,219].

Hyaluronic acid (HA) has been also used to prepare miRNA polyplexes. It is a natural anionic polysaccharide that can be used due to their targeting properties. For example, Deng *et al.* co-encapsulated miR-34a and doxorubicin into nanocomplexes composed of chitosan and hyaluronic acid prepared through a facile ionotropic gelation method in water. HA endowed tumor-targeting properties through specifically binding to CD44 molecule, an integral membrane glycoprotein over-expressed on the surface of various tumor cells. Complexes exhibit a good serum stability protecting miRNA from

degradation, characteristic suitable for *in vivo* application [124]. In another study, HA was used to construct innovative nanocapsules based on PECs between HA and protamine sulfate (PS). *In vitro* and *in vivo* experiments illustrated high miR-34a encapsulation efficiency (more than 90%) into HA-PS complexes and deliver into breast cancer cells or breast cancer tissues [130].

Table 3. Representative research on miRNA therapeutics based on polymeric delivery systems.

Delivery system	**miRNA**	**Therapeutic application**	**Polymers**	**Particle size**	**Refs.**
Polyplexes	miR-210	Ischemic heart disease	PEI-Deoxycholic acid (DA)	100-180 nm	[201]
	anti-miR 21	Breast cancer	PEI-PLL	300 nm	[202]
	miR-34a	Prostate tumor	Chitosan	-	[216]
	miR-34a	Breast cancer	Chitosan/ Hyaluronic acid	185-214 nm	[124]
	miR-34a	Breast cancer	Hyaluronic acid/Protamine sulfate	201 nm	[130]
	miR-124	Neurodegenerative disorders	Chitosan	222 nm	[220]
	miR-145	Breast cancer	Chitosan	190 nm	[217]
	miR-145	Breast cancer	Chitosan/ Carboxymethyl dextran (CMD)	30-695 nm	[221]
	miR-181a	Chronic myeloid leukemia	Pullulan spermine (PS)	200-250 nm	[222]
	miR-200 miR 141	Breast cancer	Chitosan	296-380 nm	[218]
	miR-126	Angiogenesis	Trimethyl (TMC) chitosan	98-342 nm	[223]
PLGA NPs	anti-miR10b anti-miR 21	Breast cancer	PLGA-b-PEG	100-200 nm	[206]
	miR-34a	Breast cancer	PLGA-PLL	122 nm	[21]
	miR-34a	Multiple myeloma	PLGA-Chitosan	160 nm	[40]
	miR-150	Pancreatic cancer	PLGA	183 nm	[207]
Dendrimers	miR-194-5p miR-214-3p anti-miR-122-5p	Myocardial infarction	PAMAM-His	60 nm	[212]
	anti-miR-21	Glioblastoma	PAMAM	100 nm	[213]

2.5.2 Challenges in the delivery of small RNAs

The transition from bench to bedside of small RNA-based therapies depends on the design of a safe, clinically relevant delivery system that can protect the RNA molecules from nuclease degradation and facilitate their cellular uptake into target tissues/cells, all without inducing any adverse effect [22]. The size, charge and surface properties of nanocarriers have to be tuned to ensure effective and safe delivery of the miRNA in clinical practice. Insufficient *in vivo* stability of polyplexes, in the presence of polyanions such as serum albumin and heparin, is one of the major obstacle faced by non-viral gene delivery systems [100]. Cationic polyplexes tend to aggregate and dissociate in the presence of proteins and other polyanions present in the blood and other biological fluids leading to premature nucleic acid release, in particular for small RNAs, if the formulation is not fully optimized [224–226].

The use of crosslinkers within the particle core can contribute to obtain a more stable packaging of polyplexes against undesired specific interactions with the bioenvironment [227]. TPP has been reported to enhance the siRNA-condensing capacity of polycations under both neutral and physiological conditions [124]. Xiao and colleagues found that chitosan/siRNA NPs formed via TPP-assisted ionotropic gelation technique exhibited a much higher biological activity compared to polyplexes formulate without crosslinking agent [115]. Apart of this, alternative approaches includes co-formulation with other polyanions [124,228], nucleic acid conjugation [173], hydrophilic modification with poly (ethylene glycol) (PEG) [219,223] and hydrophobic stabilization of polycations [229]. PEGylated polyplexes exhibit improved stability in serum containing media and reduced toxicity of the polycations compared with polyplexes formed from non-PEGylated polycations [230].

Delivery strategies also have to deal with the need for internalization, release, and distribution in the proper subcellular compartment [79]. Successful use of any polyplex stabilization strategy requires that the stabilization is reversible, and that nucleic acid is released in the cytoplasm [173]. The site of action differs according to the type of therapeutic nucleic acid: plasmid DNAs (pDNA) have their destination in the nucleus, whereas the targets of mRNA, siRNA or miRNA therapeutics are located in the cytosol [133].

Carriers normally are internalized by cells via endocytic pathways, and the genetic material (DNA/RNA) is then translocated from endocytic vesicles towards cytosol [231]. To avoid nucleic acid degradation, the nanocarrier should preferably escape from the endosomes into the cell cytoplasm and promptly release the payload in order to carry out its therapeutic action [94]. "Smart" biomaterials can be designed in order to release their payload upon a trigger able to respond to a range of environmental stimuli (e.g., temperature, pressure, pH, enzymes, glucose), biological signals, or pathological abnormalities [54,61,152]. A judiciously rational designed gene delivery system must be elaborated to have sufficient *in vivo* stability during circulation time of nucleic acid until it reaches targeted cells while being capable of rapid release after being taken up in order to maximize their therapeutic effect (Figure 14) [171].

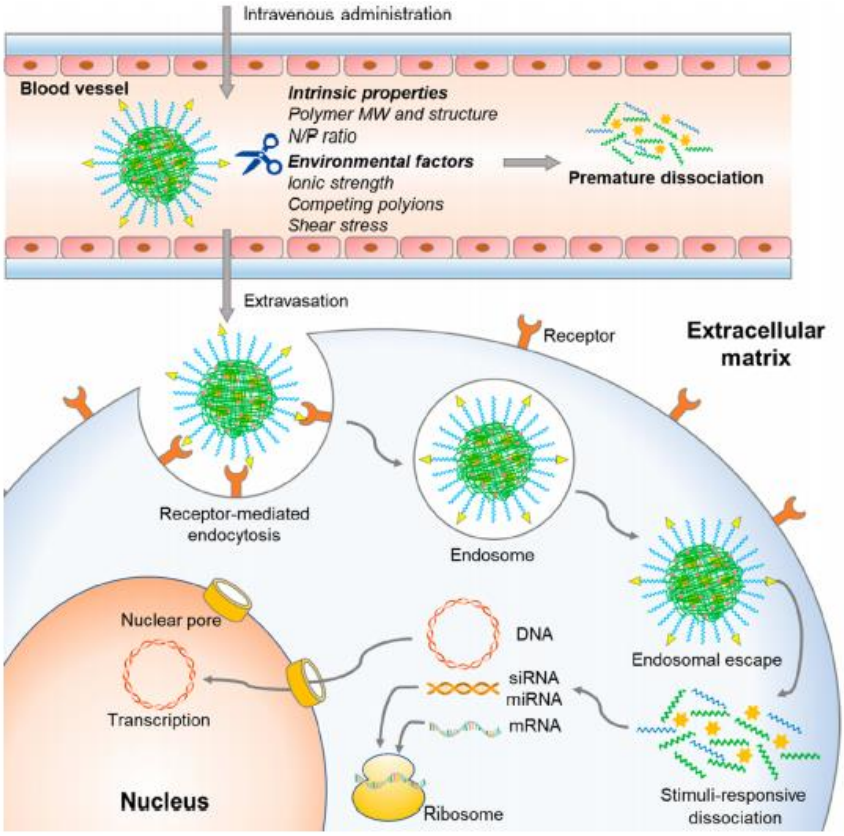

Figure 14. Schematic illustration of the barriers for a successful gene delivery to target cells [171].

3. EXPERIMENTAL WORK

3.1 CHAPTER I

Synthesis of cationic pullulan derivatives for miRNA delivery

Introduction

This work is a continuation of the work of Antunes *et al.* initiated in the laboratory to develop drug delivery systems for miRNA therapy of cardiovascular diseases [232]. Core-shell polymer-based nanoparticles loaded with miRNA were prepared by redox radical emulsion polymerization to obtain core-shell NPs, with the core composed by the synthetic and hydrophobic poly(isobutylcyanoacrylate), and the shell constituted by natural and hydrophilic polysaccharides (10% fucoidan, 20% DEAE-dextran and 70% dextran). miR-155-5p was loaded into NPs via electrostatic interactions thanks to the presence of cationic DEAE-dextran on nanoparticles surface. Fucoidan would confer NPs the ability to target P-selectin, over-expressed in activated endothelial cells. These biospecific nanosystems showed to be able to be internalized by activated endothelial cells and decreased the levels of target gene BACH 1, providing a proof of concept of *in vitro* functional validation of miR-155-5p delivery. However, the cytotoxicity associated with cyanoacrylate NPs was the main obstacle to the development of these nanosystems.

In this context, this project aims at developing miRNA polymeric NPs using positively charged pullulan derivatives. Pullulan is a natural polysaccharide of potential interest for biomedical applications due to its non-toxic, non-immunogenic and biodegradable properties. Cationic pullulan derivatives were obtained by grafting tertiary amines (DEAE-pullulan) and quaternary ammonium groups (QA-pullulan). The ability of different cationic derivatives to form complexes with miRNAs driven by electrostatic interaction (polyplexes) was evaluated. As for the previous study, fucoidan was introduced to confer biospecificity to the NPs toward activated endothelial cells.

This chapter is divided in two parts: the first part has been published in International Journal of Pharmaceutics and a second part presents complementary results (complementary work).

The first study investigated the use of cationic quaternized pullulan as an alternative to classical polycations to form complexes with miRNA and their transfection into vascular cells.

Briefly, cationic pullulan derivatives grafted with quaternary ammonium groups (QA-pullulan) were synthetized and characterized. The product showed to be cytocompatible towards human endothelial cells whithin a wide dose range. QA-pullulan is a promising polycation due to its capacity to form complexes with miRNA via electrostatic

interactions in a wide range of pH owing to permanent positive charges, an advantage when compared to chitosan, a classical natural cationic polymer used in gene therapy. Polyplexes formed between QA-pullulan and miRNA exhibited nanometric size (133 ± 30 nm) and spherical shape. The negative surface charge (-12 ± 5 mV) of polyplexes suggested the presence of anionic miRNA, which was confirmed by agarose gel electrophoresis. QA-pullulan was able to promote miRNA delivery into cells when compared to miRNA alone.

Unpublished complementary works constitutes the second part of the chapter. DEAE-pullulan derivatives were prepared and their capacity to form polyplexes with miRNA was evaluated and compared to that of QA-pullulans. The feasibility to incorporate fucoidan into polyplexes formulation was also evaluated.

In order to facilitate the reading of the manuscript and to allow a better understanding of the strategies chosen and their evolution, the published part of this chapter has been integrated into the continuity of the text, the printed proof beeing presented in the appendix.

Chapter I- Part I

Publication in International Journal of Pharmaceutics, 2020,

doi: 10.1016/j.ijpharm.2020.119041 (the PDF proof is provided in annex 6):

Synthesis of cationic quaternized pullulan derivatives for miRNA delivery

Fernanda C. Moraes, Joana C. Antunes, Laura Marcela Forero Ramirez, Paola Aprile, Gregory Franck, Cédric Chauvierre, Frédéric Chaubet, Didier Letourneur

Keywords: Pullulan, Cationic derivatives, Polyplexes, microRNA, Gene therapy

Graphical abstract

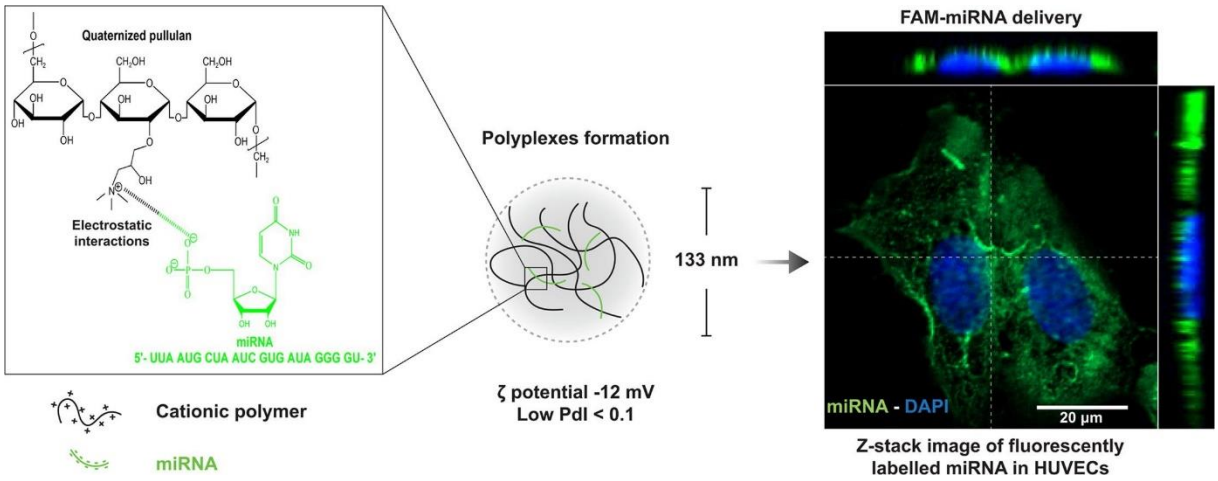

Abstract: Pullulan is a natural polysaccharide of potential interest for biomedical applications due to its non-toxic, non-immunogenic and biodegradable properties. The aim of this work was to synthesize cationic pullulan derivatives to be able to form complexes with microRNAs (miRNAs) driven by electrostatic interaction (polyplexes). Quaternized ammonium groups were linked to pullulan backbone by adding the reactive glycidyltrimethylammonium chloride (GTMAC). The presence of these cationic groups within the pullulan was confirmed by elemental analysis, Fourier-transform infrared spectroscopy (FTIR) and proton nuclear magnetic resonance (1H-NMR). The alkylated pullulan was able to interact with miRNA and form stable polyplexes that were characterized regarding size, zeta potential and morphology. The presence of miRNA was confirmed by agarose gel electrophoresis and UV spectrophotometry. *In vitro* tests on human umbilical vein endothelial cells did not show any cytotoxicity after 1 day of incubation with nanosized polyplexes up to 200 µg/mL. QA-pullulan was able to promote miRNA delivery inside cells as demonstrated by fluorescence microscopy images of labelled miRNA. In conclusion, the formation of polyplexes using cationic derivatives of pullulan with miRNA provided an easy and versatile method for polysaccharide nanoparticle production in aqueous media and could be a new promising platform for gene delivery.

1. Introduction

Gene therapy uses nucleic acids (DNA or RNA) for the treatment, cure or prevention of human disorders by the insertion of new genes into target cells [153]. The use of nucleic acids as drugs has been described for two decades [233], being mainly based on viral vectors and plasmid DNA technology [155,234]. More recently, small non coding RNAs (ncRNAs), namely microRNAs (miRNAs), have emerged as key regulators of gene expression as a promising alternative to conventional plasmid DNA (pDNA) due to its multiple unique features and advantages when compared to DNA-based therapy [155,235].

miRNAs are small endogenous single stranded non-coding RNA molecules that play important roles in many cellular processes such as cell differentiation, proliferation and survival acting on post-transcriptional level by binding to complementary target mRNAs, resulting in mRNA translational inhibition or degradation [236]. miRNAs have been proposed and investigated as therapeutics and biomarkers for various diseases such as cancer, diabetes, cardiovascular diseases and other pathologies whose etiology is related to aberrant gene expression [159,216,237–240]. At the target, miRNAs can generate strong, sustained and comprehensive biological effects, through endogenous gene silencing with very low concentrations (at least 0.5 nM) [160,161]. Additionally, miRNAs are able to affect multiple pathways/cellular processes rather than specific targets [19]. The success of miRNA-based therapies depends on the development of suitable vehicles able to specifically target cells for the efficient delivery of the nucleic acids, with minimum toxicity [154].

Compared to DNA-based gene therapy, the delivery of miRNA is more challenging due to important differences in terms of size and structure. Most of the polymeric delivery strategies originally developed for plasmid DNA (pDNA) in gene therapy cannot be used for miRNA delivery without formulation optimization since miRNA are much smaller molecules (21-23 bp) than DNA (several kilo bp). Thereby, small RNAs are more difficult to be packaged and condensed into stable systems for protection against early clearance and degradation [174,175]. Moreover, the vulnerability of RNA to enzymatic degradation (hydrolyses) by serum nucleases due to an extra hydroxyl group in the 2’ position of pentose ring in ribose structure, instead of a hydrogen atom present in DNA structure, induced additional challenges to RNA delivery [177,241].

Several types of biomaterials have been used as platforms for gene delivery, and in particular positively-charged polymers represent a high proportion. They can bind nucleic acids via electrostatic interactions to form particulate structures named polyplexes [144]. Polyplexes are formed in solution by the direct mixing of two oppositely charged polyelectrolytes and the main driving force that guides polyplex formation is an increase in the entropy of the system due to the release of low-molecular weight counterions which is able to produce nanoparticles containing the nucleic acid payload in a compacted and protected structure [133,242]. The easy manipulation and versatility of physicochemical properties are some of the most important advantages of polymeric gene carriers [157].

Cationic polymers that have been used for the delivery of miRNAs include polyethyleneimine (PEI), polyamidoamine (PAMAM) dendrimers and chitosan [174,241]. Polymers derived from natural sources could be preferable in gene therapy applications because they are naturally biocompatible, biodegradable and nontoxic and can overcome the cytotoxicity associate with the use of several synthetic polymers which does not satisfy the requirements for clinical applications. However, cationic chitosan, one of the most studied polymers of the list, has its own drawbacks such as low water solubility at physiological pH because of partial protonation of primary amino groups which can affects nucleic acid interactions and stability of complexes in bloodstream [177,219]. Thus, the design of biocompatible, stable and efficient nanocarriers is needed [204]. In contrast to the large amount of synthetic non-viral gene delivery systems, there is only a small number of polycations of natural origin [243].

Pullulan is a natural polysaccharide derived from *Aureobasidium pullulans* that consists of maltotriose units and due to its non-toxic, non-immunogenic and biodegradable properties, is considered as a promising material for biomedical applications [244]. It is admitted safe in the United States for a wide range of applications, such as an excipient in pharmaceutical tablets and listed in the Japanese Standards as accepted adjuvant for drug delivery [245,246]. Cationic pullulan derivatives grafted with primary or tertiary amine groups were previously demonstrated to be able to form complexes with plasmid DNA as well as siRNA in cationized pullulan-based hydrogels [247,248]. However, the ionic interaction between the macromolecules closely depend on the pH. Hydroxyl groups of pullulan can be easily substituted with quaternized ammonium groups (QA) to improve the interaction with negatively charged nucleic acids [247,249]. QA derivatives are an interesting strategy for gene therapy due to their permanent positive charges independent of the pH [116]. In this work, polycations have been obtained by grafting QA using

glycidyltrimethylammonium chloride at different feeding ratios into the pullulan backbone. Then, QA-pullulan formulations were used to form nanosized polyplexes with miRNAs opening the way to their use as a platform for gene delivery.

2. Materials and Methods

2.1 Materials

Pullulan (Mw 200 kg/mol) was purchased from Hayashibara Company (Okayama, Japan). Glycidyltrimethylammonium chloride (GTMAC) (Mw 151.63 g/mol) was purchased from Sigma-Aldrich (St. Louis, MO, USA). Dialysis membranes of 20 kDa was purchased from Spectrum Laboratories (New Brunswick, NJ, USA). Single-stranded miRNA and 6-Fluorescein AMidite (6-FAM)-miRNA scramble oligonucleotides with 23 bp of length (RNA sequence: 5'-UUA AUG CUA AUC GUG AUA GGG GU-3') used to mimic the natural human mature microRNA miR-155-5p were purchased from Sigma-Aldrich (Saint Quentin Fallavier, France). Sequence was reconstituted in RNase-free water to achieve a final concentration of 20 μM and stock solutions were stored at -20°C. Ultrapure water was prepared by ion-exchange of running tap water (Millipore, France).

2.2 Synthesis of cationized pullulan

2.2.1 Alkylation with GTMAC

Pullulan was synthetized based on a protocol previously described by San Juan *et al.* to graft primary and tertiary amine groups into pullulan backbone [247]. Briefly, pullulan (500 mg) was dissolved in 5 mL of an aqueous solution of 10 M NaOH. Then, the solution was placed at 4°C under magnetic stirring until pullulan was completely solubilized. Glycidyltrimethylammonium chloride (GTMAC) was added to polysaccharide solution at different feeding ratios (1 eq = 3.1 mmol; 2 eq = 6.2 mmol, and 3 eq = 9.3 mmol) drop by drop and under high magnetic stirring at 4°C. The solution was placed under magnetic stirring at 55°C for 4 hours. After cooling down to room temperature, the pH was adjusted to 7 with concentrated hydrochloric acid solution. The mixture was exhaustively dialyzed (MWCO of 20 kDa) for 48 hours with ultrapure water and the derivatives were obtained as fluffy white materials after freeze-drying.

2.3 Chemical characterization of modified pullulan

2.3.1 Elemental analysis

Elemental analysis (C, H, N, O) was performed by the Microanalysis service of Centre National de la Recherche Scientifique (CNRS) (Gif/Yvette, France) (Table 4 and Table 5). Degree of substitution was estimated using N content values.

2.3.2 Molecular weight determination

Weight-average molecular weight (Mw) and number-average molecular weight (Mn) were determined by size exclusion chromatography (SEC) coupled to a multiangle laser light scattering (MALLS) detector (DAWN-F, Wyatt Technology, Santa Barbara, CA, USA). The SEC line consisted of a TSK-Gel PWXL Guardcolumn and TSK-Gel GMPWXL in series (Tosoh Bioscience, Stuttgart, Germany). The eluent was 0.2 M NaNO3 containing 0.02% (w/v) NaN3 at 0.5 mL/min flow rate. The samples were dissolved in the eluent at a concentration of 10 mg/mL. The dn/dc value used for the molecular weight distribution calculations was 0.14. The collected data were analyzed using the software Astra V-6.1.2 (Santa Barbara, CA).

2.3.3 FTIR spectroscopy

FTIR spectroscopy was carried out with KBr pellets on a Thermo-Nicolet-AVATAR 370 FTIR (Thermo Electron Corporation, Waltham, MA). A first pellet with 200 mg of KBr was prepared. Then, pellets were made using 200 mg KBr and 2 mg of polymer. A 32-scan interferogram was collected in transmittance mode. Scans were taken from 400 cm^{-1} to 4000 cm^{-1} at a resolution of 2 cm^{-1}. The spectrum of KBr pellet was used as background.

2.3.4 NMR spectroscopy

1H-NMR spectra was recorded with a Bruker-400 Ultrashield (Bruker, Germany) operating at 400 MHz. Polymers samples were prepared in D2O at a concentration of 20 mg/mL.

2.4 Synthesis of QA-pullulan/miRNA Polyplexes

Briefly, cationic pullulan and anionic miRNA were dissolved in ultrapure water to obtain stock solutions at 0.08 mg/mL and 0.04 mg/mL, respectively. All polysaccharide solutions were filtered before use (0.2 µm). Nanosized polyplexes were produced by

dropping 1 mL of miRNA solution over 1 mL of quaternized pullulan solution under high magnetic stirring at room temperature in aqueous solution. Samples were placed at 4ºC during 20 min for stabilization before use.

2.5 Characterization of QA-pullulan/miRNA Polyplexes

2.5.1 Size and zeta potential measurements

Particle size and zeta potential of polyplexes were measured by Dynamic Light Scattering (DLS) and Electrophoretic Light Scattering (ELS) using a Zetasizer Nano-ZS (Malvern Instruments, Malvern, UK) respectively. Size and zeta potential measurements were performed at 25°C using a 173° and 13° scattering angle for size and zeta potential measurements, respectively, equipped with a 4 mW HeNe laser beam with a wavelength of 633 nm. Size and ζ potential values were automatically calculated through the software DTS Nano v.6.30 (Malvern, UK) using the Stokes-Einstein equation and the Henry equation with the Smoluchowski approximation, respectively. Size measurements were performed in water using disposable polystyrene cuvettes and zeta potential measurements were performed in 1 mM KCl solution using a DTS1070-folded capillary cell (ELS, Malvern, UK). Data were acquired in triplicate.

2.5.2 Morphology

The morphology of optimized polyplexes was assessed using a Transmission Electron Microscope (TEM) Tecnai 12 (80 kV; FEI; Hillsboro, OR, USA) with a 1K x 1K KeenView camera (OSiS). Nanosized polyplexes were produced as previously described. Then, 3 µL of polyplexes suspension was placed onto a 400 µL mesh copper grid coated with carbon (EMS) without any sample dilution. Uranyl acetate 1% (w/v) was used for negative staining. TEM pictures was performed at the platform ImagoSeine of the Institute Jacques Monod (Paris, France).

2.5.3 miRNA presence into polyplexes

The presence of the miRNA was monitored by agarose gel electrophoresis (AGE) and UV spectrophotometry after miRNA desorption. Agarose gel electrophoresis was perfomed using 5% agarose gels containing ethidium bromide in TBE (Tris-Borate-EDTA, Thermo Fisher Scientific, Vilnius, Lithuania) buffer. An Ultra-Low Range GeneRuler DNA Ladder (10-300 bp; Thermo Fisher Scientific, Bleiswijk, Netherlands)

was used to monitor miRNA presence. Samples included solution of free polymer (QA-pullulan), plus additional controls from different steps of the miRNA loading: miRNA alone (at the concentration used for loading), QA-pullulan polysaccharide solution and QA-pullulan/miRNA polyplexes. Samples were run by electrophoresis (50 V, 120 min) and detected through a UV transilluminator (Vilber Lourmat smart imaging system, Collegien, France). Additional miRNA quantification was performed by UV spectrophotometry using NanoDrop™ 2000/2000c Spectrophotometer (Thermo Fisher Scientific, Wilmington, DE, USA).

2.5.4 Stability of QA-pullulan/miRNA Polyplexes

The stability of complexes was evaluated over time while stored at 4°C in aqueous media. Size and PdI (Polydispersity Index) evolutions of polyplexes suspensions were monitored by DLS (n= 3) at each time point (0h, 6h, 12h, 18h, 24h).

2.5.5 Cytotoxicity of QA-pullulan and QA-pullulan/miRNA Polyplexes

Cytotoxicity was evaluated in Human Umbilical Vein Endothelial Cells (HUVECs, ATCC CRL-1730, Manassas, VA, USA) by resazurin conversion assay (Sigma-Aldrich, Saint Louis, MO, USA). Cells were seeded at a concentration of 10,000 cells/well onto 96-well plates in Dulbecco's Modified Eagle Medium (DMEM) (Thermo Fisher Scientific, Carlsbad, CA, USA) supplemented with 10% (v/v) of fetal bovine serum, 1% (v/v) of penicillin and 1% (v/v) of streptomycin in a humidified atmosphere with 5% CO2 at 37°C. At a subconfluent to confluent stage, cells were detached with 0.05% trypsin/EDTA (Gibco) and re-seeded until the required number of cells for the subsequent experiments was obtained. Cell metabolic activity was assessed after different culture conditions by resazurin conversion. Cells were incubated with medium containing 10% resazurin for 2 hours at 37°C. Fluorescence intensity (530 nm/590 nm) of the cell culture supernatants was measured with an Infinite® 200 PRO microplate reader (TECAN Group Ltd., Männedorf, Switzerland). A blank control comprising only medium was also included. Bright field images (EVOS™ XL Core Cell Imaging System, Thermo Fisher Scientific, Carlsbad, CA, USA) were taken during culture to monitor cell morphology.

2.5.6 miRNA delivery

Human Umbilical Vein Endothelial Cells (HUVECs, ATCC CRL-1730, Manassas, VA, USA) cells were seeded at a concentration of 8,000 cells/well onto Nunc™ Lab-Tek™

chamber slides (Thermo Fisher Scientific) and grown for 48 hours. Polyplexes of QA-pullulan and scramble FAM-miRNA were prepared as previously described on the same day of treatment and incubated for 20 min at 4°C before adding to the cells. After 30 min of incubation using serum-free supplemented cell culture medium, cells were washed with PBS and fixed with fresh 4% paraformaldehyde. Cell nucleus was stained with 4',6-DiAmidino-2-PhenylIndole (DAPI) (Sigma Aldrich, St. Louis, MO, USA). Coverslips were mounted using Ibidi Mounting Medium (IMM) for fluorescence microscopy (ibidi GmbH, Germany). Fluorescence images were taken to evaluate miRNA delivery (Axiovert Observer Z1 inverted microscope, Zeiss, Germany).

2.6 Statistical analysis

The data were expressed as mean ± SD (standard deviation). Statistical analysis was performed using GraphPad Prism (version: 5.0a, San Diego, CA, USA). Since data followed a non-parametric distribution, Wilcoxon matched-pairs test was performed to compare each paired group and p smaller than 0.05 was considered to be statistically significant.

3. Results and discussion

3.1 Chemical modification of pullulan and characterization

Pullulan was grafted with glycidyltrimethylammonium chloride to give QA groups (Figure 15) with molar feeding ratios of 1, 2 and 3 to get QA-pullulan.

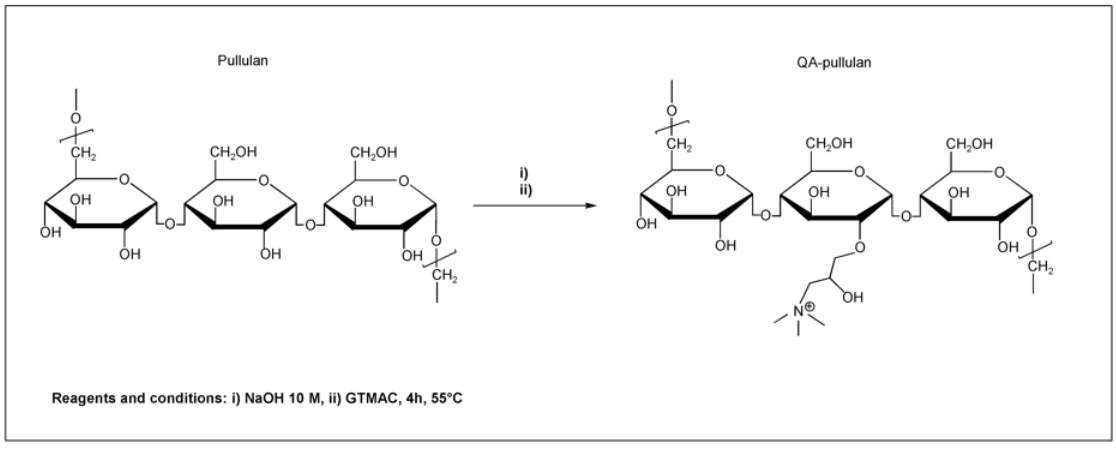

Figure 15. Schematic representation of synthesis route for alkylation of pullulan using glycidyltrimethylammonium chloride (GTMAC).

Cationic derivatives were characterized to confirm the success of incorporation of trimethylammonium groups into the pullulan backbone. Nitrogen elemental analysis confirmed the substitution reaction with N content ranging from 1.8 to 3.3% (w/w) corresponding to 1.3 to 2.3 mmol of QA groups per g of polymer. SEC-MALLS analysis evidenced monomodal molecular weight distributions (PdI ranging from 1.1 to 1.4) (Table 4 and Table 5).

Table 4. Characterization of pullulan and cationic pullulan derivatives.

Amine	Feeding[a]	M_n [b,c] (kDa)	M_w [b,c] (kDa)	PdI[b]	N[d] (%)	DS[e]
No amine (pullulan)	0	113	298	2.6	0	0
QA-pullulan	1	125	186	1.4	1.83 ± 0.25	0.3
	2	240	270	1.1	2.75 ± 0.34	0.4
	3	275	320	1.2	3.27 ± 0.04	0.5

[a]Feeding: $mol_{amine}/mol_{hydroxyl\ groups}$, [b]Measured by SEC-MALLS, [c]SD ± 5-10%, [d]From nitrogen elemental analysis, [e]Degree of substitution of QA-pullulan calculated per anydroglucose unit.

Table 5. Elemental analysis of pullulan and cationic pullulan derivatives.

Amine	Feeding[a]	N (%)	C (%)	H (%)	O (%)
No amine (pullulan)	0	Absence	41.92 ± 0.06	6.35 ± 0.01	51.88 ± 011
QA-pullulan	1	1.83 ± 0.25	42.52 ± 0.34	7.09 ± 0.06	46.99 ± 0.55
	2	2.75 ± 0.34	41.88 ± 0.43	7.27 ± 0.19	44.04 ± 0.91
	3	3.27 ± 0.04	43.40 ± 0.14	7.49 ± 0.09	43.26 ± 0.07

[a]Feeding: $mol_{amine}/mol_{hydroxyl\ groups}$

The extent of the derivatisation reaction was given by the degree of substitution (DS) defined as the number of substituted hydroxyls groups per AGU (AnhydroGlucose Unit) [108]. DS can be calculated using N content from elemental analysis results. Derivatives with a degree of substitution in QA groups around 0.3-0.5 were obtained in one step and in a shorter time (4 hours) compared to others protocols used to obtain quaternized polymers with reaction time of 8, 14 and 24 hours [112,250,251]. Moreover, the protocol of Liu *et al.* performed in 8h used a mixture of water and isopropanol as reaction medium contrary to our protocol performed only in water without organic solvent [251].

IR spectra of pullulan and its cationic derivative presented the general pattern characteristic of polysaccharides [252]. The substitution with QA groups was confirmed

by a signal at 1470 cm-1 (Figure 16) due to C-H scissoring in methyl groups [250,253]. This was further confirmed by 1H-NMR spectra (Figure 17) with signals at 3.2 ppm and 4.4 ppm [112,250].

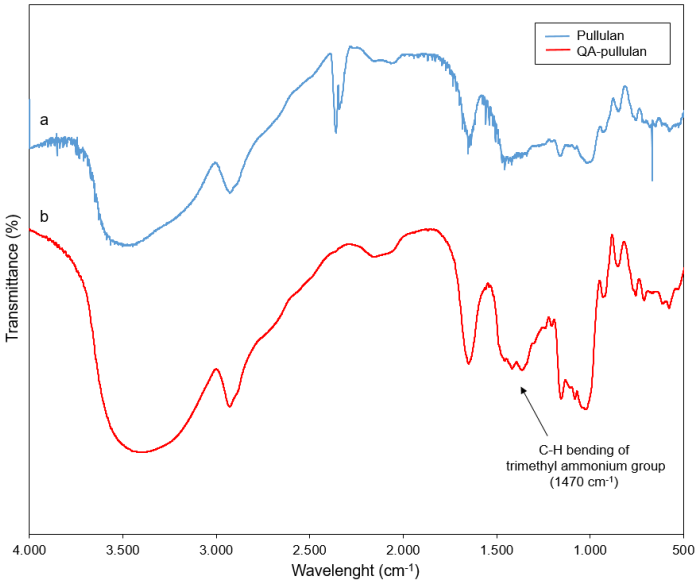

Figure 16. FTIR spectra of (a) non-modified pullulan and (b) QA-pullulan.

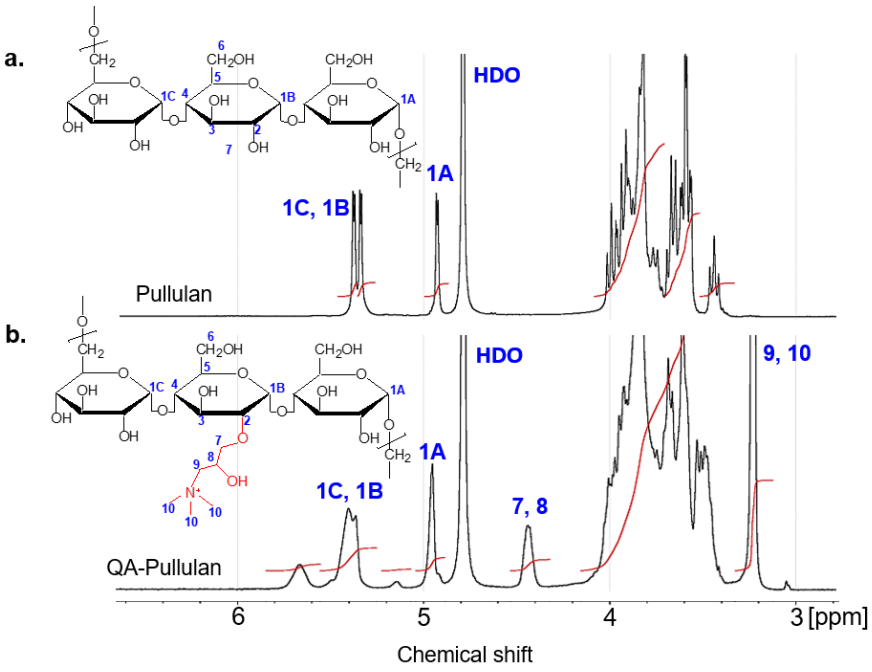

Figure 17. 1H-NMR spectra of (a) non-modified pullulan and (b) QA-pullulan in D2O. 1A, 1B, 1C signals depicted anomeric H from maltotriose base unit of pullulan. Numbers 2-6 corresponded to H on anydroglucose unit. H from GTMAC substituent (b) were depicted with numbers from 7 to 10.

Highly charged cationic polymers can have non-specific interactions with polyanionic biomolecules in the bloodstream leading to the inhibition of many crucial cellular processes and causing severe inflammatory reactions [204,246]. When compared to non-modified pullulan, cationic pullulan did not show toxicity up to 72h of incubation with increasing concentrations of QA-pullulan until 1,000 µg/mL (Figure 18) and supports results of literature that pullulan modified with glycidyltrimethylammonium chloride is a nontoxic polymer [250].

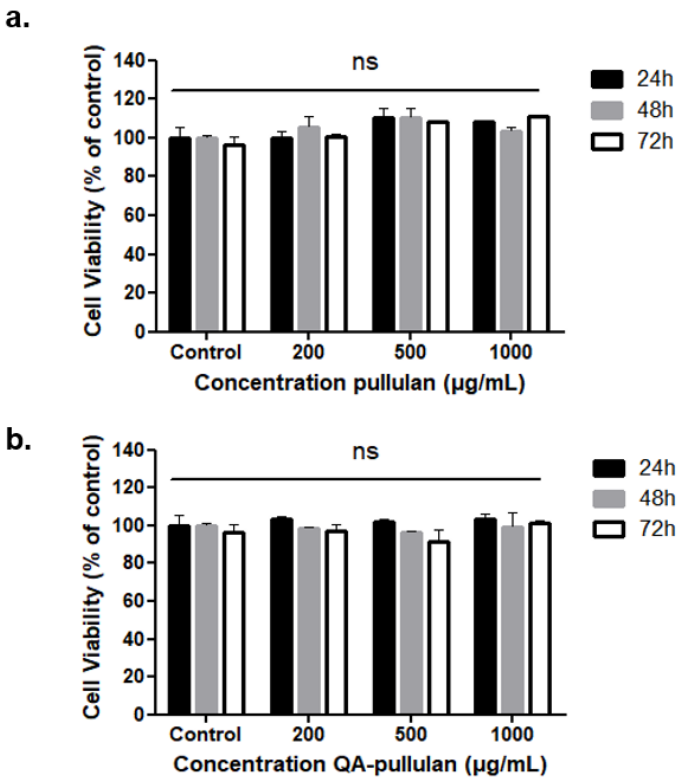

Figure 18. Cytocompatibility of (a) non-modified pullulan and (b) QA-pullulan towards HUVECs at 200, 500 and 1000 µg/mL after 24, 48 and 72h of incubation. Results are shown as mean ± SD from 3 independent experiments with no statistical differences detected using the Wilcoxon matched-pairs signed rank test.

3.2 Synthesis and characterization of QA-pullulan/miRNA Polyplexes

Polyplexes were prepared by mixing miRNA and QA-pullulan at different concentrations under strong magnetic stirring (Figure 19). They were incubated at 4°C for 20 minutes for stabilization of complexes before use. Once QA-pullulan modified with 1.83% of N showed to be enough to form complexes with miRNA by electrostatic interactions this derivative was selected for all further optimizations. To optimize the production of stable

polyplexes, a fixed concentration of miRNA of 5 nmol (0.04 mg/mL) was selected based on previous works performed by Antunes *et al.* 2019 [232]. Different N/P ratios (0.5-15) were tested by increasing the concentration of QA-pullulan.

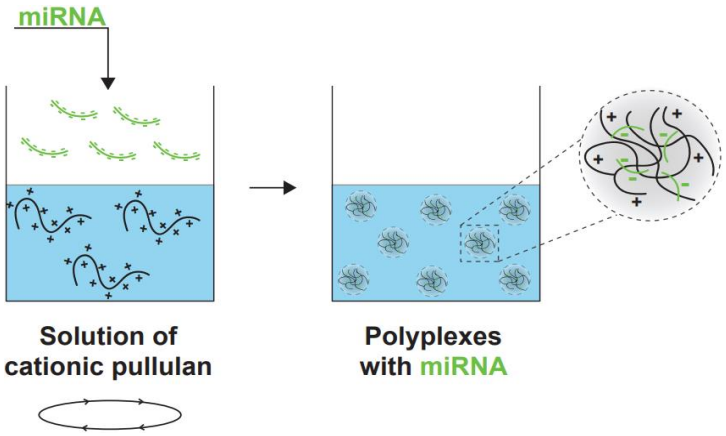

Figure 19. Schematic representation of preparation of QA-pullulan/miRNA polyplexes by electrostatic interactions.

All physicochemical characterizations are summarized in Figure 20. Samples were characterized by DLS/ELS regarding size, PdI and zeta potential values (Figure 20C). Complexes were formed at an optimized N/P molar ratio of 0.8 producing polyplexes in the nanosized range with a diameter around 130 ± 30 nm and narrow distribution as shown by the polydispersity index (0.07 ± 0.04). More negative zeta potential values of QA-pullulan/miRNA polyplexes (-12 ± 5 mV) as compared to zeta potential of cationic pullulan solution alone (31 ± 6 mV), suggested the presence of additional negative charges at the surface due to miRNA presence in the complex. The morphology of complexes was characterized by TEM (Figure 20B) evidencing the formation of homogeneous spherical particles. The observed sizes were well-correlated with those determined by DLS.

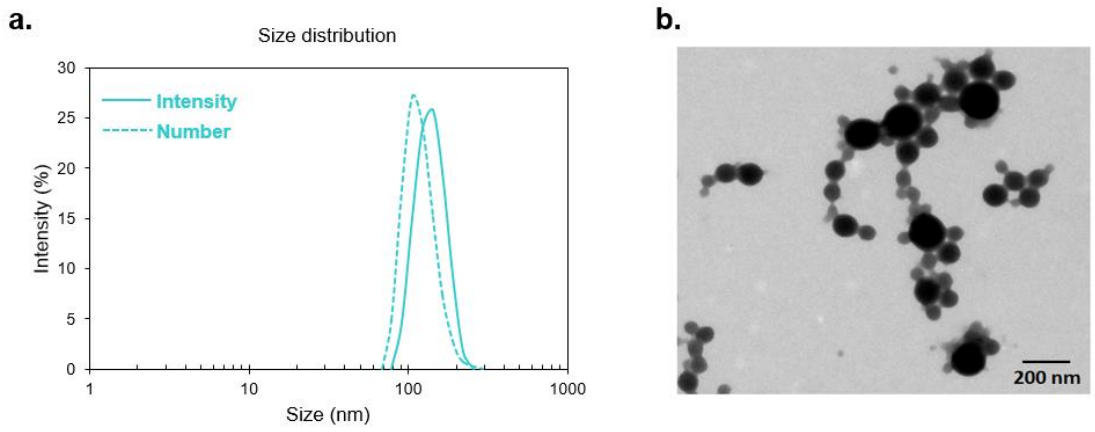

c.

Size (nm)	PdI	Attenuator	Count rate (kcps)	ζ potential (mV)
133 ± 30	0.07 ± 0.04	7	178	-12 ± 5

Figure 20. Physico-chemical characterization of QA-pullulan/miRNA polyplexes: (a) Size distribution from Light Scattering (LS) expressed by intensity and number percentages; (b) Morphology of polyplexes obtained by TEM microscopy; (c) Size (nm), PdI, attenuator and count rate values measured by LS and zeta potential (mV) measured by Doppler laser electrophoresis. Results are shown as mean ± standard deviation of 3 different samples.

miRNA presence was confirmed by agarose gel electrophoresis by the presence of a band in the expected region of 23 bp after miRNA desorption from QA-pullulan (Figure 21A). miRNA was quantified using the software ImageJ by the intensity of the band of polyplexes in the agarose gel normalized by the control naked miRNA and the loading efficiency was around 80%. There was no miRNA degradation or fragmentation after loading as suggested by the absence of smeared bands in AGE indicating that QA-pullulan could effectively protected miRNA. Further miRNA quantification by UV spectrophotometry (Figure 21B) displayed a similar trend as in AGE results.

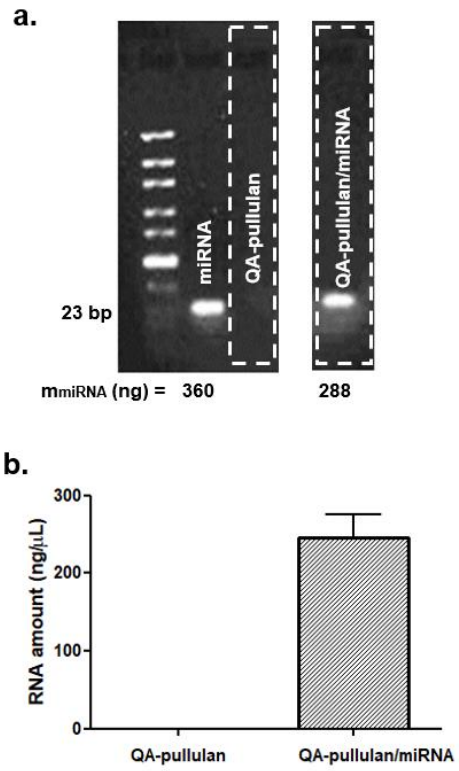

Figure 21. miRNA presence onto polyplexes: (a) miRNA presence onto polyplexes after miRNA desorption confirmed by agarose gel electrophoresis using an Ultra-Low Range GeneRuler DNA Ladder (10-300 bp) as control and RNA amount (ng) quantified by the intensity of the band when compared to miRNA alone (0.04 mg/mL, 9 µL) using ImageJ software; (b) RNA amount (ng/µL) quantified by UV absorbance (n=3).

The N/P ratio, which corresponds to the ratio between QA groups of pullulan derivatives to the phosphate groups of nucleic acid, plays an important role in the capacity of complexation, particle diameter, stability and cytotoxicity of carriers [254–256]. Generally, polyplexes can be formed between polycations and nucleic acids at relatively low N/P ratios [249]. In our case, this optimum was found at N/P of 0.8. Furthermore, it was described that an increase in the average molecular weight (Mn) of polymer dramatically improved oligonucleotides encapsulation at low N/P ratios [116,254,257]. In a study of Liu and co-workers chitosan with chains having 5 to 10 times the length of siRNA (i.e. with a molecular weight ranging from 65 to 170 kDa) were most suitable to form stable complexes [258]. Further studies could investigate the effect of the molecular weight of pullulan and its consequence in terms of both physicochemical characteristics of the polyplexes and *in vivo* biodistribution/biodegradation.

Stability of complexes in aqueous media was evaluated here under storage at 4°C over 1 day without forming aggregates (Figure 22). In addition, it is noteworthy that our method of complex formation was developed without the use of any chemical crosslinking agent.

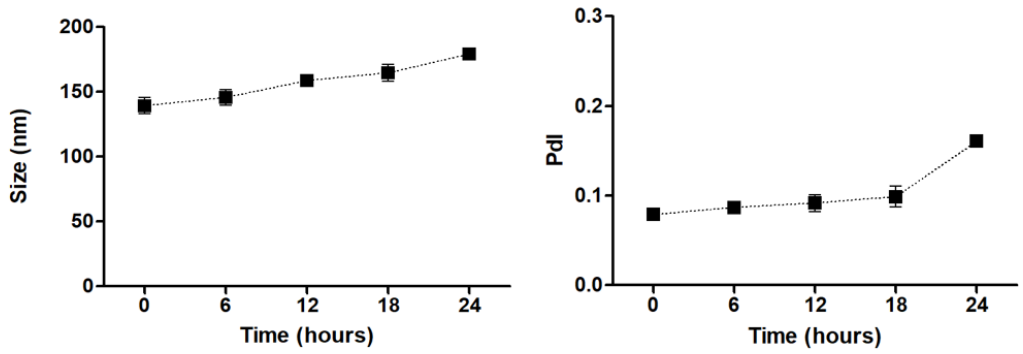

Figure 22. Stability of QA-pullulan/miRNA polyplexes evaluated by size (left) and PdI evolution (right) measured by Light Scattering as function of time of incubation in water at 4°C (mean ± SD, n=3).

The increase of the ionic strength has a significant impact on colloidal stability with aggregate formation, and higher PdI values correlated with the heterogeneity of complexes in this medium. Alameh *et al.* described that the colloidal instability in 150 mM NaCl increased with the increase of molecular weight when comparing chitosan with low (10 kDa) and high (120 kDa) Mn [259]. Keeping a good stability in physiological conditions is one of the major challenges when designing vectors intended for intravenous administration [219]. To achieve this goal, several strategies were thought to overcome this limitation and improve stability in biological fluids [241]. A classical strategy uses crosslinkers such as sodium tripolyphosphate (TPP) for the preparation of chitosan NPs with nucleic acids [129,130]. However, TPP is a chemical agent with limited sites of interaction for ionotropic gelation [260]. Hence, the colloidal stability of polyplexes nanosystems in physiological conditions was far from being fully addressed in the previous investigations [261].

To assess if the developed polyplexes could be used in biomedical applications, namely as vectors for gene therapy, the cytocompatibility towards HUVECs was evaluated here through an *in vitro* toxicological assay based on resazurin conversion. *In vitro* tests did not evidence any toxic effect of the QA-pullulan/miRNA complexes after 1 day of

incubation up to the maximum tested dose of 200 µg/mL of polyplexes (n=3) (Figure 23A). We did not observe any alteration in cell morphology (Figure 23B). This important result is a key aspect to further investigate the potential use of the new biocompatible systems.

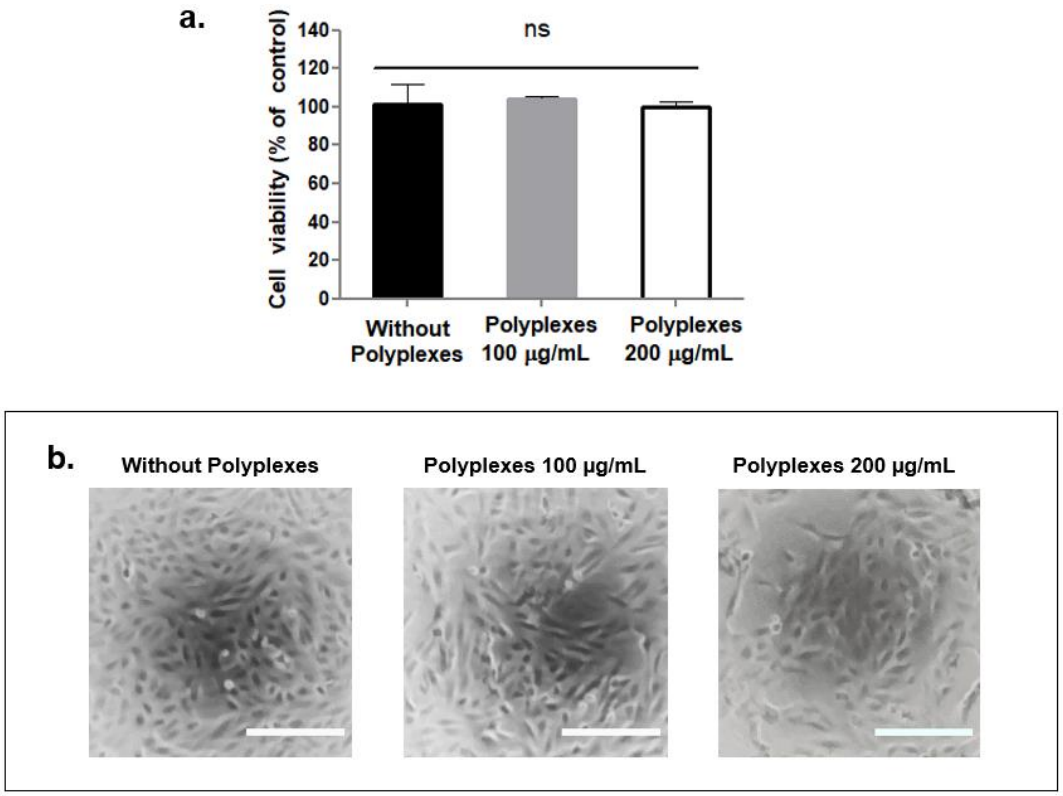

Figure 23. Cytocompatibility of complexes. (a) Cytocompatibility of complexes towards HUVECs exposed to increasing concentrations of QA-pullulan/miRNA polyplexes measured by resazurin conversion after 1 day of incubation. Results are shown as mean ± SD from 3 independent experiments with no statistical differences detected using the Wilcoxon matched-pairs signed rank test. (b) Optical images of confluent cells without polyplexes and with 100 µg/mL and 200 µg/mL of polyplexes. Scale bar corresponds to 200 µm.

Finally, a comparative study of free miRNA, neutral pullulan/miRNA and polyplexes of QA-pullulan/miRNA, was done using a fluorescently labeled miRNA to evaluate their cellular uptake. As it can be seen from Figure 24B and Figure 24C, no miRNA could be detected inside cells in case of administration of free miRNA or unmodified pullulan and miRNA indicating that free miRNA could hardly be internalized by cells. miRNA from polyplexes, in contrast, was clearly incorporated by cells (Figure 24D) by forming complexes with QA-pullulan that is able to promote their internalization usually via

endocytic pathways being 150 nm the accepted size limit for cellular uptake by non-specific endocytosis [177,231,262].

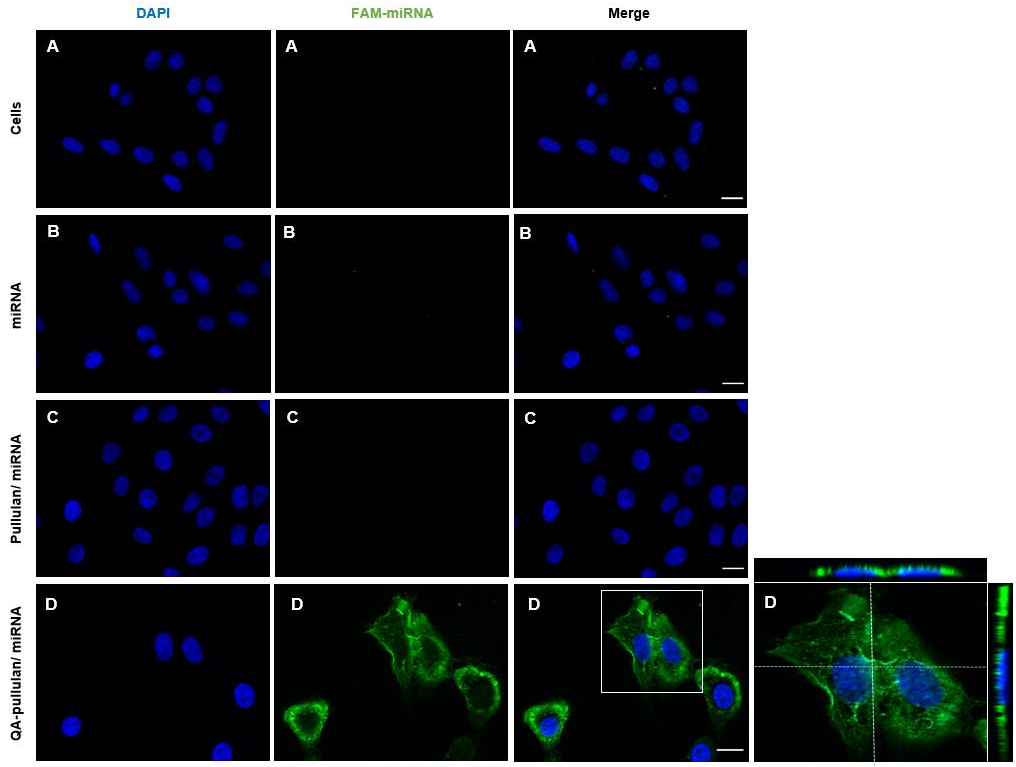

Figure 24. FAM-miRNA delivery. Fluorescence microscopy images of HUVECs evidencing miRNA delivery. Left column: cells' nuclei stained with DAPI (depicted in blue); middle column: FAM labelled miRNA (depicted in green); right column: merged images. (A) Without treatment, (B) cells treated with FAM-labelled miRNA, (C) cells treated with FAM-labelled miRNA in presence of unmodified pullulan; (D) cells treated with polyplexes formed by FAM-labelled miRNA and QA-pullulan including Z-stack-assembled fluorescence images (zoom). Treatments were performed for 30 min at 37°C. Scale bar: 20 µm.

4. Conclusions

This work demonstrated that nanosized polyplexes are formed and are stable in aqueous medium by simply mixing miRNA with pullulan substituted with quaternized ammonium groups. Such pullulan derivatives have been previously used by André and co-workers to modify the surface of nanoparticles based on sorbitan monooleate (Span® 80) in order to increase the interaction of this system with siRNA for cellular therapy [263]. To the best of our knowledge, cationized pullulan have been used for the first time to build miRNA delivery nanosystems. The obtained nanoparticles proved to be non-cytotoxic on HUVECs cells after 1 day incubation. Neither toxic reagent nor organic solvent were used. With further experiments proving the efficacy of the systems *in vivo*, we expect to

contribute for the development of new safe pullulan-based delivery systems for miRNA therapeutics.

Chapter I- Part II

CHAPTER I –

COMPLEMENTARY WORK

1. Introduction

In order to form complexes with negatively charged miRNA, cationic pullulan derivatives can be easily obtained by chemical grafting of amino groups in pullulan backbone. It is described that the complexation of nucleic acids with cationic pullulan derivatives can be modulated by changing the density and the nature of amino groups grafted on the pullulan backbone [248]. Polycations containing tertiary amino groups have demonstrated improved capacity for condensation of nucleic acids [264]. Here, cationic pullulan derivatives grafted with tertiary amine groups (DEAE-pullulan) were synthetized and characterized. Then, the ability of DEAE-pullulan to form complexes with anionic miRNA was evaluated and compared to QA-pullulan.

Finally, the feasibility to incorporate fucoidan in polyplexes formulation was evaluated using QA-pullulan/miRNA polyplexes as example. Fucoidan would confer targeting properties to the system. The formation of polyelectrolyte complexes between QA-pullulan and fucoidan was first optimized, followed by miRNA loading to produce ternary complexes.

2. Materials and Methods

2.1 Materials

2-Chloro-N,N-diethylethylamine hydrochloride (Mw 172.10 g/mol) was purchased from Sigma-Aldrich. Fucoidan low molecular weight (Mw 7 kg/mol) was a gift from Algues & Mer (île d'Ouessant, France).

2.2 Synthesis of DEAE-pullulan

Pullulan (1 g) was dissolved in 5 mL of distilled water. The solution was placed at 4°C until complete solubilisation of pullulan. Then, 5 mL of soda (10 M NaOH) was added to activate the hydroxyl functions. The solution was kept at 4°C under magnetic stirring for 20 min. Then, 1 mL of the 2-chloro-N, N-diethylamine hydrochloride (1 eq = 6.2 mmol, 2 eq= 12.4 mmol, and 3 eq = 18.6 mmol) was added to the solution under magnetic stirring at 4°C. The solution was placed under magnetic stirring at 55°C for 40 min. The mixture was placed at room temperature and the pH was adjusted to 7 with hydrochloric acid 10M (10M HCl) solution. The mixture was exhaustively dialyzed (MWCO of 20 kDa) for 48h

with ultrapure water and the derivatives were obtained as fluffy white materials after freeze-drying. Molar ratio was calculated as mol of reagent per mol of anydroglucose.

2.3 Synthesis of polyplexes

Briefly, cationic pullulan and anionic miRNA were dissolved in ultrapure water to obtain stock solutions at 0.08 mg/mL and 0.04 mg/mL, respectively. All polysaccharide solutions were filtered before use (0.2 µm). Nanosized polyplexes were produced by dropping 1 mL of miRNA solution over 1 mL of cationic pullulan solution under high magnetic stirring at room temperature in aqueous solution. Samples were placed at 4ºC during 20 min for stabilization before use.

2.4 Synthesis of polyelectrolyte complexes (PECs) with fucoidan

Cationic pullulan and fucoidan were dissolved in ultrapure water to obtain stock solutions at 0.08 mg/ml and 0.04 mg/mL, respectively. All polysaccharide solutions were filtered before use (0.2 µm). Nanosized PECs were produced by dropping 1 mL of fucoidan solution over 1 mL of cationic pullulan derivatives solution under high magnetic stirring at room temperature in aqueous solution. Samples were placed at 4ºC during 20 min for stabilization before use. Loaded PECs were produced by adding 1 mL of fucoidan (0.04 mg/mL) and miRNA (0.04 mg/mL) solution over 1 mL of cationic pullulan solution (0.08 mg/mL).

3. Results and discussion

3.1 Chemical modification and characterization of pullulan

Cationic pullulan derivatives modified with tertiary amine groups were synthetized by the addition of 2-chloro-N,N-diethylethylamine hydrochloride to pullulan backbone to produce diethylaminoethyl pullulan (DEAE-pullulan) [247]. DEAE-pullulan has a peculiar structure with two possible cationic charges: a tertiary amine function at the end of DEAE group and a quaternary ammonium function when the DEAE group are linked to another DEAE group on the same anhydroglucose due to Hoffman addition (Figure 25) [66]. Since the positive charge of the tertiary ammmonium depends on the pH, the overall charge of the derivatives is related to the amount of unsubstituted DEAE groups grafted on the pullulan backbone. At pH 7.4, all substituents are positively charged.

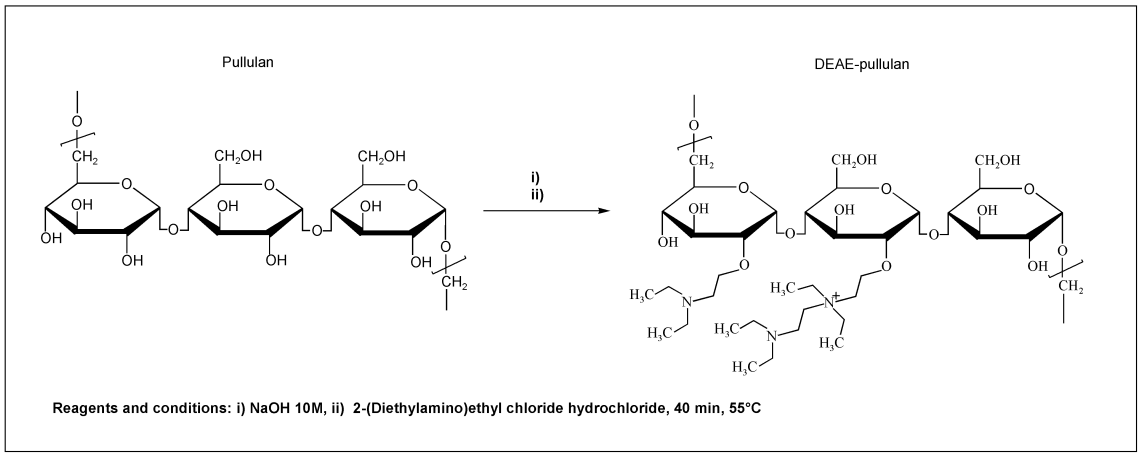

Figure 25. Synthesis route for amination of pullulan grafted with 2-chloro-N, N-diethyl ethylamine hydrochloride.

The data obtained by elemental analysis allowed to verify the amount of amine groups grafted as indicated by the nitrogen content. Values ranging from 1.5 to 2.5% N (w/w) were obtained depending on the amount of reagent added (Table 6). This gives derivatives with a degree of substitution ranging between 0.2-0.5 obtained in a one single step performed in aqueous medium. The amount of grafted amine was proportional to the feeding ratio of reactives. As we can see, by increasing the quantity of reagent added (molar feeding ratio), higher N content values were obtained suggesting an increase of the number of chemical groups grafted. SEC-MALLS analysis evidenced monomodal molecular weight distributions (PdI ranging from 1.3 to 1.5).

Table 6. Characterization of pullulan and cationic pullulan derivatives.

Amine	Feeding[a]	M_n [b,c] (kDa)	M_w [b,c] (kDa)	PdI[b]	N[d] (%)	DS[e]
No amine (pullulan)	0	113	298	2.6	0	0
DEAE-pulullan	1	155	236	1.5	1.5 ± 0.05	0.2
	2	210	272	1.3	2.4 ± 0.12	0.3
	3	161	246	1.5	2.5 ± 0.07	0.3

[a]Feeding: $mol_{amine}/mol_{hydroxyl\ groups}$; [b]Measured by SEC-MALLS; [c]SD ± 5-10%; [d] From nitrogen elemental analysis; [e]Degree of substitution of DEAE-pullulan calculated per anydroglucose unit.

Cell viability was evaluated by a rezasurin conversion assay. Compared to unmodified pullulan, DEAE-pullulan showed to be non-toxic up to 1000 µg/mL confirming that cationic pullulan is a non-toxic polymer. Figure 26 evidences the absence of cytotoxicity of DEAE-substituted derivatives. Comparison is made with previously studied QA-

pullulan. This important result is a key aspect to further investigate the potential use of the new cytocompatible pullulan-based derivatives.

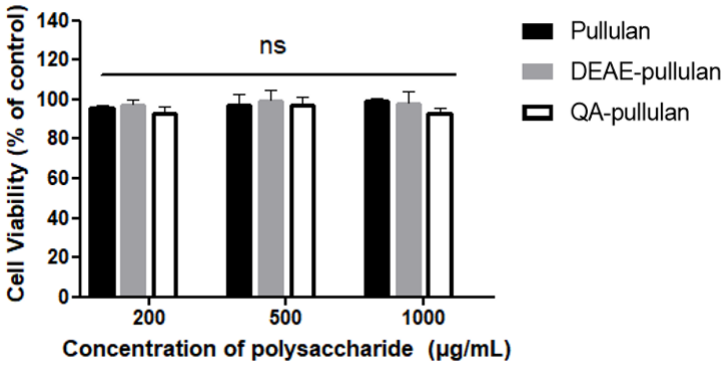

Figure 26. Cytocompatibility of non-modified pullulan, DEAE-pullulan and QA-pullulan towards HUVECs at 200, 500 and 1000 µg/mL after 24h of incubation. Results are shown as mean ± SD from 3 independent experiments with no statistical differences detected using the Wilcoxon matched-pairs signed rank test.

3.2 Synthesis and characterization of nanoparticles

Two strategies were investigated here to produce miRNA nanoparticles: (a) direct complexation of cationic pullulan derivatives with miRNA (polyplexes) and (b) the addition of a negatively charged polymer, fucoidan, and its effect on the formation of PECs between cationic pullulan derivatives and miRNA.

3.2.1 Polyplexes between cationic pullulan derivatives and miRNA

Cationic pullulan/miRNA polyplexes were prepared by dropping 1 mL of miRNA solution to 1 mL of cationic pullulan solutions under high magnetic stirring (Figure 27). The mixed solution was incubated for 20 min at 4°C to form polyplexes completely. Polyplexes were prepared at different charge (N/P) ratios (from 0.5 to 15) using constant miRNA concentration of 5 nmol (0.04 mg/mL) selected based on previous works performed by Antunes *et al.* [232]. Samples were characterized by DLS/ELS regarding size, PdI and zeta potential values. Polyplexes were also characterized regarding miRNA presence and morphology.

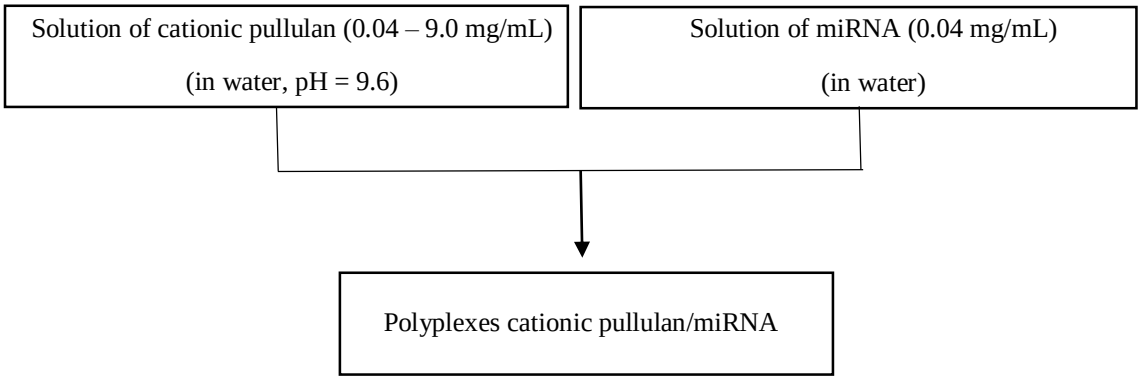

Figure 27. Scheme of polyplexes production. All the solutions were filtered (0.2 µm) before use.

Size, zeta-potential and the loaded amount of miRNA of polyplexes prepared with DEAE-substituted pullulan (1.5%N) and QA-pullulan (1.8%N) with similar amine contents and N/P molar ratio of respectively 1.0 and 0.8 are compared on Figure 28. Polyplexes showed a nanosized range with a diameter of less than 200 nm and narrow size distribution as confirmed by the low polydispersity index values (0.12 ± 0.01 and 0.07 ± 0.04). Negative zeta potential values of DEAE-substituted pullulan/miRNA (−14.8 ± 1.67 mV) and QA-pullulan/miRNA (−12.0 ± 5.42 mV) polyplexes, suggested the presence of negative charges at the surface. miRNA presence was confirmed by agarose gel electrophoresis through the appearance of a band in the expected region of 23 bp after miRNA desorption from DEAE and QA-pullulan polyplexes. miRNA was quantified using the software ImageJ by the intensity of the band of polyplexes in the agarose gel normalized by the control naked miRNA and the loading efficiency was around 80%. There was no miRNA degradation or fragmentation after loading as suggested by the absence of smeared bands in AGE indicating that polyplexes could effectively protect miRNA from degradation.

A.

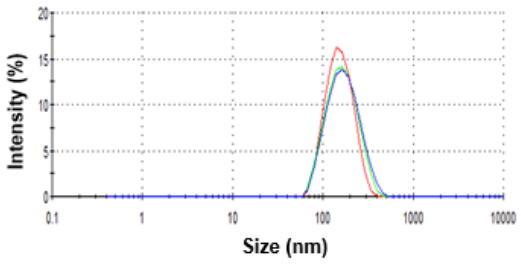

B.

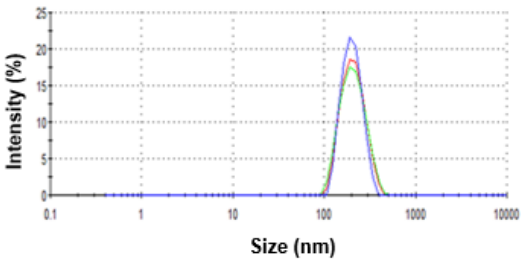

C.

Cationic pullulan	Size (nm)	PdI	ζ pot (mV)
DEAE-pullulan	169 ± 9	0.12 ± 0.01	-14.8 ± 1.67
QA-pullulan	133 ± 30	0.07 ± 0.04	-12.0 ± 5.42

D.

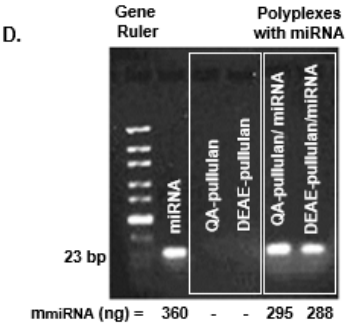

Figure 28. Physico-chemical characterization of polyplexes: Size distribution of (A) DEAE-pullulan/miRNA and (B) QA-pullulan/miRNA polyplexes from Light Scattering (LS) expressed by intensity percentages; (C) Size (nm) and PdI values measured by LS and zeta potential (mV) measured by Doppler laser electrophoresis. (D) miRNA presence onto polyplexes after miRNA desorption confirmed by agarose gel electrophoresis using an Ultra-Low Range GeneRuler DNA Ladder (10–300 bp) as control and RNA amount (ng) quantified by the intensity of the band when compared to miRNA alone (0.04 mg/mL, 9 µL) using ImageJ software; Results are shown as mean ± standard deviation of 3 different samples.

Keeping a good stability in physiological conditions is one of the major challenges when designing vectors intended for intravenous administration. Polyplexes formed between QA-pullulan and miRNA have previously showed to be stable in aqueous media. As chemical and physical stability of polyplexes must be defined also in the presence of serum, we investigated the effect of physiological salt concentration on the integrity of the polyplexes by their incubation in 0.9% NaCl. As we can see in Figure 29, an increase in the ionic strenght caused polyplexes disassembly leading to aggregation. High PdI values correlated with the heterogeneity of complexes in this medium during the first 1h for both DEAE and QA-pullulan polyplexes.

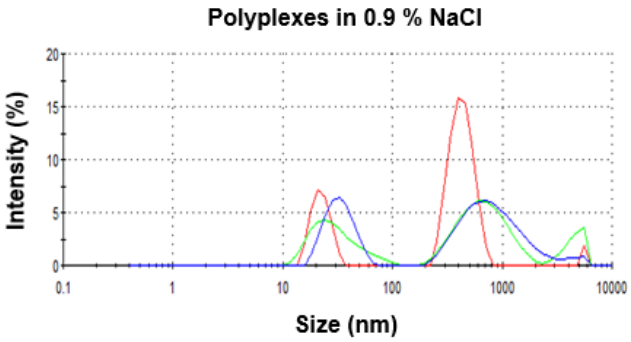

Figure 29. Size distribution from Light Scattering (LS) expressed by intensity percentages of DEAE-pullulan/miRNA polyplexes dissolved in 0.9% NaCl. Data was acquired in triplicate.

3.2.2 Polyelectrolyte complexes with fucoidan

Since it was possible to form complexes with both cationic pullulan derivatives, QA-pullulan was selected to continuous the work due to its permanently positive charged groups independent of the pH of the medium. The formation of PECs between QA-pullulan and fucoidan, was first optimized without miRNA in order to achieve the best conditions to formulate PECs. Fucoidan low molecular weight (LMWF) of 7 kDa was selected for this purpose (Table 7).

Table 7. Characterization of LMWF by elemental analysis.

Sample	**S (%)**	**C (%)**	**H (%)**	**N (%)**
Fucoidan	**7.35 ± 0.11**	28.71 ± 0.10	4.78 ± 0.13	Ab*

*Absent

As the formation of PEC nanoparticles can be influenced by several parameters, we investigated in this work the influence of polyelectrolyte concentrations, mixing and volume ratio of charged units. The influence of pH was excluded from the present investigation, since quaternary ammonium groups are not sensitive to pH changes [265]. In addition, fucoidans are considered as strong polyelectrolytes (pKa 1.0- 2.5) and are likely to be fully charged in the range of pH used in the study [266].

PECs were produced by dropping fucoidan solution over QA-pullulan (Figure 30) solution under high magnetic stirring via electrostatic interactions between negatively charged sulfate groups of fucoidan ($-OSO_3^-$) and quaternary ammonium of QA-pullulan.

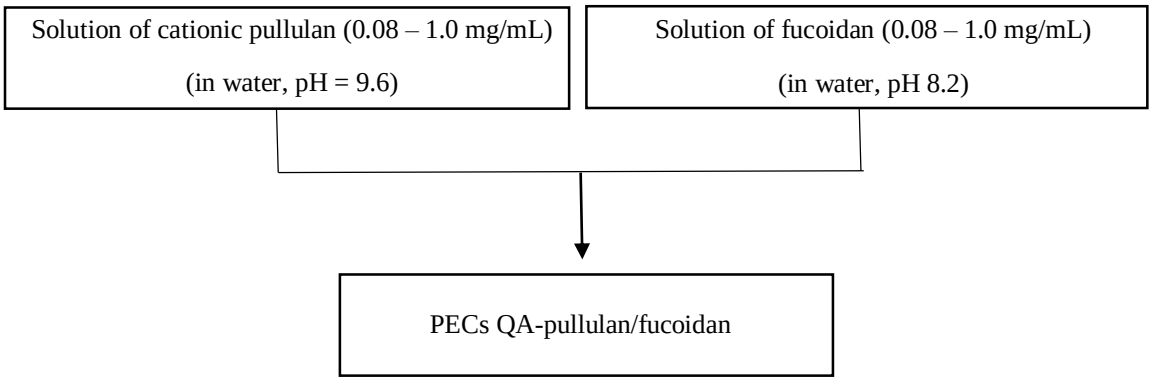

Figure 30. Scheme to produce polyelectrolyte complexes between QA-pullulan and fucoidan. All the solutions were filtered (0.2 µm) before use.

In general, PECs are formed using very diluted solutions. To better understanding the effect of polymer concentration on electrostatic interaction and complex formation, four total polymer concentrations were studied: 0.08, 0.2, 0.5 and 1.0 mg/mL. As we can see, from Table 8, increasing the concentration of polyelectrolytes leads to an increase in both nanoparticles size and PdI.

Table 8. Size (nm) and polydispersity index for QA-pullulan/fucoidan PECs at different polyelectrolyte concentrations and volumes.

Concentration polyelectrolytes	Final Volume					
	2 mL		10 mL		20 mL	
	Size	PdI	Size	PdI	Size	PdI
0.08 mg/mL	125.0	0.173	142.8	0.120	169.4	0.098
0.2 mg/mL	156.5	0.077	182.8	0.050	202.8	0.031
0.5 mg/mL	288.0	0.164	357.3	0.135	445.0	0.160
1.0 mg/mL	431.8	0.217	776.6	0.479	2039	0.834

The Figure 31 shows the turbidity of the formed PEC dispersions in dependence on polyelectrolytes concentration. At low polyelectrolytes concentrations (0.08 and 0.2 mg/mL), PECs appear soluble as indicated by transparent solutions, while turbidity was

observed when PEs concentrations was higher than 0.5 mg/mL, indicating that concentrations above the mentionated conditions induced aggregation and are not suitable for nanocomplex preparation.

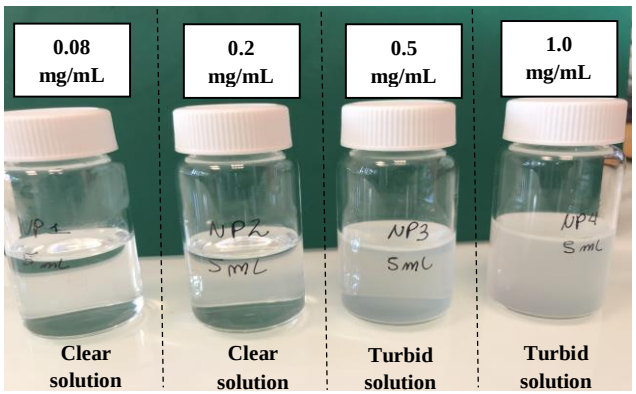

Figure 31. Visual turbidity for PECs with different polyelectrolyte concentrations (0.08, 0.2, 0.5 and 1.0 mg/mL).

Next, different volume ratios between polyelectrolytes were evaluated for three different concentrations of polyelectrolytes ranging from 0.08-0.5 mg/mL. As we can see in Table 9, PECs with diameter less than 200 nm with homogeneous distribution (PdI of 0.053 and 0.067) were only obtained for equivalent PE volume ratios of 1:1 and low PE concentration values of 0.08 and 0.2 mg/mL. We can assume that the volume ratio 1:1 presented the best results due to the better charge balance between the oppositely charged polyelectrolytes.

Table 9. Size (nm) and polydispersity index for QA-pullulan/fucoidan PECs at different polyelectrolyte concentrations and volume ratios.

Concentration polyelectrolytes	QA-pullulan: fucoidan volume ratio							
	1:0.1		1:0.2		1:0.5		1:1	
	Size	PdI	Size	PdI	Size	PdI	Size	PdI
0.08 mg/mL	-	-	-	-	-	-	137.7	0.067
0.2 mg/mL	-	-	-	-	677.8	0.182	198.3	0.053
0.5 mg/mL	342.2	0.133	-	-	-	-	305.8	0.192

Finally, the effect of two different PE weight ratios was studied. Equally weight ratios of polyelectrolytes solutions (QA-pullulan: fucoidan, 1:1) showed the best results producing particles in a nanometric range and low PdI values (Table 10). Solutions with weight ratios of 1:0.5 leads to particle aggregates and were turbid.

Table 10. Size (nm) and Polydispersity Index for QA-pullulan/fucoidan PECs at different polyelectrolyte concentrations and weight ratios.

Concentration of QA-pullulan	QA-pullulan: fucoidan weight ratio			
	1:0.5		1:1	
	Size	PdI	Size	PdI
0.08 mg/mL	563.3	0.088	157.8	0.061
0.2 mg/mL	1533	0.451	164.0	0.063

From all previous results, it can be highlithed that the formation of small and monodisperse particles required the following conditions: the same volume ratio and weight ratio − and low concentration of polyelectrolytes (from 0.008% up to 0.02%, w/v).

Following these optimal conditions, colloidal PECs produced by dropping 1 mL of 0.008% (w/v) fucoidan (Mw 7 kDa, pH 8.2) over 1 mL of 0.008% (w/v) of QA-pullulan (N=1.83%, Mw= 108.2 kDa, pH 9.6) displayed an average diameter of 164.0 ± 3.56 nm, polydispersity index about 0.06 ± 0.03 and negative zeta potential of -8.56 ± 6.59 mV (Figure 32) probably due to the excess of fucoidan on the nanocomplex surface.

A.

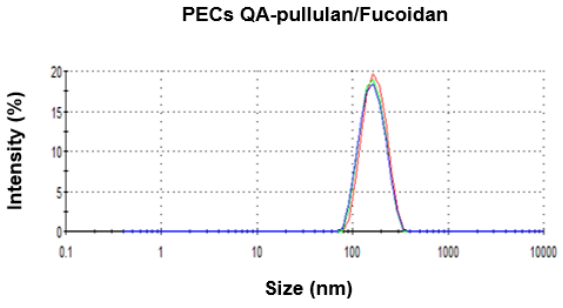

B.

Cationic pullulan	Size (nm)	PdI	ζ pot (mV)
QA-pullulan	164.0 ± 3.56	0.06 ± 0.03	-8.56 ± 6.59

Figure 32. Characterization QA-pullulan/fucoidan PECs prepared at equally PEs concentration of 0.008% (w/v): (A) Size distribution measured from Light Scattering (LS) expressed by intensity

percentages and (B) Size (nm) and PdI values measured by LS and zeta potential (mV) measured by Doppler laser electrophoresis. Results are shown as mean ± standard deviation of 3 different samples.

Once, the protocol to obtain polyelectrolyte complexes was optimized, miRNA was incorporated in the formulation at the previously optimized N/P ratio of 0.8. To produced loaded PECs, 1 mL of miRNA (0.04 mg/mL) and fucoidan (0.04 mg/mL) solution were added dropwise to 1 mL of QA-pullulan solution (0.08 mg/mL) (Figure 33).

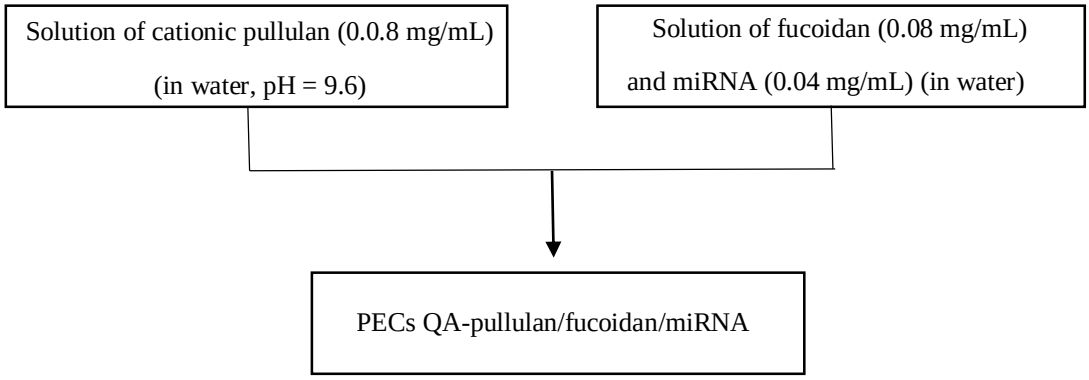

Figure 33. Scheme to produce polyelectrolyte complexes between QA-pullulan and fucoidan loaded with miRNA.

As we can see from Figure 34, the size of the PECs formulated with the miRNA slighty increase to 210 nm while keeping low PdI values (0.07 ± 0.04). More negative zeta potential (-14.62 ± 5.06 mV) compared to PECs formulated without miRNA (-8.56 ± 6.59 mV) suggest the incorporation of additional negative charges in the complexes due to miRNA presence, which was confirmed by agarose gel electrophoresis after miRNA dessorption.

A.

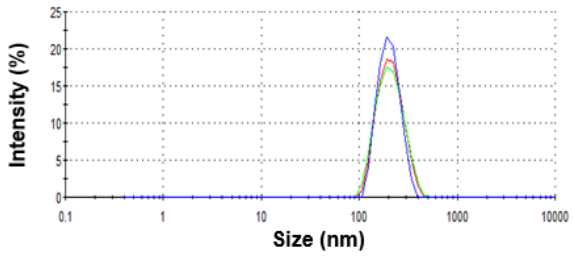

C.

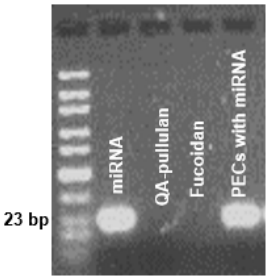

B.

Cationic pullulan	Size (nm)	PdI	ζ pot (mV)
QA-pullulan	210.47 ± 4.56	0.07 ± 0.04	- 14.62 ± 5.06

Figure 34. Physico-chemical characterization of loaded PECs: (A) Size distribution from Light Scattering (LS) expressed by intensity percentages; (B) Size (nm) and PdI values measured by LS and zeta potential (mV) measured by Doppler laser electrophoresis. (C) miRNA presence onto PECs after miRNA desorption confirmed by agarose gel electrophoresis using an Ultra-Low Range GeneRuler DNA Ladder (10–300 bp) as control and RNA amount (ng) quantified by the intensity of the band when compared to miRNA alone (0.04 mg/mL, 9 µL). Results are shown as mean ± standard deviation of 3 different samples.

The stability of PECs was evaluated in pure water and in 0.9% (w/v) NaCl. They show to form a stable colloidal solution for at least one week (Figure 35), suggesting that the presence of fucoidan is able to increase the stability of polyplexes when compared to polypexes formulated without fucoidan.

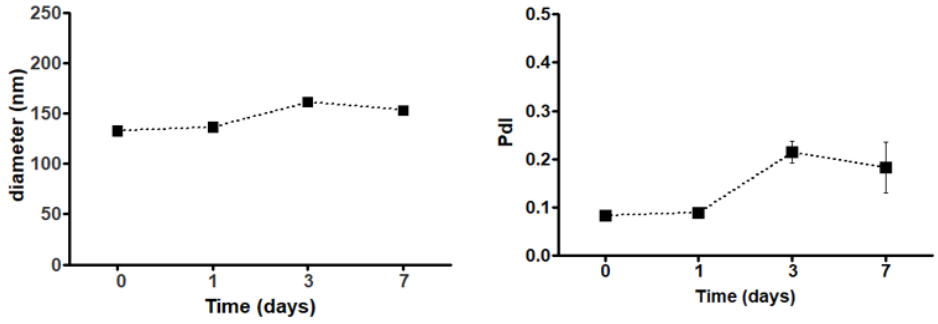

Figure 35. Stability of PECs QA-pullulan/fucoidan loaded with miRNA evaluated by size (left) and PdI (right) measured by Light Scattering as function of time of incubation in water at 4°C (mean ± SD, n = 3).

Finally, the stability of PECs in 0.9% NaCl was evaluated over time. After only 1h of incubation in this medium, DLS measurements showed the presence of large peaks due to the increase in ionic strenght leading to polyplexes destabilization and aggregates formation illustrated by high PdI values (Figure 36).

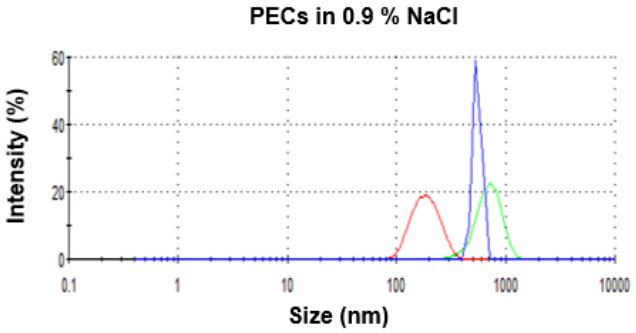

Figure 36. Size distribution from Light Scattering (LS) expressed by intensity percentages of PECs dissolved after 1h incubation in 0.9% NaCl. Data was acquired in triplicate.

Despite the addition of fucoidan into QA-pullulan/miRNA polyplexes contributed to increase the polyplex integrity in water, it was not enough to avoid polyplexes dissociation in a medium with higher ionic strength. Stability issues of polyplexes need to be adressed for its *in vivo* success.

3.3 *In vitro* tests

The cytocompatibility of polyelectrolyte complexes formulated with QA-pullulan and fucoidan was evaluated through an *in vitro* toxicological assay based on resazurin conversion using serum free cell culture medium. *In vitro* tests did not evidence any toxic effect of the PECs after 1 day of incubation up to the maximum tested dose of 200 µg/mL (Figure 37). The dissociation of QA-pullulan from polyplexes after incubation in cell culture medium did not induce any cell toxicity due to the presence of free or weakly bonded polycations. These results are in agreement with our previous results showing that cationic pullulan modified with QA groups is a non-toxic polymer.

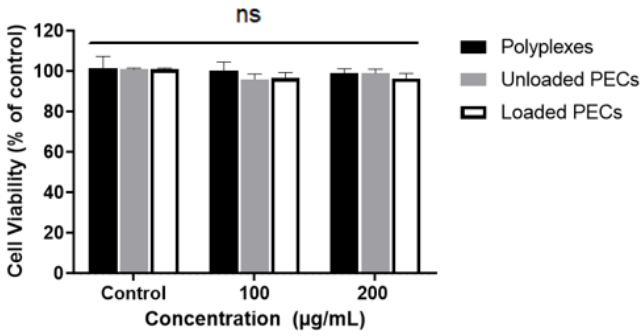

Figure 37. Cytocompatibility of polyplexes, unloaded PECs and loaded miRNA PECs towards HUVECs at 100 and 200 µg/mL after 24h of incubation. Results are shown as mean ± SD from 3 independent experiments with no statistical differences detected using the Wilcoxon matched-pairs signed rank test.

4. Conclusion

Here cationic pullulan derivatives were produced by grafting diethylaminoethylamine (DEAE) groups in pullulan backbone. These derivatives showed to be non cytotoxic in HUVECs up to 1000 µg/mL. When comparing with pullulan derivatives modified with quaternary groups, both DEAE-pullulan and QA-pullulan showed to be able to form polyplexes with miRNA via eletrostatic interactions. The modification of pullulan with DEAE groups did not improve the stability of polyplexes in serum. When fucoidan was incorporated in the formulation to form ternary complexes, their stability was improved up to one week in aqueous media. However, the lack of stability in physiological conditions limited their application and *in vivo* functional validation.

CHAPTER I - DISCUSSION

The aim of the work presented in this chapter was to synthetize cationic pullulan derivatives able to integrate miRNA in nanoparticulate structures via electrostatic interactions between positive amine groups grafted in pullulan backbone and phosphate groups present in miRNA structure. Nanoparticles was further functionalized with fucoidan in order to target P-selectin overexpressed by endothelial cells in cardiovascular diseases.

Pullulan was chosen because it is a non-toxic FDA-approved natural polysaccharide presenting non immunogenic properties with very interesting characteristics for biomedical applications, including gene delivery once cationized. Cationic pullulan derivatives grafted with primary or tertiary amine groups were previously demonstrated to be able to form complexes with high affinity towards both plasmid DNA and siRNA in cationized pullulan-based hydrogels [247,248]. To the best of our knowledge, only one other study used cationic pullulan derivatives (spermine-pullulan) for miRNA delivery [222]. However, as this polycation acquires its positive charge from primary and secondary amino groups, its cationic charge is hence pH dependent and vectors intended for intravenous injection need to be more robust in order to face *in vivo* pH variations.

In the present study, pullulan was grafted with diethylaminoethylamine (DEAE) or glycidyltrimethylammonium (GTMAC) to obtain two types of cationized pullulans at different amine contents. It was possible to obtain a N content ranging from 1.5 to 3.3% (w/w) which corresponds to 1.3 to 2.3 mmol of QA groups per g of polymer (N content from 1.8 to 3.3%) and 1.1 to 1.8 mmol of DEAE groups per g of poymer (N content from 1.5 to 2.5%). Cationic pullulan derivatives with 2.1 mmol/g of DEAE groups was previously demonstrated to complex plasmid DNA [247].

As highly charged cationic polymers can have non-specific interactions with polyanionic biomolecules in the bloodstream leading to the inhibition of many crucial cellular processes and causing severe inflammatory reactions, cytotoxicity of cationic pullulan derivatives was evaluated. When compared to non-modified pullulan, cationic pullulan derivatives did not show any toxicity with increasing concentrations up to 1000 µg/mL. Results are in agreement with the literature in which polysaccharides modified with tertiary and quaternary ammonium groups showed to be non toxic being comparable with unmodified polyssacharides [142,250,267]. Modification of pullulan has made it convenient to be used as gene carrier.

Cationic pullulan derivatives were further employed to prepare polyssacharide-based nanoparticles by the simple polyelectrolyte complexation (PECs) approach. PECs

between oppositely charged polyelectrolytes under sterile conditions provide an easy and versatile synthesis method for the production of nanoparticles avoiding the use of organic solvents or other toxic chemicals. This type of connection is undemanding in terms of directionality and in which the distance between functional groups of opposite charges present the lowest steric requirements of all chemical bonds and the possibility of forming multicentric connections [268]. In addition, assembling miRNA via eletrostatic interactions should facilitate their release after reaching the target, compared to covalent bonds which would be more difficult to break.

When constructing polyplexes with nucleic acids, the molar ratio of nitrogen on polycation to phosphate on miRNA, plays an important role in determining the degree of complexation, particle stability, transfection efficiency, and cytotoxicity [269]. Every polymer has a different optimal N/P ratio that may vary by several orders of magnitude. Typically, a polymer with a higher charge density and molecular weight tends to be more stable and requires a lower N/P ratio for efficient gene delivery [171]. Rekha and Sharma investigated N/P ratios ranging from 0.5 to 5 in order to form polyplexes between cationic pullulan derivatives of 58 kDa modified with GTMAC groups and plasmid DNA [246]. Ma *et al.* prepared pullulan spermine (Ps)-miRNA nanoparticles at N/P ratio of 1.2 [222]. The authors did not specify the Mw of the polymer. In our study, an optimum Mw was found to be between 0.8-1.0. Increasing this value leads to an increase in the size and distribution of nanoplexes probably due to an excess of polycation that did not bind to miRNA.

Anionic fucoidan was then incorporated to the formulation in order to form ternary complexes. Nanoparticles functionalized with fucoidan were shown to be able to target P-selectin expressed by activated platelets [270]. Also, the incorporation of polyanions, e.g. dextran sulfate and hyaluronic acid, in PEC drug formulations has been described to result in more compact and stable polyplexes contributing to increase their stability [94]. Indeed, we showed that polyelectrolyte complexes with fucoidan were more stable (up to one week) than polyplexes merely formed between cationic pullulan and miRNA (stable for 24h).

The increase of the ionic strength, however, had a significant impact on colloidal stability with aggregate formation, and higher PdI values correlated with the heterogeneity of complexes in this medium. Polyplexes formed solely by electrostatic interactions generally possess insufficient stability in physiological conditions due to various characteristics of building components (i.e., concentration and Mw) and environmental

conditions (i.e., pH, temperature, and especially ionic strength) [261]. Especially with regard to *in vivo* applications, polyplex stability becomes an even more important issue, as polyplexes face a much harsher environment in the blood circulation than in cell culture medium [224]. It was reported that the size of chitosan/pDNA polyplexes increased from 100 nm to more than 1 micron after 1 h of incubation in PBS [271]. Several strategies were thought to overcome this limitation and improve the stability of poyplexes in biological fluids including PEGlyation and crosslinking. For example, PEGylation of trimethyl chitosan/miRNA polyplexes increased their serum stability in PBS containing 50% FBS up to 72h [223]. The use of TPP is a classical crosslinking strategy used to improve the quality of electrostatic interaction between chitosan and nucleic acids [124,129]. Zhou *et al.* demonstrated the superior colloidal stability of the covalent conjugate hyaluronic acid (HA)-polyethylenimine (PEI) complex in the presence of serum in comparison to non-covalent polyplex HA/PEI [272].

Then, *in vitro* tests were performed to evaluate cytocompatibility and cellular uptake. The good biocompatibility is a pre requisite for the drug/gene delivery systems. The *in vitro* cytotoxicity of nanoplexes was evaluated by resazurin assays on HUVECs. Results indicated that there was no difference between polyplexes and PECs formulated with fucoidan, as both of them had no cytotoxicity and good biocompatibility.

Finally, miRNA delivery towards HUVECs was evaluated using serum-free medium. One of the most important therapeutic challenges for miRNAs is failing to reach the target cell and tissue, cellular uptake, because of a negative charged backbone, leading to electrostatic repulsion [218]. No miRNA could be detected inside cells in case of administration of free miRNA or unmodified pullulan and miRNA indicating that free miRNA could hardly be internalized by cells. miRNA from polyplexes, in contrast, was clearly incorporated by cells. The strong and difuse green fluorescence from FAM-miRNA indicated the distribution of the polyplexes in the cytoplasm. Similar FAM-miRNA distributions profiles were observed in the literature [130,223]. Chemical modification of vectors, including quaternization, are expected to increase transfection efficiency by modulating complex interactions with cells, such as adsorption on cell surfaces [141]. Similary to our results, effective carriers of DEAE-chitosan showed good transfection activities and low cytotoxicity at low charge ratios (N/P ratios of 2-3) [257]. Ideally, polyplexes should be designed to have a positive surface charge, in order to improve the interaction with the negative phospholipid components of the cell membrane, and to avoid electrostatic repulsion allowing NP internalization. However, this interaction

causes membrane cell damages and may be toxic. Recent evidence proves that anionic NPs can also be effectively internalized by cells suggesting that high positive global net charge for polyplexes is not necessarily a requirement for cell transfection [263,273]. As a result we provided the important insight that in contrast to reported studies, formulations with substantially lower ratios can be formulated and achieve nucleic acid delivery. We believe that this approach can contribute to a rational formulation strategy for the design of pullulan-based miRNA formulations by avoiding the use of polycations in excess, contributing for the development of less toxic and more efficient polyplexes. Nevertheless, these exciting *in vitro* insights need to be corroborated *in vivo* before generalized statements can be made.

CHAPTER I - CONCLUSION

Polyelectrolyte complexes functionalized with fucoidan were developed here for miRNA delivery using biocompatible cationic pullulan derivatives. Neither toxic reagent nor harsh conditions of preparation were used, this way avoiding any possible damage to miRNA during the complexation. Extensive characterization was achieved with known size, zeta potential, morphology and miRNA loading. Chemical and physical stability of polyplexes were studied in aqueous solution and in the presence of serum. Despite good stability in aqueous medium, an increase in the ionic strenght leads to polyplexes instability, which was reflected by the high PdI values of polyplexes when incubated in 0.9% NaCl. Colloidal stability of nanoparticles in complex physiological media is demanded for systemic administration of miRNAs. In the previous investigations the colloidal stability of the polyplexes in physiological conditions was not fully addressed. However, it should be highlighted that our method was developed without the use of any crosslinking agent. The obtained nanoparticles proved to be non-cytotoxic on HUVECs after 1 day of incubation and was able to promote *in vitro* miRNA delivery. Biological evaluation is necessary to evaluate the reduction of targeted miRNA levels relative to appropriate controls. With further formulation optimizations and experiments proving the efficacy of the systems, these PECs could represent an interesting platform for miRNA-based therapeutics for cardiovascular diseases.

3.2 CHAPTER II

Biospecific polysaccharide-based nanogels crosslinked with genipin for miRNA delivery

Introduction

In the first chapter, we demonstrated that cationic pullulan derivatives modified with both tertiary amine and quaternary ammonium groups showed to be able to form polyelectrolyte complexed nanoparticles with anionic miRNA via electrostatic interactions. However, the stability of these complexes under physiological conditions largely limited their application as small nucleic acids delivery systems.

Hence, in order to increase the stability of the complexes, a crosslinking agent was added to the formulation. Genipin, a natural crosslinking agent able to make bridges between primary amine groups containing materials was chosen to improve the stability of the complexes in physiological conditions without impairing their cytocompatibility.

Briefly, we developed a new synthesis protocol to produce crosslinked cationic pullulan-based nanogels entirely performed in aqueous media using genipin. For this purpose, pullulan derivatives modified with primary amine groups were produced and characterized. Then, the formation of polyelectrolyte complexes between cationic pullulan derivatives bearing primary amines and fucoidan was optimized. Next, genipin was incorporated to the formulation in order to produce nanosized crosslinked polysaccharide-based polyelectrolyte complexes. They were fully characterized regarding their physicochemical properties, stability and cytocompatibility towards endothelial cells. Their capacity to aim at human activated platelets was demonstrated.

Finally, we presented the results of miRNA loading into the developed nanogels. Under acid conditions, it was possible to modulate their surface charge allowing miRNA loading via electrostatic interactions with primary ammonium. Although these nanosystems were able to penetrate into endothelial cells, further experiments remain to be performed to evaluate their potentiality as nanotherapeutics, i.e., if the loaded miRNA induces a proper biological response once inside the cell.

This work has been published in International Journal of Pharmaceutics.

Chapter II

Publication in International Journal of Pharmaceutics, 2021,

doi: 10.1016/j.ijpharm.2021.120302 (the PDF proof is provided in annex 6):

P-selectin targeting polysaccharide-based nanogels for miRNA delivery

Fernanda C. Moraes, Laura Marcela Forero Ramirez, Rachida Aid, Samira Benadda, Murielle Maire, Cédric Chauvierre, Joana C. Antunes, Frédéric Chaubet, Didier Letourneur

Keywords: Genipin crosslinking; Pullulan; Nanogels; Fucoidan; P-selectin; miRNA

Graphical abstract

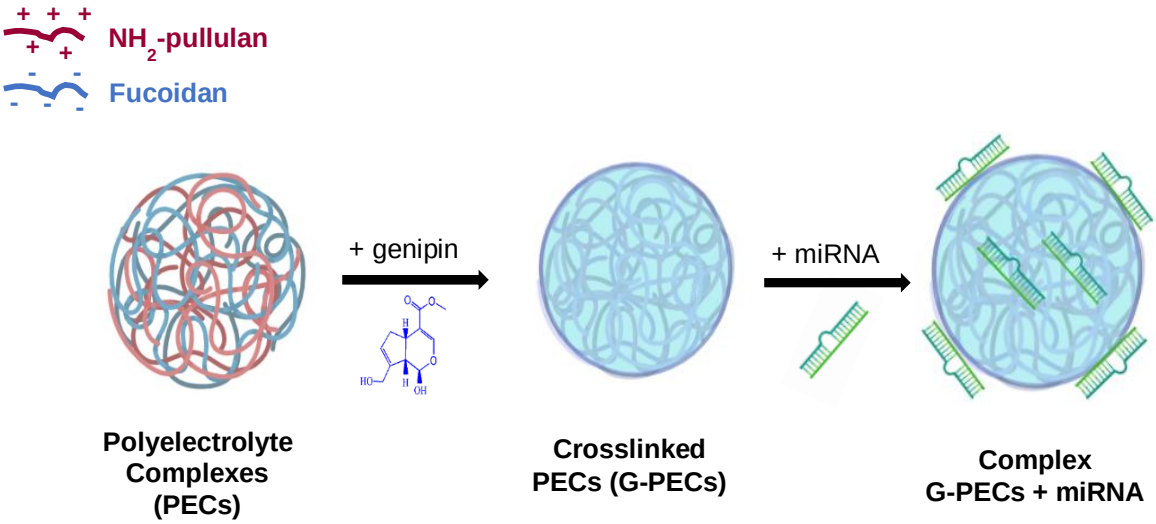

Abstract

Nanogels were prepared in aqueous media without the use of any organic solvent via a simple polyelectrolyte complexation method between aminated pullulan and fucoidan followed by covalent crosslinking with genipin. Homogeneously distributed genipin crosslinked nanogels (G-PECs) were obtained with a mean hydrodynamic diameter of 155.9 ± 9.72 nm and zeta potential of 0.86 ± 4.35 mV. Their capacity to bind to human activated platelets was evaluated *in vitro*, as well as their cytocompatibility within human endothelial cells after 1 day of incubation up to 1000 µg/mL of G-PECs (94.56 ± 7.82% of viable cells). Additional hemolysis tests support the biocompatible character of the developed nanosystems (hemolysis rate of 2.09 ± 0.06% for 1000 µg/mL of G-PECs). Under acid conditions, the surface charge of G-PECs was tuned to around ~10 mV allowing miRNA incorporation via electrostatic interactions. G-PECs were able to promote miRNA delivery inside cells, as demonstrated by fluorescence microscopy images of labelled miRNA. With further studies to demonstrate the biological activity of delivered miRNA, these nanogels could be an interesting platform for miRNA-based therapeutics in atherothrombotic-related diseases thanks to the possibility to target over-expressed P-selectin.

1. Introduction

In the past few years, small non-coding microRNAs (miRNAs) have emerged as key regulators of gene expression and are some of the most important biopharmaceuticals candidates as future medicines due to their multiple unique features and advantages when compared to conventional plasmid DNA (pDNA)-based therapy [154,155]. RNA therapeutics do not have the risk of genomic integration, do not need to cross the nucleus membrane to their function, and are expressed instantaneously [156,157,197]. They play important roles in many cellular processes and have been investigated as therapeutics and biomarkers for various diseases such as cancer, diabetes, cardiovascular diseases and other pathologies whose etiology is related to aberrant gene expression [159,216,237–240]. However, unfavorable physicochemical features of miRNAs such as their anionic charge, sensitivity to nuclease degradation, and inefficient cellular uptake are major hindrances for their clinical application. The success of miRNA-based therapies relies on the development of suitable vehicles able to specifically target cells for the efficient delivery of the nucleic acid with minimum toxicity [154,207].

Recently, nanogels have arised as a class of interesting polymeric materials for the delivery of biopharmaceuticals because of their hydrophilic three-dimensional macromolecular networks that allow a high loading capacity for hydrophilic biotherapeutics, protecting the loaded molecules against degradation. Additionally, they possess stimuli-responsive behavior potential and can participate in versatile drug release protocols [66,113,158]. Nanogels can either be composed of natural or synthetic polymers and may contain more than one type of polymer [274]. Cationic polymers are widely used in gene therapy applications since they form interpolyelectrolyte complexes with nucleic acids through ionic interactions with their negatively charged phosphate groups [141,202,216,275]. Polymers derived from natural sources are preferable because they are naturally biocompatible, biodegradable and nontoxic, and can overcome the cytotoxicity associated with the use of several synthetic polymers, which do not satisfy the requirements for clinical applications.

Pullulan is a natural water-soluble homopolysaccharide produced by the fungus *Aureobasidium pullulans* considered as a promising material for biomedical applications such as drug/gene delivery and tissue engineering because of its inherent non-toxic, non-immunogenic, and biodegradable characters [245]. Charged hydrophilic derivatives of

pullulan provide the possibility to formulate nanoparticles via electrostatic interactions with oppositely charged materials of interest [49]. Electrostatic interactions between oppositely charged polymers are becoming an interesting alternative to produce nanogel systems. Since the polyelectrolyte complexation method can be performed in aqueous media, this process is environment-friendly and does not require the use of organic solvents which is interesting for pharmaceutical applications [138].

Cationic pullulan derivatives grafted with primary or tertiary amine groups were previously demonstrated to be able to form complexes with plasmid DNA as well as siRNA in cationized pullulan-based hydrogels [247,248]. In previous work from our group, we demonstrated the feasibility of quaternized cationic pullulan (QA-pullulan) nanosized polyelectrolyte complexes (PECs) for *in vitro* miRNA delivery [276]. To the best of our knowledge, it was the first time that QA-pullulan was used to build miRNA delivery nanosystems. However, in this study, the colloidal stability of the developed nanosystems in physiological conditions was not addressed. One of the major drawbacks associated with the use of PECs is the lack of stability in physiological conditions due to the presence of electrolytes and changes in pH values responsible for a decrease in the charge density of polyions [261]. Especially with regard to *in vivo* applications, PECs´ stability becomes an even more important issue, as they face a much harsher environment in the blood circulation than in cell culture media [224].

Chemical crosslinking is an effective approach to stabilize PECs upon the formation of permanent networks allowing the free diffusion of water and enhancing the mechanical properties of the nanogels [121]. However, the majority of crosslinking agents used are synthetic reactants (e.g. glutaraldehyde) that are highly cytotoxic often impairing the biocompatibility of crosslinked products [277]. Hence, many investigations have focused on finding suitable crosslinking agents for use in biomedical applications. Genipin is an alternative natural crosslinking agent extracted from the fruit of *Gardenia jasminoides* Ellis that is commonly used in herbal medicine and as a food dye [121,278,279]. It can spontaneously react with materials containing primary amine groups, such as chitosan and some peptides and polypeptides, to form covalently crosslinked networks. Genipin is described to be 10,000 times less cytotoxic than glutaraldehyde being a great promise for the preparation of biocompatible crosslinked materials [280]. A few researchers used genipin to crosslink chitosan nanoparticles improving their physical and chemical

stability with good biocompatibility profile [127,128,278]. To the best of our knowledge, no report of nanogel made from pullulan derivatives crosslinked with genipin exists.

Here we propose a simple miRNA delivery system based on two polyelectrolytes derived from naturally occurring, highly biocompatible polysaccharides, pullulan and fucoidan, which instantly and spontaneously self-assembly to form nanosized hydrogels. A cationic pullulan derivative was first obtained by grafting primary amine groups. The addition of genipin produced nanosized hydrogels with high colloidal stability. Then, their functionalization with fucoidan confered them the ability to target P-selectin, an adhesion molecule over-expressed at the surface of activated platelets and endothelial cells in atherothrombotic-related diseases [34]. The capacity of these novel polysaccharide-based PECs to cargo nucleic acids, in particular miRNA, into endothelial cells was investigated.

2. Materials and Methods

2. 1 Materials

Pullulan (Mw 200 kg/mol) was purchased from Hayashibara Company (Okayama, Japan). 2-chloro-ethylamine hydrochloride (Mw 115.99 g/mol) was purchased from Sigma-Aldrich (St. Louis, MO, USA). Fucoidan low molecular weight (Mw 7 kg/mol) was a gift from Algues & Mer (île d'Ouessant, France). Carboxymethyl-dextran (Mw 10 kg/mol) was purchased from Sigma-Aldrich (St. Louis, MO, USA). Genipin (CAS number 6902-77-8) was purchased from TCI chemicals (Chennai, Tamilnadu, India). Dialysis membranes of 20 kDa was purchased from Spectrum Laboratories (New Brunswick, NJ, USA). Chemically modified, double-stranded RNA oligonucleotides from Qiagen were used to mimic the natural human mature microRNA miR-155-5p (miRNA sequence: 5'-UUA AUG CUA AUC GUG AUA GGG GU-3'). Single-stranded miRNA and 6-Fluorescein AMidite (6-FAM)-miRNA scramble oligonucleotides with 23 bp of length (RNA sequence: 5′-UUA AUG CUA AUC GUG AUA GGG GU-3′) were purchased from Sigma-Aldrich (Saint Quentin Fallavier, France). Sequences were reconstituted in RNase-free water to achieve a final concentration of 20 μM and stock solutions were stored at −20 °C. Ultrapure water was prepared by ion-exchange of running tap water (Millipore, France).

2.2 Synthesis of cationic pullulan derivatives

Pullulan (1 g) was dissolved in 5 mL of distilled water. The solution was placed at 4°C until complete solubilisation of pullulan. Then, 5 mL of soda (6.2 M NaOH) was added to activate the hydroxyl functions. The solution was kept at 4°C under magnetic stirring for 20 min followed by the addition of 1.43 g of 2-chloro-ethylamine hydrochloride (2 equivalents per AGU). The solution was placed under magnetic stirring at 55°C for 3 h. The mixture was placed at room temperature and the pH was adjusted to 7 with 37% hydrochloric acid (HCl) solution. The mixture was dialyzed with a 20 kg/mol membrane and freeze-dried before characterization. Final product was named as ethylamine-pullulan (EA-pullulan).

2.3 Synthesis of fluorescent cationic pullulan

Ethylamine-pullulan (500 mg) was dissolved in anhydrous DMSO. Few drops of pyridine were added, followed by the addition of 500 µL of Rhodamine B isothiocyanate (RBITC) solution (100 mg RBITC dissolved in 1 mL of DMSO) and 10 µL of dibutyltin dilaureate. The reaction was performed for 2h at 95°C under inert atmosphere using nitrogen. The grafted polysaccharide was recovered by cooled precipitation (4°C) in absolute ethanol. Final product was freeze-dryer before use.

2.4 Chemical characterization of modified pullulan

2.4.1 Elemental analysis

The weight percentages of N of pullulan and cationic pullulan derivatives were determined using a combustion method with catharometric detection (CHNS Vario EL III, Elementar Analyzer). Degree of substitution of primary amine groups was estimated by elemental analysis of nitrogen.

2.4.2 Size exclusion chromatography equipped with multi-angle light scattering (SEC-MALS)

Apparent molecular weight-average (M_w) and number-average molecular weight (M_n) were determined by size exclusion chromatography (SEC) coupled online to a multiangle laser light scattering (MALLS) detector. The SEC line consisted of an TSK-Gel PW_{XL} Guardcolumn and TSK-Gel $GMPW_{XL}$ in series (Tosoh Bioscience, Stuttgart, Germany). The eluent was 0.2 M $NaNO_3$ containing 0.02% w/v NaN_3 at 0.5 mL/min flow rate. The

samples were dissolved in the eluent at a concentration of 10 mg/mL. The dn/dc used in the molecular weight distribution calculations were 0.14. The collected data were analysed using the software Astra V-4.81.05.

2.4.3 NMR spectroscopy

^{1}H- NMR spectra was recorded with a Bruker-400 Ultrashield operating at 400 MHz. Polymers samples were prepared in D_2O in a concentration of 20 mg/mL.

2.5 Synthesis of polyelectrolyte complexes and crosslinked nanoparticles

Cationic pullulan derivatives containing primary amine groups (EA-pullulan) were dissolved in 1% acetic acid at a final concentration of 1.0 mg/mL and the pH of the solution was adjusted to pH 5 using 10 M NaOH. Low molecular weight fucoidan was dissolved in distillated water at 0.25 mg/mL. Polyelectrolytes complexes (PECs) were produced by dropping 2 mL of fucoidan over 2 mL of EA-pullulan under high magnetic stirring at room temperature. Crosslinked PECs (G-PECs) were produced by adding 1 mL of genipin at 1.25 mg/mL to polyelectrolyte solution. The mixture was placed under moderate magnetic stirring (250 rpm) for 48h at room temperature. G-PECs were recovered by ultracentrifugation at 15,000 g during 20 min at 21°C.

2.6 Characterization of crosslinked nanoparticles

2.6.1 Size and zeta potential measurements

Particle size and zeta potential of nanoparticles were measured by Dynamic Light Scattering (DLS) and Electrophoretic Light Scattering (ELS) using a Zetasizer Nano-ZS (Malvern Instruments, Malvern, UK) respectively. Size and zeta potential measurements were performed at 25°C using a 173° and 13° scattering angle for size and zeta potential measurements, respectively, equipped with a 4 mW HeNe laser beam with a wavelength of 633 nm. Size and ζ potential values were automatically calculated through the software DTS Nano v.6.30 (Malvern, UK) using the Stokes-Einstein equation and the Henry equation with the Smoluchowski approximation, respectively. Size measurements were performed in water using disposable polystyrene cuvettes and zeta potential measurements were performed in 1mM KCl solution using a DTS1070-folded capillary cell (ELS, Malvern, UK). Data were acquired in triplicate.

2.6.2 Nanoparticles concentration

Nanoparticle concentration was assessed by Tunable Resistive Pulse Sensing (TRPS). TRPS technology measures nanoparticles suspended in electrolytes on a particle-by-particle basis as they pass through a nanopore. To perform TRPS analysis nanoparticles were isolated by ultracentrifugation and redispersed in 0.9% NaCl.

2.6.3 Morphology

Transmission Electron Microscopy and Environmental Scanning Electron Microscopy were employed to assess the morphology of crosslinked PECs.

Transmission Electron Microscope (TEM) was performed in a Tecnai 12 (80 kV; FEI; Hillsboro, OR, USA) with a 1K x 1K KeenView camera (OSiS). Samples were prepared by placing 3 μL of G-PECs suspension onto a 400 μL mesh copper grid coated with carbon (EMS). Uranyl acetate 1% (w/v) was used for negative staining.

Environmental Scanning Electron Microscopy (ESEM) was performed using a Philips XL30 ESEM-FEG (Amsterdam, The Netherlands) in aqueous media with no special sample preparation.

2.6.4 Fourier transform infrared spectroscopy (FTIR)

FTIR spectroscopy was carried out with KBr pellets on a Thermo-Nicolet-AVATAR 370 FTIR (Thermo Electron Corporation, Waltham, MA). A first pellet with 200 mg of KBr was prepared. Then, pellets were made using 200 mg KBr and 2 mg of sample. A 32-scan interferogram was collected in transmittance mode. Scans were taken from 400 cm^{-1} to 4000 cm^{-1} at a resolution of 2 cm^{-1}. The spectrum of KBr pellet was used as background.

2.6.5 Swelling behavior

The swelling behavior of nanoparticles was determined by incubating them in either NaCl 0.9%, PBS 1x or distilled water, solutions with different ionic strengths. Their hydrodynamic diameter was measured by DLS.

2.6.6 Stability of nanoparticles

The stability of crosslinked polyelectrolyte complexes was evaluated over time while stored at 4ºC in water or 0.9% NaCl solution. Size, PdI (Polydispersity Index) and surface

charge evolutions were monitored by DLS and ELS (n= 3) at each time point up to 28 days of storage.

2.6.7 Freeze-drying nanoparticles

With the aim of developing a pharmaceutically acceptable dry form of the nanoparticle suspensions, nanoparticles were submitted to a freeze-drying study. Samples were freeze-dried in MUT (Cryotec®) in three steps. First, samples were frozen until -20ºC at -0.1°C/min. Then, the primary drying was performed under 5Pa and gradually increasing of temperature in two phases until reaches 10°C (+0.1°C/min until -5°C during 8h and +0.2°C/min until 10°C during 4h). Finally, secondary drying was performed at 25ºC and 0.1Pa for at least 1h. After the freeze-drying procedure, nanoparticles were resuspended by adding the volume of water corresponding to the initial volume of nanoparticles (1 ml), and their size was assessed by DLS measurements.

2.6.8 Cytotoxicity assays

Cytotoxicity was evaluated on Human Umbilical Vein Endothelial Cells (HUVECs, ATCC CRL-1730, Manassas, VA, USA) by resazurin conversion assay (Sigma-Aldrich, Saint Louis, MO, USA). Cells were seeded at a concentration of 10,000 cells/well onto 96-well plates in Dulbecco's Modified Eagle Medium (DMEM) (Thermo Fisher Scientific, Carlsbad, CA, USA) supplemented with 10% (v/v) of fetal bovine serum, 1% (v/v) of penicillin and 1% (v/v) of streptomycin in a humidified atmosphere with 5% CO_2 at 37°C. At a subconfluent to confluent stage, cells were detached with 0.05% trypsin/EDTA (Gibco) and re-seeded until the required number of cells for the subsequent experiments was obtained. Cell metabolic activity was assessed after different culture conditions by resazurin conversion. Cells were incubated with medium containing 10% resazurin for 2 hours at 37°C. Fluorescence intensity (530nm/590 nm) of the cell culture supernatants was measured with an Infinite® 200 PRO microplate reader (TECAN Group Ltd., Männedorf, Switzerland). A blank control comprising only medium was also included. Bright field images (EVOS™ XL Core Cell Imaging System, Thermo Fisher Scientific, Carlsbad, CA, USA) were taken during culture to monitor cell morphology.

2.6.9 Hemolysis test

The blood compatibility of crosslinked polyelectrolyte complexes was evaluated by hemolysis tests on human red blood cells (RBC). In brief, the anti-coagulated blood was

centrifuged at 800g at 4°C for 10 min. Then, the erythrocytes pellet was incubated with different concentrations of nanogels (250, 500 and 1000 µg/mL). Water and PBS 1x were used as positive and negative controls, respectively. The resulting mixtures were incubated at 37°C for 2h and centrifuged at 3,000g at 4°C for 10 min. The absorbance of the supernatant solution of the test sample (Atest), positive control (Apos), and negative control (Aneg) at 540 nm was determined by UV–Vis spectrophotometry. Each set of experiments was carried out three times and the hemolysis (%) was calculated by the formula = [(Atest−Aneg)/ (Apos−Aneg)] × 100%.

2.6.10 Cell internalization

Human Umbilical Vein Endothelial Cells (HUVECs, ATCC CRL-1730, Manassas, VA, USA) cells were seeded at a concentration of 8,000 cells/well onto Nunc™ Lab-Tek™ chamber slides (Thermo Fisher Scientific). Fluorescent labelled pullulan derivatives was used to produce crosslinked polyelectrolyte complexes for cell internalization assays. After 24h of incubation using serum supplemented cell culture medium, cells were washed with PBS and fixed with fresh 4% paraformaldehyde. Cytoplasm was stained with FITC-phalloidin (Invitrogen) (dilution 1/200 on PBS from stock at 1 mg/mL) and cell nucleus was stained with 4',6-DiAmidino-2-PhenylIndole (DAPI) (dilution 1/50 000 in PBS from stock at 5 mg/mL) (Sigma Aldrich, St. Louis, MO, USA). Coverslips were mounted using Ibidi Mounting Medium (IMM) for fluorescence microscopy (ibidi GmbH, Germany). Confocal images were taken to evaluate nanoparticles internalization (Microscope Confocal Zeiss LSM 780, Germany).

2.6.11 Targeting assays

The interaction of genipin crosslinked NPs with P-selectin was evaluated *in vitro* as previously reported [281]. Briefly, micro-channels of Vena8 Fluoro+ chambers (Cellix Ltd, Dublin, Ireland) were coated overnight with 50 µg/mL of collagen and then washed with NaCl 0.9%. Human whole blood labeled with DiOC6 (a green fluorescent dye) was perfused under arterial flow conditions for 5 min to induce platelet activation and aggregation on the collagen-coated channel. Rhodamine labeled G-PECs at 1mg/mL in NaCl 0.9% were then perfused during 5 min. Their accumulation onto preformed platelet aggregates was monitored in real time by fluorescence microscopy (Axio Observer, Carl Zeiss Microscopy, Oberkochen, Germany). Fluorescence images were taken along each

micro-channel after washing with NaCl 0.9%. G-PECs formulated with carboxymethyl-dextran were used as negative control.

2.7 miRNA loading and characterization

2.7.1 miRNA loading

Loaded G-PECs nanogels were produced by adding 1 mL of miRNA solution (0.04 mg/mL) to 1 mL of nanoparticle solution at 1 mg/mL (N/P ratio 10) redispersed in 1% acetic acid solution (pH 3) or ultrapure water (pH 7). Nanoparticles were placed at 4°C during 30 min for stabilization. Then, ultracentrifugation at 15,000 g during 20 min at 4°C was performed to remove the free or poorly adsorbed miRNA. The entrapment efficiency (EE) of miRNA into G-PECs, was determine by UV spectrophotometry using NanoDrop™ 2000/2000c Spectrophotometer (Thermo Fisher Scientific, Wilmington, DE, USA) by measuring the concentration of free miRNA in the supernatant. The entrapment efficiency was calculated as EE% = (miRNA initially added − miRNA in the supernatant/miRNA initially added) × 100%.

2.7.2 Presence of miRNA within loaded G-PECs

The presence of the miR-155-5p was monitored by agarose gel electrophoresis (AGE). Agarose gel electrophoresis was perfomed using 5% agarose gels containing ethidium bromide in TBE (Tris-Borate-EDTA, Thermo Fisher Scientific, Vilnius, Lithuania) buffer. An Ultra-Low Range GeneRuler DNA Ladder (10–300 bp; Thermo Fisher Scientific, Bleiswijk, Netherlands) was used to monitor miRNA presence. Samples included solution of unloaded G-PECs, plus additional controls from different steps of the miRNA loading: miRNA alone (at the concentration used for loading), loaded G-PECs before ultracentrifugation, loaded G-PECs after ultracentrifugation and the supernatant of loaded G-PECs after ultracentrifugation. Samples were run by electrophoresis (50 V, 120 min) and detected through a UV transilluminator (Vilber Lourmat smart imaging system, Collegien, France).

2.7.3 miRNA release

To assess miRNA release from nanogels, the loaded G-PECs were resuspended in PBS and subjected to strong orbital shaking at 250 rpm at 37°C. At each time point (15 min, 30 min, 1 hour, 3 hours and 6 hours), G-PECs were centrifuged (15,000 g, 20 min, 4°C) and the supernatant was separate to quantify released miRNA by UV spectrophotometry

using NanoDrop™ 2000/2000c Spectrophotometer (Thermo Fisher Scientific, Wilmington, DE, USA).

2.7.4 miRNA delivery

Human Umbilical Vein Endothelial Cells (HUVECs, ATCC CRL-1730, Manassas, VA, USA) cells were seeded at a concentration of 8,000 cells/ well onto Nunc™ Lab-Tek™ chamber slides (Thermo Fisher Scientific) and grown for 48 h. Loaded G-PECs nanogels were prepared as previously described using scramble FAM-miRNA. After 2h of incubation using serum-free supplemented cell culture medium, cells were washed with PBS and fixed with fresh 4% paraformaldehyde. Cell nucleus was stained with 4′,6-DiAmidino-2- PhenylIndole (DAPI) (Sigma Aldrich, St. Louis, MO, USA). Coverslips were mounted using Ibidi Mounting Medium (IMM) for fluorescence microscopy (ibidi GmbH, Germany). Fluorescence images were taken to evaluate miRNA delivery (Axiovert Observer Z1 inverted microscope, Zeiss, Germany).

2.7.5 Cellular uptake analysis by flow cytometry

HUVECs were seeded on a 24-well plate at a density of 50,000 cells/well and incubated overnight in 500 µL of DMEM containing 10% FBS. Then, the cells were incubated with 500 µL of G-PECs nanogel/miRNA solution at 1 mg/mL containing 5 nmol of scramble fluorescein-labeled miRNA. After incubation for 2 h, the medium was removed and the cells were washed with phosphate buffer saline (PBS). The cells were then trypsinized and collected by centrifugation (1500 rpm, 4 °C, 5 min). Finally, the cells were suspended in 200 µL of PBS. Flow cytometric analysis was carried out using LSRII flow cytometer (BD Biosciences, Le Pont de Claix, France). The mean fluorescence intensity (MFI) of fluorescein was measured for each condition. Naked FAM-miRNA was used as negative control.

2.8 Statistical analysis

The data were expressed as mean ± SD (standard deviation). Statistical analysis was performed using GraphPad Prism (version: 5.0a, San Diego, CA, USA). Since data followed a non-parametric distribution, Wilcoxon matched-pairs test was performed to compare each paired group and p smaller than 0.05 was considered statistically significant.

3. Results and Discussion

3.1 Synthesis and characterization of cationic pullulan derivatives

In this work, cationic pullulan/fucoidan nanoparticles were prepared in a two-step procedure based on polyelectrolyte complexation followed by polycationic crosslinking through the addition of genipin which forms bridges between primary amines [280]. Cationic pullulan derivatives with primary amine groups were prepared by substitution of hydroxyl groups from pullulan with chloroethylamine in basic aqueous media (Figure 48) [276].

Successful introduction of amine moieties was confirmed by elemental analysis of nitrogen content (%N) and ^{1}H-NMR spectroscopy (see Figure 49 and Figure 50 in supplementary data). It was possible to synthetize derivatives with N content of 1.60 ± 0.05% N (1.18 mmol/g) and monomodal molecular weight distributions (PdI of 1.6) in two synthesis steps using a molar feeding ratio of 2 equivalents (mol amine/mol OH) of chloroethylamine (Table 11). San Juan *et al.* obtained a similar N content of 1 mmol/g for 40 min of reaction at 55°C to modify pullulan but using a feeding ratio of 8 equivalents of bromoethylamine [247]. We found that in order to get higher degree of substitution (DS), the reaction should be performed once more on the substituted derivatives rather than increasing the quantity of ethylamine (see Table 14 and Table 15 in supplementary data).

Table 11. Characterization of cationic pullulan derivative with primary amine groups.

Amine	Feeding[a]	M_n[b] (kDa)	M_w[b] (kDa)	PdI[b]	N[c] (%)	DS[d]
No amine (pullulan)	0	113	298	2.6	0	0
EA-pullulan	2	178	298	1.6	1.60 ± 0.05	0.20

[a] Feeding: $mol_{amine}/mol_{hydroxyl\ groups}$; [b]Measured by SEC-MALLS; [c]Calculated from nitrogen elemental analysis; [d]Degree of substitution calculated per anydroglucose unit

3.2 Crosslinking of polyelectrolyte complexes nanoparticles

PECs formed merely by electrostatic interactions are known to have limited stability in physiological media. To obtain nanogels with interesting characteristics, the use of covalent crosslinkers is necessary. Crosslinked PECs (G-PECs) were produced by using genipin as crosslinking agent in a two steps process.

First, PECs of EA-pullulan and fucoidan were prepared by simple dropping process and their physicochemical properties were studied without covalent crosslinking. PECs are formed using very diluted solutions and the effect of pH and mass ratio between polyelectrolytes was investigated. As the charge of primary amines (-NH_2) from EA-pullulan derivatives are dependent on the pH (Figure 52), four different pH settings were selected in order to obtain polymer solutions with different charges during the formation of the PECs. As expected, increasing the pH values of polycations solution lead to an increase in the size of polyplexes, PdI values and a decrease in zeta potential due to to the lower number of positively charged groups from EA-pullulan (Table 12).

Table 12. Effect of pH on PECs formation by mixing EA-pullulan (0.2 mg/mL) and fucoidan (0.2 mg/mL). Results are expressed as mean ± SD (n=3).

pH	Size (nm)	PdI	ʃ-potential (mV)
pH 2	181.53 ± 17.17	0.120 ± 0.00	-2.02 ± 4.93
pH 3	130.23 ± 29.52	0.156 ± 0.01	-4.29 ± 3.79
pH 5	205.46 ± 38.94	0.123 ± 0.02	-5.49 ± 5.55
pH 6	472.26 ± 59.01	0.213 ± 0.01	-8.36 ± 5.28

As it was possible to form PECs in the nanometric range and with nice distribution at pH values up to 5, this value was thus selected. The effect of mass ratio between polyelectrolytes was evaluated by keeping constant the concentration of the polycation. PECs prepared with lower concentrations of fucoidan showed increased size values and PdI, probably due to lower contribution of the polyanion counterpart to form compacted PECs. Interestingly, it should be noted that by varying the polymer ratios, it was possible to modulate zeta potential values of PECs. Decreasing the concentration of fucoidan in PECs formulation led to a decrease in zeta potential values (Table 13).

Table 13. Effect of EA-pullulan/fucoidan mass ratio on PECs formation. Results are expressed as mean ± SD (n=3).

pH	EA-pullulan (mg/mL)	Fucoidan (mg/mL)	EA-pullulan/fucoidan mass ratio	Size (nm)	PdI	ζ-potential (mV)
		0.50	1/2	109.6 ± 10.2	0.155 ± 0.08	-3.75 ± 5.82
		0.34	1/3	141.8 ± 25.3	0.138 ± 0.12	-2.47 ± 4.33
pH 5	1.0	0.25	1/4	150.9 ± 8.92	0.142 ± 0.03	0.51 ± 2.76
		0.20	1/5	181.7 ± 14.7	0.098 ± 0.08	4.25 ± 4.98
		0.10	1/10	251.6 ± 6.07	0.215 ± 0.01	4.06 ± 0.53

Then, genipin was added to a solution of EA-pullulan (1.0 mg/mL) and fucoidan (0.25 mg/mL) at pH 5 to get G-PECs. The crosslinking reaction was monitored by the appearance of blue coloration in the reaction mixture. After 48h of reaction, particles were isolated by ultracentrifugation at 15,000 g for 20 min.

The crosslinking reaction occurs by mean of a complex mechanism, which consists in two reactions involving different sites on the genipin molecule. The first reaction is a nucleophilic attack of the genipin C3 carbon atom from a primary amine group to form an intermediate aldehyde group. The opening of the dihydropyran ring is then followed by attack on the resulting aldehyde group by the secondary amine formed in the first step of the reaction. A heterocyclic compound of genipin crosslinked to the primary amine groups of EA-pullulan is thereby formed (Figure 38C) [280,282].

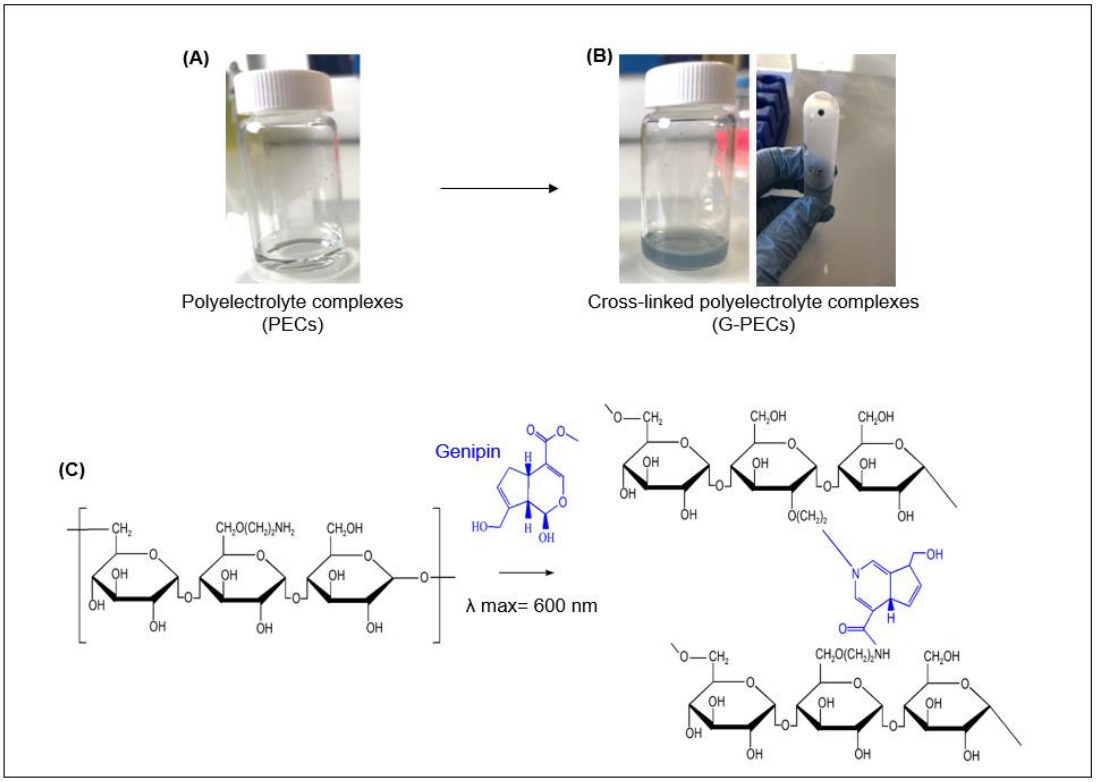

Figure 38. Polyelectrolyte complexes nanoparticles of EA-pullulan and fucoidan: (A) before crosslinking, (B) after crosslinking with genipin and (C) schematic representation of crosslinking bridges between genipin and primary amine groups of EA-pullulan.

The crosslinking reaction in function of time and temperature was monitored by UV–Vis spectroscopy by the apparition of a blue color (λ max= 600 nm). Genipin-crosslinked PECs gradually turned from uncolored solution into a light blue colored one within 48h (Figure 39). Several studies with chitosan reported that a crosslinking reaction time of 2h was enough to produce nanoparticles without specifying the temperature [128,283,284]. Razi *et al.* performed the crosslinking reaction with genipin during 24h at 30°C to produced chitosan crosslinked nanoparticles [127]. In the work of Pujana *et al.* the crosslinking reaction was carried out for 4 days at 25ºC using W/O microemulsions to produce chitosan nanogels [285]. Our protocol of 48h of reaction was performed at room temperature and can be decreased to 6h by increasing the temperature to 50°C while keeping nanoparticles characteristics.

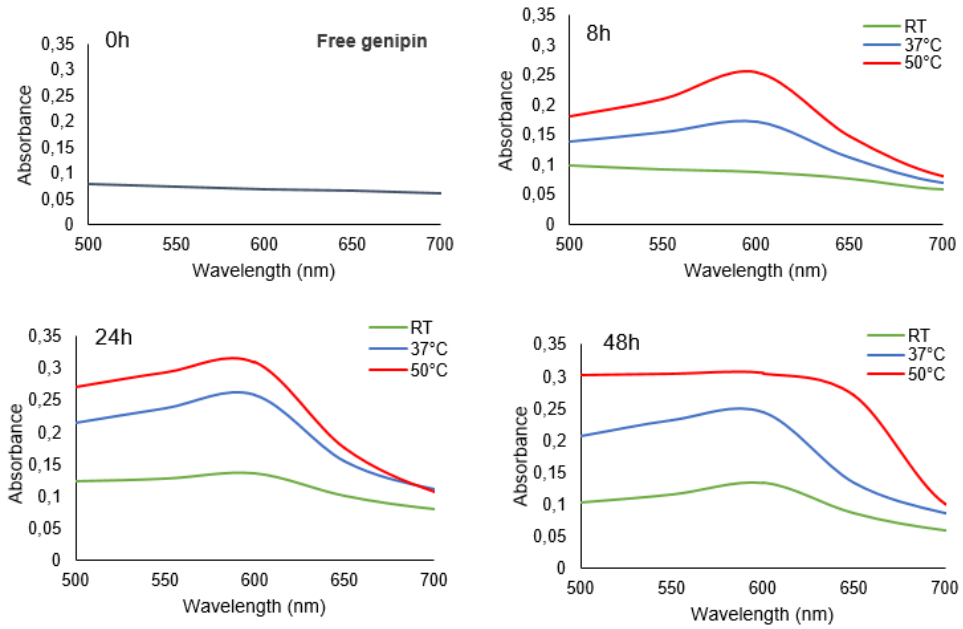

Figure 39. Absorption spectra of free genipin and genipin crosslinked PECs (G-PECs) at different temperatures (room temperature, 37°C and 50°C) over time (0h, 8h, 24h, 48h).

Different concentrations of genipin were evaluated (0.125 mg/mL, 0.25 mg/mL, 0.50 mg/mL). Both the low (0.125 mg/mL) and high (0.50 mg/mL) concentration of genipin produced nanoparticles after 48h treatment, indicating that highly crosslinked PECs could be obtained even from a low genipin concentration (Figure 54). Since the concentration of 0.25 mg/mL allowed the production of nanoparticles with a diameter lower than 200 nm with low PdI this concentration was selected for all further experiments.

Crosslinked PECs were comprehensively characterized by size, surface charge, polydispersity, morphology and swelling properties (Figure 40). Crosslinked nanoparticles exhibited a size of 155.9 ± 9.8 nm in water with zeta potential value of 0.86 ± 4.35 mV. The presence of fucoidan in G-PECs was confirmed by elemental analysis (7% w/w of the total nanoparticles weight) (Figure 40C). No notable differences in particle size and zeta potential were observed between PECs and G-PECs, suggesting that interpolyelectrolyte structures remained unaffected by the crosslinking process. FTIR spectroscopy was employed to characterize the chemical structure of the prepared sample (Figure 53). TEM and E-SEM images exhibited spherical morphology and uniform particle size distribution of G-PECs (Figure 40B).

When incubated in either PBS 1x or 0.9%NaCl, G-PECs exhibited a swelling behavior (Figure 40A) that characterize them as nanogels, even if the swelling ability of polymeric

networks was reduced due to chemical crosslinking. The polymeric matrix of nanogels whould be able to retain a significant amount of low molecular weight drugs and releasing them in a controlled manner [158,286].

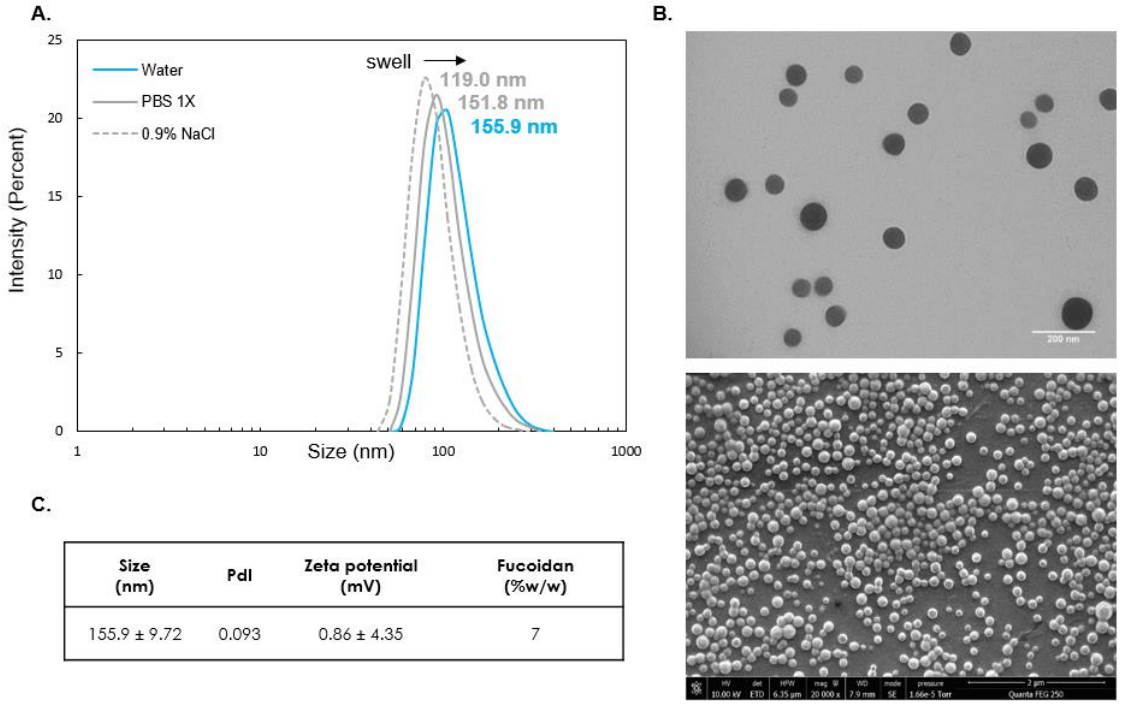

Size (nm)	PdI	Zeta potential (mV)	Fucoidan (%w/w)
155.9 ± 9.72	0.093	0.86 ± 4.35	7

Figure 40. Physico-chemical characterization of crosslinked nanoparticles: (A) Dynamic diffusion of light measured in intensity. (B) Images obtained by transmission electron microscopy (upper image) and environmental scanning electron microscopy (bottom image). (C) Size (nm), polydispersion index and zeta potential (mV) measured by Zetasizer Nano-ZS. The percent of fucoidan by weight of the total nanoparticle weight was determined by elemental analysis.

Long-term stability of G-PECs was evaluated in distilled water and NaCl upon storage of the nanoparticles suspensions at 4°C. By genipin crosslinking, the colloidal stability of interpolyelectrolyte complexes was improved up to 1 month of incubation in 0.9%NaCl (Figure 41A, B and C). The formation of PECs, based only in electrostatic interactions, was found to be poor against pH and ionic strength because of repulsive forces and salt-screening effects [127]. The covalent crosslinking of EA-pullulan with genipin in the presence of fucoidan has led to the formation of permanent networks in which fucoidan has been retained by ionic interactions between the sulfate groups and the primary ammoniums. In addition, it was possible to freeze-dry G-PECs while keeping the same size after re-dispersion in 0.9% NaCl, using 5% (w/w) of sucrose as cryoprotectant agent (Figure 41D). Freeze-dryer process is useful for long-term storage of pharmaceutical

formulations and to concentrate PECs nanoparticles prior to use by rehydrating them in reduced volumes.

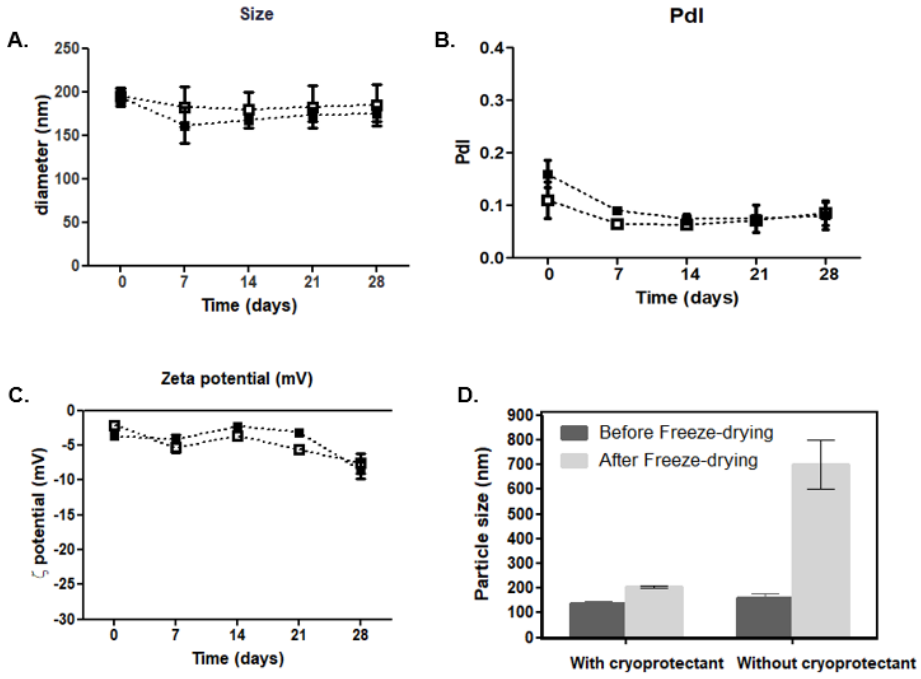

Figure 41. Stability of G-PECs in water (·□·) and NaCl 0.9% (·■·) after preparation (day 0), and after 1, 7, 14, 21 and 28 days of storage at 4°C. (A) NP size (nm) and (B) PdI were measured by DLS; (C) ζ potential values (mV) by ELS; (D) Effect of the addition of a cryoprotectant on nanoparticles size before and after freeze-drying. Results are shown as mean ± SD from three independent experiments.

3.3 Cell viability, hemocompatibility and cellular uptake studies

EA-pullulan showed to be biocompatible up to 200 µg/mL (Figure 51). When increasing the concentration of polycation up to 1000 µg/mL, the cell viability decreased for less than 70% (48.19 ± 3.59 %). Lou *et al.* tested the toxicity of different polycations for much lower concentrations ranging from 2 to 100 µg/mL [225]. Similarly, Huang *et al.* evaluated the toxicity of chitosan derivatives reconstructed with different alkylamines for concentrations only up to 200 µg/mL [287]. Cationic pullulan derivatives modified with quaternary amine groups have previously showed to be non-cytotoxic [276]. It is known that the cytotoxicity of polycations is a function that results from their polyamine nature (i.e., primary, secondary, tertiary, and quaternary amino groups) [288]. In comparison to primary amines, higher order amines can induce lower toxicity by reducing the cationic

polymer's ability to bind to and disrupt the organization of cell membrane lipid bilayer [225,289,290]. Cytotoxicity assays of G-PECs showed that no decrease in cell viability was observed up to 1000 µg/mL (Figure 42A). Results were confirmed by optical (Figure 42B) and fluorescence (Figure 42C) images, in which no alteration of cell morphology was observed when compared with control.

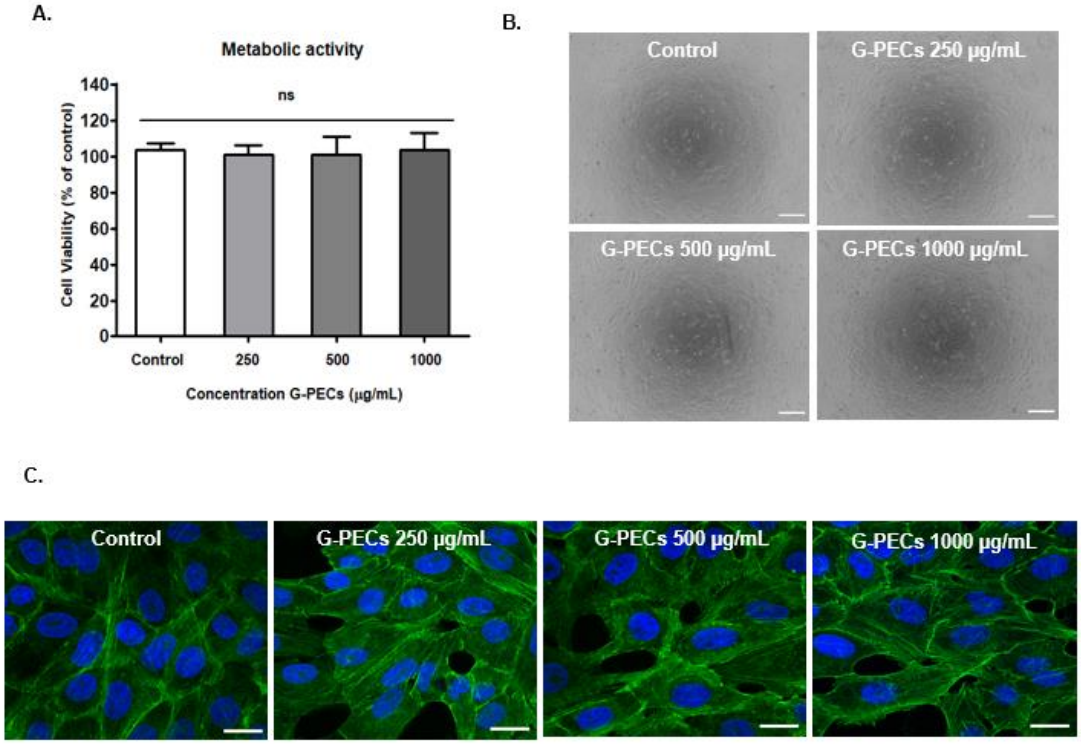

Figure 42. (A) Cytocompatibility of G-PECs towards HUVECs exposed to increasing concentrations of G-PECs measured by resazurin conversion after 1 day of incubation. Results are shown as mean ± SD from 3 independent experiments with no statistical differences detected using the Wilcoxon matched-pairs signed rank test. (B) Optical and (C) fluorescence images of confluent cells without G-PECs and with 250, 500 and 1000 µg/mL of G-PECs, respectively. Scale bar corresponds to 200 µm (top image) and 20 µm (bottom image).

For further clinical safety evaluation, we investigated the hemolytic property of G-PECs on human erythrocytes (Figure 43). Hemolysis assays are generally considered valuable in testing the hemocompatibility of new nanoformulations [291]. All tested concentrations (250 –1000 µg/mL) had a hemolytic value below 5% (hemolysis rate of 0.79 ± 0.04%, 1.45 ± 0.15% and 2.09 ± 0.06% for G-PECs concentrations of 250, 500 and 1000 µg/mL respectively). According to the American Society for Testing and Materials International (ASTM, 2013) materials with < 5% hemolytic reaction can be

considered as non-hemolytic and G-PECs nanogels could be thereby classified as non-hemolytic material [292].

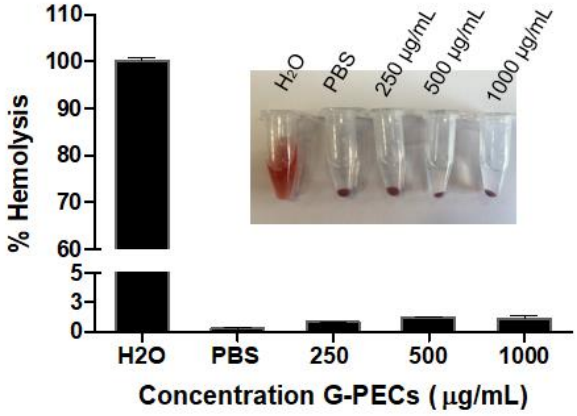

Figure 43. Blood hemolysis percentage of human blood from healthy donors after incubation with increasing concentrations of 250,500 and 1000 µg/mL of G-PECs nanogels. Water and PBS were used as positive and negative control, respectively. Results are shown as mean ± SD from three independent experiments.

The cellular uptake was evaluated in HUVECs after 24h of incubation. For this purpose, G-PECs were produced using fluorescent-labelled EA-pullulan with rhodamine-B isothiocyanate. The cells incubated with G-PECs exhibited intense red accumulations in the cytoplasm, indicating an efficient cell internalization (Figure 44 and Figure 56) probably via non-specific endocytosis due to their relatively small size of less than 200 nm [262].

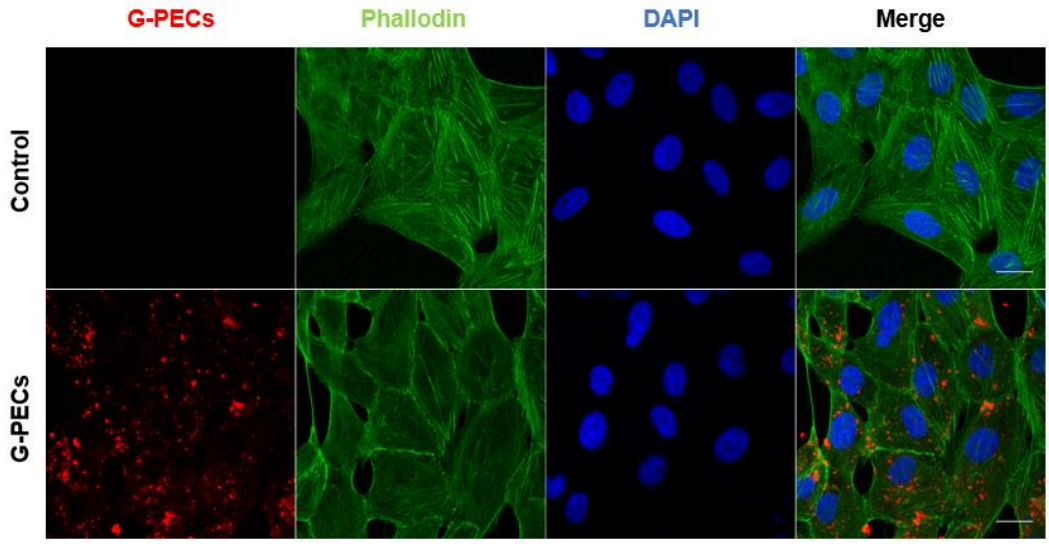

Figure 44. Confocal microscopy images of HUVECs treated without G-PECs and with G-PECs produced using fluorescent labelled EA-pullulan (RBITC-EA-pullulan). G-PECs were incubated with HUVECs for 24h at 37˚C. HUVECs were then washed, fixed, and observed under fluorescence microscopy. Red, G-PECs; green, phalloidin; blue, cell nuclei. Scale bars, 20 µm.

3.4 Biospecificity of G-PECs

Nanosystems decorated with fucoidan have been previously shown to be able to target P-selectin [270,281,293,294]. *In vitro* capacity of rhodamine-B labelled G-PECs to target human activated platelets was evaluated via flow adhesion assay. Control fluorescent polyplexes were formulated using carboxymethyl-dextran as polyanion. As evidenced on Figure 45, G-PECs with fucoidan were able to target P-selectin expressed in activated platelets.

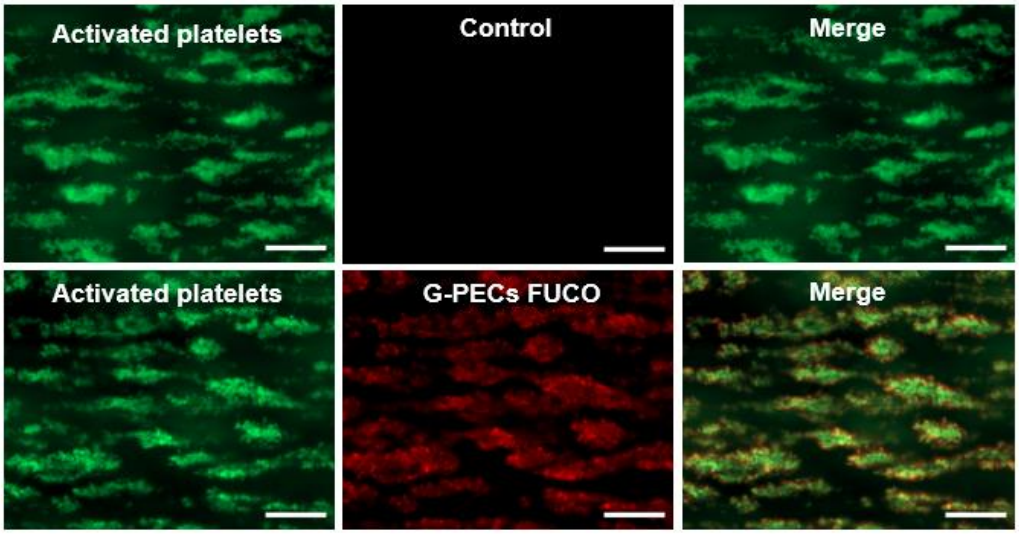

Figure 45. Evaluation of G-PECs binding on activated platelets under arterial flow conditions. Particles and platelets aggregates co-localization was evaluated by merged fluorescence microscopy images (right). G-PECs without fucoidan were used as control. Scale bars corresponds to 50 µm.

3.5 miRNA loading, release and delivery

Nanogels can be used as highly efficient and biodegradable carriers for the transport of drugs in controlled drug delivery devices. Strongly charged biotherapeutics, such as nucleic acids, are generally post-loaded into oppositely charged nanogels by electrostatic interactions with oppositely charged groups.

In order to evaluate the influence of the surface charge of G-PECs on miRNA interactions, two different pHs (pH 3 and pH 7) were studied for miRNA loading. Under neutral conditions, the primary amine groups chains of G-PECs were deprotonated, thereby leading to nearly neutral surface charge of developed nanogels (0.86 ± 4.35 mV). However, in a more acidic environment, the amount of primary ammonium groups led to G-PECs with a positive zeta potential (9.23 ± 0.81 mV) which could contribute for miRNA loading onto the particle surface through electrostatic interactions.

After miRNA addition, loaded G-PECs were characterized regarding size, polydispersity, surface charge and agarose gel electrophoresis. miRNA loaded as well as unloaded G-PECs showed equivalent diameters around 200 nm, although the PdI increased considerably for the loaded ones indicating a more heterogeneous population (Figure 57). Similary, Raemdonck *et al.* revelead that siRNA-loaded cationic dextran nanogels had

nearly the same hydrodynamic size as the nanogels prior to loading with siRNA [295]. The charge of surface G-PECs slightly decreased indicating the presence of additional negative charges (Figure 46A). A loading efficiency of 70.23 ± 5.33% at pH 3 was achieved compared to 33.11 ± 6.51% at pH 7 (Figure 46B). This difference was likely due to the higher affinity the particles had for miRNA as a direct result of polymer protonation in acidic conditions. The agarose gel electrophoresis supports more effectively miRNA retardation from nanogels loaded with miRNA in acidic conditions when compared to miRNA loaded in neutral pH (Figure 58). For all the subsequent experiments, the miRNA was loaded into G-PECs only at pH 3.

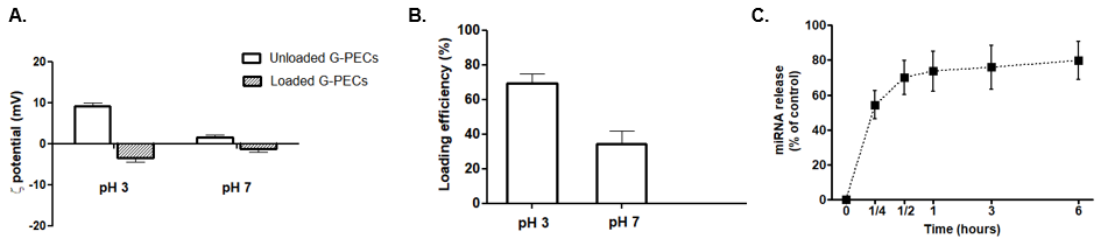

Figure 46. miRNA loading and release. (A) Zeta potential (mV) measured by the Zetasizer Nano-ZS at pH 3 and pH 7 before and after miRNA loading. (B) Loading efficiency of miRNA at pH 3 and 7 and (C) miRNA release from G-PECs nanogels at 37°C in PBS. Results are shown as mean ± SD from three independent experiments.

These results are in agreement with the literature. Pereira *et al.* performed siRNA loading onto glycol chitosan-based nanogels by simple mixing nanogels supensions in 0.2M acetate buffer at pH 4.5 with siRNA [296]. Its positive charge (25-30 mV) under slightly acidic conditions allowed the electrostatic interaction between glycol chitosan and negatively charged siRNA. Under neutral or alkaline conditions, the siRNA binding was essentially stabilized by hydrogen bonding and hydrophobic interactions of modified chitosan. Pilipenko *et al.*, demonstrated that the ability of chitosan–heparin complexes to encapsulate the siRNA was also depending on pH of the medium due to the pH sensitive behavior of chitosan [228]. Under acidic conditions, almost 100% of siRNA was entrapped into polyplexes due to the greatest protonation of the amino groups of chitosan in acidic media resulting in maximum binding efficiency. Thus, they determined the optimal pH for oligonucleotide entrapment around pH 6.0 or below. Khaled *et al.* also evaluated the siRNA loading efficiency into hybrid nanogel particles formed by a nanostructured inorganic silica core and an organic pH-responsive hydrogel shell at acidic

and physiological pH conditions. They obtained a loading efficiency of 95% of siRNA at pH 6 compared to 70% at pH 7.4 [297].

Further, to evaluate if the miRNA could be released from G-PECs, the release profile was studied in physiological conditions. When placed under strong orbital shaking at 37°C in PBS, loaded G-PECs released nucleic acids up to 6 hours, with a $t_{1/2}$ of 15 min after incubation (Figure 46C). Antunes *et al.* obtained similar release profiles from core-shell polymer based nanoparticles loaded with miR-155-5p [232].

Finally, a comparative study of naked miRNA and miRNA loaded into G-PECs was done using a fluorescently labeled miRNA to evaluate their cellular uptake. As it can be seen from Figure 47A, no miRNA could be detected inside cells in case of administration of free miRNA confirming that free miRNA cannot be internalized by cells. miRNA from G-PECs nanogels, in contrast, was clearly incorporated by cells. The strong and difuse green fluorescence from FAM-miRNA indicated the distribution of the polyplexes in the cytoplasm after 2h incubation with G-PECs. Flow cytometry analysis confirmed quantitative differences in FAM-miRNA uptake levels upon loading into G-PECs (Figure 47B).

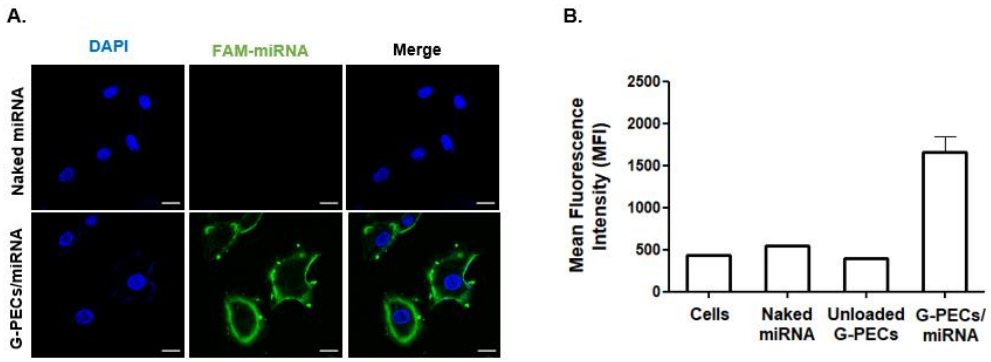

Figure 47. FAM-miRNA delivery. (A) Fluorescence microscopy images of HUVECs evidencing miRNA delivery. Left column: cells' nuclei stained with DAPI (depicted in blue); middle column: FAM labelled miRNA (depicted in green); right column: merged images for cells treated with naked FAM-labelled miRNA and cells treated with G-PECs nanogels loaded with FAM-labelled miRNA; Treatments were performed for 2h at 37°C. Scale bar: 20 µm. (B) Mean fluorescence intensity (MFI) of fluorescein amidite (FAM) measured by flow cytometry analysis. Results are shown as mean ± SD from three experiments.

4. Conclusion

In this work, we demonstrated the development of a simple and versatile drug delivery system based on two polyelectrolytes derived from natural biocompatible polysaccharides, pullulan and fucoidan, which spontaneously interact to form PECs of adjustable size and surface charge for miRNA delivery. The ability of our nanosystems to target P-selectin make them attractive candidates for the delivery of small sized nucleic acids, while foccused on the cardiovascular field. Future studies about the potency of these systems for gene silencing should clarify if the amount of delivered miRNA is able to induce the desired pharmacological effect.

APPENDIX- SUPPLEMENTARY DATA

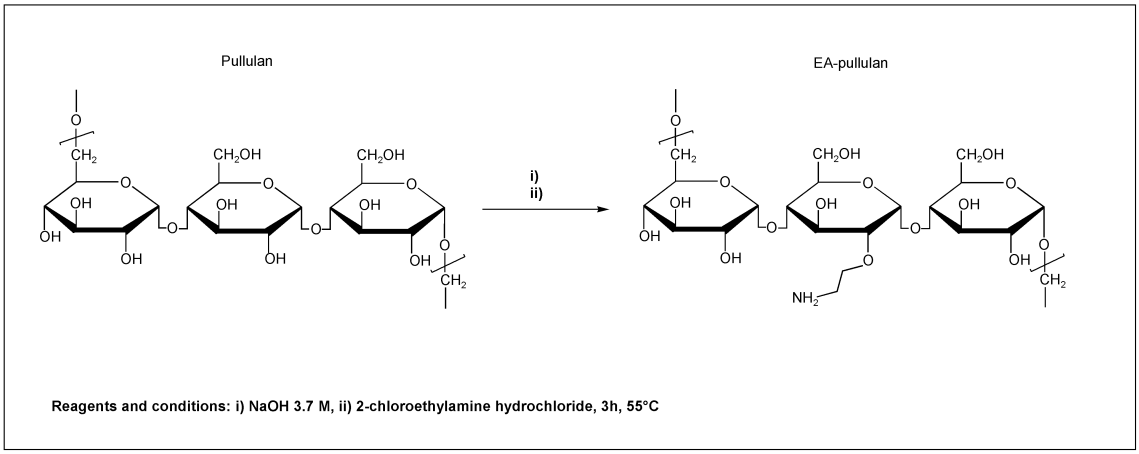

Figure 48. Synthesis route for amination of pullulan grafted with 2-chloroethylamine hydrochloride.

Table 14. Characterization of cationic pullulan derivatives with primary amine groups performed in one-step of synthesis.

R.	$\frac{[NH2]}{[OH]}$	Time (h)	N [a] (%)
1	2	1.5	0.26
2	2	3.0	0.68
3	2	6.0	0.71
4	2	14.0	0.87
5	3	3.0	0.87
6	3	6.0	1.36
7	4	3.0	1.01
8	4	6.0	1.79
9	5	3.0	0.77
10	8	3.0	1.11

[a]Calculated by elemental analysis

Table 15. Characterization of cationic pullulan derivatives with primary amine groups performed in two steps of synthesis during 3h at 55°C each step.

R.	$\frac{[NH2]}{[OH]}$	Time (h)	N[a] (%)
11	2	3.0 (x2)	1.58
12	3	3.0 (x2)	2.09

[a]Calculated by elemental analysis

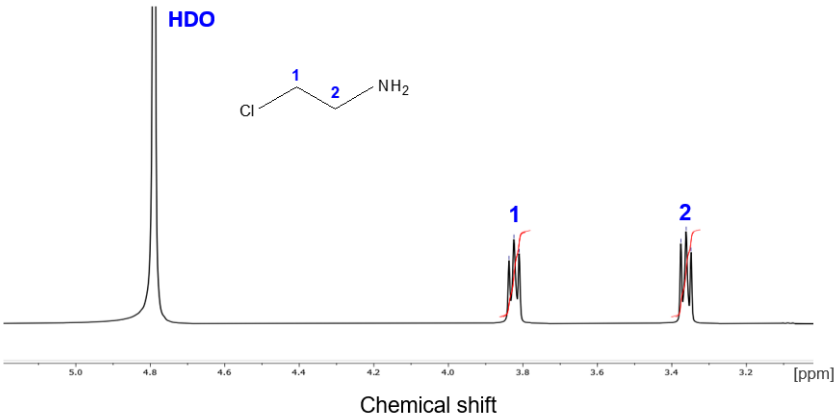

Figure 49. 1H NMR spectrum at 400 Mhz of 2-chloro-ethylamine hydrochloride in D2O.

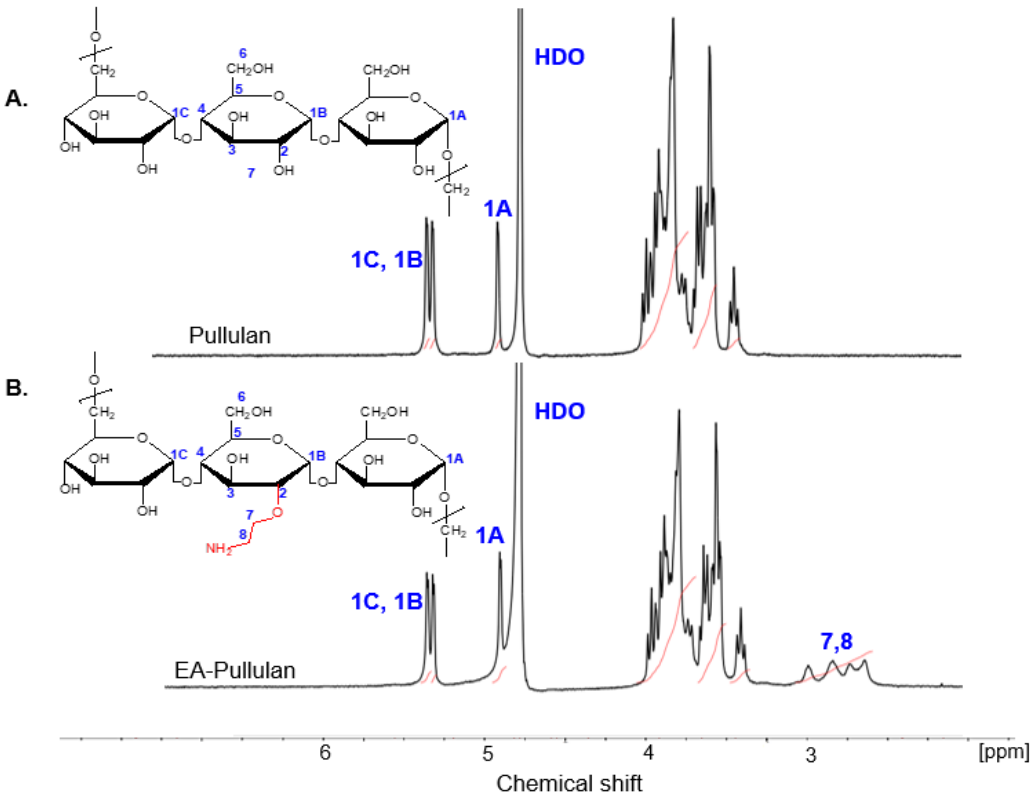

Figure 50. 1H NMR spectra at 400 Mhz of (A) non-modified pullulan and (B) EA-pullulan in D2O. 1A, 1B, 1C signals depicted anomeric H from maltotriose base unit of pullulan. Numbers 2–6 corresponded to H on anydroglucose unit. H from ethylamine (B) were depicted with numbers 7 and 8.

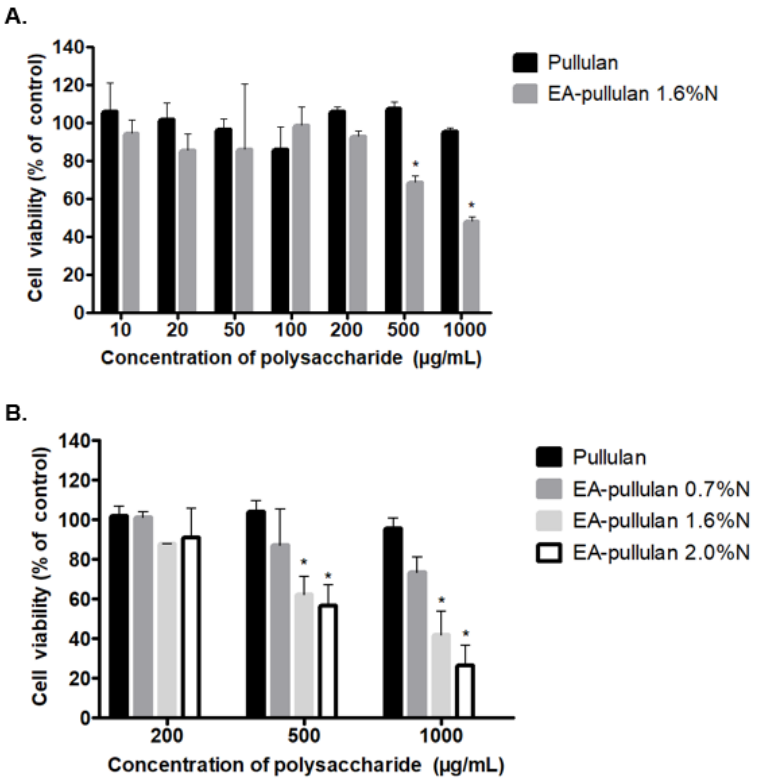

Figure 51. Cytocompatibility of EA-pullulan derivatives. (A) Cytocompatibility of EA-pullulan (1.6%N) measured by resazurin assay after 1-day exposure to increasing concentrations ranging from 10-1000 µg/mL compared to unmodified pullulan. (B) Cytocompatibility of EA-pullulan with different N contents (0.7, 1.6 and 2.0 %N) after 1-day exposure to increasing concentrations ranging from 200-1000 µg/mL of EA-pullulan compared to unmodified pullulan. Results are shown as mean ± SD from 3 independent experiments. *p < 0.05 using the Wilcoxon matched-pairs signed rank test.

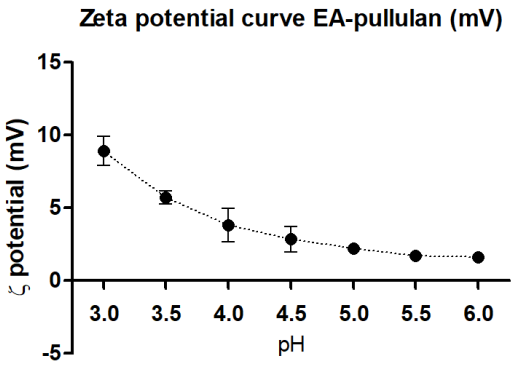

Figure 52. Zeta potential (mV) curve of EA-pullulan solution at 2.5 mg/mL at different pH values (mean ± SD, n = 3).

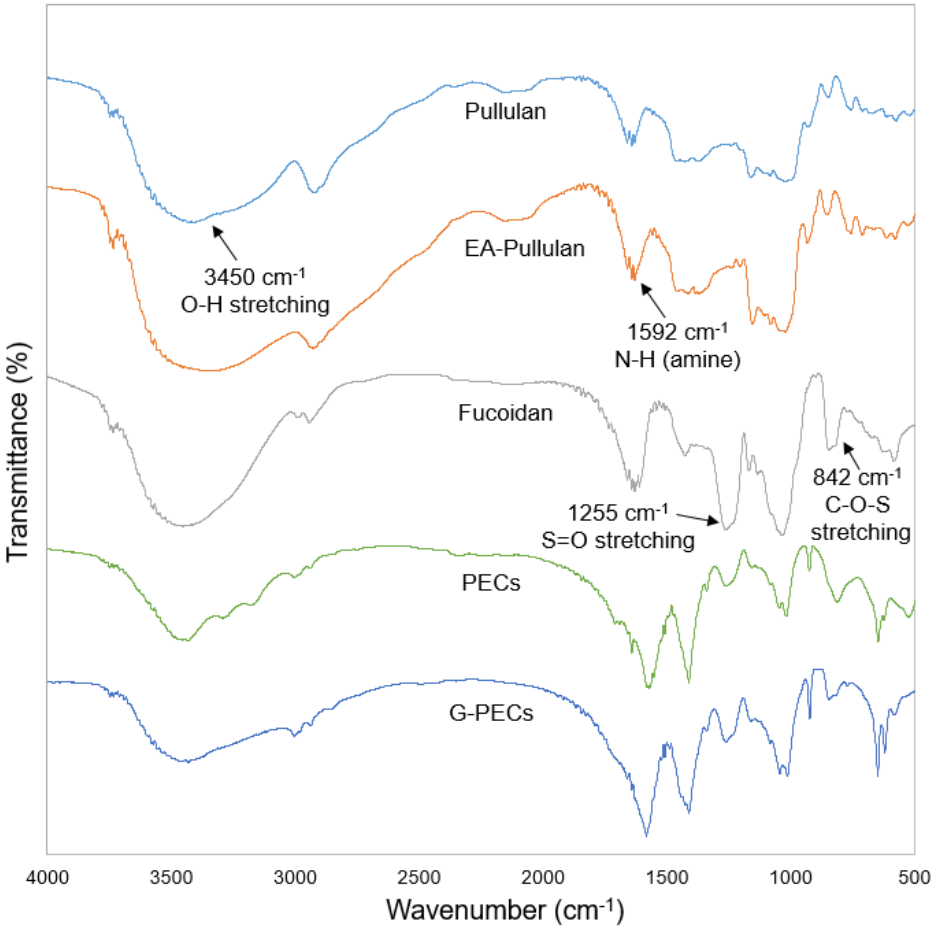

Figure 53. FTIR spectra of unmodified pullulan, EA-pullulan, fucoidan, PECs and G-PECs.

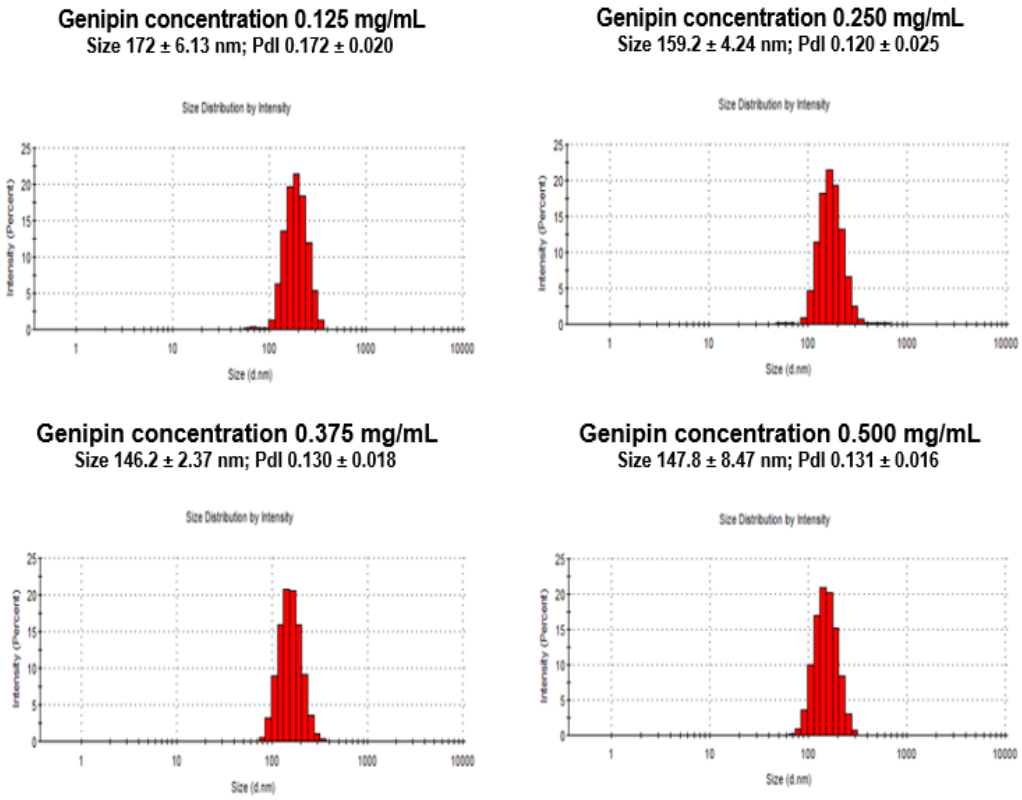

Figure 54. Histograms of particle size distribution at different genipin concentrations from Light Scattering (LS) expressed by intensity percentages (mean ± SD, n=3).

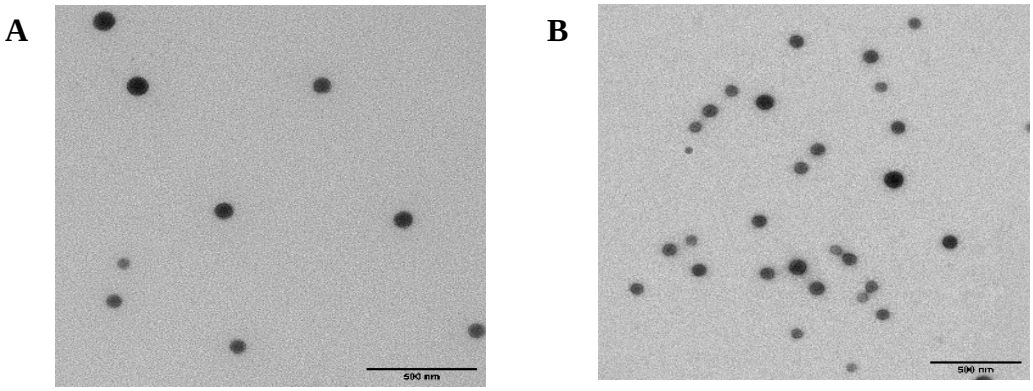

Figure 55. TEM pictures of polyelectrolyte complexes (A) before and (B) after crosslinking. Scale bars represents 500 nm.

Table 16. Nanoparticles concentration before and after purification by ultracentrifugation (UC).

Sample	Mean Diameter (nm)	Mode Diameter (nm)	d90/d10 (PdI)	Raw concentration (NP/mL)	Particle count
Before UC	134	134	1.4	5.25e+0.09	757
After UC	139	133	1.5	4.49e+0.09	620

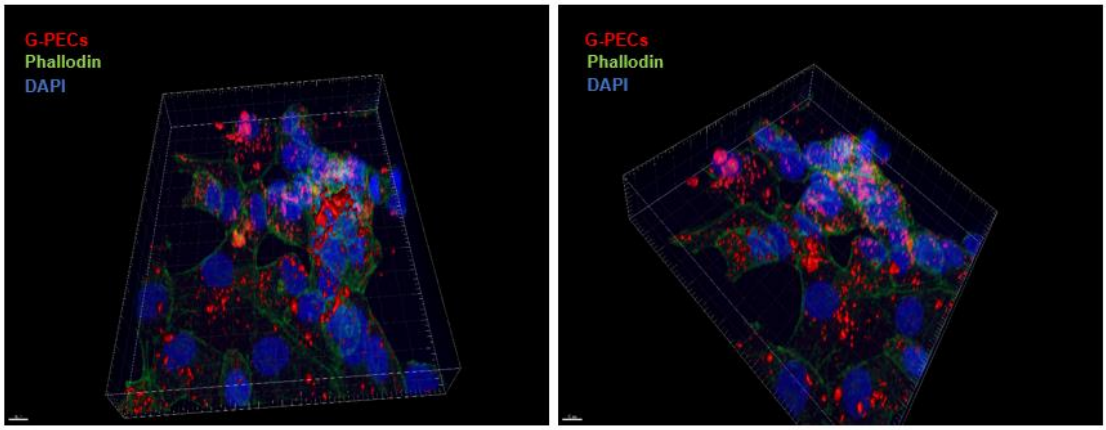

Figure 56. Reconstructed 3D images of G-PECs internalization in HUVECs using the Imaris® software. Scale bars corresponds to 10µm.

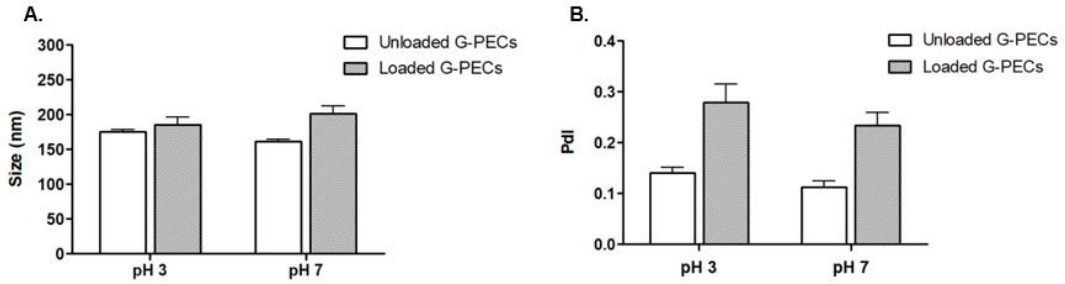

Figure 57. (A) Size (nm) and (B) polydispersity index measured by the Zetasizer Nano-ZS at pH 3 and pH 7 before and after miRNA loading. Results are shown as mean ± SD from three independent experiments.

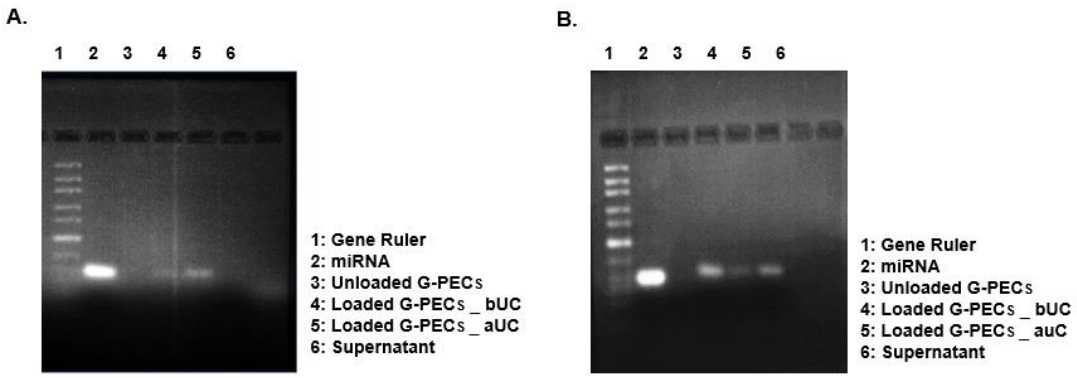

Figure 58. Agarose gel electrophoresis of unloaded G-PECs, loaded G-PECs before ultracentrifugation (bUC) and after ultracentrifugation (aUC) and supernatant for miRNA loading performed at (A) acid pH (pH 3) and (B) neutral pH (pH 7). An ultra-low weight GeneRuler (10–300 base pairs) was used as a control and the amount of RNA incorporated was compared to miRNA alone at the same concentration used for loading (0.04 mg/mL, 9 µL).

4. GENERAL DISCUSSION

In this work, we have designed and synthetized polysaccharide-based nanoparticles focused on miRNA delivery. miRNA instability and inefficient delivery are the main hindrances for their clinical application. Uncomplexed miRNAs are unstable and would be rapidly degraded after entering the systemic circulation before reaching targeted tissue. Among the many challenges involved with *in vivo* miRNA delivery, the development of safe and efficient carriers remain one of the most prominent.

A wide range of vehicles has been proposed for developing miRNA delivery systems. Non-viral vectors (inorganic nanoparticles, lipid-based nanoparticles and polymer-based carriers) have considerable advantages over viral vectors such as relatively low immunogenicity, low cost and versatility. The lower transfection efficiency of non-viral vectors compared to viral vectors can be improved by adding targeting moieties to the carries [18,162]. Suitable carriers must be non-toxic and non-immunogenic, provide serum stability and enhance miRNA cellular uptake. Once inside cells, they should also be able to release their payloads efficiently to trigger a biological response [171]. The choice of the appropriate carrier is influenced by the route of administration and therapeutic purposes [197].

Among the different types of nanoparticles, lipid-based NPs (LNPs), a relatively mature technology, are widely used for *in vivo* delivery of small interfering RNAs [189,190,194]. They are composed of a lipid bilayer that contains the miRNA encapsulated in the hydrophilic aqueous core or, complexed with the lipids on the surface [182,191]. The development of ionizable cationic lipids that are positively charged at acidic pH values, but nearly neutral at physiological pH, has proven to be essential for the development of clinically viable LNPs [189,298]. For example, the first siRNA-based therapy to be approved by the FDA, Onpattro®, is a LNP composed of heptatriaconta-6,9,28,31-tetraen-19-yl 4-(dimethylamino)butanoate (DLin-MC3-DMA) ionizable lipid [190,197].

Regarding miRNA therapeutics, they have not yet be translated into FDA-approved candidates for medical intervention, but some miRNA candidates have shown potential (e.g. Miravirsen, RG-101), while some have failed [164]. It is worth mentioning that MRX34, a liposomal injection of miR-34 has been the first compound based on miRNA mimics to enter a phase I clinical trial to treat patients with advanced solid tumors. The trial was prematurely closed because of serious immune-related events which were potentially attributable to the liposome carrier instead of the miR-34 mimics themselves [187,299,300]. A search for the ideal vector capable of successfully deliver miRNAs is

still underway and several efforts has been made to move miRNAs from the bench to clinics.

Cationic polymer-based systems are other relevant candidates, which have been widely investigated. The gold standard for the polymer-based gene delivery is polyethylenimine (PEI). PEI is rich in amine groups and thus can bind to small RNAs to form nanosized complexes. Lin *et al.* have shown that branched PEIs were more effective at transferring miR-494 in mouse embryonic fibroblast cells than the lipofectamine reagent [301]. Despite being an efficient transfecting agent, it suffers from high cytotoxicity. Eventually, it is clear that the clinical translation of miRNA therapeutics heavily depends on the development of delivery systems presenting a satisfactory balance between therapeutic efficacy and toxicity, since the intrinsic adverse effects of polycationic systems cannot be fully avoided. This is the main objective of our study and the main reason of our choice to develop pullulan-based polycations due, in one hand to the excellent biocompatibility of this polysaccharide and, in another hand, to the versatility of the possible chemical modifications of this material.

After preparing cationic pullulan derivatives, polyplexes were produced by direct polyelectrolyte complexation approach with miRNA. Polyplexes have many advantages for nanoparticles formulations such as non-toxicity and excellent biocompatibility and have proven to be very useful in gene therapy [228,231]. By comparison with covalent assemblies, the efficiency of these complexes involves only the breaking of ionic bonds without altering the structure of one or the other of the polyions. The advantage is a release of miRNA in an intact form. The downside is the significant risk of competition with other polyions in the physiological medium, or local ionic conditions capable of destroying the complexes, before the therapeutic target has been reached.

In the first part of our study, we demonstrated that cationic pullulan derivatives were able to form complexes with anionic miRNAs and deliver them into HUVECs despite the stability issues in physiological conditions. Some studies have shown that an excess of free or weakly associated polycation chains plays an important role on the uptake process and transfection efficiency [264,302]. From the *in vitro* cellular uptake, this hypothesis is supported. miRNA delivery inside cells is a prerequisite for their action. The uptake mechanism of polyplexes with similar size around 80–200 nm was found to be clathrin-mediated endocytosis [225]. Here the exact mechanism of miRNA internalization, release and biological activity of delivery miRNA was not explored since these polyplexes

presented instability issues. As previously mentioned, when an intravenous administration is intended, an effective miRNA delivery system should retain its colloidal stability under physiological conditions in order to protect miRNA during systemic circulation until it reaches its targeted tissues.

In the second part of the study, we stabilized the complexes by forming some covalent bridges between the chains of the cationic pullulan without impairing their complexation capacity. We improved their efficacy through the complexation with fucoidan. Fucoidan is a sulfated polysaccharide able to aim at P-selectin, a strong marker of atherothrombotic disorders [270,281,293,294]. The challenge was to develop a very simple strategy to endow the complexes with biospecificity by maintaining their capacity to efficiently cargo and carry miRNA to the cellular targets. We selected genipin as crosslinking agent. Genipin is a natural compound, described to be 10,000 times less cytotoxic when compared to synthetic glutaraldehyde, being a great promise for the preparation of biocompatible crosslinked materials [280].

Cationic pullulan derivatives were modified with primary amine groups to allow genipin crosslinking reaction. A versatile method to synthetize pullulan/fucoidan PECs was developed for the first time. Their low cytotoxicity and hemolysis rate make them a safe material for potential gene delivery. These nanosystems showed high stability when incubated in 0.9% NaCl without aggregates formation. The presence of fucoidan allowed the *in vitro* targeting of P-selectin over-expressed in cardiovascular diseases as demonstrated by flow assays. It is consistent with the results that had been reported by Juenet *et al.* using fucoidan functionalized based polysaccharide nanoparticles to interact with activated platelets [270].

The efficacy of the carriers is also related to their loading capacity. Consequently, the amount of loaded miRNA should be maximized. Generally, nucleic acids can be loaded into nanogels via electrostatic interaction (post-synthetic loading). We have shown that under acidic environement it was possible to increase the global positive charge of our PECs from ~ 0.86 mV to 9.23 mV due to the greatest protonation of the amino groups from cationic pullulan. In this condition, a loading efficiency of about 70% was achieved. Several studies have demonstrated the influence of the surrounding pH of the medium on nucleic acid loading [228,296,297,303].

A future approach to increase miRNA loading would be the use of cationic pullulan derivatives bearing both primary amines and quaternary ammonium groups following a strategy similar to that of Yung *et al.* with cationic LNPs [198]. Some polymers containing quaternary ammonium groups have been described to make polyplexes with nucleic acids more efficiently than the polymers having primary or secondary amine groups [211]. For example, in the work of Tamura and colleagues, quaternary ammonium groups were introduced into a polyamine nanogel resulting in an increment in their surface charge from ~1 mV to 23 mV, which allowed an enhanced siRNA loading [304]. Quaternary ammonium groups have several advantages for nucleic acid delivery, including the reduction of cytotoxicity and the improvement of the binding capacity with nucleic acids compared to the amino groups with pKa values. The nature of cationic groups should be considered as a critical factor to develop biocompatible derivatives.

Another greatest challenge in miRNA therapy is the evaluation of the changes in the target after miRNA delivery. When designing miRNA-based complexes, additional quantitative assays would be necessary to check the amount of delivered miRNA and the effects on the protein production. Traditional approaches to assess miRNA silencing activity include the analysis of mRNA products such as relative quantity of the relevant RNA by real-time quantitative polymerase chain reaction (qPCR) or the expression of the encoded protein as measured by western blot (WB) [305,306]. However, those techniques are labor intensive and time-consuming. In addition, they also require cell lysis which make them unsuitable for dynamic analysis of expression level or *in vivo* detection of miRNAs.

Recent approaches on the analysis of the extent of gene silencing efficiency were done by using RNAi against a reporter gene such as luciferase [275,307,308] or green fluorescence protein (GFP) [231,309,310]. Culture cells must stably express the reporter gene or be transfected first with a plasmid containing the reporter gene and then with the polyplex containing the relevant RNAi [178]. According to the design of the imaging system, an increase or reduction in light emission in cells is generated and can be detected using conventional optical imaging methods [305]. Turk *et al.* developed a GFP-based reporter system to monitor the cellular levels of the tumor suppressor miRNA let-7 in single Human embryonic kidney 293 (HEK 293) cells. Using qPCR, they confirmed the inverse relationship of GFP fluorescence and miRNA levels [311]. However, major drawbacks of reporter gene-based techniques include genetic modification of the studied objects, high tissue auto-fluorescence background (especially for fluorescence-based

miRNA imaging) and poor tissue penetration of the light *in vivo*, which limit their use as a research tool in cells and small animal models.

The development of alternatives imaging modalities to monitor miRNA delivery and its therapeutic efficacy is of great interest. Besides the applications of optical imaging in miRNA research, other imaging modalities have been explored. For example, magnetic resonance imaging (MRI) provides a non-invasive image with better anatomical information and high spatial resolution [306]. Gadolinium is the mostly used contrastophore for MRI. It has seven unpaired outer shell electrons and a large magnetic moment. Gadolinium-based contrast agents can be incorporated into nanoparticles to enable real-time imaging of their in vivo biodistribution [312]. Yang *et al.* developed a poly(amidoamine) dendrimer-grafted gadolinium-functionalized nanographene oxide (Gd-NGO) nanoparticles for combined miRNA delivery and magnetic resonance imaging. Together with the use of FAM labeled miRNA, these systems allowed the quantification of miRNA delivery in real time *in vivo* [188].

More recently some studies about siRNA *in vivo* imaging have used the radionuclide technique [80,313]. Single-photon emission computed tomography (SPECT) is a noninvasive and sensitive method. A SPECT scan can reach resolution of ~0.4 mm with no depth penetration limit. This technique requires efficient methods of miRNA labeling and purification from excesses of radiolabel. In the work of Merkel *et al.*, SPECT images are used to monitor the pharmacokinetics and biodistribution of siRNA polyplexes using both ^{111}Indium radiolabeled siRNA and polymer [80].

For a while, there is no method capable of combining all the advantages of the different ways of monitoring miRNA. The combination of several molecular imaging modalities should offer synergy to collect complementary information about molecular and cellular processes about miRNA functions. The use of nanoparticles as imaging agents can facilitate multimodal imaging due to their ability to incorporate different imaging markers in a single imaging compound thus enabling image-guided gene therapy. Tracking miRNA is essential to improve our understandings of a wide range of diseases, which may lead to the development of more effective treatment strategies.

Finally, in the future, the proper manufacturing and quality control of the developed nanosystems should be adressed. Scalable manufacturing methods are crucial for the translational success of new nanomedicines in order to ensure robust products with good physicochemical properties. It should be highlighted that a major drawback associated with polyelectrolyte-based nanoparticles is the use of very diluted solutions, which limits the production of enough doses for clinical applications using the conventional preparation methods of polyplexes [314]. Manual pipetting is restricted to relatively small volumes and it is poorly controlled which may result in irreproducibility and to batch-to-batch variations. A controlled and repeatable production method of polyplexes in large quantities is essential for their advance into clinical settings. For this purpose, Kasper *et al.* described the development of an up-scaled micro-mixer method using a T-connector fixed into two common syringe drivers for the preparation of plasmid/LPEI polyplexes. Plasmid/LPEI polyplexes prepared at varied mixing speeds were compared to those prepared by classical pipetting. Traditionally pipetting and the up-scaled micro-mixer method led to the production of polyplexes with comparable physicochemical characteristics and biological activity [315]. Similarly, Naeini *et al.* used an automated in-line mixing system for large-scale production of chitosan based polyplexes with both pDNA and siRNA. It was possible to increase the flow rate up to 300 mL/min for polyplexes production instead of the maximum of 2 mL of product delivered when using manual mixing [316].

Despite significant progress in the field of polysaccharide-based NPs for the development of nucleic acid condensation agents, the discovery of an ideal delivery vehicle is still far away to be accomplished [96]. To achieve successful gene therapy, the development of a proper delivery vector is essential. Consideration of the major drawbacks to gene delivery is necessary to understand the limitations of current carriers and is important for the rational design of new ones. With a growing understanding of gene-delivery mechanisms and polymer chemistry, it is likely that polysaccharide-based nanosystems will become an important tool for gene therapy [40,166,204]. The recent approval of the first messenger RNA-based vaccine against COVID-19 pandemic and ongoing clinical trials with therapeutic nucleic acids highlight the feasibility of their use as therapeutics providing ground for the development of the next generation of biodegradable, stabilized, biospecific and efficient formulations.

5. GENERAL CONCLUSION

Heart failure is a complex and debilitating disease, and the last stage of most heart and vascular wall diseases. Despite a relative risk reduction achieved by the best therapies targeting systemic risk factor for cardiovascular diseases, the majority of events are not prevented. miRNA therapeutics associated with nanocarriers should show great promise as therapeutic molecules for the treatment of cardiovascular diseases.

The aim of this project was to develop new and safe polysaccharide-based nanosystems for miRNA delivery in particular as potential injectable cardio-protective therapy for myocardial infarction. Ideally, these nanosystems should be able to appropriately target the diseased area after intravenous injection, protect the miRNA until its destination, internalize targeted cells, release the payload, being subsequently biodegraded into residues or quickly excreted through normal routes.

In the first chapter, PECs between cationic pullulan derivatives and miRNA were developed. These nanosystems were able to deliver miRNA *in vitro*. This work is a proof of concept that cationic pullulan derivatives modified with quaternary ammonium groups are able to interact with small RNAs by simple mixing and delivery them into human endothelial cells. The poor stability of the PECs under physiological conditions led us to consider a crosslinking strategy.

In the second chapter, we thus developed PECs formed by cationic pullulan derivatives crosslinked with genipin for miRNA delivery. The crosslinking of pullulan networks allowed the production of highly stable polysaccharide NPs in physiological conditions. When associated with fucoidan (through interactions of anionic sulfate groups with cations on the pullulan backbone) PECs are able to bind to P-selectin overexpressed by human activated platelets under flow *in vitro*. Their successful application for miRNA delivery depends now on their ability to release sufficient active miRNA molecules to induce a therapeutic effect.

With the work presented in this manuscript, we expect to contribute for the development of novel safe pullulan-based delivery systems for miRNA therapeutics. The facile synthesis, possibility of scalability and ease of formulation depict excellent clinical translation potential for a variety of biomedical applications. Proven safe and effective, such compounds are eagerly awaited by pharmaceutical partners as well as the cardiovascular community.

6. REFERENCES

1. Paiva, S.; Agbulut, O. MiRroring the Multiple Potentials of MicroRNAs in Acute Myocardial Infarction. *Front Cardiovasc Med* **2017**, *4*, doi:10.3389/fcvm.2017.00073.
2. Insull, W. The Pathology of Atherosclerosis: Plaque Development and Plaque Responses to Medical Treatment. *The American Journal of Medicine* **2009**, *122*, S3–S14, doi:10.1016/j.amjmed.2008.10.013.
3. Nascimento, D.S.; Valente, M.; Esteves, T.; de Pina, M. de F.; Guedes, J.G.; Freire, A.; Quelhas, P.; Pinto-do-Ó, P. MIQuant – Semi-Automation of Infarct Size Assessment in Models of Cardiac Ischemic Injury. *PLoS ONE* **2011**, *6*, e25045, doi:10.1371/journal.pone.0025045.
4. Kura, B.; Szeiffova Bacova, B.; Kalocayova, B.; Sykora, M.; Slezak, J. Oxidative Stress-Responsive MicroRNAs in Heart Injury. *IJMS* **2020**, *21*, 358, doi:10.3390/ijms21010358.
5. Zia, A.; Wu, Y.; Nguyen, T.; Wang, X.; Peter, K.; Ta, H.T. The Choice of Targets and Ligands for Site-Specific Delivery of Nanomedicine to Atherosclerosis. *Cardiovascular Research* **2020**, cvaa047, doi:10.1093/cvr/cvaa047.
6. Frangogiannis, N. The Immune System and Cardiac Repair. *Pharmacological Research* **2008**, *58*, 88–111, doi:10.1016/j.phrs.2008.06.007.
7. Frost, R.J.A.; van Rooij, E. MiRNAs as Therapeutic Targets in Ischemic Heart Disease. *J. of Cardiovasc. Trans. Res.* **2010**, *3*, 280–289, doi:10.1007/s12265-010-9173-y.
8. Palasubramaniam, J.; Wang, X.; Peter, K. Myocardial Infarction—From Atherosclerosis to Thrombosis: Uncovering New Diagnostic and Therapeutic Approaches. *ATVB* **2019**, *39*, doi:10.1161/ATVBAHA.119.312578.
9. Pepine CJ, C.J. The Effects of Angiotensin-Converting Enzyme Inhibition on Endothelial Dysfunction: Potential Role in Myocardial Ischemia. **1998**, 5.
10. Patti, G.; Cavallari, I. Extended Duration Dual Antiplatelet Therapy in Patients with Myocardial Infarction: A Study-Level Meta-Analysis of Controlled Randomized Trials. *American Heart Journal* **2016**, *176*, 36–43, doi:10.1016/j.ahj.2016.03.005.
11. Gong, W.; Feng, S.; Wang, X.; Fan, J.; Li, A.; Nie, S. Beta-Blockers Reduced the Risk of Cardiac Rupture in Patients with Acute Myocardial Infarction: A Meta-Analysis of Randomized Control Trials. *International Journal of Cardiology* **2017**, *232*, 171–175, doi:10.1016/j.ijcard.2017.01.035.
12. Yang, H.; Qin, X.; Wang, H.; Zhao, X.; Liu, Y.; Wo, H.-T.; Liu, C.; Nishiga, M.; Chen, H.; Ge, J.; et al. An *in Vivo* MiRNA Delivery System for Restoring Infarcted Myocardium. *ACS Nano* **2019**, doi:10.1021/acsnano.9b03343.
13. Chauvierre, C.; Letourneur, D. The European Project NanoAthero to Fight Cardiovascular Diseases Using Nanotechnologies. *Nanomedicine* **2015**, *10*, 3391–3400, doi:10.2217/nnm.15.170.
14. Bejarano, J.; Navarro-Marquez, M.; Morales-Zavala, F.; Morales, J.O.; Garcia-Carvajal, I.; Araya-Fuentes, E.; Flores, Y.; Verdejo, H.E.; Castro, P.F.; Lavandero, S.; et al. Nanoparticles for Diagnosis and Therapy of Atherosclerosis and Myocardial Infarction: Evolution toward Prospective Theranostic Approaches. *Theranostics* **2018**, *8*, 4710–4732, doi:10.7150/thno.26284.
15. Parviz, Y.; Vijayan, S.; Lavi, S. A Review of Strategies for Infarct Size Reduction during Acute Myocardial Infarction. *Cardiovascular Revascularization Medicine* **2017**, *18*, 374–383, doi:10.1016/j.carrev.2017.02.004.
16. Saparov, A.; Ogay, V.; Nurgozhin, T.; Chen, W.C.W.; Mansurov, N.; Issabekova, A.; Zhakupova, J. Role of the Immune System in Cardiac Tissue Damage and

Repair Following Myocardial Infarction. *Inflammation Research* **2017**, *66*, 739–751, doi:10.1007/s00011-017-1060-4.

17. Wojciechowska, A.; Osiak, A.; Kozar-Kamińska, K. MicroRNA in Cardiovascular Biology and Disease. *Advances in Clinical and Experimental Medicine* **2017**, *26*, 868–874, doi:10.17219/acem/62915.
18. Zhang, Y.; Wang, Z.; Gemeinhart, R.A. Progress in MicroRNA Delivery. *Journal of Controlled Release* **2013**, *172*, 962–974, doi:10.1016/j.jconrel.2013.09.015.
19. van Rooij, E.; Marshall, W.S.; Olson, E.N. Toward MicroRNA–Based Therapeutics for Heart Disease: The Sense in Antisense. *Circulation Research* **2008**, *103*, 919–928, doi:10.1161/CIRCRESAHA.108.183426.
20. Gori, M.; Trombetta, M.; Santini, D.; Rainer, A. Tissue Engineering and MicroRNAs: Future Perspectives in Regenerative Medicine. *Expert Opinion on Biological Therapy* **2015**, *15*, 1601–1622, doi:10.1517/14712598.2015.1071349.
21. Kapadia, C.H.; Luo, B.; Dang, M.N.; Irvin-Choy, N.; Valcourt, D.M.; Day, E.S. Polymer Nanocarriers for MicroRNA Delivery. *J Appl Polym Sci* **2020**, *137*, 48651, doi:10.1002/app.48651.
22. Lam, J.K.W.; Chow, M.Y.T.; Zhang, Y.; Leung, S.W.S. SiRNA Versus MiRNA as Therapeutics for Gene Silencing. *Molecular Therapy - Nucleic Acids* **2015**, *4*, e252, doi:10.1038/mtna.2015.23.
23. Yu, A.-M.; Choi, Y.H.; Tu, M.-J. RNA Drugs and RNA Targets for Small Molecules: Principles, Progress, and Challenges. *Pharmacol Rev* **2020**, *72*, 862–898, doi:10.1124/pr.120.019554.
24. Chen, Z.; Li, Y.; Zhang, H.; Huang, P.; Luthra, R. Hypoxia-Regulated MicroRNA-210 Modulates Mitochondrial Function and Decreases ISCU and COX10 Expression. *Oncogene* **2010**, *29*, 4362–4368, doi:10.1038/onc.2010.193.
25. Cheng, X.; Ku, C.-H.; Siow, R.C.M. Regulation of the Nrf2 Antioxidant Pathway by MicroRNAs: New Players in Micromanaging Redox Homeostasis. *Free Radical Biology and Medicine* **2013**, *64*, 4–11, doi:10.1016/j.freeradbiomed.2013.07.025.
26. Pulkkinen, K.H.; Ylä-Herttuala, S.; Levonen, A.-L. Heme Oxygenase 1 Is Induced by MiR-155 via Reduced BACH1 Translation in Endothelial Cells. *Free Radical Biology and Medicine* **2011**, *51*, 2124–2131, doi:10.1016/j.freeradbiomed.2011.09.014.
27. Gong, Y.-Y.; Luo, J.-Y.; Wang, L.; Huang, Y. MicroRNAs Regulating Reactive Oxygen Species in Cardiovascular Diseases. *Antioxidants & Redox Signaling* **2018**, *29*, 1092–1107, doi:10.1089/ars.2017.7328.
28. Mitsuishi, Y.; Motohashi, H.; Yamamoto, M. The Keap1–Nrf2 System in Cancers: Stress Response and Anabolic Metabolism. *Front. Oncol.* **2012**, *2*, doi:10.3389/fonc.2012.00200.
29. Yin, Y.; Zhao, X.; Yang, Z.; Min, X. Downregulation of MiR-93 Elevates Nrf2 Expression and Alleviates Reactive Oxygen Species and Cell Apoptosis in Diabetic Retinopathy. 9.
30. Schrottmaier, W.C.; Oskolkova, O.V.; Schabbauer, G.; Afonyushkin, T. MicroRNA MiR-320a Modulates Induction of HO-1, GCLM and OKL38 by Oxidized Phospholipids in Endothelial Cells. *Atherosclerosis* **2014**, *235*, 1–8, doi:10.1016/j.atherosclerosis.2014.03.026.
31. Yano, Y.; Ozono, R.; Oishi, Y.; Kambe, M.; Yoshizumi, M.; Ishida, T.; Omura, S.; Oshima, T.; Igarashi, K. Genetic Ablation of the Transcription Repressor Bach1 Leads to Myocardial Protection against Ischemia/Reperfusion in Mice. *Genes to Cells* **2006**, *11*, 791–803, doi:10.1111/j.1365-2443.2006.00979.x.

32. Bajan, S.; Hutvagner, G. RNA-Based Therapeutics: From Antisense Oligonucleotides to MiRNAs. *Cells* **2020**, *9*, 137, doi:10.3390/cells9010137.
33. Silva, A.K.A.; Letourneur, D.; Chauvierre, C. Polysaccharide Nanosystems for Future Progress in Cardiovascular Pathologies. *Theranostics* **2014**, *4*, 579–591, doi:10.7150/thno.7688.
34. Bachelet, L.; Bertholon, I.; Lavigne, D.; Vassy, R.; Jandrot-Perrus, M.; Chaubet, F.; Letourneur, D. Affinity of Low Molecular Weight Fucoidan for P-Selectin Triggers Its Binding to Activated Human Platelets. *Biochimica et Biophysica Acta (BBA) - General Subjects* **2009**, *1790*, 141–146, doi:10.1016/j.bbagen.2008.10.008.
35. Chauvierre, C.; Aid-Launais, R.; Aerts, J.; Chaubet, F.; Maire, M.; Chollet, L.; Rolland, L.; Bonafé, R.; Rossi, S.; Bussi, S.; et al. Pharmaceutical Development and Safety Evaluation of a GMP-Grade Fucoidan for Molecular Diagnosis of Cardiovascular Diseases. *Marine Drugs* **2019**, *17*, 699, doi:10.3390/md17120699.
36. Dilnawaz, F.; Acharya, S.; Sahoo, S.K. Recent Trends of Nanomedicinal Approaches in Clinics. *International Journal of Pharmaceutics* **2018**, *538*, 263–278, doi:10.1016/j.ijpharm.2018.01.016.
37. Wolfram, J.; Zhu, M.; Yang, Y.; Shen, J.; Gentile, E.; Paolino, D.; Fresta, M.; Nie, G.; Chen, C.; Shen, H.; et al. Safety of Nanoparticles in Medicine. **2016**, 25.
38. Chaubet, F.; Rodriguez-Ruiz, V.; Boissière, M.; Velasquez, D. Pharmacology: Drug Delivery. In *Encyclopedia of Biomedical Engineering*; Elsevier, 2019; pp. 440–453 ISBN 978-0-12-805144-3.
39. Li, C.; Wang, J.; Wang, Y.; Gao, H.; Wei, G.; Huang, Y.; Yu, H.; Gan, Y.; Wang, Y.; Mei, L.; et al. Recent Progress in Drug Delivery. *Acta Pharmaceutica Sinica B* **2019**, *9*, 1145–1162, doi:10.1016/j.apsb.2019.08.003.
40. Cosco, D.; Cilurzo, F.; Maiuolo, J.; Federico, C.; Di Martino, M.T.; Cristiano, M.C.; Tassone, P.; Fresta, M.; Paolino, D. Delivery of MiR-34a by Chitosan/PLGA Nanoplexes for the Anticancer Treatment of Multiple Myeloma. *Sci Rep* **2015**, *5*, 17579, doi:10.1038/srep17579.
41. Wu, L.-P.; Wang, D.; Li, Z. Grand Challenges in Nanomedicine. *Materials Science and Engineering: C* **2020**, *106*, 110302, doi:10.1016/j.msec.2019.110302.
42. Bobo, D.; Robinson, K.J.; Islam, J.; Thurecht, K.J.; Corrie, S.R. Nanoparticle-Based Medicines: A Review of FDA-Approved Materials and Clinical Trials to Date. *Pharm Res* **2016**, *33*, 2373–2387, doi:10.1007/s11095-016-1958-5.
43. Soares, S.; Sousa, J.; Pais, A.; Vitorino, C. Nanomedicine: Principles, Properties, and Regulatory Issues. *Front. Chem.* **2018**, *6*, 360, doi:10.3389/fchem.2018.00360.
44. Cicha, I.; Chauvierre, C.; Texier, I.; Cabella, C.; Metselaar, J.M.; Szebeni, J.; Dézsi, L.; Alexiou, C.; Rouzet, F.; Storm, G.; et al. From Design to the Clinic: Practical Guidelines for Translating Cardiovascular Nanomedicine. *Cardiovascular Research* **2018**, *114*, 1714–1727, doi:10.1093/cvr/cvy219.
45. Ragelle, H.; Danhier, F.; Préat, V.; Langer, R.; Anderson, D.G. Nanoparticle-Based Drug Delivery Systems: A Commercial and Regulatory Outlook as the Field Matures. *Expert Opinion on Drug Delivery* **2017**, *14*, 851–864, doi:10.1080/17425247.2016.1244187.
46. Mirza, A.Z.; Siddiqui, F.A. Nanomedicine and Drug Delivery: A Mini Review. *Int Nano Lett* **2014**, *4*, 94, doi:10.1007/s40089-014-0094-7.
47. Simpson; Smith; Thurecht; Such Engineered Polymeric Materials for Biological Applications: Overcoming Challenges of the Bio–Nano Interface. *Polymers* **2019**, *11*, 1441, doi:10.3390/polym11091441.

48. Hassan, S.; Prakash, G.; Bal Ozturk, A.; Saghazadeh, S.; Farhan Sohail, M.; Seo, J.; Remzi Dokmeci, M.; Zhang, Y.S.; Khademhosseini, A. Evolution and Clinical Translation of Drug Delivery Nanomaterials. *Nano Today* **2017**, *15*, 91–106, doi:10.1016/j.nantod.2017.06.008.
49. dos Santos, M.A.; Grenha, A. Polysaccharide Nanoparticles for Protein and Peptide Delivery. In *Advances in Protein Chemistry and Structural Biology*; Elsevier, 2015; Vol. 98, pp. 223–261 ISBN 978-0-12-802828-5.
50. Lakkireddy, H.R.; Bazile, D.V. Nano-Carriers for Drug Routeing – towards a New Era. *Journal of Drug Targeting* **2019**, *27*, 525–541, doi:10.1080/1061186X.2018.1561891.
51. Conniot, J.; Silva, J.M.; Fernandes, J.G.; Silva, L.C.; Gaspar, R.; Brocchini, S.; Florindo, H.F.; Barata, T.S. Cancer Immunotherapy: Nanodelivery Approaches for Immune Cell Targeting and Tracking. *Front. Chem.* **2014**, *2*, doi:10.3389/fchem.2014.00105.
52. Patra, J.K.; Das, G.; Fraceto, L.F.; Campos, E.V.R.; Rodriguez-Torres, M. del P.; Acosta-Torres, L.S.; Diaz-Torres, L.A.; Grillo, R.; Swamy, M.K.; Sharma, S.; et al. Nano Based Drug Delivery Systems: Recent Developments and Future Prospects. *J Nanobiotechnol* **2018**, *16*, 71, doi:10.1186/s12951-018-0392-8.
53. Chenthamara, D.; Subramaniam, S.; Ramakrishnan, S.G.; Krishnaswamy, S.; Essa, M.M.; Lin, F.-H.; Qoronfleh, M.W. Therapeutic Efficacy of Nanoparticles and Routes of Administration. *Biomater Res* **2019**, *23*, 20, doi:10.1186/s40824-019-0166-x.
54. Fenton, O.S.; Olafson, K.N.; Pillai, P.S.; Mitchell, M.J.; Langer, R. Advances in Biomaterials for Drug Delivery. *Adv. Mater.* **2018**, *30*, 1705328, doi:10.1002/adma.201705328.
55. Havel, H.A. Where Are the Nanodrugs? An Industry Perspective on Development of Drug Products Containing Nanomaterials. *AAPS J* **2016**, *18*, 1351–1353, doi:10.1208/s12248-016-9970-6.
56. Ventola, C.L. Progress in Nanomedicine: Approved and Investigational Nanodrugs. **2017**, 14.
57. Anselmo, A.C.; Mitragotri, S. Nanoparticles in the Clinic: An Update. *Bioeng Transl Med* **2019**, *4*, doi:10.1002/btm2.10143.
58. Anselmo, A.C.; Mitragotri, S. Nanoparticles in the Clinic. *Bioeng Transl Med* **2016**, *1*, 10–29, doi:10.1002/btm2.10003.
59. Metselaar, J.M.; Lammers, T. Challenges in Nanomedicine Clinical Translation. *Drug Deliv. and Transl. Res.* **2020**, doi:10.1007/s13346-020-00740-5.
60. Svenson, S. Clinical Translation of Nanomedicines. *Current Opinion in Solid State and Materials Science* **2012**, *16*, 287–294, doi:10.1016/j.cossms.2012.10.001.
61. Abed, S.N.; Deb, P.K.; Surchi, H.S.; Kokaz, S.F.; Jamal, S.M.; Bandopadhyay, S.; Tekade, R.K. Nanocarriers in Different Preclinical and Clinical Stages. In *Basic Fundamentals of Drug Delivery*; Elsevier, 2019; pp. 685–731 ISBN 978-0-12-817909-3.
62. Macdougall, I.C. Evolution of IV Iron Compounds over the Last Century. *Journal of Renal Care* **2009**, *35*, 8–13, doi:10.1111/j.1755-6686.2009.00127.x.
63. Na, H.B.; Song, I.C.; Hyeon, T. Inorganic Nanoparticles for MRI Contrast Agents. *Adv. Mater.* **2009**, *21*, 2133–2148, doi:10.1002/adma.200802366.
64. Schütz, C.A.; Juillerat-Jeanneret, L.; Mueller, H.; Lynch, I.; Riediker, M. Therapeutic Nanoparticles in Clinics and under Clinical Evaluation. *Nanomedicine* **2013**, *8*, 449–467, doi:10.2217/nnm.13.8.

65. Jeevanandam, J.; Barhoum, A.; Chan, Y.S.; Dufresne, A.; Danquah, M.K. Review on Nanoparticles and Nanostructured Materials: History, Sources, Toxicity and Regulations. *Beilstein J. Nanotechnol.* **2018**, *9*, 1050–1074, doi:10.3762/bjnano.9.98.
66. Li, D.; van Nostrum, C.F.; Mastrobattista, E.; Vermonden, T.; Hennink, W.E. Nanogels for Intracellular Delivery of Biotherapeutics. *Journal of Controlled Release* **2017**, *259*, 16–28, doi:10.1016/j.jconrel.2016.12.020.
67. Coty, J.-B.; Vauthier, C. Characterization of Nanomedicines: A Reflection on a Field under Construction Needed for Clinical Translation Success. *Journal of Controlled Release* **2018**, *275*, 254–268, doi:10.1016/j.jconrel.2018.02.013.
68. Farjadian, F.; Ghasemi, A.; Gohari, O.; Roointan, A.; Karimi, M.; Hamblin, M.R. Nanopharmaceuticals and Nanomedicines Currently on the Market: Challenges and Opportunities. *Nanomedicine* **2019**, *14*, 93–126, doi:10.2217/nnm-2018-0120.
69. Hickey, J.W.; Santos, J.L.; Williford, J.-M.; Mao, H.-Q. Control of Polymeric Nanoparticle Size to Improve Therapeutic Delivery. *Journal of Controlled Release* **2015**, *219*, 536–547, doi:10.1016/j.jconrel.2015.10.006.
70. Majumder, J.; Taratula, O.; Minko, T. Nanocarrier-Based Systems for Targeted and Site Specific Therapeutic Delivery. *Advanced Drug Delivery Reviews* **2019**, *144*, 57–77, doi:10.1016/j.addr.2019.07.010.
71. Vinogradov, S.V.; Bronich, T.K.; Kabanov, A.V. Nanosized Cationic Hydrogels for Drug Delivery: Preparation, Properties and Interactions with Cells. *Advanced Drug Delivery Reviews* **2002**, *54*, 135–147, doi:10.1016/S0169-409X(01)00245-9.
72. Goldberg, M.; Langer, R.; Jia, X. Nanostructured Materials for Applications in Drug Delivery and Tissue Engineering. *Journal of Biomaterials Science, Polymer Edition* **2007**, *18*, 241–268, doi:10.1163/156856207779996931.
73. Ahmadzada, T.; Reid, G.; McKenzie, D.R. Fundamentals of SiRNA and MiRNA Therapeutics and a Review of Targeted Nanoparticle Delivery Systems in Breast Cancer. *Biophysical Reviews* **2018**, *10*, 69–86, doi:10.1007/s12551-017-0392-1.
74. Li, Y.; Kröger, M.; Liu, W.K. Shape Effect in Cellular Uptake of PEGylated Nanoparticles: Comparison between Sphere, Rod, Cube and Disk. *Nanoscale* **2015**, *7*, 16631–16646, doi:10.1039/C5NR02970H.
75. St, B. Marina A. Dobrovolskaia* and Scott E. McNeil. *nature nanotechnology* **2007**, *2*, 10.
76. Lin, P.-C.; Lin, S.; Wang, P.C.; Sridhar, R. Techniques for Physicochemical Characterization of Nanomaterials. *Biotechnology Advances* **2014**, *32*, 711–726, doi:10.1016/j.biotechadv.2013.11.006.
77. Mohanraj, V.J.; Chen, Y. Nanoparticles - A Review. *Trop. J. Pharm Res* **2007**, *5*, 561–573, doi:10.4314/tjpr.v5i1.14634.
78. Hoshyar, N.; Gray, S.; Han, H.; Bao, G. The Effect of Nanoparticle Size on *in Vivo* Pharmacokinetics and Cellular Interaction. *Nanomedicine* **2016**, *11*, 673–692, doi:10.2217/nnm.16.5.
79. Guo, X.; Huang, L. Recent Advances in Nonviral Vectors for Gene Delivery. *Acc. Chem. Res.* **2012**, *45*, 971–979, doi:10.1021/ar200151m.
80. Merkel, O.M.; Librizzi, D.; Pfestroff, A.; Schurrat, T.; Buyens, K.; Sanders, N.N.; De Smedt, S.C.; Béhé, M.; Kissel, T. Stability of SiRNA Polyplexes from Poly(Ethylenimine) and Poly(Ethylenimine)-g-Poly(Ethylene Glycol) under in Vivo Conditions: Effects on Pharmacokinetics and Biodistribution Measured by Fluorescence Fluctuation Spectroscopy and Single Photon Emission Computed Tomography (SPECT) Imaging. *Journal of Controlled Release* **2009**, *138*, 148–159, doi:10.1016/j.jconrel.2009.05.016.

81. Martins, G.O.; Segalla Petrônio, M.; Furuyama Lima, A.M.; Martinez Junior, A.M.; de Oliveira Tiera, V.A.; de Freitas Calmon, M.; Leite Vilamaior, P.S.; Han, S.W.; Tiera, M.J. Amphipathic Chitosans Improve the Physicochemical Properties of SiRNA-Chitosan Nanoparticles at Physiological Conditions. *Carbohydrate Polymers* **2019**, S0144861719303777, doi:10.1016/j.carbpol.2019.03.098.
82. Avramović, N.; Mandić, B.; Savić-Radojević, A.; Simić, T. Polymeric Nanocarriers of Drug Delivery Systems in Cancer Therapy. **2020**, 18.
83. George, A.; Shah, P.A.; Shrivastav, P.S. Natural Biodegradable Polymers Based Nano-Formulations for Drug Delivery: A Review. *International Journal of Pharmaceutics* **2019**, *561*, 244–264, doi:10.1016/j.ijpharm.2019.03.011.
84. Rai, R.; Alwani, S.; Badea, I. Polymeric Nanoparticles in Gene Therapy: New Avenues of Design and Optimization for Delivery Applications. *Polymers* **2019**, *11*, 745, doi:10.3390/polym11040745.
85. Kean, T.; Roth, S.; Thanou, M. Trimethylated Chitosans as Non-Viral Gene Delivery Vectors: Cytotoxicity and Transfection Efficiency. *Journal of Controlled Release* **2005**, *103*, 643–653, doi:10.1016/j.jconrel.2005.01.001.
86. Bravo-Anaya, L.M.; Fernández-Solís, K.G.; Rosselgong, J.; Nano-Rodríguez, J.L.E.; Carvajal, F.; Rinaudo, M. Chitosan-DNA Polyelectrolyte Complex: Influence of Chitosan Characteristics and Mechanism of Complex Formation. *International Journal of Biological Macromolecules* **2019**, *126*, 1037–1049, doi:10.1016/j.ijbiomac.2019.01.008.
87. Wang, F.; Zhang, Q.; Huang, K.; Li, J.; Wang, K.; Zhang, K.; Tang, X. Preparation and Characterization of Carboxymethyl Cellulose Containing Quaternized Chitosan for Potential Drug Carrier. *International Journal of Biological Macromolecules* **2019**, S0141813019360076, doi:10.1016/j.ijbiomac.2019.11.019.
88. Jo, A.; Ringel-Scaia, V.M.; McDaniel, D.K.; Thomas, C.A.; Zhang, R.; Riffle, J.S.; Allen, I.C.; Davis, R.M. Fabrication and Characterization of PLGA Nanoparticles Encapsulating Large CRISPR–Cas9 Plasmid. *J Nanobiotechnol* **2020**, *18*, 16, doi:10.1186/s12951-019-0564-1.
89. Ban, E.; Kwon, T.-H.; Kim, A. Delivery of Therapeutic MiRNA Using Polymer-Based Formulation. *Drug Deliv. and Transl. Res.* **2019**, doi:10.1007/s13346-019-00645-y.
90. Debele, T.A.; Mekuria, S.L.; Tsai, H.-C. Polysaccharide Based Nanogels in the Drug Delivery System: Application as the Carrier of Pharmaceutical Agents. *Materials Science and Engineering: C* **2016**, *68*, 964–981, doi:10.1016/j.msec.2016.05.121.
91. Seidi, F.; Jenjob, R.; Phakkeeree, T.; Crespy, D. Saccharides, Oligosaccharides, and Polysaccharides Nanoparticles for Biomedical Applications. *Journal of Controlled Release* **2018**, *284*, 188–212, doi:10.1016/j.jconrel.2018.06.026.
92. Yang, J.; Han, S.; Zheng, H.; Dong, H.; Liu, J. Preparation and Application of Micro/Nanoparticles Based on Natural Polysaccharides. *Carbohydrate Polymers* **2015**, *123*, 53–66, doi:10.1016/j.carbpol.2015.01.029.
93. Chen, F.; Huang, G. Preparation and Immunological Activity of Polysaccharides and Their Derivatives. *International Journal of Biological Macromolecules* **2018**, *112*, 211–216, doi:10.1016/j.ijbiomac.2018.01.169.
94. Raemdonck, K.; Martens, T.F.; Braeckmans, K.; Demeester, J.; De Smedt, S.C. Polysaccharide-Based Nucleic Acid Nanoformulations. *Advanced Drug Delivery Reviews* **2013**, *65*, 1123–1147, doi:10.1016/j.addr.2013.05.002.

95. Hassani, L.N.; Hendra, F.; Bouchemal, K. Auto-Associative Amphiphilic Polysaccharides as Drug Delivery Systems. *Drug Discovery Today* **2012**, *17*, 608–614, doi:10.1016/j.drudis.2012.01.016.
96. Thomas, T.J.; Tajmir-Riahi, H.-A.; Pillai, C.K.S. Biodegradable Polymers for Gene Delivery. *Molecules* **2019**, *24*, 3744, doi:10.3390/molecules24203744.
97. Swierczewska, M.; Han, H.S.; Kim, K.; Park, J.H.; Lee, S. Polysaccharide-Based Nanoparticles for Theranostic Nanomedicine. *Advanced Drug Delivery Reviews* **2016**, *99*, 70–84, doi:10.1016/j.addr.2015.11.015.
98. Zhang, H.; Ma, Y.; Sun, X.-L. Recent Developments in Carbohydrate-Decorated Targeted Drug/Gene Delivery. *Med. Res. Rev.* **2009**, n/a-n/a, doi:10.1002/med.20171.
99. Lee, J.W.; Park, J.H.; Robinson, J.R. Bioadhesive-Based Dosage Forms: The next Generation. *JOURNAL OF PHARMACEUTICAL SCIENCES* **2000**, *89*, 17.
100. Serrano-Sevilla, I.; Artiga, Á.; Mitchell, S.G.; De Matteis, L.; de la Fuente, J.M. Natural Polysaccharides for SiRNA Delivery: Nanocarriers Based on Chitosan, Hyaluronic Acid, and Their Derivatives. *Molecules* **2019**, *24*, 2570, doi:10.3390/molecules24142570.
101. Miao, T.; Wang, J.; Zeng, Y.; Liu, G.; Chen, X. Polysaccharide-Based Controlled Release Systems for Therapeutics Delivery and Tissue Engineering: From Bench to Bedside. *Adv. Sci.* **2018**, *5*, 1700513, doi:10.1002/advs.201700513.
102. Nair, L.S.; Laurencin, C.T. Biodegradable Polymers as Biomaterials. *Progress in Polymer Science* **2007**, *32*, 762–798, doi:10.1016/j.progpolymsci.2007.05.017.
103. Zhang, N.; Wardwell, P.; Bader, R. Polysaccharide-Based Micelles for Drug Delivery. *Pharmaceutics* **2013**, *5*, 329–352, doi:10.3390/pharmaceutics5020329.
104. Islam, N.; Dmour, I.; Taha, M.O. Degradability of Chitosan Micro/Nanoparticles for Pulmonary Drug Delivery. *Heliyon* **2019**, *5*, e01684, doi:10.1016/j.heliyon.2019.e01684.
105. Mohandas, A.; Anisha, B.S.; Chennazhi, K.P.; Jayakumar, R. Chitosan–Hyaluronic Acid/VEGF Loaded Fibrin Nanoparticles Composite Sponges for Enhancing Angiogenesis in Wounds. *Colloids and Surfaces B: Biointerfaces* **2015**, *127*, 105–113, doi:10.1016/j.colsurfb.2015.01.024.
106. Mi, F.-L.; Sung, H.-W.; Shyu, S.-S.; Su, C.-C.; Peng, C.-K. Synthesis and Characterization of Biodegradable TPP/Genipin Co-Crosslinked Chitosan Gel Beads. *Polymer* **2003**, *44*, 6521–6530, doi:10.1016/S0032-3861(03)00620-7.
107. Farshbaf, M.; Davaran, S.; Zarebkohan, A.; Annabi, N.; Akbarzadeh, A.; Salehi, R. Significant Role of Cationic Polymers in Drug Delivery Systems. *Artificial Cells, Nanomedicine, and Biotechnology* **2017**, 1–20, doi:10.1080/21691401.2017.1395344.
108. Cumpstey, I. Chemical Modification of Polysaccharides. *ISRN Organic Chemistry* **2013**, *2013*, 1–27, doi:10.1155/2013/417672.
109. Mizrahy, S.; Peer, D. ChemInform Abstract: Polysaccharides as Building Blocks for Nanotherapeutics. *ChemInform* **2012**, *43*, no-no, doi:10.1002/chin.201227260.
110. Bawa, P.; Pillay, V.; Choonara, Y.E.; du Toit, L.C.; Ndesendo, V.M.K.; Kumar, P. A Composite Polyelectrolytic Matrix for Controlled Oral Drug Delivery. *AAPS PharmSciTech* **2011**, *12*, 227–238, doi:10.1208/s12249-010-9576-8.
111. Sampaolesi, S.; Nicotra, F.; Russo, L. Glycans in Nanomedicine, Impact and Perspectives. *Future Medicinal Chemistry* **2019**, *11*, 43–60, doi:10.4155/fmc-2018-0368.
112. Dionísio, M.; Braz, L.; Corvo, M.; Lourenço, J.P.; Grenha, A.; Rosa da Costa, A.M. Charged Pullulan Derivatives for the Development of Nanocarriers by

Polyelectrolyte Complexation. *International Journal of Biological Macromolecules* **2016**, *86*, 129–138, doi:10.1016/j.ijbiomac.2016.01.054.

113. Zhang, T.; Yang, R.; Yang, S.; Guan, J.; Zhang, D.; Ma, Y.; Liu, H. Research Progress of Self-Assembled Nanogel and Hybrid Hydrogel Systems Based on Pullulan Derivatives. *Drug Delivery* **2018**, *25*, 278–292, doi:10.1080/10717544.2018.1425776.
114. Wen, Y.; Oh, J.K. Recent Strategies to Develop Polysaccharide-Based Nanomaterials for Biomedical Applications. *Macromol. Rapid Commun.* **2014**, n/a-n/a, doi:10.1002/marc.201400406.
115. Xiao, B.; Ma, P.; Ma, L.; Chen, Q.; Si, X.; Walter, L.; Merlin, D. Effects of Tripolyphosphate on Cellular Uptake and RNA Interference Efficiency of Chitosan-Based Nanoparticles in Raw 264.7 Macrophages. *Journal of Colloid and Interface Science* **2017**, *490*, 520–528, doi:10.1016/j.jcis.2016.11.088.
116. Ahmed, T.; Aljaeid, B. Preparation, Characterization, and Potential Application of Chitosan, Chitosan Derivatives, and Chitosan Metal Nanoparticles in Pharmaceutical Drug Delivery. *Drug Design, Development and Therapy* **2016**, 483, doi:10.2147/DDDT.S99651.
117. Saravanakumar, G.; Jo, D.-G.; H. Park, J. Polysaccharide-Based Nanoparticles: A Versatile Platform for Drug Delivery and Biomedical Imaging. *CMC* **2012**, *19*, 3212–3229, doi:10.2174/092986712800784658.
118. Mokhtarzadeh, A.; Alibakhshi, A.; Yaghoobi, H.; Hashemi, M.; Hejazi, M.; Ramezani, M. Recent Advances on Biocompatible and Biodegradable Nanoparticles as Gene Carriers. *Expert Opinion on Biological Therapy* **2016**, *16*, 771–785, doi:10.1517/14712598.2016.1169269.
119. Basu, A.; Kunduru, K.R.; Abtew, E.; Domb, A.J. Polysaccharide-Based Conjugates for Biomedical Applications. *Bioconjugate Chem.* **2015**, *26*, 1396–1412, doi:10.1021/acs.bioconjchem.5b00242.
120. Nitta, S.; Numata, K. Biopolymer-Based Nanoparticles for Drug/Gene Delivery and Tissue Engineering. *IJMS* **2013**, *14*, 1629–1654, doi:10.3390/ijms14011629.
121. Berger, J.; Reist, M.; Mayer, J.M.; Felt, O.; Peppas, N.A.; Gurny, R. Structure and Interactions in Covalently and Ionically Crosslinked Chitosan Hydrogels for Biomedical Applications. *European Journal of Pharmaceutics and Biopharmaceutics* **2004**, *57*, 19–34, doi:10.1016/S0939-6411(03)00161-9.
122. Banerjee, T.; Mitra, S.; Kumar Singh, A.; Kumar Sharma, R.; Maitra, A. Preparation, Characterization and Biodistribution of Ultrafine Chitosan Nanoparticles. *International Journal of Pharmaceutics* **2002**, *243*, 93–105, doi:10.1016/S0378-5173(02)00267-3.
123. Ballantyne, B.; Jordan, S.L. Toxicological, Medical and Industrial Hygiene Aspects of Glutaraldehyde with Particular Reference to Its Biocidal Use in Cold Sterilization Procedures. *J. Appl. Toxicol.* **2001**, *21*, 131–151, doi:10.1002/jat.741.
124. Deng, X.; Cao, M.; Zhang, J.; Hu, K.; Yin, Z.; Zhou, Z.; Xiao, X.; Yang, Y.; Sheng, W.; Wu, Y.; et al. Hyaluronic Acid-Chitosan Nanoparticles for Co-Delivery of MiR-34a and Doxorubicin in Therapy against Triple Negative Breast Cancer. *Biomaterials* **2014**, *35*, 4333–4344, doi:10.1016/j.biomaterials.2014.02.006.
125. Lu, H.-T.; Lu, T.-W.; Chen, C.-H.; Mi, F.-L. Development of Genipin-Crosslinked and Fucoidan-Adsorbed Nano-Hydroxyapatite/Hydroxypropyl Chitosan Composite Scaffolds for Bone Tissue Engineering. *International Journal of Biological Macromolecules* **2019**, *128*, 973–984, doi:10.1016/j.ijbiomac.2019.02.010.

126. Pujana, M.A.; Pérez-Álvarez, L.; Iturbe, L.C.C.; Katime, I. Water Soluble Folate-Chitosan Nanogels Crosslinked by Genipin. *Carbohydrate Polymers* **2014**, *101*, 113–120, doi:10.1016/j.carbpol.2013.09.014.
127. Razi, M.A.; Wakabayashi, R.; Tahara, Y.; Goto, M.; Kamiya, N. Genipin-Stabilized Caseinate-Chitosan Nanoparticles for Enhanced Stability and Anti-Cancer Activity of Curcumin. *Colloids and Surfaces B: Biointerfaces* **2018**, *164*, 308–315, doi:10.1016/j.colsurfb.2018.01.041.
128. Lin, Y.-H.; Tsai, S.-C.; Lai, C.-H.; Lee, C.-H.; He, Z.S.; Tseng, G.-C. Genipin-Cross-Linked Fucose–Chitosan/Heparin Nanoparticles for the Eradication of Helicobacter Pylori. *Biomaterials* **2013**, *34*, 4466–4479, doi:10.1016/j.biomaterials.2013.02.028.
129. Karimi, M.; Avci, P.; Ahi, M.; Gazori, T.; Hamblin, M.R.; Naderi-Manesh, H. Evaluation of Chitosan-Tripolyphosphate Nanoparticles as a p-ShRNA Delivery Vector: Formulation, Optimization and Cellular Uptake Study. *Journal of Nanopharmaceutics and Drug Delivery* **2013**, *1*, 266–278, doi:10.1166/jnd.2013.1027.
130. Wang, S.; Cao, M.; Deng, X.; Xiao, X.; Yin, Z.; Hu, Q.; Zhou, Z.; Zhang, F.; Zhang, R.; Wu, Y.; et al. Degradable Hyaluronic Acid/Protamine Sulfate Interpolyelectrolyte Complexes as MiRNA-Delivery Nanocapsules for Triple-Negative Breast Cancer Therapy. *Advanced Healthcare Materials* **2015**, *4*, 281–290, doi:10.1002/adhm.201400222.
131. Chen, K.-Y.; Zeng, S.-Y. Fabrication of Quaternized Chitosan Nanoparticles Using Tripolyphosphate/Genipin Dual Cross-Linkers as a Protein Delivery System. *Polymers* **2018**, *10*, 1226, doi:10.3390/polym10111226.
132. Liu, Z.; Jiao, Y.; Wang, Y.; Zhou, C.; Zhang, Z. Polysaccharides-Based Nanoparticles as Drug Delivery Systems. *Advanced Drug Delivery Reviews* **2008**, *60*, 1650–1662, doi:10.1016/j.addr.2008.09.001.
133. Lächelt, U.; Wagner, E. Nucleic Acid Therapeutics Using Polyplexes: A Journey of 50 Years (and Beyond). *Chemical Reviews* **2015**, *115*, 11043–11078, doi:10.1021/cr5006793.
134. Folchman-Wagner, Z.; Zaro, J.; Shen, W.-C. Characterization of Polyelectrolyte Complex Formation Between Anionic and Cationic Poly(Amino Acids) and Their Potential Applications in PH-Dependent Drug Delivery. *Molecules* **2017**, *22*, 1089, doi:10.3390/molecules22071089.
135. Meka, V.S.; Sing, M.K.G.; Pichika, M.R.; Nali, S.R.; Kolapalli, V.R.M.; Kesharwani, P. A Comprehensive Review on Polyelectrolyte Complexes. *Drug Discovery Today* **2017**, *22*, 1697–1706, doi:10.1016/j.drudis.2017.06.008.
136. Hartig, S.M.; Greene, R.R.; Dikov, M.M.; Prokop, A.; Davidson, J.M. Multifunctional Nanoparticulate Polyelectrolyte Complexes. *Pharm Res* **2007**, *24*, 2353–2369, doi:10.1007/s11095-007-9459-1.
137. Raik, S.V.; Gasilova, E.R.; Dubashynskaya, N.V.; Dobrodumov, A.V.; Skorik, Y.A. Diethylaminoethyl Chitosan–Hyaluronic Acid Polyelectrolyte Complexes. *International Journal of Biological Macromolecules* **2019**, S0141813019365936, doi:10.1016/j.ijbiomac.2019.10.054.
138. Bourganis, V.; Karamanidou, T.; Kammona, O.; Kiparissides, C. Polyelectrolyte Complexes as Prospective Carriers for the Oral Delivery of Protein Therapeutics. *European Journal of Pharmaceutics and Biopharmaceutics* **2017**, *111*, 44–60, doi:10.1016/j.ejpb.2016.11.005.

139. Hu, B.; Wang, S.S.; Li, J.; Zeng, X.X.; Huang, Q.R. Assembly of Bioactive Peptide–Chitosan Nanocomplexes. *The Journal of Physical Chemistry B* **2011**, *115*, 7515–7523, doi:10.1021/jp2013557.
140. Sarmento, B.; Ferreira, D.C.; Jorgensen, L.; van de Weert, M. Probing Insulin's Secondary Structure after Entrapment into Alginate/Chitosan Nanoparticles. *European Journal of Pharmaceutics and Biopharmaceutics* **2007**, *65*, 10–17, doi:10.1016/j.ejpb.2006.09.005.
141. Safari, S.; Dorkoosh, F.A.; Soleimani, M.; Zarrintan, M.H.; Akbari, H.; Larijani, B.; Tehrani, M.R. N-Diethylmethyl Chitosan for Gene Delivery to Pancreatic Cancer Cells and the Relation between Charge Ratio and Biologic Properties of Polyplexes via Interpolations Polynomial. *International Journal of Pharmaceutics* **2011**, *420*, 350–357, doi:10.1016/j.ijpharm.2011.08.050.
142. Thomas, J.J.; Rekha, M.R.; Sharma, C.P. Dextran–Glycidyltrimethylammonium Chloride Conjugate/DNA Nanoplex: A Potential Non-Viral and Haemocompatible Gene Delivery System. *International Journal of Pharmaceutics* **2010**, *389*, 195–206, doi:10.1016/j.ijpharm.2010.01.011.
143. Amaduzzi, F.; Bomboi, F.; Bonincontro, A.; Bordi, F.; Casciardi, S.; Chronopoulou, L.; Diociaiuti, M.; Mura, F.; Palocci, C.; Sennato, S. Chitosan–DNA Complexes: Charge Inversion and DNA Condensation. *Colloids and Surfaces B: Biointerfaces* **2014**, *114*, 1–10, doi:10.1016/j.colsurfb.2013.09.029.
144. Shen, Z.; Xia, Y.; Yang, Q.; Tian, W.; Chen, K.; Ma, Y. Polymer–Nucleic Acid Interactions. *Top Curr Chem (Z)* **2017**, *375*, 44, doi:10.1007/s41061-017-0131-x.
145. Kim, I.-S.; Oh, I.-J. Preparation and Characterization of Stearic Acid-Pullulan Nanoparticles. *Arch. Pharm. Res.* **2010**, *33*, 761–767, doi:10.1007/s12272-010-0516-7.
146. Henni-Silhadi, W.; Deyme, M.; Boissonnade, M.-M.; Appel, M.; Le Cerf, D.; Picton, L.; Rosilio, V. Enhancement of the Solubility and Efficacy of Poorly Water-Soluble Drugs by Hydrophobically-Modified Polysaccharide Derivatives. *Pharm Res* **2007**, *24*, 2317–2326, doi:10.1007/s11095-007-9461-7.
147. Chen, S.; Cheng, S.-X.; Zhuo, R.-X. Self-Assembly Strategy for the Preparation of Polymer-Based Nanoparticles for Drug and Gene Delivery. *Macromol. Biosci.* **2011**, *11*, 576–589, doi:10.1002/mabi.201000427.
148. Alhaique, F.; Matricardi, P.; Di Meo, C.; Coviello, T.; Montanari, E. Polysaccharide-Based Self-Assembling Nanohydrogels: An Overview on 25-Years Research on Pullulan. *Journal of Drug Delivery Science and Technology* **2015**, *30*, 300–309, doi:10.1016/j.jddst.2015.06.005.
149. Morimoto, N.; Hirano, S.; Takahashi, H.; Loethen, S.; Thompson, D.H.; Akiyoshi, K. Self-Assembled PH-Sensitive Cholesteryl Pullulan Nanogel As a Protein Delivery Vehicle. *Biomacromolecules* **2013**, *14*, 56–63, doi:10.1021/bm301286h.
150. Zhu, C.; Jung, S.; Luo, S.; Meng, F.; Zhu, X.; Park, T.G.; Zhong, Z. Co-Delivery of SiRNA and Paclitaxel into Cancer Cells by Biodegradable Cationic Micelles Based on PDMAEMA–PCL–PDMAEMA Triblock Copolymers. *Biomaterials* **2010**, *31*, 2408–2416, doi:10.1016/j.biomaterials.2009.11.077.
151. Khan, W.; Hosseinkhani, H.; Ickowicz, D.; Hong, P.-D.; Yu, D.-S.; Domb, A.J. Polysaccharide Gene Transfection Agents. *Acta Biomaterialia* **2012**, *8*, 4224–4232, doi:10.1016/j.actbio.2012.09.022.
152. Dinçer, S.; Türk, M.; Pişkin, E. Intelligent Polymers as Nonviral Vectors. *Gene Ther* **2005**, *12*, S139–S145, doi:10.1038/sj.gt.3302628.

153. Cao, Y.; Tan, Y.F.; Wong, Y.S.; Liew, M.W.J.; Venkatraman, S. Recent Advances in Chitosan-Based Carriers for Gene Delivery. *Marine Drugs* **2019**, *17*, 381, doi:10.3390/md17060381.
154. Chakraborty, C.; Sharma, A.R.; Sharma, G.; Doss, C.G.P.; Lee, S.-S. Therapeutic MiRNA and SiRNA: Moving from Bench to Clinic as Next Generation Medicine. *Molecular Therapy - Nucleic Acids* **2017**, *8*, 132–143, doi:10.1016/j.omtn.2017.06.005.
155. Xiong, Q.; Lee, G.Y.; Ding, J.; Li, W.; Shi, J. Biomedical Applications of MRNA Nanomedicine. *Nano Res.* **2018**, *11*, 5281–5309, doi:10.1007/s12274-018-2146-1.
156. Itani, R.; Al Faraj, A. SiRNA Conjugated Nanoparticles—A Next Generation Strategy to Treat Lung Cancer. *IJMS* **2019**, *20*, 6088, doi:10.3390/ijms20236088.
157. Patil, S.D.; Rhodes, D.G.; Burgess, D.J. DNA-Based Therapeutics and DNA Delivery Systems: A Comprehensive Review. *AAPS J* **2005**, *7*, E61–E77, doi:10.1208/aapsj070109.
158. Shatsberg, Z.; Zhang, X.; Ofek, P.; Malhotra, S.; Krivitsky, A.; Scomparin, A.; Tiram, G.; Calderón, M.; Haag, R.; Satchi-Fainaro, R. Functionalized Nanogels Carrying an Anticancer MicroRNA for Glioblastoma Therapy. *Journal of Controlled Release* **2016**, *239*, 159–168, doi:10.1016/j.jconrel.2016.08.029.
159. Falzone; Lupo; Rosa; Crimi; Anfuso; Salemi; Rapisarda; Libra; Candido Identification of Novel MicroRNAs and Their Diagnostic and Prognostic Significance in Oral Cancer. *Cancers* **2019**, *11*, 610, doi:10.3390/cancers11050610.
160. Devaux, Y.; Stammet, P.; Friberg, H.; Hassager, C.; Kuiper, M.A.; Wise, M.P.; Nielsen, N.; for the Biomarker subcommittee of the TTM trial (Target Temperature Management After Cardiac Arrest, NCT01020916) MicroRNAs: New Biomarkers and Therapeutic Targets after Cardiac Arrest? *Critical Care* **2015**, *19*, 54, doi:10.1186/s13054-015-0767-2.
161. Qiagen Guidelines for MiRNA Mimic and MiRNA Inhibitor Experiments. Https://Www.Qiagen.Com/Fr/Resources/Resourcedetail?Id=3e1477ad-74a2-4ee6-9c31- 54b1997f2941&lang=en. **2018**.
162. Fernandez-Piñeiro, I.; Badiola, I.; Sanchez, A. Nanocarriers for MicroRNA Delivery in Cancer Medicine. *Biotechnology Advances* **2017**, *35*, 350–360, doi:10.1016/j.biotechadv.2017.03.002.
163. Gadde, S.; Rayner, K.J. Nanomedicine Meets MicroRNA: Current Advances in RNA-Based Nanotherapies for Atherosclerosis. *Arteriosclerosis, Thrombosis, and Vascular Biology* **2016**, *36*, doi:10.1161/ATVBAHA.116.307481.
164. Hanna, J.; Hossain, G.S.; Kocerha, J. The Potential for MicroRNA Therapeutics and Clinical Research. *Front. Genet.* **2019**, *10*, 478, doi:10.3389/fgene.2019.00478.
165. Zhu, Y.; Liang, G.; Sun, B.; Tian, T.; Hu, F.; Xiao, Z. A Novel Type of Self-Assembled Nanoparticles as Targeted Gene Carriers: An Application for Plasmid DNA and AntimicroRNA Oligonucleotide Delivery. *IJN* **2016**, 399, doi:10.2147/IJN.S84927.
166. Pack, D.W.; Hoffman, A.S.; Pun, S.; Stayton, P.S. Design and Development of Polymers for Gene Delivery. *Nat Rev Drug Discov* **2005**, *4*, 581–593, doi:10.1038/nrd1775.
167. Mansouri, S.; Lavigne, P.; Corsi, K.; Benderdour, M.; Beaumont, E.; Fernandes, J.C. Chitosan-DNA Nanoparticles as Non-Viral Vectors in Gene Therapy: Strategies to Improve Transfection Efficacy. *European Journal of Pharmaceutics and Biopharmaceutics* **2004**, *57*, 1–8, doi:10.1016/S0939-6411(03)00155-3.

168. Jiang, H.-L.; Cui, P.-F.; Xie, R.-L.; Cho, C.-S. Chemical Modification of Chitosan for Efficient Gene Therapy. In *Advances in Food and Nutrition Research*; Elsevier, 2014; Vol. 73, pp. 83–101 ISBN 978-0-12-800268-1.
169. Ballarín-González, B.; Howard, K.A. Polycation-Based Nanoparticle Delivery of RNAi Therapeutics: Adverse Effects and Solutions. *Advanced Drug Delivery Reviews* **2012**, *64*, 1717–1729, doi:10.1016/j.addr.2012.07.004.
170. Pereira, P.; Jorge, A.F.; Martins, R.; Pais, A.A.C.C.; Sousa, F.; Figueiras, A. Characterization of Polyplexes Involving Small RNA. *Journal of Colloid and Interface Science* **2012**, *387*, 84–94, doi:10.1016/j.jcis.2012.07.088.
171. Wang, Y.; Ye, M.; Xie, R.; Gong, S. Enhancing the In Vitro and In Vivo Stabilities of Polymeric Nucleic Acid Delivery Nanosystems. *Bioconjugate Chem.* **2019**, *30*, 325–337, doi:10.1021/acs.bioconjchem.8b00749.
172. O'Driscoll, C.M.; Bernkop-Schnürch, A.; Friedl, J.D.; Préat, V.; Jannin, V. Oral Delivery of Non-Viral Nucleic Acid-Based Therapeutics - Do We Have the Guts for This? *European Journal of Pharmaceutical Sciences* **2019**, *133*, 190–204, doi:10.1016/j.ejps.2019.03.027.
173. Chen, Y.; Li, J.; Oupický, D. Conjugate Polyplexes with Anti-Invasive Properties and Improved SiRNA Delivery In Vivo. *Bioconjugate Chem.* **2018**, *29*, 296–305, doi:10.1021/acs.bioconjchem.7b00622.
174. Scholz, C.; Wagner, E. Therapeutic Plasmid DNA versus SiRNA Delivery: Common and Different Tasks for Synthetic Carriers. *Journal of Controlled Release* **2012**, *161*, 554–565, doi:10.1016/j.jconrel.2011.11.014.
175. Nuhn, L.; Tomcin, S.; Miyata, K.; Mailänder, V.; Landfester, K.; Kataoka, K.; Zentel, R. Size-Dependent Knockdown Potential of SiRNA-Loaded Cationic Nanohydrogel Particles. *Biomacromolecules* **2014**, *15*, 4111–4121, doi:10.1021/bm501148y.
176. Chiu, Y.-L. SiRNA Function in RNAi: A Chemical Modification Analysis. *RNA* **2003**, *9*, 1034–1048, doi:10.1261/rna.5103703.
177. Gary, D.J.; Puri, N.; Won, Y.-Y. Polymer-Based SiRNA Delivery: Perspectives on the Fundamental and Phenomenological Distinctions from Polymer-Based DNA Delivery. *Journal of Controlled Release* **2007**, *121*, 64–73, doi:10.1016/j.jconrel.2007.05.021.
178. Scomparin, A.; Polyak, D.; Krivitsky, A.; Satchi-Fainaro, R. Achieving Successful Delivery of Oligonucleotides — From Physico-Chemical Characterization to in Vivo Evaluation. *Biotechnology Advances* **2015**, *33*, 1294–1309, doi:10.1016/j.biotechadv.2015.04.008.
179. Sukumar, U.K.; Bose, R.J.C.; Malhotra, M.; Babikir, H.A.; Afjei, R.; Robinson, E.; Zeng, Y.; Chang, E.; Habte, F.; Sinclair, R.; et al. Intranasal Delivery of Targeted Polyfunctional Gold–Iron Oxide Nanoparticles Loaded with Therapeutic MicroRNAs for Combined Theranostic Multimodality Imaging and Presensitization of Glioblastoma to Temozolomide. *Biomaterials* **2019**, *218*, 119342, doi:10.1016/j.biomaterials.2019.119342.
180. Leder, A.; Raschzok, N.; Schmidt, C.; Arabacioglu, D.; Butter, A.; Kolano, S.; de Sousa Lisboa, L.S.; Werner, W.; Polenz, D.; Reutzel-Selke, A.; et al. Micron-Sized Iron Oxide-Containing Particles for MicroRNA-Targeted Manipulation and MRI-Based Tracking of Transplanted Cells. *Biomaterials* **2015**, *51*, 129–137, doi:10.1016/j.biomaterials.2015.01.065.
181. Conde, J.; Ambrosone, A.; Hernandez, Y.; Tian, F.; McCully, M.; Berry, C.C.; Baptista, P.V.; Tortiglione, C.; de la Fuente, J.M. 15 Years on SiRNA Delivery:

Beyond the State-of-the-Art on Inorganic Nanoparticles for RNAi Therapeutics. *Nano Today* **2015**, *10*, 421–450, doi:10.1016/j.nantod.2015.06.008.

182. Lee, S.W.L.; Paoletti, C.; Campisi, M.; Osaki, T.; Adriani, G.; Kamm, R.D.; Mattu, C.; Chiono, V. MicroRNA Delivery through Nanoparticles. *Journal of Controlled Release* **2019**, *313*, 80–95, doi:10.1016/j.jconrel.2019.10.007.
183. Boca, S. Nanoscale Delivery Systems for MicroRNAs in Cancer Therapy. 28.
184. Coradeghini, R.; Gioria, S.; García, C.P.; Nativo, P.; Franchini, F.; Gilliland, D.; Ponti, J.; Rossi, F. Size-Dependent Toxicity and Cell Interaction Mechanisms of Gold Nanoparticles on Mouse Fibroblasts. *Toxicology Letters* **2013**, *217*, 205–216, doi:10.1016/j.toxlet.2012.11.022.
185. Muthiah, M.; Park, I.-K.; Cho, C.-S. Nanoparticle-Mediated Delivery of Therapeutic Genes: Focus on MiRNA Therapeutics. *Expert Opinion on Drug Delivery* **2013**, *10*, 1259–1273, doi:10.1517/17425247.2013.798640.
186. Tivnan, A.; Orr, W.S.; Gubala, V.; Nooney, R.; Williams, D.E.; McDonagh, C.; Prenter, S.; Harvey, H.; Domingo-Fernández, R.; Bray, I.M.; et al. Inhibition of Neuroblastoma Tumor Growth by Targeted Delivery of MicroRNA-34a Using Anti-Disialoganglioside GD2 Coated Nanoparticles. *PLoS ONE* **2012**, *7*, e38129, doi:10.1371/journal.pone.0038129.
187. Panebianco, F.; Climent, M.; Malvindi, M.A.; Pompa, P.P.; Bonetti, P.; Nicassio, F. Delivery of Biologically Active MiR-34a in Normal and Cancer Mammary Epithelial Cells by Synthetic Nanoparticles. *Nanomedicine: Nanotechnology, Biology and Medicine* **2019**, *19*, 95–105, doi:10.1016/j.nano.2019.03.013.
188. Yang, H.-W.; Huang, C.-Y.; Lin, C.-W.; Liu, H.-L.; Huang, C.-W.; Liao, S.-S.; Chen, P.-Y.; Lu, Y.-J.; Wei, K.-C.; Ma, C.-C.M. Gadolinium-Functionalized Nanographene Oxide for Combined Drug and MicroRNA Delivery and Magnetic Resonance Imaging. *Biomaterials* **2014**, *35*, 6534–6542, doi:10.1016/j.biomaterials.2014.04.057.
189. Semple, S.C.; Akinc, A.; Chen, J.; Sandhu, A.P.; Mui, B.L.; Cho, C.K.; Sah, D.W.Y.; Stebbing, D.; Crosley, E.J.; Yaworski, E.; et al. Rational Design of Cationic Lipids for SiRNA Delivery. *Nat Biotechnol* **2010**, *28*, 172–176, doi:10.1038/nbt.1602.
190. Campani, V.; Zappavigna, S.; Scotti, L.; Abate, M.; Porru, M.; Leonetti, C.; Caraglia, M.; De Rosa, G. Hybrid Lipid Self-Assembling Nanoparticles for Brain Delivery of MicroRNA. *International Journal of Pharmaceutics* **2020**, *588*, 119693, doi:10.1016/j.ijpharm.2020.119693.
191. Granot, Y.; Peer, D. Delivering the Right Message: Challenges and Opportunities in Lipid Nanoparticles-Mediated Modified MRNA Therapeutics—An Innate Immune System Standpoint. *Seminars in Immunology* **2017**, *34*, 68–77, doi:10.1016/j.smim.2017.08.015.
192. Campani, V.; Salzano, G.; Lusa, S.; Rosa, G.D. Lipid Nanovectors to Deliver RNA Oligonucleotides in Cancer. **2016**, 22.
193. Scheideler, M.; Vidakovic, I.; Prassl, R. Lipid Nanocarriers for MicroRNA Delivery. *Chemistry and Physics of Lipids* **2020**, *226*, 104837, doi:10.1016/j.chemphyslip.2019.104837.
194. Kulkarni, J.A.; Cullis, P.R.; van der Meel, R. Lipid Nanoparticles Enabling Gene Therapies: From Concepts to Clinical Utility. *Nucleic Acid Therapeutics* **2018**, *28*, 146–157, doi:10.1089/nat.2018.0721.
195. Kulkarni, A.D.; Vanjari, Y.H.; Sancheti, K.H.; Patel, H.M.; Belgamwar, V.S.; Surana, S.J.; Pardeshi, C.V. Polyelectrolyte Complexes: Mechanisms, Critical

Experimental Aspects, and Applications. *Artificial Cells, Nanomedicine, and Biotechnology* **2016**, *44*, 1615–1625, doi:10.3109/21691401.2015.1129624.

196. Leung, A.K.K.; Tam, Y.Y.C.; Cullis, P.R. Lipid Nanoparticles for Short Interfering RNA Delivery. In *Advances in Genetics*; Elsevier, 2014; Vol. 88, pp. 71–110 ISBN 978-0-12-800148-6.
197. Uchida, S.; Perche, F.; Pichon, C.; Cabral, H. Nanomedicine-Based Approaches for MRNA Delivery. *Mol. Pharmaceutics* **2020**, *17*, 3654–3684, doi:10.1021/acs.molpharmaceut.0c00618.
198. Yung, B.C.; Li, J.; Zhang, M.; Cheng, X.; Li, H.; Yung, E.M.; Kang, C.; Cosby, L.E.; Liu, Y.; Teng, L.; et al. Lipid Nanoparticles Composed of Quaternary Amine–Tertiary Amine Cationic Lipid Combination (QTsome) for Therapeutic Delivery of AntimiR-21 for Lung Cancer. *Mol. Pharmaceutics* **2016**, *13*, 653–662, doi:10.1021/acs.molpharmaceut.5b00878.
199. Trang, P.; Wiggins, J.F.; Daige, C.L.; Cho, C.; Omotola, M.; Brown, D.; Weidhaas, J.B.; Bader, A.G.; Slack, F.J. Systemic Delivery of Tumor Suppressor MicroRNA Mimics Using a Neutral Lipid Emulsion Inhibits Lung Tumors in Mice. *Molecular Therapy* **2011**, *19*, 1116–1122, doi:10.1038/mt.2011.48.
200. Nogueira, E.; Freitas, J.; Loureiro, A.; Nogueira, P.; Gomes, A.C.; Preto, A.; Carmo, A.M.; Moreira, A.; Cavaco-Paulo, A. Neutral PEGylated Liposomal Formulation for Efficient Folate-Mediated Delivery of MCL1 SiRNA to Activated Macrophages. *Colloids and Surfaces B: Biointerfaces* **2017**, *155*, 459–465, doi:10.1016/j.colsurfb.2017.04.023.
201. Radmanesh, F.; Abandansari, H.S.; Pahlavan, S.; Alikhani, M.; Karimi, M.; Rajabi, S.; Kazemi, B.; Baharvand, H. Optimization of MiRNA Delivery by Using a Polymeric Conjugate Based on Deoxycholic Acid-Modified Polyethylenimine. *International Journal of Pharmaceutics* **2019**, *565*, 391–408, doi:10.1016/j.ijpharm.2019.05.009.
202. Gao, S.; Tian, H.; Guo, Y.; Li, Y.; Guo, Z.; Zhu, X.; Chen, X. MiRNA Oligonucleotide and Sponge for MiRNA-21 Inhibition Mediated by PEI-PLL in Breast Cancer Therapy. *Acta Biomaterialia* **2015**, *25*, 184–193, doi:10.1016/j.actbio.2015.07.020.
203. Raik, S.; Andranovitš, S.; Petrova, V.; Xu, Y.; Lam, J.; Morris, G.; Brodskaia, A.; Casettari, L.; Kritchenkov, A.; Skorik, Y. Comparative Study of Diethylaminoethyl-Chitosan and Methylglycol-Chitosan as Potential Non-Viral Vectors for Gene Therapy. *Polymers* **2018**, *10*, 442, doi:10.3390/polym10040442.
204. Shi, B.; Zheng, M.; Tao, W.; Chung, R.; Jin, D.; Ghaffari, D.; Farokhzad, O.C. Challenges in DNA Delivery and Recent Advances in Multifunctional Polymeric DNA Delivery Systems. *Biomacromolecules* **2017**, *18*, 2231–2246, doi:10.1021/acs.biomac.7b00803.
205. Yao, J.; Fan, Y.; Du, R.; Zhou, J.; Lu, Y.; Wang, W.; Ren, J.; Sun, X. Amphoteric Hyaluronic Acid Derivative for Targeting Gene Delivery. *Biomaterials* **2010**, *31*, 9357–9365, doi:10.1016/j.biomaterials.2010.08.043.
206. Devulapally, R.; Sekar, N.M.; Sekar, T.V.; Foygel, K.; Massoud, T.F.; Willmann, J.K.; Paulmurugan, R. Polymer Nanoparticles Mediated Codelivery of AntimiR-10b and AntimiR-21 for Achieving Triple Negative Breast Cancer Therapy. *ACS Nano* **2015**, *9*, 2290–2302, doi:10.1021/nn507465d.
207. Singh, A.; Arora, S.; Swaminathan, S.K.; Kirtane, A.; Srivastava, S.; Bhardwaj, A.; Singh, S.; Panyam, J. Synthesis, Characterization, and Evaluation of Poly (D,L-Lactide-Co-Glycolide)-Based Nanoformulation of MiRNA-150: Potential

Implications for Pancreatic Cancer Therapy. *IJN* **2014**, 2933, doi:10.2147/IJN.S61949.

208. Nishio, H.; Masumoto, H.; Sakamoto, K.; Yamazaki, K.; Ikeda, T.; Minatoya, K. MicroRNA-145-Loaded Poly(Lactic-Co-Glycolic Acid) Nanoparticles Attenuate Venous Intimal Hyperplasia in a Rabbit Model. *The Journal of Thoracic and Cardiovascular Surgery* **2019**, *157*, 2242–2251, doi:10.1016/j.jtcvs.2018.08.115.
209. Abedi-Gaballu, F.; Dehghan, G.; Ghaffari, M.; Yekta, R.; Abbaspour-Ravasjani, S.; Baradaran, B.; Ezzati Nazhad Dolatabadi, J.; Hamblin, M.R. PAMAM Dendrimers as Efficient Drug and Gene Delivery Nanosystems for Cancer Therapy. *Applied Materials Today* **2018**, *12*, 177–190, doi:10.1016/j.apmt.2018.05.002.
210. Liu, X.; Liu, C.; Catapano, C.V.; Peng, L.; Zhou, J.; Rocchi, P. Structurally Flexible Triethanolamine-Core Poly(Amidoamine) Dendrimers as Effective Nanovectors to Deliver RNAi-Based Therapeutics. *Biotechnology Advances* **2014**, *32*, 844–852, doi:10.1016/j.biotechadv.2013.08.001.
211. Lee, J.H.; Lim, Y.; Choi, J.S.; Lee, Y.; Kim, T.; Kim, H.J.; Yoon, J.K.; Kim, K.; Park, J. Polyplexes Assembled with Internally Quaternized PAMAM-OH Dendrimer and Plasmid DNA Have a Neutral Surface and Gene Delivery Potency. *Bioconjugate Chem.* **2003**, *14*, 1214–1221, doi:10.1021/bc034095g.
212. Sayed, N.; Tambe, P.; Kumar, P.; Jadhav, S.; Paknikar, K.M.; Gajbhiye, V. MiRNA Transfection via Poly(Amidoamine)-Based Delivery Vector Prevents Hypoxia/Reperfusion-Induced Cardiomyocyte Apoptosis. *Nanomedicine* **2020**, *15*, 163–181, doi:10.2217/nnm-2019-0363.
213. Ren, Y.; Kang, C.-S.; Yuan, X.-B.; Zhou, X.; Xu, P.; Han, L.; Wang, G.X.; Jia, Z.; Zhong, Y.; Yu, S.; et al. Co-Delivery of as-MiR-21 and 5-FU by Poly(Amidoamine) Dendrimer Attenuates Human Glioma Cell Growth in Vitro. *Journal of Biomaterials Science, Polymer Edition* **2010**, *21*, 303–314, doi:10.1163/156856209X415828.
214. Martirosyan, A.; Olesen, M.J.; Howard, K.A. Chitosan-Based Nanoparticles for Mucosal Delivery of RNAi Therapeutics. In *Advances in Genetics*; Elsevier, 2014; Vol. 88, pp. 325–352 ISBN 978-0-12-800148-6.
215. Holzerny, P.; Ajdini, B.; Heusermann, W.; Bruno, K.; Schuleit, M.; Meinel, L.; Keller, M. Biophysical Properties of Chitosan/SiRNA Polyplexes: Profiling the Polymer/SiRNA Interactions and Bioactivity. *Journal of Controlled Release* **2012**, *157*, 297–304, doi:10.1016/j.jconrel.2011.08.023.
216. Gaur, S.; Wen, Y.; Song, J.H.; Parikh, N.U.; Mangala, L.S.; Blessing, A.M.; Ivan, C.; Wu, S.Y.; Varkaris, A.; Shi, Y.; et al. Chitosan Nanoparticle-Mediated Delivery of MiRNA-34a Decreases Prostate Tumor Growth in the Bone and Its Expression Induces Non-Canonical Autophagy. *Oncotarget* **2015**, *6*, doi:10.18632/oncotarget.4971.
217. Santos-Carballal, B.; Aaldering, L.J.; Ritzefeld, M.; Pereira, S.; Sewald, N.; Moerschbacher, B.M.; Götte, M.; Goycoolea, F.M. Physicochemical and Biological Characterization of Chitosan-MicroRNA Nanocomplexes for Gene Delivery to MCF-7 Breast Cancer Cells. *Sci Rep* **2015**, *5*, 13567, doi:10.1038/srep13567.
218. Kaban, K.; Salva, E.; Akbuga, J. *In Vitro* Dose Studies on Chitosan Nanoplexes for MicroRNA Delivery in Breast Cancer Cells. *Nucleic Acid Therapeutics* **2017**, *27*, 45–55, doi:10.1089/nat.2016.0633.
219. Ragelle, H.; Riva, R.; Vandermeulen, G.; Naeye, B.; Pourcelle, V.; Le Duff, C.S.; D'Haese, C.; Nysten, B.; Braeckmans, K.; De Smedt, S.C.; et al. Chitosan

Nanoparticles for SiRNA Delivery: Optimizing Formulation to Increase Stability and Efficiency. *Journal of Controlled Release* **2014**, *176*, 54–63, doi:10.1016/j.jconrel.2013.12.026.

220. Louw, A.M. Chitosan Polyplex Mediated Delivery of MiRNA-124 Reduces Activation of Microglial Cells in Vitro and in Rat Models of Spinal Cord Injury. 39.
221. Tekie, F.S.M.; Kiani, M.; Zakerian, A.; Pilevarian, F.; Assali, A.; Soleimani, M.; Dinarvand, R.; Arefian, E.; Atashi, A.; Amini, M.; et al. Nano Polyelectrolyte Complexes of Carboxymethyl Dextran and Chitosan to Improve Chitosan-Mediated Delivery of MiR-145. *Carbohydrate Polymers* **2017**, *159*, 66–75, doi:10.1016/j.carbpol.2016.11.067.
222. Ma, W.; Liu, J.; Xie, J.; Zhang, X.; Zhou, H.; Yao, H.; Zhang, W.; Guo, D.; Zhu, L.; Xiao, L.; et al. Modulating the Growth and Imatinib Sensitivity of Chronic Myeloid Leukemia Stem/Progenitor Cells with Pullulan/MicroRNA Nanoparticles <I>In</I> <I>Vitro</I>. *j biomed nanotechnol* **2015**, *11*, 1961–1974, doi:10.1166/jbn.2015.2147.
223. Zhou, F.; Jia, X.; Yang, Q.; Yang, Y.; Zhao, Y.; Fan, Y.; Yuan, X. Targeted Delivery of MicroRNA-126 to Vascular Endothelial Cells via REDV Peptide Modified PEG-Trimethyl Chitosan. *Biomater. Sci.* **2016**, *4*, 849–856, doi:10.1039/C5BM00629E.
224. Fröhlich, T.; Edinger, D.; Russ, V.; Wagner, E. Stabilization of Polyplexes via Polymer Crosslinking for Efficient SiRNA Delivery. *European Journal of Pharmaceutical Sciences* **2012**, *47*, 914–920, doi:10.1016/j.ejps.2012.09.006.
225. Lou, B.; Beztsinna, N.; Mountrichas, G.; van den Dikkenberg, J.B.; Pispas, S.; Hennink, W.E. Small Nanosized Poly(Vinyl Benzyl Trimethylammonium Chloride) Based Polyplexes for SiRNA Delivery. *International Journal of Pharmaceutics* **2017**, *525*, 388–396, doi:10.1016/j.ijpharm.2017.03.036.
226. Wang, Y.; Ma, B.; Abdeen, A.A.; Chen, G.; Xie, R.; Saha, K.; Gong, S. Versatile Redox-Responsive Polyplexes for the Delivery of Plasmid DNA, Messenger RNA, and CRISPR-Cas9 Genome-Editing Machinery. *ACS Appl. Mater. Interfaces* **2018**, *10*, 31915–31927, doi:10.1021/acsami.8b09642.
227. Labatut, A.E.; Mattheolabakis, G. Non-Viral Based MiR Delivery and Recent Developments. *European Journal of Pharmaceutics and Biopharmaceutics* **2018**, *128*, 82–90, doi:10.1016/j.ejpb.2018.04.018.
228. Pilipenko, I.; Korzhikov-Vlakh, V.; Sharoyko, V.; Zhang, N.; Schäfer-Korting, M.; Rühl, E.; Zoschke, C.; Tennikova, T. PH-Sensitive Chitosan–Heparin Nanoparticles for Effective Delivery of Genetic Drugs into Epithelial Cells. *Pharmaceutics* **2019**, *11*, 317, doi:10.3390/pharmaceutics11070317.
229. Liu, Z.; Zhang, Z.; Zhou, C.; Jiao, Y. Hydrophobic Modifications of Cationic Polymers for Gene Delivery. *Progress in Polymer Science* **2010**, *35*, 1144–1162, doi:10.1016/j.progpolymsci.2010.04.007.
230. Tamura, A.; Nagasaki, Y. Smart SiRNA Delivery Systems Based on Polymeric Nanoassemblies and Nanoparticles. *Nanomedicine* **2010**, *5*, 1089–1102, doi:10.2217/nnm.10.76.
231. Ganas, C.; Weiß, A.; Nazarenus, M.; Rösler, S.; Kissel, T.; Rivera_Gil, P.; Parak, W.J. Biodegradable Capsules as Non-Viral Vectors for in Vitro Delivery of PEI/SiRNA Polyplexes for Efficient Gene Silencing. *Journal of Controlled Release* **2014**, *196*, 132–138, doi:10.1016/j.jconrel.2014.10.006.
232. Antunes, J.C.; Benarroch, L.; Moraes, F.C.; Juenet, M.; Gross, M.-S.; Aubart, M.; Boileau, C.; Caligiuri, G.; Nicoletti, A.; Ollivier, V.; et al. Core-Shell Polymer-

Based Nanoparticles To Deliver MiR-155-5p To Endothelial Cells. *Molecular Therapy - Nucleic Acids* **2019**, S2162253119301465, doi:10.1016/j.omtn.2019.05.016.

233. Wolff JA; Malone RW; Williams P; Chong W; Acsadi G; Jani A; Felgner PL Direct Gene Transfer into Mouse Muscle in Vivo. *Science* **1990**, *247*, 1465–1468.
234. Zarghampoor, F.; Azarpira, N.; Khatami, S.R.; Behzad-Behbahani, A.; Foroughmand, A.M. Improved Translation Efficiency of Therapeutic MRNA. *Gene* **2019**, *707*, 231–238, doi:10.1016/j.gene.2019.05.008.
235. Bernardo, B.C.; Ooi, J.Y.; Lin, R.C.; McMullen, J.R. MiRNA Therapeutics: A New Class of Drugs with Potential Therapeutic Applications in the Heart. *Future Medicinal Chemistry* **2015**, *7*, 1771–1792, doi:10.4155/fmc.15.107.
236. Rupaimoole, R.; Slack, F.J. MicroRNA Therapeutics: Towards a New Era for the Management of Cancer and Other Diseases. *Nature Reviews Drug Discovery* **2017**, *16*, 203–222, doi:10.1038/nrd.2016.246.
237. Zhu, L.; Chen, T.; Ye, W.; Wang, J.-Y.; Zhou, J.-P.; Li, Z.-Y.; Li, C.-C. Circulating MiR-182-5p and MiR-5187-5p as Biomarkers for the Diagnosis of Unprotected Left Main Coronary Artery Disease. *Journal of Thoracic Disease* **2019**, *11*, 1799–1808, doi:10.21037/jtd.2019.05.24.
238. Hou, W.; Tian, Q.; Steuerwald, N.M.; Schrum, L.W.; Bonkovsky, H.L. The Let-7 MicroRNA Enhances Heme Oxygenase-1 by Suppressing Bach1 and Attenuates Oxidant Injury in Human Hepatocytes. *Biochimica et Biophysica Acta (BBA) - Gene Regulatory Mechanisms* **2012**, *1819*, 1113–1122, doi:10.1016/j.bbagrm.2012.06.001.
239. Poddar, S.; Kesharwani, D.; Datta, M. MiR-449a Regulates Insulin Signalling by Targeting the Notch Ligand, Jag1 in Skeletal Muscle Cells. *Cell Communication and Signaling* **2019**, *17*, doi:10.1186/s12964-019-0394-7.
240. Candido, S.; Lupo, G.; Pennisi, M.; Basile, M.; Anfuso, C.; Petralia, M.; Gattuso, G.; Vivarelli, S.; Spandidos, D.; Libra, M.; et al. The Analysis of MiRNA Expression Profiling Datasets Reveals Inverse MicroRNA Patterns in Glioblastoma and Alzheimer's Disease. *Oncology Reports* **2019**, doi:10.3892/or.2019.7215.
241. Mao, S.; Sun, W.; Kissel, T. Chitosan-Based Formulations for Delivery of DNA and SiRNA. *Advanced Drug Delivery Reviews* **2010**, *62*, 12–27, doi:10.1016/j.addr.2009.08.004.
242. Lounis, F.M.; Chamieh, J.; Gonzalez, P.; Cottet, H.; Leclercq, L. Prediction of Polyelectrolyte Complex Stoichiometry for Highly Hydrophilic Polyelectrolytes. *Macromolecules* **2016**, *49*, 3881–3888, doi:10.1021/acs.macromol.6b00463.
243. Thanou, M.; Florea, B.I.; Geldof, M.; Junginger, H.E.; Borchard, G. Quaternized Chitosan Oligomers as Novel Gene Delivery Vectors in Epithelial Cell Lines. *Biomaterials* **2002**, *23*, 153–159, doi:10.1016/S0142-9612(01)00090-4.
244. K.R., S.; V., P. Review on Production, Downstream Processing and Characterization of Microbial Pullulan. *Carbohydrate Polymers* **2017**, *173*, 573–591, doi:10.1016/j.carbpol.2017.06.022.
245. Prajapati, V.D.; Jani, G.K.; Khanda, S.M. Pullulan: An Exopolysaccharide and Its Various Applications. *Carbohydrate Polymers* **2013**, *95*, 540–549, doi:10.1016/j.carbpol.2013.02.082.
246. Rekha, M.R.; Sharma, C.P. Blood Compatibility and in Vitro Transfection Studies on Cationically Modified Pullulan for Liver Cell Targeted Gene Delivery. *Biomaterials* **2009**, *30*, 6655–6664, doi:10.1016/j.biomaterials.2009.08.029.

247. San Juan, A.; Ducrocq, G.; Hlawaty, H.; Bataille, I.; Guénin, E.; Letourneur, D.; Feldman, L.J. Tubular Cationized Pullulan Hydrogels as Local Reservoirs for Plasmid DNA. *Journal of Biomedical Materials Research Part A* **2007**, *83A*, 819–827, doi:10.1002/jbm.a.31413.
248. San Juan, A.; Bala, M.; Hlawaty, H.; Portes, P.; Vranckx, R.; Feldman, L.J.; Letourneur, D. Development of a Functionalized Polymer for Stent Coating in the Arterial Delivery of Small Interfering RNA. *Biomacromolecules* **2009**, *10*, 3074–3080, doi:10.1021/bm900740g.
249. Shao, Z.; Xu, T.; Wang, S.; Liu, W. Elucidating the Role of Free Polycationic Chains in Polycation Gene Carriers by Free Chains of Polyethylenimine or N,N,N-Trimethyl Chitosan plus a Certain Polyplex. *IJN* **2014**, 3231, doi:10.2147/IJN.S64308.
250. Stefan, J.; Kus, K.; Wisniewska, A.; Kaminski, K.; Szczubialka, K.; Jawien, J.; Nowakowska, M.; Korbut, R. New Cationically Modified Pullulan Attenuates Atherogenesis and Influences Lipid Metabolism in ApoE-Knockout Mice. *J Physiol Pharmacol* **2016**, *67*, 739–749.
251. Liu, P.; Meng, W.; Wang, S.; Sun, Y.; Aqeel Ashraf, M. Quaternary Ammonium Salt of Chitosan: Preparation and Antimicrobial Property for Paper. *Open Medicine* **2015**, *10*, doi:10.1515/med-2015-0081.
252. Stuart, B.H. Infrared Spectroscopy: Fundamentals and Applications. **2004**, 208.
253. Li, Q.; Tan, W.; Zhang, C.; Gu, G.; Guo, Z. Synthesis of Water Soluble Chitosan Derivatives with Halogeno-1,2,3-Triazole and Their Antifungal Activity. *International Journal of Biological Macromolecules* **2016**, *91*, 623–629, doi:10.1016/j.ijbiomac.2016.06.006.
254. Vauthier, C.; Zandanel, C.; Ramon, A.L. Chitosan-Based Nanoparticles for in Vivo Delivery of Interfering Agents Including SiRNA. *Current Opinion in Colloid & Interface Science* **2013**, *18*, 406–418, doi:10.1016/j.cocis.2013.06.005.
255. Zhao, Q.-Q.; Chen, J.-L.; Lv, T.-F.; He, C.-X.; Tang, G.-P.; Liang, W.-Q.; Tabata, Y.; Gao, J.-Q. N/P Ratio Significantly Influences the Transfection Efficiency and Cytotoxicity of a Polyethylenimine/Chitosan/DNA Complex. *Biological & Pharmaceutical Bulletin* **2009**, *32*, 706–710, doi:10.1248/bpb.32.706.
256. Tekie, F.S.M.; Atyabi, F.; Soleimani, M.; Arefian, E.; Atashi, A.; Kiani, M.; Khoshayand, M.R.; Amini, M.; Dinarvand, R. Chitosan Polyplex Nanoparticle Vector for MiR-145 Expression in MCF-7: Optimization by Design of Experiment. *International Journal of Biological Macromolecules* **2015**, *81*, 828–837, doi:10.1016/j.ijbiomac.2015.09.014.
257. de Paula Pansani Oliveira, F.; Picola, I.P.D.; Shi, Q.; Barbosa, H.F.G.; de Oliveira Tiera, V.A.; Fernandes, J.C.; Tiera, M.J. Synthesis and Evaluation of Diethylethylamine–Chitosan for Gene Delivery: Composition Effects on the *in Vitro* Transfection Efficiency. *Nanotechnology* **2013**, *24*, 055101, doi:10.1088/0957-4484/24/5/055101.
258. Liu, X.; Howard, K.A.; Dong, M.; Andersen, M.Ø.; Rahbek, U.L.; Johnsen, M.G.; Hansen, O.C.; Besenbacher, F.; Kjems, J. The Influence of Polymeric Properties on Chitosan/SiRNA Nanoparticle Formulation and Gene Silencing. *Biomaterials* **2007**, *28*, 1280–1288, doi:10.1016/j.biomaterials.2006.11.004.
259. Alameh, M.; Lavertu, M.; Tran-Khanh, N.; Chang, C.-Y.; Lesage, F.; Bail, M.; Darras, V.; Chevrier, A.; Buschmann, M.D. SiRNA Delivery with Chitosan: Influence of Chitosan Molecular Weight, Degree of Deacetylation, and Amine to Phosphate Ratio on in Vitro Silencing Efficiency, Hemocompatibility,

Biodistribution, and in Vivo Efficacy. *Biomacromolecules* **2018**, *19*, 112–131, doi:10.1021/acs.biomac.7b01297.

260. Avadi, M.R.; Sadeghi, A.M.M.; Mohammadpour, N.; Abedin, S.; Atyabi, F.; Dinarvand, R.; Rafiee-Tehrani, M. Preparation and Characterization of Insulin Nanoparticles Using Chitosan and Arabic Gum with Ionic Gelation Method. *Nanomedicine: Nanotechnology, Biology and Medicine* **2010**, *6*, 58–63, doi:10.1016/j.nano.2009.04.007.
261. Wu, D.; Delair, T. Stabilization of Chitosan/Hyaluronan Colloidal Polyelectrolyte Complexes in Physiological Conditions. *Carbohydrate Polymers* **2015**, *119*, 149–158, doi:10.1016/j.carbpol.2014.11.042.
262. Goyal, R.; Kapadia, C.H.; Melamed, J.R.; Riley, R.S.; Day, E.S. Layer-by-Layer Assembled Gold Nanoshells for the Intracellular Delivery of MiR-34a. *Cel. Mol. Bioeng.* **2018**, *11*, 383–396, doi:10.1007/s12195-018-0535-x.
263. André, E.M.; Pensado, A.; Resnier, P.; Braz, L.; Rosa da Costa, A.M.; Passirani, C.; Sanchez, A.; Montero-Menei, C.N. Characterization and Comparison of Two Novel Nanosystems Associated with SiRNA for Cellular Therapy. *International Journal of Pharmaceutics* **2016**, *497*, 255–267, doi:10.1016/j.ijpharm.2015.11.020.
264. Siewert, C.; Haas, H.; Nawroth, T.; Ziller, A.; Nogueira, S.S.; Schroer, M.A.; Blanchet, C.E.; Svergun, D.I.; Radulescu, A.; Bates, F.; et al. Investigation of Charge Ratio Variation in MRNA – DEAE-Dextran Polyplex Delivery Systems. *Biomaterials* **2019**, *192*, 612–620, doi:10.1016/j.biomaterials.2018.10.020.
265. Souguir, Z.; Roudesli, S.; About-Jaudet, E.; Picton, L.; Le Cerf, D. Novel Cationic and Amphiphilic Pullulan Derivatives II: PH Dependant Physicochemical Properties. *Carbohydrate Polymers* **2010**, *80*, 123–129, doi:10.1016/j.carbpol.2009.11.003.
266. Ho, T.T.M.; Bremmell, K.E.; Krasowska, M.; Stringer, D.N.; Beattie, D.A. Tuning Polyelectrolyte Multilayer Structure by Exploiting Natural Variation in Fucoidan Chemistry. 43.
267. Gök, M.K. In Vitro Evaluation of Synergistic Effect of Primary and Tertiary Amino Groups in Chitosan Used as a Non-Viral Gene Carrier System. *European Polymer Journal* **2019**, *115*, 375–383, doi:10.1016/j.eurpolymj.2019.03.048.
268. Jc, A.; Rm, G.; Ma, B. Chitosan/Poly(γ-Glutamic Acid) Polyelectrolyte Complexes: From Self- Assembly to Application in Biomolecules Delivery and Regenerative Medicine. *Res. Rev. J Mat. Sci* **2016**, *04*, doi:10.4172/2321-6212.1000153.
269. Liu, X.; Ma, L.; Qin, W.; Gao, C. Effect of N/P Ratios on Physicochemical Stability, Cellular Association, and Gene Silencing Efficiency for Trimethyl Chitosan/Small Interfering RNA Complexes. *Journal of Bioactive and Compatible Polymers* **2013**, *28*, 590–604, doi:10.1177/0883911513508495.
270. Juenet, M.; Aid-Launais, R.; Li, B.; Berger, A.; Aerts, J.; Ollivier, V.; Nicoletti, A.; Letourneur, D.; Chauvierre, C. Thrombolytic Therapy Based on Fucoidan-Functionalized Polymer Nanoparticles Targeting P-Selectin. *Biomaterials* **2018**, *156*, 204–216, doi:10.1016/j.biomaterials.2017.11.047.
271. Strand, S.P.; Issa, M.M.; Christensen, B.E.; Vårum, K.M.; Artursson, P. Tailoring of Chitosans for Gene Delivery: Novel Self-Branched Glycosylated Chitosan Oligomers with Improved Functional Properties. *Biomacromolecules* **2008**, *9*, 3268–3276, doi:10.1021/bm800832u.
272. Zhou, Z.; Zhang, M.; Liu, Y.; Li, C.; Zhang, Q.; Oupicky, D.; Sun, M. Reversible Covalent Cross-Linked Polycations with Enhanced Stability and ATP-Responsive

Behavior for Improved SiRNA Delivery. *Biomacromolecules* **2018**, *19*, 3776–3787, doi:10.1021/acs.biomac.8b00922.

273. Resina, S.; Prevot, P.; Thierry, A.R. Physico-Chemical Characteristics of Lipoplexes Influence Cell Uptake Mechanisms and Transfection Efficacy. *PLoS ONE* **2009**, *4*, e6058, doi:10.1371/journal.pone.0006058.
274. Baipaywad, P.; Udomluck, N.; Pyo, S.-G.; Park, H.H.; Park, H. Fabrication of Nanogels for Delivery of Molecules. *Journal of Nanoscience and Nanotechnology* **2014**, *14*, 7363–7373, doi:10.1166/jnn.2014.9579.
275. Zintchenko, A.; Philipp, A.; Dehshahri, A.; Wagner, E. Simple Modifications of Branched PEI Lead to Highly Efficient SiRNA Carriers with Low Toxicity. *Bioconjugate Chem.* **2008**, *19*, 1448–1455, doi:10.1021/bc800065f.
276. Moraes, F.C.; Antunes, J.C.; Forero Ramirez, L.M.; Aprile, P.; Franck, G.; Chauvierre, C.; Chaubet, F.; Letourneur, D. Synthesis of Cationic Quaternized Pullulan Derivatives for MiRNA Delivery. *International Journal of Pharmaceutics* **2020**, *577*, 119041, doi:10.1016/j.ijpharm.2020.119041.
277. Sung, H.-W.; Huang, R.-N.; Huang, L.L.H.; Tsai, C.-C. In Vitro Evaluation of Cytotoxicity of a Naturally Occurring Cross-Linking Reagent for Biological Tissue Fixation. *Journal of Biomaterials Science, Polymer Edition* **1999**, *10*, 63–78, doi:10.1163/156856299X00289.
278. Yu, S.-H.; Wu, S.-J.; Wu, J.-Y.; Wen, D.-Y.; Mi, F.-L. Preparation of Fucoidan-Shelled and Genipin-Crosslinked Chitosan Beads for Antibacterial Application. *Carbohydrate Polymers* **2015**, *126*, 97–107, doi:10.1016/j.carbpol.2015.02.068.
279. Hu, B.; Xie, M.; Zhang, C.; Zeng, X. Genipin-Structured Peptide–Polysaccharide Nanoparticles with Significantly Improved Resistance to Harsh Gastrointestinal Environments and Their Potential for Oral Delivery of Polyphenols. *Journal of Agricultural and Food Chemistry* **2014**, *62*, 12443–12452, doi:10.1021/jf5046766.
280. Butler, M.F.; Ng, Y.-F.; Pudney, P.D.A. Mechanism and Kinetics of the Crosslinking Reaction between Biopolymers Containing Primary Amine Groups and Genipin. *J. Polym. Sci. A Polym. Chem.* **2003**, *41*, 3941–3953, doi:10.1002/pola.10960.
281. Li, B.; Juenet, M.; Aid-Launais, R.; Maire, M.; Ollivier, V.; Letourneur, D.; Chauvierre, C. Development of Polymer Microcapsules Functionalized with Fucoidan to Target P-Selectin Overexpressed in Cardiovascular Diseases. *Adv. Healthcare Mater.* **2017**, *6*, 1601200, doi:10.1002/adhm.201601200.
282. Mi, F.-L.; Shyu, S.-S.; Peng, C.-K. Characterization of Ring-Opening Polymerization of Genipin and PH-Dependent Cross-Linking Reactions between Chitosan and Genipin. *J. Polym. Sci. A Polym. Chem.* **2005**, *43*, 1985–2000, doi:10.1002/pola.20669.
283. Kumar, G.V.; Su, C.-H.; Velusamy, P. Ciprofloxacin Loaded Genipin Cross-Linked Chitosan/Heparin Nanoparticles for Drug Delivery Application. *Materials Letters* **2016**, *180*, 119–122, doi:10.1016/j.matlet.2016.05.108.
284. Lin, Y.-H.; Lu, K.-Y.; Tseng, C.-L.; Wu, J.-Y.; Chen, C.-H.; Mi, F.-L. Development of Genipin-Crosslinked Fucoidan/Chitosan- *N* -Arginine Nanogels for Preventing *Helicobacter* Infection. *Nanomedicine* **2017**, *12*, 1491–1510, doi:10.2217/nnm-2017-0055.
285. Arteche Pujana, M.; Pérez-Álvarez, L.; Cesteros Iturbe, L.C.; Katime, I. Biodegradable Chitosan Nanogels Crosslinked with Genipin. *Carbohydrate Polymers* **2013**, *94*, 836–842, doi:10.1016/j.carbpol.2013.01.082.
286. Lachowicz, D.; Mielczarek, P.; Wirecka, R.; Berent, K.; Karewicz, A.; Szuwarzyński, M.; Zapotoczny, S. Nanohydrogels Based on Self-Assembly of

Cationic Pullulan and Anionic Dextran Derivatives for Efficient Delivery of Piroxicam. *Pharmaceutics* **2019**, *11*, 622, doi:10.3390/pharmaceutics11120622.

287. Huang, G.; Chen, Q.; Wu, W.; Wang, J.; Chu, P.K.; Bai, H.; Tang, G. Reconstructed Chitosan with Alkylamine for Enhanced Gene Delivery by Promoting Endosomal Escape. *Carbohydrate Polymers* **2020**, *227*, 115339, doi:10.1016/j.carbpol.2019.115339.
288. Fischer, D.; Li, Y.; Ahlemeyer, B.; Krieglstein, J.; Kissel, T. In Vitro Cytotoxicity Testing of Polycations: Influence of Polymer Structure on Cell Viability and Hemolysis. *Biomaterials* **2003**, *24*, 1121–1131, doi:10.1016/S0142-9612(02)00445-3.
289. Toy, R.; Pradhan, P.; Ramesh, V.; Di Paolo, N.C.; Lash, B.; Liu, J.; Blanchard, E.L.; Pinelli, C.J.; Santangelo, P.J.; Shayakhmetov, D.M.; et al. Modification of Primary Amines to Higher Order Amines Reduces in Vivo Hematological and Immunotoxicity of Cationic Nanocarriers through TLR4 and Complement Pathways. *Biomaterials* **2019**, *225*, 119512, doi:10.1016/j.biomaterials.2019.119512.
290. Palermo, E.F.; Lee, D.-K.; Ramamoorthy, A.; Kuroda, K. Role of Cationic Group Structure in Membrane Binding and Disruption by Amphiphilic Copolymers. *J. Phys. Chem. B* **2011**, *115*, 366–375, doi:10.1021/jp1083357.
291. Naeye, B. Hemocompatibility of SiRNA Loaded Dextran Nanogels. **2011**, 8.
292. Chatzitaki, A.-T.; Jesus, S.; Karavasili, C.; Andreadis, D.; Fatouros, D.G.; Borges, O. Chitosan-Coated PLGA Nanoparticles for the Nasal Delivery of Ropinirole Hydrochloride: In Vitro and Ex Vivo Evaluation of Efficacy and Safety. *International Journal of Pharmaceutics* **2020**, *589*, 119776, doi:10.1016/j.ijpharm.2020.119776.
293. Forero Ramirez, L.M.; Gobin, E.; Aid-Launais, R.; Journe, C.; Moraes, F.C.; Picton, L.; Le Cerf, D.; Letourneur, D.; Chauvierre, C.; Chaubet, F. Gd(DOTA)-Grafted Submicronic Polysaccharide-Based Particles Functionalized with Fucoidan as Potential MR Contrast Agent Able to Target Human Activated Platelets. *Carbohydrate Polymers* **2020**, *245*, 116457, doi:10.1016/j.carbpol.2020.116457.
294. Suzuki, M.; Bachelet-Violette, L.; Rouzet, F.; Beilvert, A.; Autret, G.; Maire, M.; Menager, C.; Louedec, L.; Choqueux, C.; Sabourał, P.; et al. Ultrasmall Superparamagnetic Iron Oxide Nanoparticles Coated with Fucoidan for Molecular MRI of Intraluminal Thrombus. *Nanomedicine* **2015**, *10*, 73–87, doi:10.2217/nnm.14.51.
295. Raemdonck, K.; Naeye, B.; Buyens, K.; Vandenbroucke, R.E.; Høgset, A.; Demeester, J.; De Smedt, S.C. Biodegradable Dextran Nanogels for RNA Interference: Focusing on Endosomal Escape and Intracellular SiRNA Delivery. *Advanced Functional Materials* **2009**, *19*, 1406–1415, doi:10.1002/adfm.200801795.
296. Pereira, P.; Morgado, D.; Crepet, A.; David, L.; Gama, F.M. Glycol Chitosan-Based Nanogel as a Potential Targetable Carrier for SiRNA: Glycol Chitosan-Based Carrier of SiRNA. *Macromol. Biosci.* **2013**, *13*, 1369–1378, doi:10.1002/mabi.201300123.
297. Khaled, S.Z.; Cevenini, A.; Yazdi, I.K.; Parodi, A.; Evangelopoulos, M.; Corbo, C.; Scaria, S.; Hu, Y.; Haddix, S.G.; Corradetti, B.; et al. One-Pot Synthesis of PH-Responsive Hybrid Nanogel Particles for the Intracellular Delivery of Small Interfering RNA. *Biomaterials* **2016**, *87*, 57–68, doi:10.1016/j.biomaterials.2016.01.052.

298. Akinc, A. The Onpattro Story and the Clinical Translation of Nanomedicines Containing Nucleic Acid-Based Drugs. *Nature Nanotechnology* **2019**, *14*, 4.
299. Hong, D.S.; Kang, Y.-K.; Borad, M.; Sachdev, J.; Ejadi, S.; Lim, H.Y.; Brenner, A.J.; Park, K.; Lee, J.-L.; Kim, T.-Y.; et al. Phase 1 Study of MRX34, a Liposomal MiR-34a Mimic, in Patients with Advanced Solid Tumours. *Br J Cancer* **2020**, *122*, 1630–1637, doi:10.1038/s41416-020-0802-1.
300. Moro, M. Coated Cationic Lipid-Nanoparticles Entrapping MiR-660 Inhibit Tumor Growth in Patient-Derived Xenografts Lung Cancer Models. *Journal of Controlled Release* **2019**, 13.
301. Lin, C.-W.; Jan, M.-S.; Kuo, J.-H.S. The Vector-Related Influences of Autophagic MicroRNA Delivery by Lipofectamine 2000 and Polyethylenimine 25K on Mouse Embryonic Fibroblast Cells. *European Journal of Pharmaceutical Sciences* **2017**, *101*, 11–21, doi:10.1016/j.ejps.2017.01.031.
302. de Souza, R.H.F.V.; Picola, I.P.D.; Shi, Q.; Petrônio, M.S.; Benderdour, M.; Fernandes, J.C.; Lima, A.M.F.; Martins, G.O.; Martinez Junior, A.M.; de Oliveira Tiera, V.A.; et al. Diethylaminoethyl- Chitosan as an Efficient Carrier for SiRNA Delivery: Improving the Condensation Process and the Nanoparticles Properties. *International Journal of Biological Macromolecules* **2018**, *119*, 186–197, doi:10.1016/j.ijbiomac.2018.07.072.
303. Jeyaram, A.; Lamichhane, T.N.; Wang, S.; Zou, L.; Dahal, E.; Kronstadt, S.M.; Levy, D.; Parajuli, B.; Knudsen, D.R.; Chao, W.; et al. Enhanced Loading of Functional MiRNA Cargo via PH Gradient Modification of Extracellular Vesicles. *Molecular Therapy* **2020**, *28*, 975–985, doi:10.1016/j.ymthe.2019.12.007.
304. Tamura, A.; Oishi, M.; Nagasaki, Y. Efficient SiRNA Delivery Based on PEGylated and Partially Quaternized Polyamine Nanogels: Enhanced Gene Silencing Activity by the Cooperative Effect of Tertiary and Quaternary Amino Groups in the Core. *Journal of Controlled Release* **2010**, *146*, 378–387, doi:10.1016/j.jconrel.2010.05.031.
305. Baril, P.; Ezzine, S.; Pichon, C. Monitoring the Spatiotemporal Activities of MiRNAs in Small Animal Models Using Molecular Imaging Modalities. *IJMS* **2015**, *16*, 4947–4972, doi:10.3390/ijms16034947.
306. Hernandez, R.; Orbay, H.; Cai, W. Molecular Imaging Strategies for In Vivo Tracking of MicroRNAs: A Comprehensive Review. *CMC* **2013**, *20*, 3594–3603, doi:10.2174/09298673113202900005.
307. Chang Kang, H.; Bae, Y.H. Co-Delivery of Small Interfering RNA and Plasmid DNA Using a Polymeric Vector Incorporating Endosomolytic Oligomeric Sulfonamide. *Biomaterials* **2011**, *32*, 4914–4924, doi:10.1016/j.biomaterials.2011.03.042.
308. Pinel, S.; Aman, E.; Erblang, F.; Dietrich, J.; Frisch, B.; Sirman, J.; Kichler, A.; Sibler, A.-P.; Dontenwill, M.; Schaffner, F.; et al. Quantitative Measurement of Delivery and Gene Silencing Activities of SiRNA Polyplexes Containing Pyridylthiourea-Grafted Polyethylenimines. *Journal of Controlled Release* **2014**, *182*, 1–12, doi:10.1016/j.jconrel.2014.03.001.
309. Raemdonck, K.; Van Thienen, T.G.; Vandenbroucke, R.E.; Sanders, N.N.; Demeester, J.; De Smedt, S.C. Dextran Microgels for Time-Controlled Delivery of SiRNA. *Adv. Funct. Mater.* **2008**, *18*, 993–1001, doi:10.1002/adfm.200701039.
310. Yuan, X.; Shah, B.A.; Kotadia, N.K.; Li, J.; Gu, H.; Wu, Z. The Development and Mechanism Studies of Cationic Chitosan-Modified Biodegradable PLGA Nanoparticles for Efficient SiRNA Drug Delivery. *Pharm Res* **2010**, *27*, 1285–1295, doi:10.1007/s11095-010-0103-0.

311. Turk, M.; Chung, C.; Manni, E.; Zukowski, S.; Engineer, A.; Badakhshi, Y.; Bi, Y.; Heinemann, I. MiRAR—MiRNA Activity Reporter for Living Cells. *Genes* **2018**, *9*, 305, doi:10.3390/genes9060305.
312. Arms, L.; Smith, D.W.; Flynn, J.; Palmer, W.; Martin, A.; Woldu, A.; Hua, S. Advantages and Limitations of Current Techniques for Analyzing the Biodistribution of Nanoparticles. *Front. Pharmacol.* **2018**, *9*, 802, doi:10.3389/fphar.2018.00802.
313. Kang, L.; Huo, Y.; Ji, Q.; Fan, S.; Yan, P.; Zhang, C.; Ma, H.; Hao, P.; Sun, H.; Zheng, Z.; et al. Noninvasive Visualization of MicroRNA-155 in Multiple Kinds of Tumors Using a Radiolabeled Anti-MiRNA Oligonucleotide. *Nuclear Medicine and Biology* **2016**, *43*, 171–178, doi:10.1016/j.nucmedbio.2015.11.005.
314. Veilleux, D.; Gopalakrishna Panicker, R.K.; Chevrier, A.; Biniecki, K.; Lavertu, M.; Buschmann, M.D. Lyophilisation and Concentration of Chitosan/SiRNA Polyplexes: Influence of Buffer Composition, Oligonucleotide Sequence, and Hyaluronic Acid Coating. *Journal of Colloid and Interface Science* **2018**, *512*, 335–345, doi:10.1016/j.jcis.2017.09.084.
315. Kasper, J.C.; Schaffert, D.; Ogris, M.; Wagner, E.; Friess, W. The Establishment of an Up-Scaled Micro-Mixer Method Allows the Standardized and Reproducible Preparation of Well-Defined Plasmid/LPEI Polyplexes. *European Journal of Pharmaceutics and Biopharmaceutics* **2011**, *77*, 182–185, doi:10.1016/j.ejpb.2010.11.012.
316. Tavakoli Naeini, A.; Soliman, O.Y.; Alameh, M.G.; Lavertu, M.; Buschmann, M.D. Automated In-Line Mixing System for Large Scale Production of Chitosan-Based Polyplexes. *Journal of Colloid and Interface Science* **2017**, *500*, 253–263, doi:10.1016/j.jcis.2017.04.013.
317. Pitarresi, G.; Casadei, M.A.; Mandracchia, D.; Paolicelli, P.; Palumbo, F.S.; Giammona, G. Photocrosslinking of Dextran and Polyaspartamide Derivatives: A Combination Suitable for Colon-Specific Drug Delivery. *Journal of Controlled Release* **2007**, *119*, 328–338, doi:10.1016/j.jconrel.2007.03.005.

7. ANNEXES

Annex 1: Environmental scanning electron microscopy images

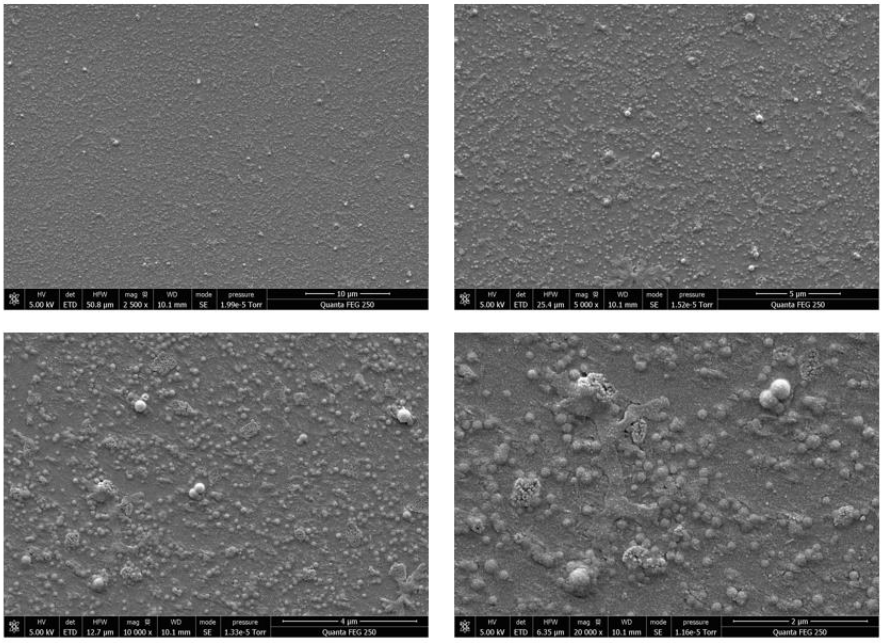

Figure 59. Environmental scanning electron microscopy images of polyelectrolyte complexes EA-pullulan and fucoidan.

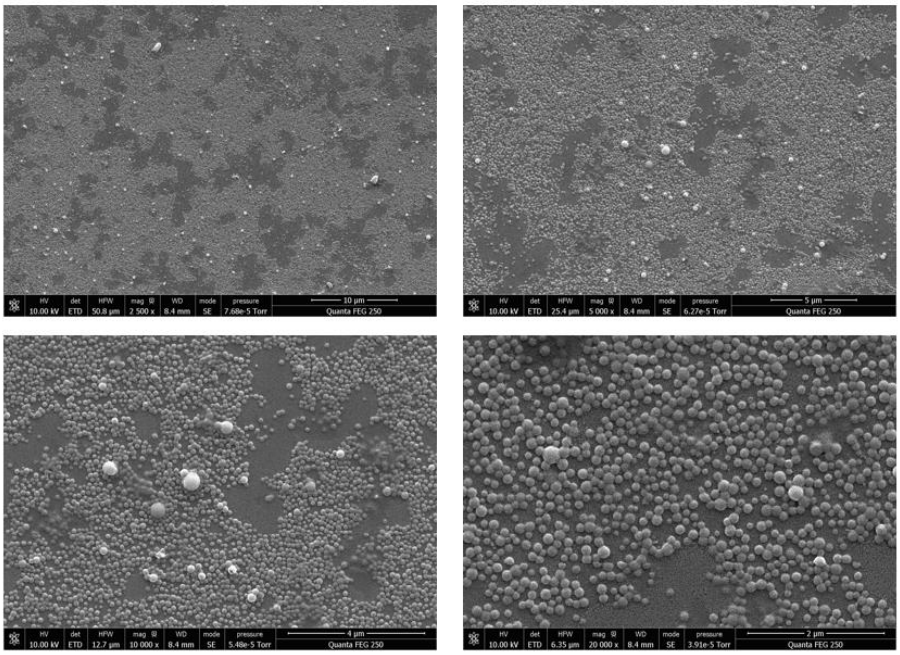

Figure 60. Environmental scanning electron microscopy images of crosslinked polyelectrolyte complexes EA-pullulan and fucoidan with genipin.

Annex 2: Synthesis and characterization of pullulan methacrylate

1. Materials

Glycidyl methacrylate (GMA) and N,N-Dimethylpyridin-4-amine, (4-DMAP) were purchased from Sigma-Aldrich (St. Louis, MO, USA). Dialysis membranes of 20 kDa was purchased from Spectrum Laboratories (New Brunswick, NJ, USA).

2. Methods

Pullulan methacrylate (Pull-MA) was synthetized based on a protocol previously described by Pitarresi *et al.*, 2007 to produce dextran methacrylate [317]. To a solution of pullulan (2.5 g) in DMSO (20 ml), 4-DMAP (0.5 g) and GMA (0.35 g, 1 mol of GMA/6 mol of repetitive unit of pullulan) were added. The solution was placed under high magnetic stirring at room temperature for 24h. After pullulan methacrylate was recovered by precipitation in 100 mL of cold ethanol. The mixture was exhaustively dialyzed (MWCO of 20 kDa) for 48 hours with ultrapure water and the derivatives were obtained as fluffy white materials after freeze-drying. The presence of methacrylate groups was confirmed by H-NMR.

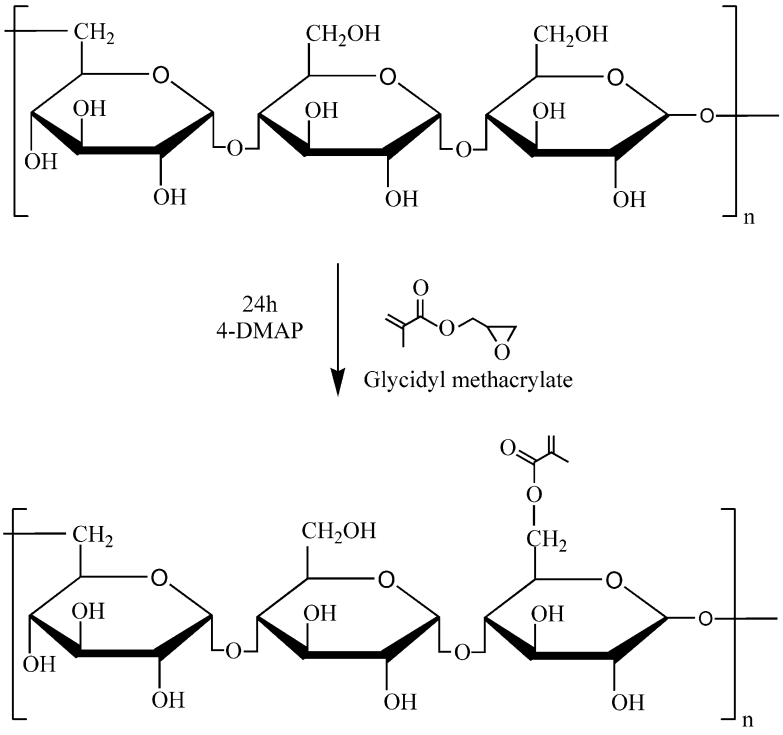

Figure 61. Synthesis of pullulan methacrylate. Pullulan were reacted with glycidyl methacrylate (GMA) during 24h at room temperature.

3. Results

3.1 Characterization of pullulan methacrylate

1H-NMR spectra was recorded with a Bruker-400 Ultrashield (Bruker, Germany) operating at 400 MHz. Polymers samples were prepared in D2O at a concentration of 20 mg/mL. Exemplary NMR spectra of Pull-MA are presented in Figure 62. The characteristics peaks of methacrylate functions was confirmed by the presence of peaks at 5.8 and 6.2 ppm. The methacrylation degree of pullulan was quantified by ^{1}H-NMR spectroscopy by comparing the integrated intensity of the double bond peak to that of pullulan backbone. Degree of methacrylation of 20% was obtained.

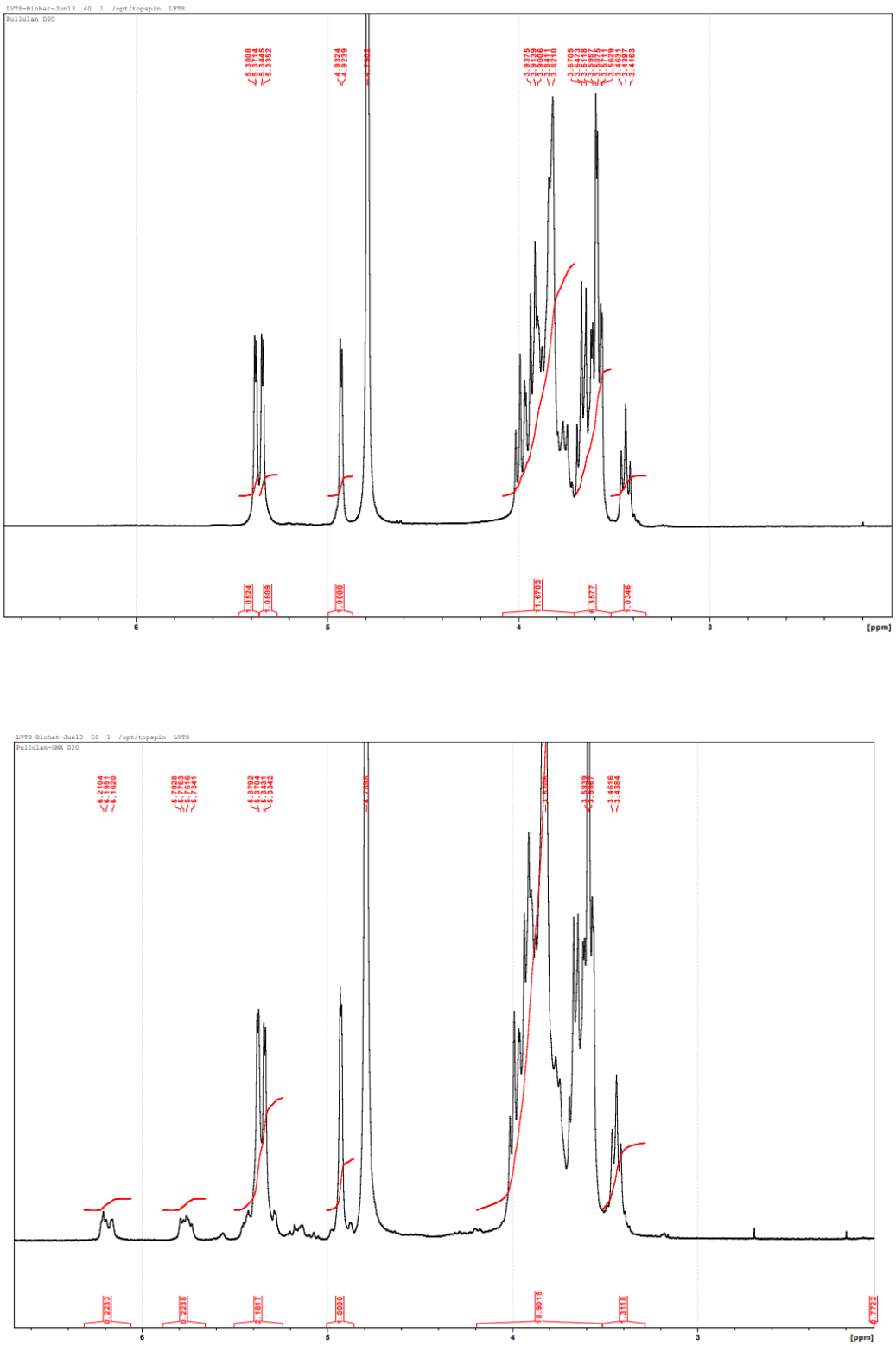

Figure 62. 1H NMR spectra at 400 Mhz of non-modified pullulan (top) and pullulan methacrylate (bottom) in D2O.

3.2 Photo-crosslinking of pullulan methacrylate

To create hydrogel networks, Pull-MA (100 mg/mL) was crosslinked by using UV irradiation at 365 nm (LC-L1V3 -UV LED, Hamamatsu Photonics, Japan) in the absence of photoinitiators. The intensity of UV light was set to 80% and the time of exposition set to 4h. Pullulan with methacrylate groups showed to be able to produce crosslinked structures after UV irradiation (Figure 63).

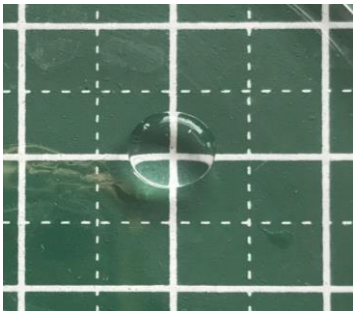

Figure 63. Crosslinked Pull-MA hydrogels after 4h exposed to UV irradiation in the absence of photoinitiators.

Annex 3: Synthesis and characterization of pullulan with primary amines and quaternary ammonium groups

1. Materials

Glycidyltrimethylammonium chloride (GTMAC) (Mw 151.63 g/mol) was purchased from Sigma-Aldrich (St. Louis, MO, USA). 3-chloropropylamine hydrochloride (Mw 130.02 g/mol) was purchased from Sigma-Aldrich (St. Louis, MO, USA). Dialysis membranes of 20 kDa was purchased from Spectrum Laboratories (New Brunswick, NJ, USA).

2. Methods

2.1 Alkylation with GTMAC

Briefly, pullulan (500 mg) was dissolved in 5 mL of an aqueous solution of 10 M NaOH. Then, the solution was placed at 4°C under magnetic stirring until pullulan was completely solubilized. Glycidyltrimethylammonium chloride (GTMAC) was added to polysaccharide solution at 1/3 equivalent feeding ratio drop by drop and under high magnetic stirring at 4°C. The solution was placed under magnetic stirring at 55°C for 4 hours. After cooling down to room temperature, the pH was adjusted to 7 with concentrated hydrochloric acid solution. The mixture was exhaustively dialyzed (MWCO of 20 kDa) for 48 hours with ultrapure water and the derivatives were obtained as fluffy white materials after freeze-drying.

2.2 Amination with propylamine

QA- pullulan (1 g) was dissolved in 5 mL of distilled water. The solution was placed at 4°C until complete solubilisation of pullulan. Then, 5 mL of soda (6.2 M NaOH) was added to activate the hydroxyl functions. The solution was kept at 4°C under magnetic stirring for 20 min. Then, 1.60 g of 3-chloropropylamine hydrochloride (2 equivalents per AGU) was added to the solution under magnetic stirring at 4°C. Then, the solution was placed under magnetic stirring at 55°C for 3 h. The mixture was placed at room temperature and the pH was adjusted to 7 with 37% hydrochloric acid (HCl) solution. The mixture was dialyzed with a 20 kg/mol membrane and freeze-dried before characterization. Final product was named as QA-pullulan-PA.

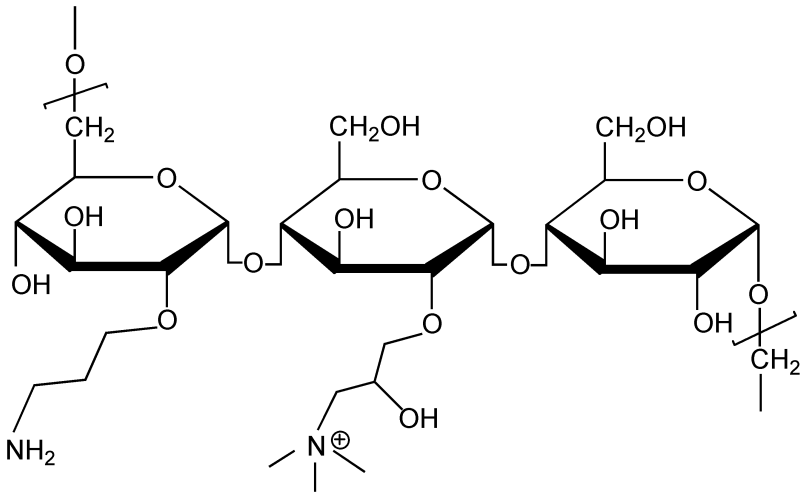

Figure 64. Chemical structure of cationic pullulan derivative with primary amines and quaternary ammonium groups.

3. Results

QA-pullulan derivatives with different DS were synthetized via the alkylation of pullulan with GTMAC. The product was characterized by elemental analysis before next step of amination. Amination was then performed by grafting 3-chloropropylamine hydrochloride at 2 equivalents feeding ratio during 3h at 55°C. The products were freeze-dryed and characterized by elemental analysis (Table 17) and ^{1}H NMR. It was possible to modify QA-pullulan only with low DS with DS ranging from 3-7.

Table 17. Characterization of cationic pullulan derivatives with quaternary ammonium and primary amines.

	1st step Alkylation (QA-pullulan)			**2nd step Amination (QA-pullulan-PA)**		
Reaction	t (h)	% N[a]	DS[b]	t (h)	% N[a]	DS_{NH2}[b]
Condition 1	4	0.25	3	3	1.24	12
Condition 2	4	0.58	7	3	1.42	11
Condition 3	4	1.03	13	3	1.07	-
Condition 4	4	1.55	21	3	1.67	-

[a] Nitrogen content estimated by elemental analyses.
[b] Degree of substitution calculated per anydroglucose unit.

^{1}H NMR spectra of QA-pullulan-PA derivatives exhibits the characteristic peaks of QA groups in the region of 3.2 ppm and 4.4 ppm, and the methylene protons of propylamine

groups in the region of 1.9 ppm and 3.1 ppm, suggesting the presence of both groups in pullulan backbone (Figure 65).

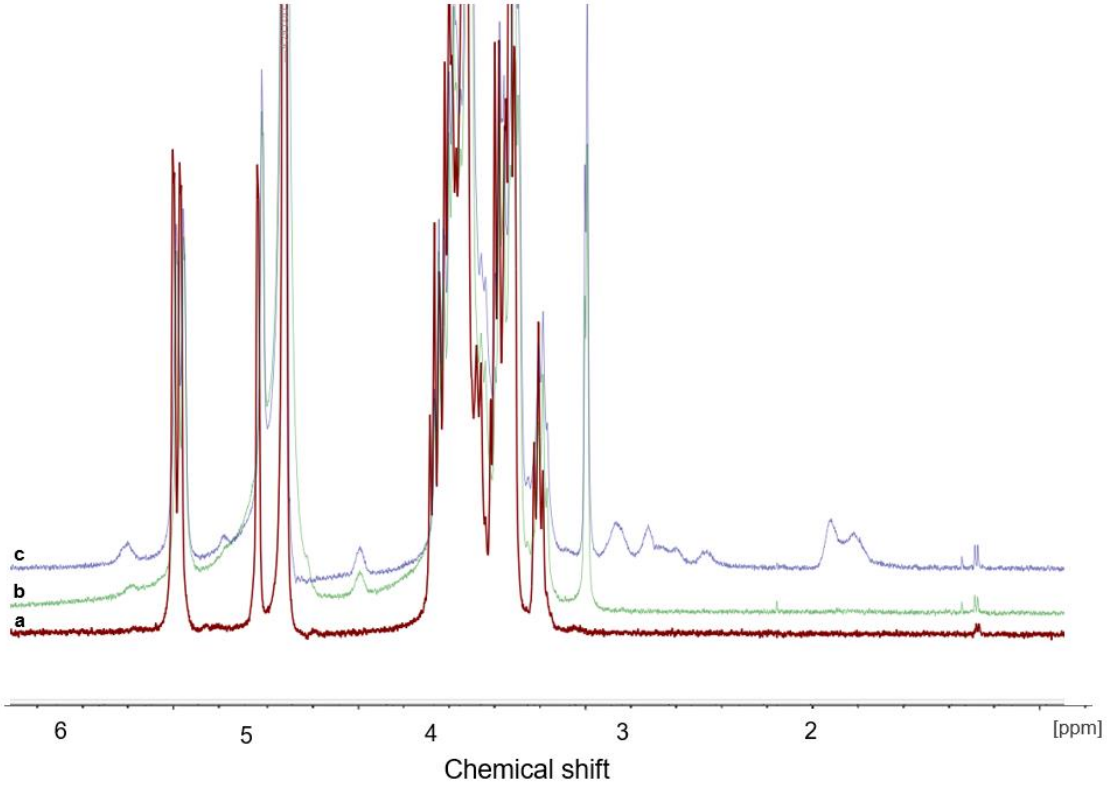

Figure 65. 1H NMR spectra at 400 Mhz of (a) non-modified pullulan, (b) QA-pullulan (0.25%N) and (c) QA-pullulan-PA (1.24%N) in D2O.

Annex 4: Flow cytometry analysis of FAM-miRNA delivery

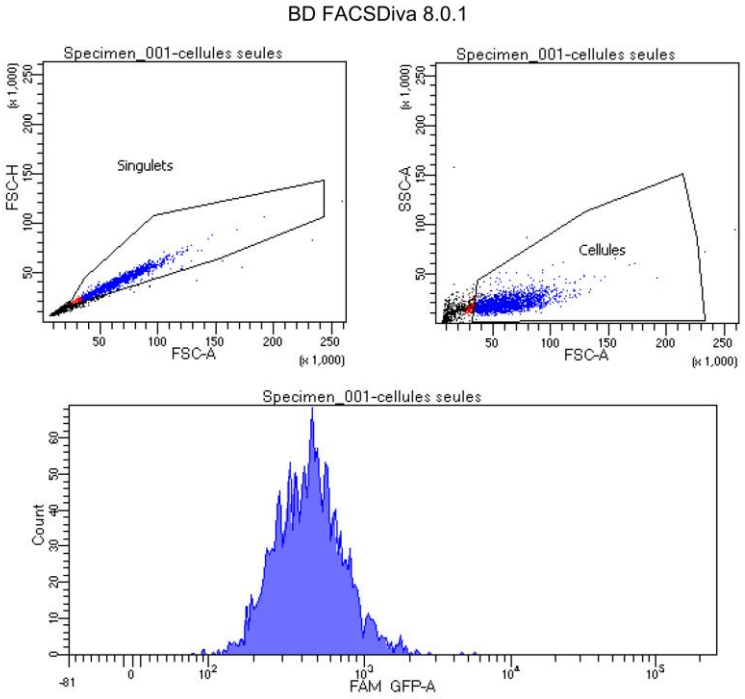

Tube: cellules seules

Population	#Events	%Parent	%Total
All Events	2,365	####	100.0
Singulets	1,793	75.8	75.8
Cellules	1,718	95.8	72.6

Population	FAM GFP-A Geo Mean	FAM GFP-A Mean	FAM GFP-A Median
Singulets	438	505	437
Cellules	432	494	431

Global Sheet1

Printed on: Mon Nov 16, 2020 03:23:38 CET

BD FACSDiva 8.0.1

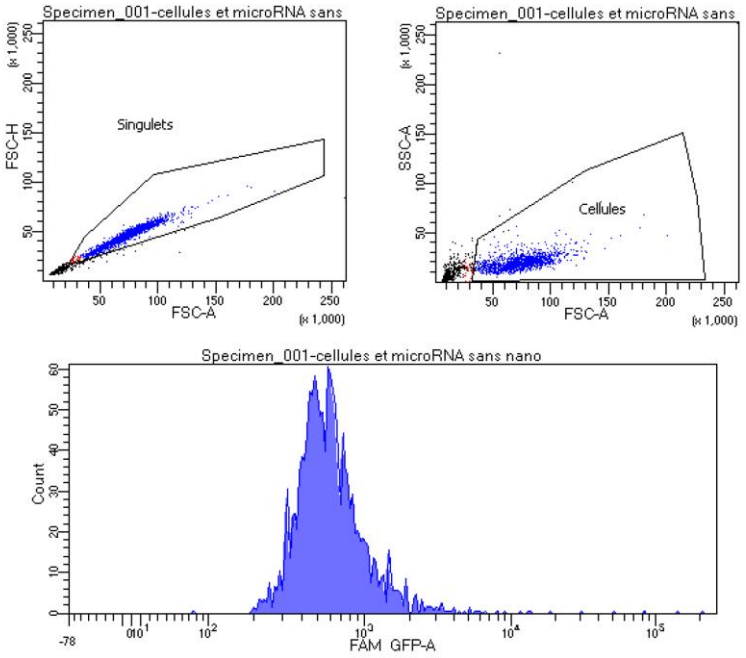

Tube: cellules et microRNA sans nano

Population	#Events	%Parent	%Total
All Events	1,938	####	100.0
Singulets	1,485	76.6	76.6
Cellules	1,460	98.3	75.3

Population	FAM GFP-A Geo Mean	FAM GFP-A Mean	FAM GFP-A Median
Singulets	####	1,669	552
Cellules	609	1,248	554

Global Sheet1

Printed on: Mon Nov 16, 2020 03:23:39 CET

BD FACSDiva 8.0.1

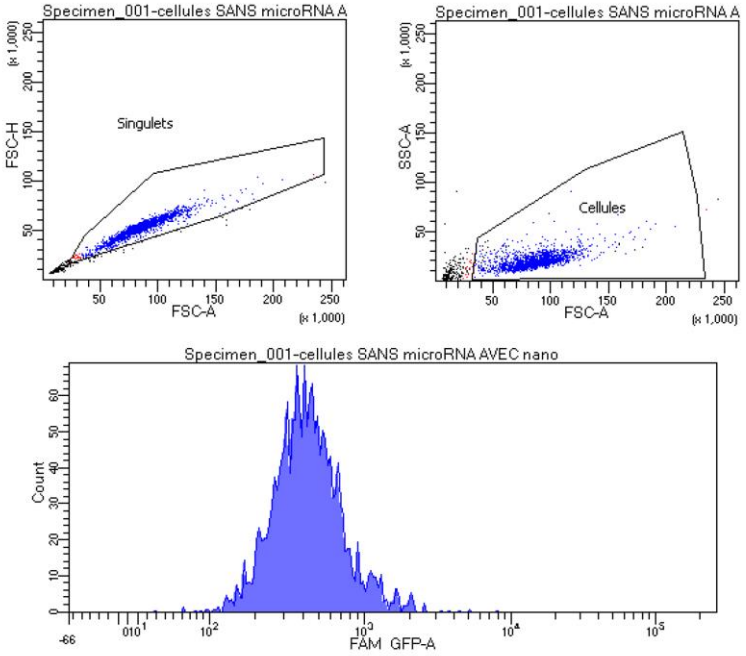

Tube: cellules SANS microRNA AVEC nano

Population	#Events	%Parent	%Total
All Events	2,115	####	100.0
Singulets	1,833	86.7	86.7
Cellules	1,814	99.0	85.8

Population	FAM GFP-A Geo Mean	FAM GFP-A Mean	FAM GFP-A Median
Singulets	414	491	401
Cellules	413	483	401

Global Sheet1

Printed on: Mon Nov 16, 2020 03:23:41 CET

BD FACSDiva 8.0.1

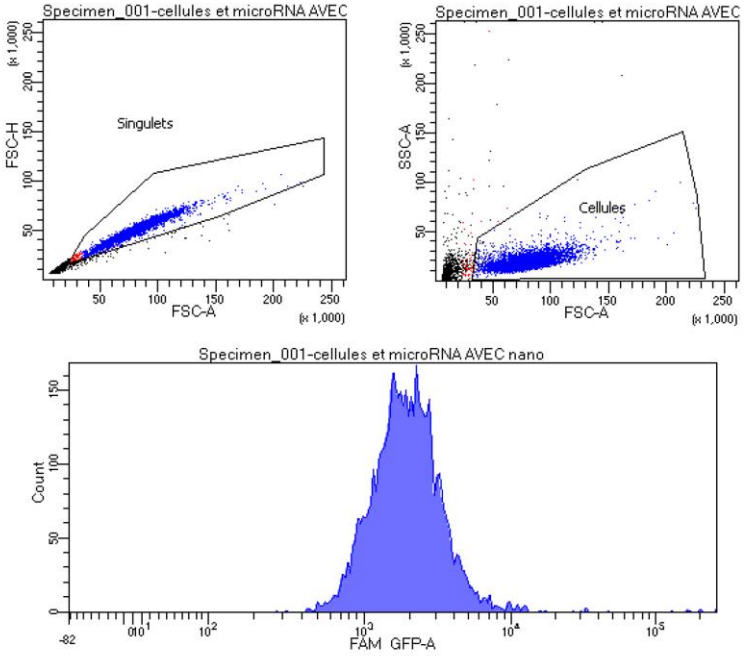

Tube: cellules et microRNA AVEC nano

Population	#Events	%Parent	%Total
All Events	6,013	####	100.0
Singulets	4,986	82.9	82.9
Cellules	4,931	98.9	82.0

Population	FAM GFP-A Geo Mean	FAM GFP-A Mean	FAM GFP-A Median
Singulets	1,942	4,015	1,844
Cellules	1,925	3,534	1,843

Global Sheet1

Printed on: Mon Nov 16, 2020 03:23:40 CET

Annex 5: Reconstructed 3D images of FAM-miRNA delivery in HUVECs

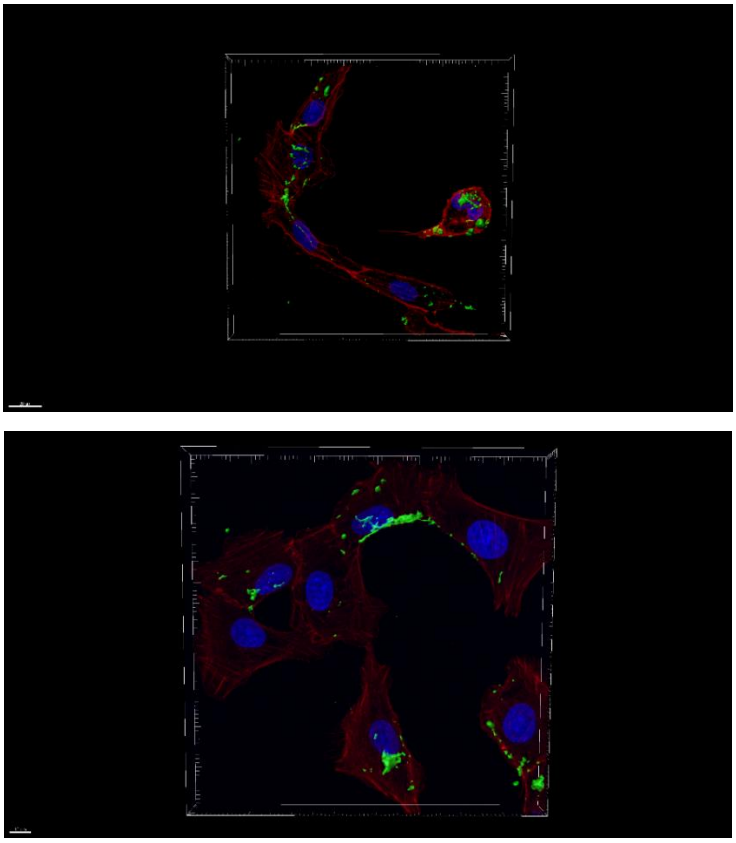

Figure 66. Reconstructed 3D images of FAM-miRNA delivery in HUVECs using the Imaris® software. Cells'nuclei were stained with DAPI (blue); Phalloidin were stained with Alexa Fluor 633 (red); miRNA was labelled with FAM (green); Scale bars corresponds to 20µm (top) and 10 µm (bottom).

Annex 6: Publications

Molecular Therapy
Nucleic Acids
Original Article

Core-Shell Polymer-Based Nanoparticles Deliver miR-155-5p to Endothelial Cells

Joana C. Antunes,[1] Louise Benarroch,[1] Fernanda C. Moraes,[1] Maya Juenet,[1] Marie-Sylvie Gross,[1] Mélodie Aubart,[1] Catherine Boileau,[1] Giuseppina Caligiuri,[1] Antonino Nicoletti,[1] Véronique Ollivier,[1] Frédéric Chaubet,[1] Didier Letourneur,[1,2] and Cédric Chauvierre[1,2]

[1]Université de Paris, LVTS, INSERM U1148, Université Paris 13, 75018 Paris, France

Heart failure occurs in over 30% of the worldwide population and most commonly originates from cardiovascular diseases such as myocardial infarction. microRNAs (miRNAs) target and silence specific mRNAs, thereby regulating gene expression. Because the endogenous miR-155-5p has been ascribed to vasculoprotection, loading it onto positively charged, core-shell poly(isobutylcyanoacrylate) (PIBCA)-polysaccharide nanoparticles (NPs) was attempted. NPs showed a decrease ($p < 0.0001$) in surface electrical charge (ζ potential), with negligible changes in size or shape when loaded with the anionic miR-155-5p. Presence of miR-155-5p in loaded NPs was further quantified. Cytocompatibility up to 100 μg/mL of NPs for 2 days with human coronary artery endothelial cells (hCAECs) was documented. NPs were able to enter hCAECs and were localized in the endoplasmic reticulum (ER). Expression of miR-155-5p was increased within the cells by 75-fold after 4 hours of incubation ($p < 0.05$) and was still noticeable at day 2. Differences between loaded NP-cultured cells and free miRNA, at days 1 ($p < 0.05$) and 2 ($p < 0.001$) suggest the ability of prolonged load release in physiological conditions. Expression of miR-155-5p downstream target *BACH1* was decreased in the cells by 4-fold after 1 day of incubation ($p < 0.05$). This study is a first proof of concept that miR-155-5p can be loaded onto NPs and remain intact and biologically active in endothelial cells (ECs). These nanosystems could potentially increase an endogenous cytoprotective response and decrease damage within infarcted hearts.

INTRODUCTION

Heart failure occurs in over 30% of the worldwide population[1] and is a leading cause of death and disability in developing countries. It most commonly arises from coronary artery disease that causes severe impairment of the coronary artery blood supply.[2–5] The sudden complete occlusion of coronary vessels leads to myocardial infarction (MI), with the resulting hypoxia triggering a cascade of events that culminates in loss of viable cardiac tissue.[3,4,6] If early reperfusion occurs,[4,7] damaged tissue is replaced with scar tissue.[4] However, after 20–40 min of sustained severe ischemia, irreversible tissue damage typically develops,[4] ultimately leading to heart failure.[3,5] The immediate clinical approach is to restore blood flow by thrombolytic treatments or coronary angioplasty,[2,5] although long-term complications and high death rates remain frequent,[3,8] particularly for the most severe cases.[4] Consequently, developing new therapeutic strategies is a vital goal of both clinical and research fields.[3,9,10]

Nanoparticles (NPs) in suspension can be easily injected,[11] and using an NP injection as a complement to reperfusion after MI would be feasible. With sizes above the renal clearance threshold (about 5 nm in diameter[12]), NPs can circulate within the body and deliver biologically active molecules into the target tissue.[11] Interestingly, biological entities such as microRNAs (miRNAs) can act intracellularly or can be secreted by cells and contribute to intercellular or cell-tissue communication.[13] miRNAs are evolutionarily conserved, ubiquitously expressed (albeit with a degree of tissue specificity), short (~22 nucleotides), non-protein-coding RNA molecules involved in post-transcriptional gene regulation. At the target, miRNAs can generate strong, sustained, and comprehensive biological effects, through endogenous gene silencing,[14] with very low concentrations (at least 0.5 nM)[15]. In addition, miRNAs affect multiple pathways and cellular processes rather than specific targets.[16]

miRNA-based therapies include the delivery of exogenous miRNA mimics, which are oligonucleotides with the same nucleotide sequence as an endogenous miRNA designed to mimic that miRNA.[17] After the miRNAs are loaded onto the NPs, an intravenous route of administration[18] would be the least invasive option. Different therapeutic candidate miRNAs have been described,[3,19–22] and different NPs for miRNA delivery are now being explored as potential treatments for cardiovascular pathologies—namely, viral,[23–30] lipid,[31–34] and polymer-based[35–37] platforms.

miR-155-5p mimics have been shown to silence the mRNA *BACH1* *in vitro* in endothelial cells (ECs)[38] and to display cytoprotective effects during inflammation through the induction of heme oxygenase 1 (a known antioxidant and cytoprotective enzyme). *BACH1*

Received 19 November 2018; accepted 20 May 2019;
https://doi.org/10.1016/j.omtn.2019.05.016.

[2]These authors contributed equally to this work.

Correspondence: Cédric Chauvierre, Ph.D., Université de Paris, LVTS, INSERM U1148, Cardiovascular Bioengineering, X. Bichat Hospital, Paris, France.
E-mail: cedric.chauvierre@inserm.fr

This is an open access article under the CC BY-NC-ND license (http://creativecommons.org/licenses/by-nc-nd/4.0/).

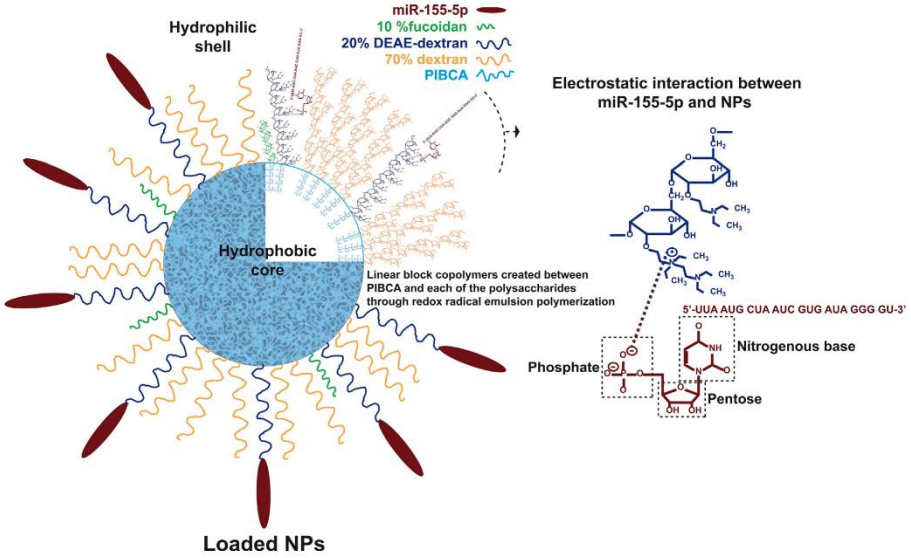

Figure 1. Schematics of Loaded NP Composition

Unloaded nanosystems prepared through redox radical emulsion polymerization included linear block copolymers composed of a hydrophobic PIBCA core and a hydrophilic shell containing fucoidan (10%), cationic DEAE-dextran (20%), and dextran (70%). miR-155-5p is bound to the NPs electrostatically by the cationic DEAE-dextran. The complete miRNA structure has been omitted for clarity.

has been confirmed as a direct target of miR-155-5p, in a study of the cell line HEK293.[38]

Knowing that an miRNA's behavior is highly dependent on cell type,[39] it is essential to pinpoint an adequate receptor to guide the nanosystem and avoid off-target effects.[16] On one hand, P-selectin, an adhesion molecule expressed at the surface of activated ECs and platelets, is highly expressed at the infarct region during a MI.[40] On the other hand, fucoidan, a naturally occurring sulfated polysaccharide developed in our laboratory,[41] has high affinity to P-selectin.[41–45] Coating NPs with fucoidan would confer on them the ability to target P-selectin-activated ECs,[40,43,46] which are directly reachable through intravenous injection.

Hence, the strategy proposed here as a proof of concept involves the use of miRNAs adsorbed onto nanocarriers to evaluate their assembly and internalization by ECs, envisioning their use as a potential injectable cardio-protective therapy for MI. Work included miR-155-5p loading onto core-shell NPs.[47–49] The NP shell included a cationic polysaccharide able to bind electrostatically to the miRNA. The NPs were characterized regarding their size and surface electrical charge (ζ potential), morphology, and miRNA presence. miRNA stability, release, and desorption were monitored. *In vitro* cell culture studies in hCAECs included cytocompatibility assays and cell internalization, in addition to mir-155-5p and *BACH1* expression level analyses under pro-inflammatory conditions.

RESULTS

Unloaded NPs were first prepared through redox radical emulsion polymerization with a core of poly(isobutylcyanoacrylate) (PIBCA) and a shell containing fucoidan, diethylaminoethyl (DEAE)-dextran, and dextran. The nitrogen content of the DEAE-dextran of the unloaded NP shell was 0.44% (Table S1), indicating availability of 26 μg of nitrogen per NP dispersion of 6 mg. After miR-155-5p addition in sterile conditions onto unloaded NPs previously subjected to UV exposure and subsequent centrifugation to remove free or poorly adsorbed miRNA, the loaded NPs were obtained. The phosphorous content of the miRNA used for the miRNA loading was 5 μg per miRNA solution of 111 μg, using the optimized N/P (nitrogen to phosphorus) molar ratio of 10. Figure 1 highlights the NP design - namely the chemical bonds driving miRNA loading. As such, the ζ potential values of positively charged unloaded NPs decreased ($p < 0.0001$) from 15.1 ± 1.1 to 1.9 ± 3.0 mV, indicating that negatively charged molecules were added to the surface (Figure 2A). Both unloaded and loaded NPs were spherical in shape, with miRNA addition tending to increase NP diameter (d) (312.4 ± 39.3–331.9 ± 30.1 nm), while

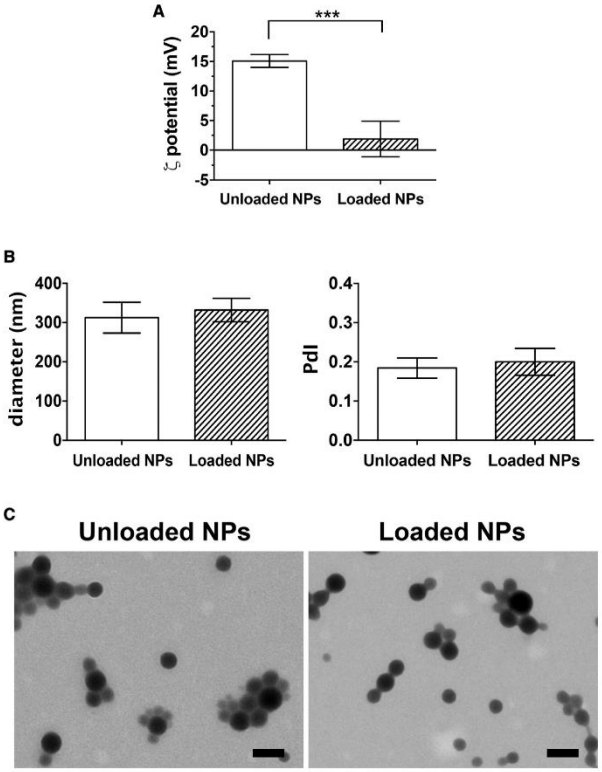

Figure 2. Surface Electrical Charge, Size, and Shape after Loading the miR-155-5p onto the Nanosystem

In ultrapure water, unloaded NPs were characterized after preparation and UV exposure before miRNA loading (white bars), and purified NPs were obtained by re-suspension after centrifugation (hatched bars). (A) ζ Potential (mV), (B) hydrodynamic diameter (nm), and polydispersity index (PdI) were determined by electrophoretic and dynamic light scattering (ELS and DLS, respectively). Results are shown as the mean ± SD of four independent experiments (n = 4). ***$p < 0.0001$, using the Wilcoxon matched-pairs signed rank test. (C) Representative transmission electron microscope (TEM) images of unloaded and loaded NPs. Scale bars represent 200 nm.

keeping a monodispersed size distribution (polydispersity index [PdI]) (0.18 ± 0.02–0.20 ± 0.03; Figure 2B). The NPs appeared on transmission electron microscopy (TEM) as electron-dense internal cores encircled by a less dense shell (Figure 2C), thereby substantiating the expected core-shell structure.[50]

The presence of miR-155-5p was further evaluated by means of agarose gel electrophoresis (AGE), using highly concentrated agarose gels and a ladder sensitive to short nucleic acids (10–300 bp; lane 1), capable of detecting this miRNA (23 bp) within the gel. Figure 3A displays miR-155-5p (lane 2) at the same concentration as for the miRNA loading, plus unloaded and loaded NPs (lanes 3 and 4, respectively). An amount of 121 ± 30 ng of the added miRNA was kept by the NPs afterward, corresponding to approximately 36% of the initially added miR-155-5p. RNases were absent from both unloaded and loaded NPs after preparation (data not shown). The RNA quantification by UV spectrophotometry after NP disruption and RNA isolation, displayed a similar trend ($p < 0.05$) as in AGE results (Figure 3B). qPCR showed that loaded NPs (Figure 3C) had a higher RNA amount than did unloaded NPs ($p < 0.001$), showing that the miR-155-5p was present within the loaded NPs.

Loaded and unloaded NPs were highly stable at 4°C for 1 day without any measurable change (Figure 4). Then, a progressive trend was observed with diameters from 317.4 ± 49.1 nm (day 1) to 381.6 ± 106.6 nm (day 14, $p < 0.05$) and PdI from 0.20 ± 0.03 (day 1) to 0.22 ± 0.05 (day 14). The ζ potential from 5.5 ± 1.8 mV (day 7) to 7.4 ± 2.0 mV (day 14, $p < 0.05$) suggests that negatively charged molecules were removed from the surface. The miRNA content decreased with storage time (Figure 4C), with 61.2% ± 25.0% nucleic acids remaining at day 7.

When subjected to strong orbital shaking at 37°C in PBS, loaded NPs released nucleic acids for 6 hours, with a half-life of 25 min after incubation (Figure 5, black symbols). After centrifugation and re-suspension in 1.5 M NaCl, an additional release of 13% was observed. As expected, we did not detect any miRNA on unloaded NPs (Figure 5, white symbols).

The biological response of unloaded and loaded NPs toward hCAECs was evaluated *in vitro*, after dynamic light scattering (DLS) measurements showed retention of the NP architecture and nanoscale size in the tested physiological conditions (data not shown), thereby showing NP stability in cell culture medium. The presence of metabolically active cells through ATP conversion during the 2-day period after NP addition, compared with the controls (cells alone, miR), demonstrated that unloaded and loaded NPs were not cytotoxic for hCAECs at the selected concentrations (5, 25, and 100 μg/mL) (Figure 6A). Light (Figure 6B) and fluorescent images of hCAECs were obtained (Figures 6B and 6C). miR-cultured cells tended to be of a slightly smaller size than the control cells, and cells incubated with unloaded NPs showed

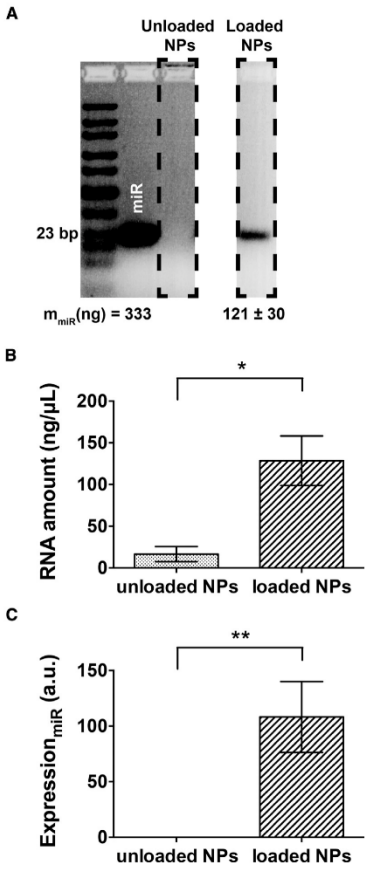

Figure 3. Stability of Loaded Nanoparticles and miRNA Content

(A) Detection of nucleic acids within the loaded NPs (n = 4), as determined by 5% agarose gel electrophoresis (AGE). (B) RNA level (ng/μL) quantified by UV absorbance, and (C) miR-155-5p expression levels within unloaded and loaded NPs, evaluated through qPCR, with 2 ng/μL of each sample. Results are shown as the mean ± SD from four independent experiments. Statistical significance was determined with the Wilcoxon matched-pairs signed rank test; *$p < 0.05$, **$p < 0.001$.

swollen features, particularly after 4 hours of incubation. miR-incubated cultures tended to have an increased number of cells, most evident after 2 days of incubation. Centrally located stress fibers (green fluorescent actin filaments) are clearly visualized in all culture conditions, but were less evident in unloaded NP-supplemented cultures, where fluorescence tended to concentrate at the cell margins. Unloaded NP-supplemented cellular membranes were also unique, as large protrusions (white arrow; Figure 6B) replaced the majority of the protruding thin filaments (thinner white arrows) that resemble the actin-rich filopodia and lamellipodia[51–53] commonly observed in migratory cells, such as the hCAECs. All evidence showed that hCAECs incubated with loaded NPs were morphologically closer to the main control cells.

Fluorescence imaging was used to monitor internalization by hCAECs of NPs fluorescently labeled with Nile red (ftNPs) in pro-inflammatory conditions after stimulation with tumor necrosis factor-α (TNF-α). The images revealed that ftNPs (red) were strongly engulfed by hCAECs (Figure 7). No difference was perceived regarding uptake of ftNPs by loaded or unloaded NPs. The increased number of Nile red-labeled features were clearly visualized within the cells with increasing culture time. In NP-enriched cells, ftNPs underwent uptake with perinuclear localization.

Since the ftNP juxtanuclear position suggested co-localization with the endoplasmic reticulum (ER), an additional ER staining with protein disulfide isomerase was performed. ftNPs were found within the ER of hCAECs (Figure 8), particularly after 2 days, with sparse red labeling detected outside the ERs (thin white arrows). No difference was noticed in the uptake of loaded or unloaded NPs cultured in pro-inflammatory conditions, other than the increase of red staining with time for unloaded and loaded NPs.

Finally, miR-155-5p and *BACH1* levels within hCAECs were examined by qPCR with cells cultured in pro-inflammatory conditions (Figures 9 and 10). In the miR-negative control groups (such as unloaded NPs), miRNA levels were minimal (expression of 1.8 ± 0.5 a.u. after 4 h, with levels being maintained with culture time). Within the TNF-α-stimulated cells, miR-supplemented cultures revealed 85- or 75-fold upper levels, respectively, for the miRNA and loaded NPs, in comparison with the unloaded NPs ($p < 0.05$). miR-155-5p levels decreased from 156.7 ± 61.4 a.u. (4 h), to 39.5 ± 21.3 a.u. (1 day), to 53.3 ± 10.6 a.u. (2 days, $p < 0.05$), whereas loaded NP values decreased from 137.3 ± 14.2 a.u. (4 h), to 82.8 ± 24.6 a.u. (1 day), to 83.1 ± 10.2 a.u. (2 days, $p < 0.05$). However, the main noticeable differences were the increased miR-155-5p values for the loaded NP condition with respect to cells cultured with miRNA, suggesting a slower load release in these physiological conditions, in contrast to the possible degradation of exogenous, free miRNA in the physiological media at 1 ($p < 0.05$) and 2 ($p < 0.001$) days of incubation. On the other hand, loaded NP-enriched cells ($48.16 \times 10^{-4} \pm 15.70 \times 10^{-4}$ a.u.) led to a decrease ($p < 0.05$) of *BACH1* levels after 1 day of incubation, when compared to the control ($177.37 \times 10^{-4} \pm 94.29 \times 10^{-4}$ a.u.). Unloaded NP-related cultures showed no indication of *BACH1* reduction through the exogenous miR-155-5p, but free miRNA-supplemented cultures resulted in further *BACH1* silencing ($p < 0.05$), as expected ($3.52 \times 10^{-4} \pm 0.53 \times 10^{-4}$ a.u.).

DISCUSSION

This study evaluated the loading of miR-155-5p onto core-shell, polymer-based NPs through electrostatic interactions (Figure 1), their

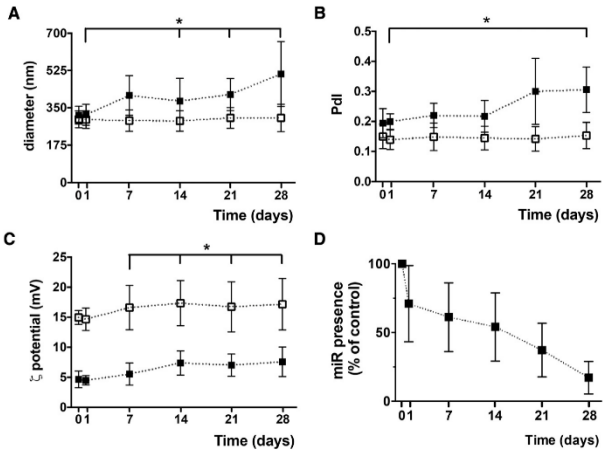

Figure 4. Stability of miR-155-5p-Loaded NPs after Preparation (Day 0) and after 1, 7, 14, 21, and 28 Days of Storage at 4°C

NP diameter (nm) (A) and PdI (B) were measured by DLS and ζ potential values (mV) by ELS (C). miRNA presence (% in relation to the control at day 0) within loaded NPs was observed through AGE (D). Outputs from unloaded NPs are also represented (white symbols). Results are shown as the mean ± SD from three to four independent experiments. Significant differences were detected for loaded NPs using the Wilcoxon matched-pairs signed rank test; *$p < 0.05$.

internalization by hCAECs, and the delivery of their miRNA cargo as a proof of concept of the feasibility of the use of miR-155-5p-loaded NPs for MI. Unloaded NPs were prepared through redox radical emulsion polymerization, containing a PIBCA core coated with a polysaccharide brush comprising 10% fucoidan for targeting, 20% DEAE-dextran for miRNA binding and promotion of cell internalization, and 70% dextran for surface stabilization. After miRNA loading under sterile conditions, unloaded and loaded NPs were analyzed through the combination of different techniques. Round-shaped NPs with a hydrodynamic size of approximately 300 nm were obtained (Figure 2), with a decrease of their ζ potential after miR-155-5p adsorption. Nucleic acids with the same size as our miRNA were detected in the loaded NPs through AGE runs (Figure 3). The RNA quantification, by UV spectrophotometry after NP disruption and RNA isolation, displayed a trend similar to that seen with AGE. miR-155-5p presence was further demonstrated by qPCR, with the additional information that the miRNA remains intact within loaded NPs, since the probe can detect only whole target sequences.

While loaded NP integrity is essential for the intended clinical application, miRNA release in physiological conditions is another essential step. Figures 4A–4C show that the main loaded NP features were highly stable up to 1 day of storage at 4°C in sterile conditions. A slight increase in NP diameter and PdI, particularly after days 1 and 14, respectively, was observed. The ζ potential showed a small increment in 28 days, which was accompanied by an apparent loss of miRNA of 38.8%, measured through AGE (Figure 4D). Since aliquots for DLS and ELS and AGE measurements were handled simultaneously, it is assumed that miRNA was released from the NP surface with some disruption of the ionic bond and/or media interaction with NP hydrophilic chain. Regardless, total miRNA release is achievable in physiological conditions, as illustrated in Figure 5 (see also Figure S1).

The previous cytocompatibility studies with human umbilical vein endothelial cells (HUVECs) performed by Matuszak and colleagues,[54] with similar but not identical compositions of core-shell (PIBCA-polysaccharide) - 10% 7 kDa fucoidan, 10% 20 kDa DEAE-dextran, and 80% 70 kDa dextran - placed the upper limit of NP concentration in direct contact with the cells used at 100 μg/mL. No cytotoxicity could be detected in our conditions until 100 μg/mL, although there was some evidence of cytotoxicity with hCAECs incubated with ≥200 μg/mL NPs (data not shown). For 100 μg/mL of NPs, a loaded amount of 650 ng/mL miRNA was obtained, corresponding to 43.1 nM of loaded biomolecule, which is well above the efficacy threshold (0.5 nM) defined by the miRNA supplier.

Analyses of cell morphology were performed with hCAECs (Figure 6). miRNA alone in solution led to increased cell shrinkage and preservation of heightened stress fiber intensity with culture time[51,53]; with unloaded NPs, cells displayed signs of oncosis and/or necrosis with substantial loss of typical topography with respect to visible actin fibers, swollen appearance, rounded periphery, and presence of large membrane protrusions suggesting membrane blebbing,[51,53,55] even though short-length polymers (7 and 20 kDa) were used for NP fabrication.[55] Regardless, cells exhibited healthier features at day 2, suggesting that these features were reversible after their eventual initial activation. Loaded NP-enriched cells showed the highest resemblance of all tested conditions to the control hCAECs cultured in basal conditions at all time points. ATP analyses showed no significant alterations in hCAEC metabolic activity. EC dysfunction and activation toward a pro-inflammatory phenotype is a key promoter of the cascade of detrimental signaling triggers to an infarcted region, which could further impair the tissue from recovering after an MI.[3] Loaded NPs maintained hCAEC basal characteristics, so promising prospects can be perceived for future treatments based on such nano-objects.

The fluorescent molecule (Nile Red) added to the NP core during NP polymerization enabled their labeling, as previously shown.[56] ftNP

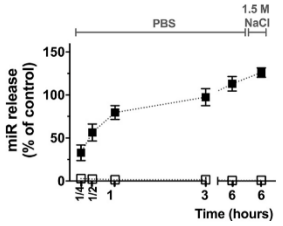

Figure 5. miRNA Release and Desorption from the NPs

NPs were re-suspended in PBS and incubated at 37°C with orbital shaking at 250 rpm, for 1/4, 1/2, 1, 3, and 6 hours, with aliquots removed at each time point. NPs at 6 hours were then centrifuged and re-suspended in 1.5 M NaCl to promote desorption of remaining miRNA. Results tracked by AGE are shown as the mean ± SD of three to four independent experiments. Loaded NPs, black symbols; unloaded NPs, white symbols.

size decreased approximately 17 nm in comparison to the non-fluorescent counterpart, and ζ potential remained unchanged (data not shown). A main interest in working with NPs is to have them cross cellular membranes and enter living cells for cargo release after intracellular targeting.[55] Some ftNPs were observed inside the cells after the 4 hour-period, but most were still outside (Figure S2). NP internalization was clearly observed after 1 day of incubation (result also noticed in basal conditions; data not shown), with even more NP accumulation within hCAEC borders after 2 days (Figure 7) and NP translocation to the perinuclearly located ER (Figure 8). The ER is the site where target mRNA binds to Argonaut-2 (Ago2) and miRNA, which precedes miRNA-mediated translation repression of target mRNA in mammalian cells,[57] events importantly linked to increased biological efficacy.[16,57,58] Possible ER transient disruption was also suggested by the cell morphology, and sparse red labeling distribution in several NPs all around cell nuclei[55,58] reinforce the latter hypothesis. Loaded NPs appeared to contain slightly more NPs encircling the hCAEC nucleus and within the ER, but internalization occurred similarly for either unloaded or loaded NPs. Endosomal entrapment is a usual endpoint of many loaded nanosystems guided toward natural cellular degradation processes through lysosomes.[55,59] No NPs have yet been reported to be capable of crossing EC ER membranes. Interestingly, our NPs clearly accumulated within hCAEC ER after 2 days.

Intracellular miR-155-5p level was studied (Figure 9) to evaluate if the load had been delivered within the cells. The massive presence of loaded ftNPs within the ER of the hCAECs reinforces the potential that the miRNA detected within the cells has been delivered to the required cell organelle for the miRNA to proceed. No information can be given, however, regarding intracellular location of the miRNA through qPCR. Even if it cannot be discounted that both exogenous and endogenous miRNAs were detected through this technique, it is clear that 4 h of incubation was sufficient to yield a 75-fold increase in miRNA within the loaded NP-supplemented TNF-α-hCAECs when compared to unloaded NPs. From 4 hours to 2 days, the miR-155-5p may have been consumed or degraded through the classic routes.[38] On the other hand, cultures with miR-155-5p alone also produced 85-fold increased miRNA expression levels. miRNAs are expected to be degraded in serum and have poor cellular uptake.[12,60] The results showed that miRNA expression was consistently lower for free miRNA than for miRNA complexed to the NPs. The intracellular level of *BACH1* was also studied to assess delivered miRNA's ability to target this gene and lead to its reduction within hCAECs. Loaded NP-enriched cultures resulted in a 4-fold reduction of *BACH1* within hCAECs in comparison to the control with cells alone. When incubated with NPs, *BACH1* levels within hCAECs were five times lower when miR-155-5p was loaded. Free miR-supplemented cultures also induced a decrease in *BACH1* expression levels when compared to the control or loaded NPs (50- or 14-fold, respectively). The results therefore indicate that the hCAECs' contact with miR-155-5p is followed by endogenous *BACH1* silencing, thus showing *in vitro* functional validation of miR-155-5p delivery through reduction of this downstream target.

The endothelial-enriched miR-155-5p is one of the TNF-α-inducible miRNAs predicted to bind to *BACH1* mRNA,[38] an important pleiotropic regulator of cell homeostasis known for its vasculoprotective effects through restrain of endothelial cell dysfunction, inflammation, and hypertension.[38,61,62] miRNA-based therapies offer an approach that can reach levels of intra- and intercellular communication so that potentiated effects can be achieved with very low doses of the bioactive compound.[16] The use of nanoscale injectable systems that are minimally invasive, able to protect and carry loads, avoid immediate renal clearance, interact with surface receptors, pass through biological barriers, be internalized into target cells, deliver loads, and influence cellular processes[11,44] is an interesting strategy for reducing the damaging effects of a MI.[18,44] Targeting this pathway is a promising *in vivo* strategy, because mice lacking *BACH1* subjected to an experimental MI were shown to have an infarct size 48.4% smaller than that in wild-type mice.[63–65] Although efficient EC targeting systems are still lacking,[33,66] miRNA carriers are now being used. Altogether, we believe that the findings in this study represent proof of concept that miR-155-5p can be successfully loaded onto polymer-based NPs and can be internalized into hCAECs, aiming at modulating hCAEC response toward their normal state through *BACH1* silencing. Delivering this miRNA to the ECs of the heart during reperfusion is hence expected to reduce their oxidative stress and, as a consequence, their barrier function and their anti-inflammatory and anti-thrombotic functions, as well as their survival.[67–70] The ultimate goal is not to regenerate the heart and obtain native healthy tissue in the long-term, but instead to decrease the overall effects of the injury, so that a decrease in the chances for heart failure can be attained.

Conclusions

Herein, we have evaluated for the first time miRNA-loaded polymer-based NPs containing a core of poly(cyanoacrylate) and a shell with dextran, DEAE-dextran, and fucoidan targeting P-selectin on

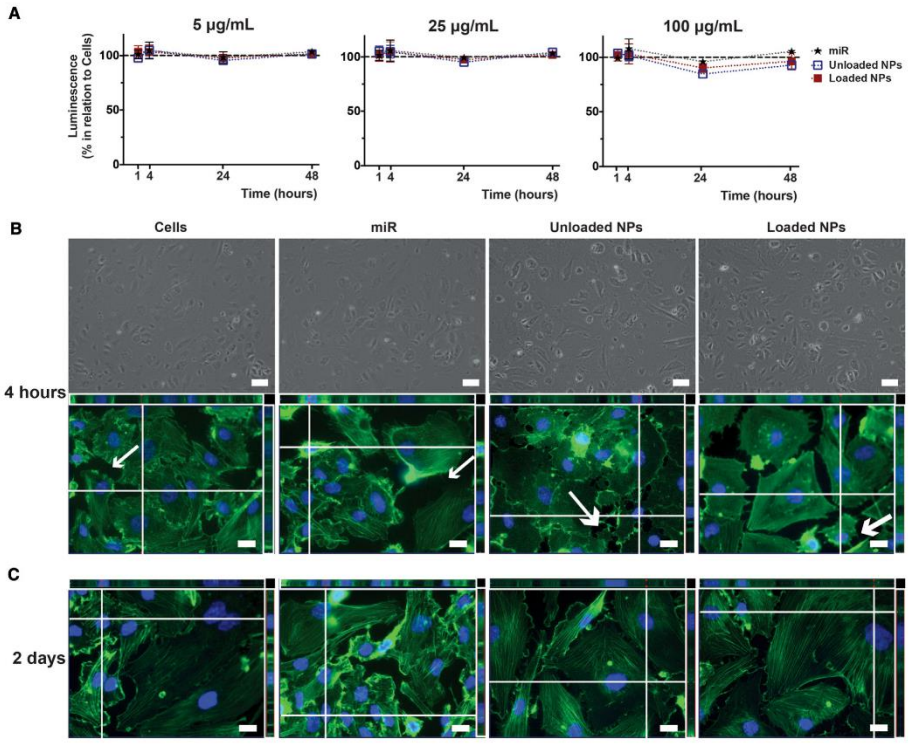

Figure 6. Cytocompatibility of Unloaded and Loaded NPs toward hCAECs in Basal Static Conditions

(A) Luminescence measurements following ATP conversion after incubation for 1 and 4 hours and 1 and 2 days, with NPs at 5, 25, or 100 µg/mL. Results are shown as the mean ± SD from three independent experiments, with no significant differences detected using the Wilcoxon matched-pairs signed rank test. (B) hCAEC morphology at an early time point (4 h) of incubation with NPs at 100 µg/mL, visualized in light micrographs of cultures in 96-well plates (scale bars represent 100 µm) and fluorescence images of hCAECs in 8-well LabTek chamber slides emphasizing cell nuclei (Hoechst; nucleic acids; blue) and cytoplasm (phalloidin; actin fibers; green). Scale bars represent 20 µm for Z-stack-assembled (25–40 slices) images. (C) Fluorescence images taken after 2 days of incubation. Images are representative of three independent experiments.

activated hCAECs. miRNA loading was successful and reproducible, as was load release in physiological conditions. Loaded NPs were cytocompatible for these cells, which presented typical hCAEC morphology. Cells cultured with the loaded NPs increased their content of miR-155-5p and decreased their content of *BACH1*. NPs were located within the ERs, thereby positioning them to bind with target mRNA and fulfill its function. Hence, this study is the first proof of concept that miR-155-5p can be loaded onto core-shell, poly(cyanoacrylate)-polysaccharide NPs and remain intact and biologically active, with the NPs located at the target site for mRNA degradation. Given *BACH1* silencing within hCAECs, a potential decrease in the overall detrimental effects within infarcted hearts through intravenous injection is envisioned, with results opening new perspectives for therapeutic approaches for cardiovascular diseases.

MATERIALS AND METHODS

Materials

Pharmaceutical grade fucoidan (7 kDa; Algues & Mer), DEAE-dextran (20 kDa; TdB Consultancy), dextran (20 kDa, Pharmacosmos) and isobutylcyanoacrylate (IBCA) monomers (AFINITICA) were used without further chemical modification. Polysaccharides were vacuum dried at 60°C overnight before use. Chemically modified, double-stranded RNA oligonucleotides from QIAGEN were used to mimic the natural human mature microRNA miR-155-5p

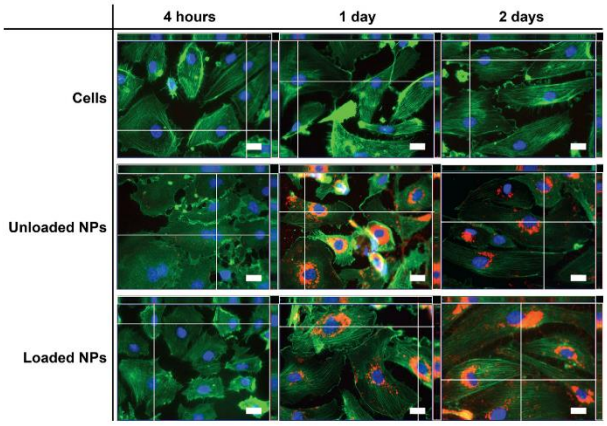

Figure 7. Fluorescence Microscopy of ftNPs (Nile Red) and Intracellular Distribution in hCAECs in TNF-α-Stimulated Cells after 4 hours and 1 and 2 Days of Incubation

Z-stack-assembled (25–40 slices) fluorescence images of hCAECs cultured with unloaded or loaded NPs, and stained to highlight the cell nucleus (Hoechst 33342; nucleic acids; blue) and cytoplasm (phalloidin; actin fibers; green) in monolayer cultured under static conditions. Scale bars represent 20 μm. Images are representative of three independent experiments. Color settings were optimized for loaded NPs at day 1 of incubation, and then used for all images, apart from the nuclear staining.

(miRNA sequence: 5′-UUA AUG CUA AUC GUG AUA GGG GU-3′). The biomolecule was received lyophilized, and then it was reconstituted, aliquoted, and stored at −20°C, according to the manufacturer's recommendations. The molecular units of the aforementioned materials are represented in Figure S3.

Preparation of the Unloaded and miR-Loaded NPs

Unloaded NPs were prepared as previously described,[47–49] by redox radical emulsion polymerization, to obtain core-shell NPs, with the core composed of the synthetic and hydrophobic cyanoacrylate PIBCA and the shell constituted of natural and hydrophilic polysaccharides. The latter were added with a proportion of 10% fucoidan, 20% DEAE-dextran, and 70% dextran, at a total concentration of 17.2 mg/mL in a nitric acid solution (0.2 M HNO_3), and then kept at 40°C under nitrogen (N_2) bubbling and magnetic stirring until solubilization. Ammonium nitrate cerium (IV) ions ($(NH_4)_2[Ce(NO_3)_6]$; Merck), previously solubilized at 0.08 M in 0.2 M HNO_3, were added to the mixture to initiate the formation of radicals, followed by addition of IBCA monomers (11.4 mg/mL) to form the NP's core. Ethanol was added 2 min later,[50,56] to synthesize non-fluorescent NPs with properties similar to those of the fluorescent ones. Reaction continued at 40°C under magnetic stirring for 50 min, with N_2 bubbling present for the first 10 min after $(NH_4)_2[Ce(NO_3)_6]$ and IBCA addition. A sodium citrate tribasic dehydrate solution (1.02 M HOC(COONa) $(CH_2COONa)_2.2H_2O$; Sigma-Aldrich) was added to the NP dispersion at room temperature to inhibit the reaction, the pH was adjusted to 6.5, and the final dispersion was dialyzed against distilled water (molecular weight cutoff [MWCO], 100 kDa; Spectrum Labs). Finally, before miRNA loading, three additional steps were performed: (1) freeze drying of unloaded NPs, to assess their mass concentration; (2) determination of their N content by elemental analysis, using a combustion method and detection through katharometry (CHNS Vario EL III Elemental Analyzer, Elementar); and (3) exposure of the NPs through UV.

miR-loaded NPs were prepared under sterile conditions, by dropwise addition of a miR-155-5p solution into a stirring NP suspension (4 mg/mL), at an N/P molar ratio of 10 at room temperature. Solutions and suspensions were prepared in UltraPure DNase/RNase-Free Distilled Water (Invitrogen), henceforth named ultrapure water. Then, the NPs were allowed to stabilize 20 min at 4°C, centrifuged (4°C, 50,000 *g*, 45 min) to remove free or poorly adsorbed miRNA, and after resuspension in ultrapure water, the loaded NPs were obtained. NPs were then maintained at 4°C until further use (maximum 24 hours). NP preparation is summarized in Figure S4. See also Figure 1.

ftNPs were used for the internalization studies. For that, NP preparation was subjected to the following modifications: Nile Red, a hydrophobic fluorescent dye (Sigma-Aldrich), was dissolved in ethanol at 0.1 mg/mL and added to the mixture 2 min after the IBCA (similarly as aforementioned) to label the hydrophobic PIBCA core.[50,56]

Characterization of the Unloaded and Loaded NPs

The size (diameter), PdI, and surface electrical charge (ζ potential) of the NPs (Figures 2A and 2B) were determined using a Zetasizer Nano ZS (Malvern Panalytical) equipped with a 4 mW HeNe laser beam with a wavelength of 633 nm and a scattering angle of 173° (for size measurements) and 13° (for ζ potential measurements). Size and ζ potential values were automatically calculated through DTS Nano v.6.30 software, using the Stokes-Einstein equation and the Henry equation with the Smoluchowski approximation, respectively. The dispersion solution used was the solvent in which the NPs were dispersed for the DLS, i.e., ultrapure water, and 1 mM KCl for the ELS. Disposable solvent-resistant microcuvettes or folded capillary cells (DLS; Sigma) with gold-plated electrodes (ELS; Malvern) were used. Data were acquired at 25°C, in triplicate.

The morphology of the NPs was observed by a transmission electron microscope (TEM, 80 kV; Tecnai 12; FEI) with a 1 K × 1 K KeenView

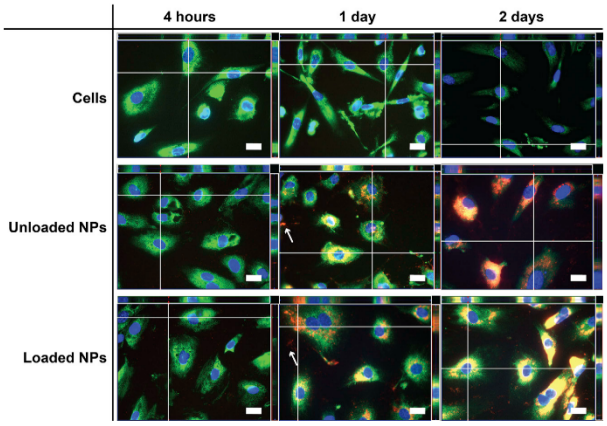

Figure 8. Fluorescence Microscopy of ftNPs (Nile Red) and Intracellular Distribution in hCAECs in TNF-α-Stimulated Cells after 4 hours and 1 and 2 Days of Incubation

Z-stack-assembled (25–40 slices) fluorescence images of hCAECs cultured with unloaded or loaded NPs, and stained to highlight cell nucleus (Hoechst; nucleic acids; blue) and endoplasmic reticulum (protein disulfide isomerase; enzyme; green) in monolayer cultured under static conditions. Scale bars represent 20 μm. Images are representative of three independent experiments. Color settings were optimized for loaded NPs at day 1 of incubation, and then used for all images, apart from the nuclear staining.

camera (OSiS). Samples were prepared by placing 3 μL of the NPs suspension onto a 400 μL mesh copper grid coated with carbon (Electron Microscopy Support). One minute after deposition, the grid was tapped with a filter paper. TEM images were obtained at different magnifications (Figure 2C).

Presence of miR-155-5p within Loaded NPs

The presence of the miR-155-5p was monitored by AGE and qPCR (Figures 3A and 3B, respectively). Five percent agarose gels, prepared in TBE (Tris-Borate-EDTA; Thermo Fisher Scientific) buffer and stained with ethidium bromide, were used to allow detection of nucleic acids within a 10–100 bp range, as well as the GeneRuler Ultra Low Range DNA Ladder (10–300 bp; Thermo Scientific). Samples included unloaded and loaded NPs, plus additional controls from different steps of the miRNA loading: miRNA alone (at the concentration used for the loading), loaded NPs right after miRNA addition, and supernatant from the ultracentrifugation. Samples were run by electrophoresis (50 V, 120 min) and detected through a UV transilluminator smart imaging system (Vilber Lourmat).

As for qPCR, miR-155-5p was detected using the Hs_miR-155_2 miScript Primer Assay (5′UUAAUGCUAAUCGUGAUAGGGGU-3′; QIAGEN), a primer able to detect specifically the human mature miRNA miR-155-5p, following the supplier's recommendations. For that, NPs were centrifuged (0.7 mL at 4°C, 20,000 *g*, 30 min), QIAzol lysis reagent (QIAGEN) was added (0.7 mL) to each sample, and the samples were vortexed until homogenization. RNA was isolated using the miRNeasy Mini Kit (QIAGEN). The quality and quantity of total RNA were determined by UV spectrophotometry. The miScript II RT Kit (QIAGEN) with a final volume of 20 μL, containing 90 ng RNA, 4 μL 5× miScript Hiflex buffer, 2 μL 10× miScript Nucleics Mix, and 2 μL miScript Reverse Transcriptase mix were used for cDNA synthesis. The final concentration of cDNA was 4.5 ng/μL. The qPCR analysis was performed using the miScript SYBR Green PCR kit (QIAGEN) for miR-155-5p with StepOnePlus Real-Time PCR System (Applied Biosystems), according to the manufacturer's recommendations. The amplification was done with a final volume of 25 μL, containing 2× QuantiTect SYBR Green PCR Master Mix, 10× miScript Universal Primer, 10× miScript Primer Assay, and 2.5 μL of each sample at 2 ng/μL. For each DNA amplification, a standard range was also generated from cDNA of a miR-155-5p solution, to determine the efficiency of the primer, as well as the negative control (without the reverse transcriptase). The qPCR conditions included 1 cycle for enzyme activation (95°C for 15 min), followed by 40 cycles of denaturation, annealing, and extension (94°C for 15 s, 55°C for 30 s, and 70°C for 34 s). By means of a standard curve, the expression of the gene encoding the miRNA was calculated using the standard curve and a geometric mean.

Loaded NP Stability, Release, and Desorption

Loaded NP stability, while stored at 4°C, was evaluated by DLS (Figures 4A and 4B), ELS (Figure 4C), and AGE (Figure 4D), right after miRNA loading (day 0) and 1, 7, 14, 21, and 28 days after miRNA inclusion. Aliquots for each time point were prepared under sterile and RNase-free conditions at day 0. Furthermore, to assess if all miRNA could be released and desorbed from the NPs under physiological and sterile conditions, loaded NPs were resuspended in PBS at 4°C (instead of the ultrapure water) after centrifugation, transferred into a clear, flat-bottomed, ultra-low attachment plate (Corning) and subjected to strong orbital shaking at 250 rpm at 37°C. At each time point (15 and 30 min and 1, 3, and 6 h), the plate was removed from the orbital shaker and incubator, and one-tenth of the volume of each well was removed and placed at −20°C and replaced by PBS. At the last time point, the remaining content of each well was centrifuged (4°C, 20,000 *g*, 30 min). Samples were resuspended in 1.5 M NaCl, supernatants collected, and a final run of re-suspension and centrifugation in 1.5 M NaCl was performed to obtain the final NPs. Samples were analyzed by AGE (Figure 5).

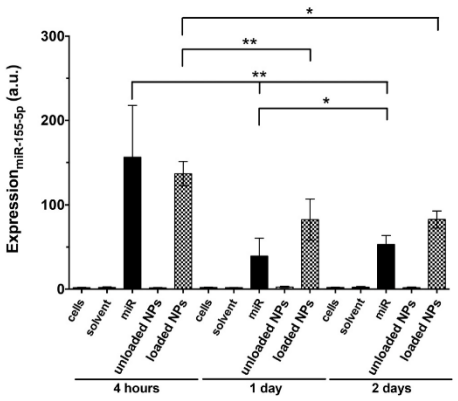

Figure 9. Expression of miR-155-5p within hCAECs after 4 hours and 1 and 2 Days, as Determined by qPCR for TNF-α-Stimulated Cells

Results are shown as the mean ± SD from four independent experiments. Significant differences were detected using the Wilcoxon matched-pairs signed rank test; *$p < 0.05$ and **$p < 0.001$. ns, nonsignificant.

In Vitro Cell Culture Studies

hCAECs (PromoCell) were expanded in monolayer culture in cell culture medium (EC basal medium MV 2 plus a supplemental pack containing 5% fetal calf serum, 5 ng/mL recombinant human epidermal growth factor, 10 ng/mL recombinant human basic fibroblast growth factor, 20 ng/mL recombinant human Long R3 insulin-like growth factor, 0.5 ng/mL recombinant human vascular endothelial growth factor 165, 1 μg/mL ascorbic acid, and 0.2 μg/mL hydrocortisone (PromoCell). Additional supplements included 1% penicillin-streptavidin (Life Technologies), 0.2% Primocin (InvivoGen), and 0.02% Plasmocin (InvivoGen), in a humidified atmosphere with 5% CO_2 at 37°C. At a subconfluent-to-confluent stage, the cells were detached with 0.05% trypsin-EDTA (Gibco) and re-seeded until the required number of cells for the subsequent experiments was obtained. Flasks, plates, and chamber slides were always pre-coated with 50 μg/mL fibronectin (PromoCell). Cells were used at passage numbers 6–7 (P6–P7) for all *in vitro* cell culture studies.

Cytocompatibility Studies

Unloaded and loaded NP cytocompatibility toward hCAECs was assessed by the CellTiter-Glo luminescent cell viability assay (Promega), which measures ATP presence by luminescence (integration time: 1,000 ms), with the result being directly proportional to the number of viable cells within the wells (Figure 6A). Bright-field images (EVOS XL Core Cell Imaging System; Thermo Fisher Scientific, Figure 6B) and fluorescence images (Axiovert Observer Z1 inverted microscope; Zeiss; Figures 6B and 6C) were taken during culture to monitor hCAEC morphology in the presence of unloaded and loaded NPs.

hCAECs were seeded at 6.25×10^4 cells/cm^2 onto Nunc white, opaque, flat-bottomed plates (Fisher Scientific) so that ATP conversion could be measured. After 24 hours and then twice per week, the medium was changed until the cells reached confluence. At this point, the medium was changed again to include the following conditions: unloaded or loaded NPs at 5, 25, and 100 μg/mL; miRNA solutions at 0.03, 0.16, and 0.65 μg/mL; with the NP dispersions and miRNA solutions within the solvent ultrapure water at one-tenth of the well volume. A blank control comprising only medium was also included, together with solvent alone at the aforementioned volume proportion and controls of all tested conditions without cells. A standard curve built from ATP sodium salt (Sigma) was prepared in the plate at each time point, according to the supplier's recommendations. Measurements were performed 1 and 4 hours and 1 and 2 days after incubation with all conditioned media.

Bright-field images were acquired at magnification 10×, after 4 hours of incubation in the tested conditions: conditioned medium with unloaded and loaded ftNPs at 100 μg/mL, miRNA solution at 0.65 μg/mL, solvent, and blank control with medium. Cells (P6–P7) were previously seeded at 6.25×10^4 cells/cm^2 onto Corning clear, flat-bottomed, 96-well plates. For acquiring fluorescence images, cells were seeded onto eight-well Nunc Lab-Tek chamber slides (Thermo Scientific) and then incubated during 4 h with each imaging condition (cells, solvent, miR, unloaded ftNPs, and loaded ftNPs). Next, the wells were fixed and cell nuclei and cytoplasm were stained. For this, cells were fixed in paraformaldehyde (PFA; 3.7%) for 15 min, washed in PBS, and stored at 4°C. Subsequently, a blocking step was introduced to reduce nonspecific background staining with 1 hour of incubation in PBS containing 1% BSA (Bio-techne). Cells were then incubated overnight in the dark at 4°C in Alexa Fluor 488-phalloidin (dilution 1:40 in blocking solution; Life Technologies). Cell nuclei were counterstained by immersion in 10 mg/mL Hoechst 33342 trihydrochloride trihydrate (dilution, 1:1,000 in PBS; Life Technologies) for 10 min at room temperature, in dark conditions. After final washes in PBS, the samples were mounted with ProLong diamond anti-fade mounting medium (Life Technologies) and sealed. Images were captured with a 40× oil objective, as Z-stack-assembled (25–40 slices, 7.44–12.09 μm) images. Color settings were optimized for each condition and time point.

Cell Internalization

To evaluate the capacity of hCAECs to internalize ftNPs, unloaded and loaded NPs were incubated with these cells under pro-inflammatory conditions (method adapted from Ollivier et al.[71]). Cell internalization was then visualized through fluorescence microscopy, as detailed in the previous section (Figures 7 and 8).

hCAECs were seeded at 6.25×10^4 cells/cm^2 onto the eight-well chamber slides described in the previous section. Once confluent, the medium was changed to include cells stimulated overnight with TNF-α-supplemented medium (10 ng/mL, TNF-α; Millipore). In the following day, medium was changed again to include unloaded and loaded NPs at 100 μg/mL, miRNA solution at 0.65 μg/mL,

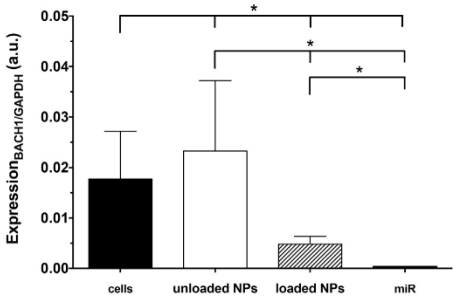

Figure 10. Expression of *BACH1* within hCAECs after 1 Day, as Determined by qPCR

Results are shown as means ± SD (n = 6). Significant differences were detected by the Wilcoxon matched-pairs signed rank test; *p < 0.05.

solvent, and control with medium (detailed in the previous section). At 4 h and 1 and 2 days of incubation, the cells were fixed and stained according to two protocols in parallel, with the first protocol staining cell nuclei and cytoplasm (detailed in the previous section), and the second protocol staining cell nuclei and ER, where SelectFX Alexa Fluor 488 Endoplasmic Reticulum Labeling Kit (Life Technologies) was used, according to the supplier's ER staining protocol. Images were captured with a 40× oil objective, as z stack-assembled (25–40 slices; 7.44–12.09 μm) images. Color settings were optimized for loaded NPs at day 1 of incubation and then used for all images, apart from the nuclear staining.

Detection of miR-155-5p and BACH1 within hCAECs

In order to verify miR-155-5p and *BACH1* presence within hCAECs, loaded NPs were incubated with these cells, as described in section 2.4. The intracellular level of the genes was then evaluated by qPCR (Figures 9 and 10).

hCAECs were seeded at 3.8×10^6 cells/cm^2 in clear, flat-bottomed, six-well plates (Corning), as described above. Once confluent, the cells were cultured under basal and pro-inflammatory conditions, and comprising the aforementioned conditioned media. At 4 hours and 1 and 2 days of incubation, the wells were washed with PBS, lysed with the QIAzol lysis reagent, and processed for qPCR, as described for digested NPs, with a final cDNA concentration of 250 ng/μL. Relative gene expression was determined for *BACH1* after 1 day of incubation, normalized by *GAPDH*. Specific primers (Eurogentec) were used to quantify the gene expression of *BACH1* (forward primer sequence: 5′-TCGCAAGAGAAAACTTGACTG-3′; reverse primer sequence: 5′-CCCAGAGTTGACAAAATGTGA-3′) and *GAPDH* (forward primer sequence: 5′-GTCGCCAGCCGAGCCACATC; reverse primer sequence: 5′-CCAGGCGCCCAATACGACCA-3′). For both genes, the amplification was done with a final volume of 25 μL, containing Absolute Blue qPCR SYBR Green ROX Mix (Thermo Fisher Scientific), forward primer, reverse primer, RNase-free water, and 10 μL of each sample at 0.8 ng/μL for *BACH1* or 0.2 ng/μL for *GAPDH*. The qPCR conditions included annealing temperatures of 62°C or 69°C, respectively.

Statistical Analysis

Statistical analysis was performed using GraphPad Prism (version: 5.0a). The parametric distribution of the data was first evaluated by the D'Agostino-Pearson omnibus normality test. Because the data followed a non-parametric distribution, statistical analysis was performed with the Wilcoxon matched-pairs signed rank test to compare each paired group. A confidence interval of at least 95% was chosen to define statistical significance (*p < 0.05, **p < 0.001, ***p < 0.0001).

SUPPLEMENTAL INFORMATION

Supplemental Information can be found online at https://doi.org/10.1016/j.omtn.2019.05.016.

AUTHOR CONTRIBUTIONS

J.C.A. designed the study, performed the experiments, collected and interpreted the data, and wrote the draft version of the manuscript. L.B. optimized qPCR protocols, provided genetics expertise, and assisted in study design and data interpretation. F.C.M. aided in miRNA release experiments and data collection, M.J. advised on nanoparticle preparation. M.-S.G., M.A., and C.B. provided genetics expertise. F.C. advised on nanoparticle characterization. G.C. aided with the immunostaining of nanoparticles and collaborated in the design of the whole study, interpretation of the results (particularly at the cell-material interface), and correction of the manuscript, together with A.N. and V.O. A.N. was also instrumental in cell internalization studies and V.O. guided the agarose gel electrophoresis, the cells used and the *in vitro* cell culture model. D.L. provided the funding, supervised the study, discussed the results and corrected the manuscript. C.C. supervised the study, discussed the results, and corrected the manuscript.

CONFLICTS OF INTEREST

The authors declare no competing interests.

ACKNOWLEDGMENTS

This work was financed by European Union project NanoAthero FP7-NMP-2012-LARGE-6-309820 and ANR-13-LAB1-0005-01 "FucoChem." The authors would like to acknowledge F.C.M.'s PhD fellowship from the Conselho Nacional de Desenvolvimento Científico e Tecnológico (CNPq) from Brazil (Process 201245/2017-5). Thanks also to B. Li, M.-P. Jacob-Lenet, C. Choqueux, R. Aid-Launais, G. Even, M. Morvan, F. Andreata, S. Loyau, L. Venisse, A. Loste, J. Aerts, and A. Grodet for technical assistance and guidance during the experiments. The authors would also like to acknowledge Marie-Françoise Bricot from the Institut de Chimie des Substances Naturelles of the Université Paris-Saclay for microanalysis of the raw polymers and NPs. We also thank the ImagoSeine core facility of the Institut Jacques Monod, member of IBiSA and France-BioImaging (ANR-10-INBS-04) infrastructures, particularly Dr. Rémi le Borgne for sample preparation and assistance with TEM imaging.

REFERENCES

1. Godier-Furnemont, A., and Vunjak-Novakovic, G. (2002). Cardiac Muscle Tissue Engineering. In Biomaterials Science: An Introduction to Materials in Medicine, Third Edition, B.D. Ratner, A.S. Hoffman, F.J. Schoen, and J.E. Lemons, eds. (Academic Press), pp. 1262–1276.
2. Chauvierre, C., and Letourneur, D. (2015). The European project NanoAthero to fight cardiovascular diseases using nanotechnologies. Nanomedicine (Lond.) *10*, 3391–3400.
3. Fiedler, J., and Thum, T. (2013). MicroRNAs in myocardial infarction. Arterioscler. Thromb. Vasc. Biol. *33*, 201–205.
4. Frangogiannis, N.G. (2008). The immune system and cardiac repair. Pharmacol. Res. *58*, 88–111.
5. Sala, V., Bergerone, S., Gatti, S., Gallo, S., Ponzetto, A., Ponzetto, C., and Crepaldi, T. (2014). MicroRNAs in myocardial ischemia: identifying new targets and tools for treating heart disease. New frontiers for miR-medicine. Cell. Mol. Life Sci. *71*, 1439–1452.
6. Frost, R.J.A., and van Rooij, E. (2010). miRNAs as therapeutic targets in ischemic heart disease. J. Cardiovasc. Transl. Res. *3*, 280–289.
7. Boersma, E., Mercado, N., Poldermans, D., Gardien, M., Vos, J., and Simoons, M.L. (2003). Acute myocardial infarction. Lancet *361*, 847–858.
8. Thum, T. (2012). MicroRNA therapeutics in cardiovascular medicine. EMBO Mol. Med. *4*, 3–14.
9. Farías, J.G., Molina, V.M., Carrasco, R.A., Zepeda, A.B., Figueroa, E., Letelier, P., and Castillo, R.L. (2017). Antioxidant Therapeutic Strategies for Cardiovascular Conditions Associated with Oxidative Stress. Nutrients *9*, E966.
10. Spath, N.B., Mills, N.L., and Cruden, N.L. (2016). Novel cardioprotective and regenerative therapies in acute myocardial infarction: a review of recent and ongoing clinical trials. Future Cardiol. *12*, 655–672.
11. Antunes, J.C., Pereira, C.L., Teixeira, G.Q., Silva, R.V., Caldeira, J., Grad, S., Gonçalves, R.M., and Barbosa, M.A. (2017). Poly(γ-glutamic acid) and poly(γ-glutamic acid)-based nanocomplexes enhance type II collagen production in intervertebral disc. J. Mater. Sci. Mater. Med. *28*, 6.
12. Wang, Y.-J., Larsson, M., Huang, W.-T., Chiou, S.-H., Nicholls, S.J., Chao, J.-I., and Liu, D.-M. (2016). The use of polymer-based nanoparticles and nanostructured materials in treatment and diagnosis of cardiovascular diseases: Recent advances and emerging designs. Prog. Polym. Sci. *57*, 153–178.
13. Cavarretta, E., and Frati, G. (2016). MicroRNAs in Coronary Heart Disease: Ready to Enter the Clinical Arena? BioMed Res. Int. *2016*, 2150763.
14. Devaux, Y., Stammet, P., Friberg, H., Hassager, C., Kuiper, M.A., Wise, M.P., and Nielsen, N.; Biomarker subcommittee of TTM trial (Target Temperature Management After Cardiac Arrest, NCT01020916) (2015). MicroRNAs: new biomarkers and therapeutic targets after cardiac arrest? Crit. Care *19*, 54.
15. Qiagen. (2018). Guidelines for miRNA mimic and miRNA inhibitor experiments, https://www.qiagen.com/fr/resources/resourcedetail?id=3e1477ad-74a2-4ee6-9c31-54b1997f2941&lang=en.
16. van Rooij, E., Marshall, W.S., and Olson, E.N. (2008). Toward microRNA-based therapeutics for heart disease: the sense in antisense. Circ. Res. *103*, 919–928.
17. Small, E.M., and Olson, E.N. (2011). Pervasive roles of microRNAs in cardiovascular biology. Nature *469*, 336–342.
18. Nguyen, M.M., Gianneschi, N.C., and Christman, K.L. (2015). Developing injectable nanomaterials to repair the heart. Curr. Opin. Biotechnol. *34*, 225–231.
19. Gadde, S., and Rayner, K.J. (2016). Nanomedicine Meets microRNA: Current Advances in RNA-Based Nanotherapies for Atherosclerosis. Arterioscler. Thromb. Vasc. Biol. *36*, e73–e79.
20. Ong, S.B., Katwadi, K., Kwek, X.Y., Ismail, N.I., Chinda, K., Ong, S.G., and Hausenloy, D.J. (2018). Non-coding RNAs as therapeutic targets for preventing myocardial ischemia-reperfusion injury. Expert Opin. Ther. Targets *22*, 247–261.
21. Small, E.M., Frost, R.J.A., and Olson, E.N. (2010). MicroRNAs add a new dimension to cardiovascular disease. Circulation *121*, 1022–1032.
22. van Rooij, E., and Olson, E.N. (2012). MicroRNA therapeutics for cardiovascular disease: opportunities and obstacles. Nat. Rev. Drug Discov. *11*, 860–872.
23. Hu, S., Huang, M., Li, Z., Jia, F., Ghosh, Z., Lijkwan, M.A., Fasanaro, P., Sun, N., Wang, X., Martelli, F., et al. (2010). MicroRNA-210 as a novel therapy for treatment of ischemic heart disease. Circulation *122* (11, Suppl), S124–S131.
24. Hutcheson, R., Terry, R., Chaplin, J., Smith, E., Musiyenko, A., Russell, J.C., Lincoln, T., and Rocic, P. (2013). MicroRNA-145 restores contractile vascular smooth muscle phenotype and coronary collateral growth in the metabolic syndrome. Arterioscler. Thromb. Vasc. Biol. *33*, 727–736.
25. Jeong, D., Yoo, J., Lee, P., Kepreotis, S.V., Lee, A., Wahlquist, C., Brown, B.D., Kho, C., Mercola, M., and Hajjar, R.J. (2018). miR-25 Tough Decoy Enhances Cardiac Function in Heart Failure. Mol. Ther. *26*, 718–729.
26. Karakikes, I., Chaanine, A.H., Kang, S., Mukete, B.N., Jeong, D., Zhang, S., Hajjar, R.J., and Lebeche, D. (2013). Therapeutic cardiac-targeted delivery of miR-1 reverses pressure overload-induced cardiac hypertrophy and attenuates pathological remodeling. J. Am. Heart Assoc. *2*, e000078.
27. Meloni, M., Marchetti, M., Garner, K., Littlejohns, B., Sala-Newby, G., Xenophontos, N., Floris, I., Suleiman, M.S., Madeddu, P., Caporali, A., and Emanueli, C. (2013). Local inhibition of microRNA-24 improves reparative angiogenesis and left ventricle remodeling and function in mice with myocardial infarction. Mol. Ther. *21*, 1390–1402.
28. Pandey, R., Velasquez, S., Durrani, S., Jiang, M., Neiman, M., Crocker, J.S., Benoit, J.B., Rubinstein, J., Paul, A., and Ahmed, R.P. (2017). MicroRNA-1825 induces proliferation of adult cardiomyocytes and promotes cardiac regeneration post ischemic injury. Am. J. Transl. Res. *9*, 3120–3137.
29. Quattrocelli, M., Crippa, S., Montecchiani, C., Camps, J., Cornaglia, A.I., Boldrin, L., Morgan, J., Calligaro, A., Casasco, A., Orlacchio, A., et al. (2013). Long-term miR-669a therapy alleviates chronic dilated cardiomyopathy in dystrophic mice. J. Am. Heart Assoc. *2*, e000284.
30. Shen, Y., Shen, Z., Miao, L., Xin, X., Lin, S., Zhu, Y., Guo, W., and Zhu, Y.Z. (2015). miRNA-30 family inhibition protects against cardiac ischemic injury by regulating cystathionine-γ-lyase expression. Antioxid. Redox Signal. *22*, 224–240.
31. Das, S., Bedja, D., Campbell, N., Dunkerly, B., Chenna, V., Maitra, A., and Steenbergen, C. (2014). miR-181c regulates the mitochondrial genome, bioenergetics, and propensity for heart failure in vivo. PLoS ONE *9*, e96820.
32. Deng, S., Zhao, Q., Zhen, L., Zhang, C., Liu, C., Wang, G., Zhang, L., Bao, L., Lu, Y., Meng, L., et al. (2017). Neonatal Heart-Enriched miR-708 Promotes Proliferation and Stress Resistance of Cardiomyocytes in Rodents. Theranostics *7*, 1953–1965.
33. Kheirolomoom, A., Kim, C.W., Seo, J.W., Kumar, S., Son, D.J., Gagnon, M.K.J., Ingham, E.S., Ferrara, K.W., and Jo, H. (2015). Multifunctional Nanoparticles Facilitate Molecular Targeting and miRNA Delivery to Inhibit Atherosclerosis in ApoE(-/-) Mice. ACS Nano *9*, 8885–8897.
34. Lesizza, P., Prosdocimo, G., Martinelli, V., Sinagra, G., Zacchigna, S., and Giacca, M. (2017). Single-Dose Intracardiac Injection of Pro-Regenerative MicroRNAs Improves Cardiac Function After Myocardial Infarction. Circ. Res. *120*, 1298–1304.
35. Gomes, R.S., das Neves, R.P., Cochlin, L., Lima, A., Carvalho, R., Korpisalo, P., Dragneva, G., Turunen, M., Liimatainen, T., Clarke, K., et al. (2013). Efficient pro-survival/angiogenic miRNA delivery by an MRI-detectable nanomaterial. ACS Nano *7*, 3362–3372.
36. Li, R.Q., Wu, Y., Zhi, Y., Yang, X., Li, Y., Xua, F.J., and Du, J. (2016). PGMA-Based Star-Like Polycations with Plentiful Hydroxyl Groups Act as Highly Efficient miRNA Delivery Nanovectors for Effective Applications in Heart Diseases. Adv. Mater. *28*, 7204–7212.
37. Xue, X., Shi, X., Dong, H., You, S., Cao, H., Wang, K., Wen, Y., Shi, D., He, B., and Li, Y. (2018). Delivery of microRNA-1 inhibitor by dendrimer-based nanovector: An early targeting therapy for myocardial infarction in mice. Nanomedicine (Lond.) *14*, 619–631.
38. Pulkkinen, K.H., Ylä-Herttuala, S., and Levonen, A.-L. (2011). Heme oxygenase 1 is induced by miR-155 via reduced BACH1 translation in endothelial cells. Free Radic. Biol. Med. *51*, 2124–2131.
39. Song, M.A., Paradis, A.N., Gay, M.S., Shin, J., and Zhang, L. (2015). Differential expression of microRNAs in ischemic heart disease. Drug Discov. Today *20*, 223–235.
40. Rouzet, F., Bachelet-Violette, L., Alsac, J.-M., Suzuki, M., Meulemans, A., Louedec, L., Petiet, A., Jandrot-Perrus, M., Chaubet, F., Michel, J.B., et al. (2011). Radiolabeled

fucoidan as a p-selectin targeting agent for in vivo imaging of platelet-rich thrombus and endothelial activation. J. Nucl. Med. *52*, 1433–1440.

41. Sabboural, P., Chaubet, F., Rouzet, F., Al-Shoukr, F., Azzouna, R.B., Bouchemal, N., Picton, L., Louedec, L., Maire, M., Rolland, L., et al. (2014). Purification of a low molecular weight fucoidan for SPECT molecular imaging of myocardial infarction. Mar. Drugs *12*, 4851–4867.

42. Bachelet, L., Bertholon, I., Lavigne, D., Vassy, R., Jandrot-Perrus, M., Chaubet, F., and Letourneur, D. (2009). Affinity of low molecular weight fucoidan for P-selectin triggers its binding to activated human platelets. Biochim. Biophys. Acta *1790*, 141–146.

43. Bonnard, T., Yang, G., Petiet, A., Ollivier, V., Haddad, O., Arnaud, D., Louedec, L., Bachelet-Violette, L., Derkaoui, S.M., Letourneur, D., et al. (2014). Abdominal aortic aneurysms targeted by functionalized polysaccharide microparticles: a new tool for SPECT imaging. Theranostics *4*, 592–603.

44. Silva, A.K.A., Letourneur, D., and Chauvierre, C. (2014). Polysaccharide nanosystems for future progress in cardiovascular pathologies. Theranostics *4*, 579–591.

45. Suzuki, M., Bachelet-Violette, L., Rouzet, F., Beilvert, A., Autret, G., Maire, M., Menager, C., Louedec, L., Choqueux, C., Sabboural, P., et al. (2015). Ultrasmall superparamagnetic iron oxide nanoparticles coated with fucoidan for molecular MRI of intraluminal thrombus. Nanomedicine (Lond.) *10*, 73–87.

46. Juenet, M., Varna, M., Aid-Launais, R., Chauvierre, C., and Letourneur, D. (2015). Nanomedicine for the molecular diagnosis of cardiovascular pathologies. Biochem. Biophys. Res. Commun. *468*, 476–484.

47. Chauvierre, C., Labarre, D., Couvreur, P., and Vauthier, C. (2003). Novel polysaccharide-decorated poly(isobutyl cyanoacrylate) nanoparticles. Pharm. Res. *20*, 1786–1793.

48. Chauvierre, C., Labarre, D., Couvreur, P., and Vauthier, C. (2003). Radical emulsion polymerization of alkylcyanoacrylates initiated by the redox system dextran-cerium(IV) under acidic aqueous conditions. Macromolecules *36*, 6018–6027.

49. Chauvierre, C., Manchanda, R., Labarre, D., Vauthier, C., Marden, M.C., and Leclerc, L. (2010). Artificial oxygen carrier based on polysaccharides-poly(alkylcyanoacrylates) nanoparticle templates. Biomaterials *31*, 6069–6074.

50. Lira, M.C.B., Santos-Magalhães, N.S., Nicolas, V., Marsaud, V., Silva, M.P.C., Ponchel, G., and Vauthier, C. (2011). Cytotoxicity and cellular uptake of newly synthesized fucoidan-coated nanoparticles. Eur. J. Pharm. Biopharm. *79*, 162–170.

51. Fink, S.L., and Cookson, B.T. (2005). Apoptosis, pyroptosis, and necrosis: mechanistic description of dead and dying eukaryotic cells. Infect. Immun. *73*, 1907–1916.

52. Hoelzle, M.K., and Svitkina, T. (2012). The cytoskeletal mechanisms of cell-cell junction formation in endothelial cells. Mol. Biol. Cell *23*, 310–323.

53. Paszek, E., Czyz, J., Woźnicka, O., Jakubiak, D., Wojnarowicz, J., Łojkowski, W., and Stepień, E. (2012). Zinc oxide nanoparticles impair the integrity of human umbilical vein endothelial cell monolayer in vitro. J. Biomed. Nanotechnol. *8*, 957–967.

54. Matuszak, J., Baumgartner, J., Zaloga, J., Juenet, M., da Silva, A.E., Franke, D., Almer, G., Texier, I., Faivre, D., Metselaar, J.M., et al. (2016). Nanoparticles for intravascular applications: physicochemical characterization and cytotoxicity testing. Nanomedicine (Lond.) *11*, 597–616.

55. Verderio, P., Avvakumova, S., Alessio, G., Bellini, M., Colombo, M., Galbiati, E., Mazzucchelli, S., Avila, J.P., Santini, B., and Prosperi, D. (2014). Delivering colloidal nanoparticles to mammalian cells: a nano-bio interface perspective. Adv. Healthc. Mater. *3*, 957–976.

56. Juenet, M., Aid-Launais, R., Li, B., Berger, A., Aerts, J., Ollivier, V., Nicoletti, A., Letourneur, D., and Chauvierre, C. (2018). Thrombolytic therapy based on fucoidan-functionalized polymer nanoparticles targeting P-selectin. Biomaterials *156*, 204–216.

57. Barman, B., and Bhattacharyya, S.N. (2015). mRNA Targeting to Endoplasmic Reticulum Precedes Ago Protein Interaction and MicroRNA (miRNA)-mediated Translation Repression in Mammalian Cells. J. Biol. Chem. *290*, 24650–24656.

58. Detzer, A., and Sczakiel, G. (2009). Phosphorothioate-stimulated uptake of siRNA by mammalian cells: a novel route for delivery. Curr. Top. Med. Chem. *9*, 1109–1116.

59. Huang, R.B., Mocherla, S., Heslinga, M.J., Charoenphol, P., and Eniola-Adefeso, O. (2010). Dynamic and cellular interactions of nanoparticles in vascular-targeted drug delivery. Mol. Membr. Biol. *27*, 312–327.

60. Singh, S., Narang, A.S., and Mahato, R.I. (2011). Subcellular fate and off-target effects of siRNA, shRNA, and miRNA. Pharm. Res. *28*, 2996–3015.

61. Cao, Y., Gong, Y., Liu, L., Zhou, Y., Fang, X., Zhang, C., Li, Y., and Li, J. (2017). The use of human umbilical vein endothelial cells (HUVECs) as an in vitro model to assess the toxicity of nanoparticles to endothelium: a review. J. Appl. Toxicol. *37*, 1359–1369.

62. Ma, X., Ma, C., and Zheng, X. (2013). MicroRNA-155 in the pathogenesis of atherosclerosis: a conflicting role? Heart Lung Circ. *22*, 811–818.

63. Mito, S., Ozono, R., Oshima, T., Yano, Y., Watari, Y., Yamamoto, Y., Brydun, A., Igarashi, K., and Yoshizumi, M. (2008). Myocardial protection against pressure overload in mice lacking Bach1, a transcriptional repressor of heme oxygenase-1. Hypertension *51*, 1570–1577.

64. Watari, Y., Yamamoto, Y., Brydun, A., Ishida, T., Mito, S., Yoshizumi, M., Igarashi, K., Chayama, K., Ohshima, T., and Ozono, R. (2008). Ablation of the bach1 gene leads to the suppression of atherosclerosis in bach1 and apolipoprotein E double knockout mice. Hypertens. Res. *31*, 783–792.

65. Yano, Y., Ozono, R., Oishi, Y., Kambe, M., Yoshizumi, M., Ishida, T., Omura, S., Oshima, T., and Igarashi, K. (2006). Genetic ablation of the transcription repressor Bach1 leads to myocardial protection against ischemia/reperfusion in mice. Genes Cells *11*, 791–803.

66. Ma, S., Tian, X.Y., Zhang, Y., Mu, C., Shen, H., Bismuth, J., Pownall, H.J., Huang, Y., and Wong, W.T. (2016). E-selectin-targeting delivery of microRNAs by microparticles ameliorates endothelial inflammation and atherosclerosis. Sci. Rep. *6*, 22910.

67. Brown, D.I., and Griendling, K.K. (2015). Regulation of signal transduction by reactive oxygen species in the cardiovascular system. Circ. Res. *116*, 531–549.

68. O'Connor, P.M., and Gutterman, D.D. (2010). Resurrecting hope for antioxidant treatment of cardiovascular disease: focus on mitochondria. Circ. Res. *107*, 9–11.

69. Seddon, M., Looi, Y.H., and Shah, A.M. (2007). Oxidative stress and redox signalling in cardiac hypertrophy and heart failure. Heart *93*, 903–907.

70. Tsutsui, H., Kinugawa, S., and Matsushima, S. (2011). Oxidative stress and heart failure. Am. J. Physiol. Heart Circ. Physiol. *301*, H2181–H2190.

71. Ollivier, V., Parry, G.C.N., Cobb, R.R., de Prost, D., and Mackman, N. (1996). Elevated cyclic AMP inhibits NF-kappaB-mediated transcription in human monocytic cells and endothelial cells. J. Biol. Chem. *271*, 20828–20835.

International Journal of Pharmaceutics 577 (2020) 119041

Contents lists available at ScienceDirect

International Journal of Pharmaceutics

journal homepage: www.elsevier.com/locate/ijpharm

Synthesis of cationic quaternized pullulan derivatives for miRNA delivery

Fernanda C. Moraes[a,b,*], Joana C. Antunes[c], Laura Marcela Forero Ramirez[a,b], Paola Aprile[a,b], Gregory Franck[a,b], Cédric Chauvierre[a,b,1], Frédéric Chaubet[a,b,1], Didier Letourneur[a]

[a] INSERM, U1148, Laboratory for Vascular Translational Science, X. Bichat Hospital, 46 rue Henri Huchard, 75018, Paris, France
[b] Université de Paris, Université Sorbonne Paris Nord, Paris, France
[c] Universidade do Minho, 2C2T, Campus de Azurém, 4800-058 Guimarães, Portugal

ARTICLE INFO

Keywords:
Pullulan
Cationic derivatives
Polyplexes
microRNA
Gene therapy

ABSTRACT

Pullulan is a natural polysaccharide of potential interest for biomedical applications due to its non-toxic, non-immunogenic and biodegradable properties. The aim of this work was to synthesize cationic pullulan derivatives able to form complexes with microRNAs (miRNAs) driven by electrostatic interaction (polyplexes). Quaternized ammonium groups were linked to pullulan backbone by adding the reactive glycidyltrimethylammonium chloride (GTMAC). The presence of these cationic groups within the pullulan was confirmed by elemental analysis, Fourier-transform infrared spectroscopy (FTIR) and proton nuclear magnetic resonance (^{1}H NMR). The alkylated pullulan was able to interact with miRNA and form stable polyplexes that were characterized regarding size, zeta potential and morphology. The presence of miRNA was confirmed by agarose gel electrophoresis and UV spectrophotometry. *In vitro* tests on human umbilical vein endothelial cells did not show any cytotoxicity after 1 day of incubation with nanosized polyplexes up to 200 µg/mL. QA-pullulan was able to promote miRNA delivery inside cells as demonstrated by fluorescence microscopy images of labelled miRNA. In conclusion, the formation of polyplexes using cationic derivatives of pullulan with miRNA provided an easy and versatile method for polysaccharide nanoparticle production in aqueous media and could be a new promising platform for gene delivery.

1. Introduction

Gene therapy uses nucleic acids (DNA or RNA) for the treatment, cure or prevention of human disorders by the insertion of new genes into target cells (Cao et al., 2019). The use of nucleic acids as drugs has been described for two decades (Wolff et al., 1990), being mainly based on viral vectors and plasmid DNA technology (Xiong et al., 2018; Zarghampoor et al., 2019). More recently, small non coding RNAs (ncRNAs), namely microRNAs (miRNAs), have emerged as key regulators of gene expression as a promising alternative to conventional plasmid DNA (pDNA) due to its multiple unique features and advantages when compared to DNA-based therapy (Bernardo et al., 2015; Xiong et al., 2018).

miRNAs are small endogenous single stranded non-coding RNA molecules that play important roles in many cellular processes such as cell differentiation, proliferation and survival acting on post-transcriptional level by binding to complementary target mRNAs, resulting in mRNA translational inhibition or degradation (Rupaimoole and Slack, 2017). miRNAs have been proposed and investigated as therapeutics and biomarkers for various diseases such as cancer, diabetes, cardiovascular diseases and other pathologies whose etiology is related to aberrant gene expression (Candido et al., 2019; Falzone et al., 2019;

Abbreviations: miRNA, MicroRNA; ncRNAs, small Non Coding RNAs; pDNA, plasmid DNA; PEI, polyethyleneimine; PAMAM, polyamidoamine; siRNA, small interfering RNA; QA-pullulan, quaternized ammonium- pullulan; Mw, weight average molecular weight; Mn, number average molecular weight; GTMAC, glycidyltrimethylammonium chloride; 6-FAM, 6-Fluorescein amidite; SEC-MALLS, size exclusion chromatography- multiangle laser light scattering; FTIR, Fourier-transform infrared spectroscopy; ^{1}H NMR, proton nuclear magnetic resonance; TBE, Tris-Borate-EDTA; PdI, Polydispersity Index; HUVECs, human umbilical vein endothelial cells; PBS, phosphate buffered saline; DS, degree of substitution; AGU, anhydroglucose unit; DAPI, 4′,6-Diamidino-2-phenylindole; TPP, tripolyphosphate; kcps, kilo counts per second

* Corresponding author.
E-mail addresses: fernanda.moraes@inserm.fr (F.C. Moraes), joana.antunes@2c2t.uminho.pt (J.C. Antunes), lmforeror@gmail.com (L.M. Forero Ramirez), paola.aprile@inserm.fr (P. Aprile), gregory.franck@inserm.fr (G. Franck), cedric.chauvierre@inserm.fr (C. Chauvierre), frederic.chaubet@univ-paris13.fr (F. Chaubet), didier.letourneur@inserm.fr (D. Letourneur).

[1] Equivalent work.

https://doi.org/10.1016/j.ijpharm.2020.119041
Received 8 November 2019; Received in revised form 5 January 2020; Accepted 11 January 2020
Available online 22 January 2020
0378-5173/ © 2020 Elsevier B.V. All rights reserved.

Gaur et al., 2015; Hou et al., 2012; Poddar et al., 2019; Zhu et al., 2019). At the target, miRNAs can generate strong, sustained and comprehensive biological effects, through endogenous gene silencing with very low concentrations (at least 0.5 nM) (Devaux et al., 2015; Qiagen, 2018). Additionally, miRNAs are able to affect multiple pathways/cellular processes rather than specific targets (van Rooij et al., 2008). The success of miRNA-based therapies depends on the development of suitable vehicles able to specifically target cells for the efficient delivery of the nucleic acids, with minimum toxicity (Chakraborty et al., 2017).

Compared to DNA-based gene therapy, the delivery of miRNA is more challenging due to important differences in terms of size and structure. Most of the polymeric delivery strategies originally developed for plasmid DNA (pDNA) in gene therapy cannot be used for miRNA delivery without formulation optimization since miRNA are much smaller molecules (21–23 bp) than DNA (several kilo bp). Thereby, small RNAs are more difficult to be packaged and condensed into stable systems for protection against early clearance and degradation (Nuhn et al., 2014; Scholz and Wagner, 2012). Moreover, the vulnerability of RNA to enzymatic degradation (hydrolyses) by serum nucleases due to an extra hydroxyl group in the 2′ position of pentose ring in ribose structure, instead of a hydrogen atom present in DNA structure, induced additional challenges to RNA delivery (Gary et al., 2007; Mao et al., 2010).

Several types of biomaterials have been used as platforms for gene delivery, and in particular positively-charged polymers represent a high proportion. They can bind nucleic acids via electrostatic interactions to form particulate structures named polyplexes (Shen et al., 2017). Polyplexes are formed in solution by the direct mixing of two oppositely charged polyelectrolytes and the main driving force that guides polyplex formation is an increase in the entropy of the system due to the release of low-molecular weight counterions which is able to produce nanoparticles containing the nucleic acid payload in a compacted and protected structure (Lächelt and Wagner, 2015; Lounis et al., 2016). The easy manipulation and versatility of physicochemical properties are some of the most important advantages of polymeric gene carriers (Patil et al., 2005).

Cationic polymers that have been used for the delivery of miRNAs include polyethyleneimine (PEI), polyamidoamine (PAMAM) dendrimers and chitosan (Mao et al., 2010; Scholz and Wagner, 2012). Polymers derived from natural sources could be preferable in gene therapy applications because they are naturally biocompatible, biodegradable and nontoxic and can overcome the cytotoxicity associate with the use of several synthetic polymers which does not satisfy the requirements for clinical applications. However, cationic chitosan, one of the most studied polymers of the list, has its own drawbacks such as low water solubility at physiological pH because of partial protonation of primary amino groups which can affects nucleic acid interactions and stability of complexes in bloodstream (Gary et al., 2007; Ragelle et al., 2014). Thus, the design of biocompatible, stable and efficient nanocarriers is needed (Shi et al., 2017). In contrast to the large amount of synthetic non-viral gene delivery systems, there is only a small number of polycations of natural origin (Thanou et al., 2002).

Pullulan is a natural polysaccharide derived from *Aureobasidium pullulans* that consists of maltotriose units and due to its non-toxic, non-immunogenic and biodegradable properties, is considered as a promising material for biomedical applications (Sugumaran and Ponnusami, 2017). It is admitted safe in the United States for a wide range of applications, such as an excipient in pharmaceutical tablets and listed in the Japanese Standards as accepted adjuvant for drug delivery (Prajapati et al., 2013; Rekha and Sharma, 2009). Cationic pullulan derivatives grafted with primary or tertiary amine groups were previously demonstrated to be able to form complexes with plasmid DNA as well as siRNA in cationized pullulan-based hydrogels (San Juan et al., 2009, 2007). However, the ionic interaction between the macromolecules closely depend on the pH. Hydroxyl groups of pullulan can be easily substituted with quaternized ammonium groups (QA) to improve the interaction with negatively charged nucleic acids (San Juan et al., 2007; Shao et al., 2014). QA derivatives are an interesting strategy for gene therapy due to their permanent positive charges independent of the pH (Ahmed and Aljaeid, 2016). In this work, polycations have been obtained by grafting QA using glycidyltrimethylammonium chloride at different feeding ratios into the pullulan backbone. Then, QA-pullulan formulations were used to form nanosized polyplexes with miRNAs opening the way to their use as a platform for gene delivery.

2. Materials and methods

2.1. Materials

Pullulan (Mw 200 kg/mol) was purchased from Hayashibara Company (Okayama, Japan). Glycidyltrimethylammonium chloride (GTMAC) (Mw 151.63 g/mol) was purchased from Sigma-Aldrich (St. Louis, MO, USA). Dialysis membranes of 20 kDa was purchased from Spectrum Laboratories (New Brunswick, NJ, USA). Single-stranded miRNA and 6-Fluorescein AMidite (6-FAM)-miRNA scramble oligonucleotides with 23 bp of length (RNA sequence: 5′-UUA AUG CUA AUC GUG AUA GGG GU-3′) used to mimic the natural human mature microRNA miR-155-5p were purchased from Sigma-Aldrich (Saint Quentin Fallavier, France). Sequence was reconstituted in RNase-free water to achieve a final concentration of 20 μM and stock solutions were stored at −20 °C. Ultrapure water was prepared by ion-exchange of running tap water (Millipore, France).

2.2. Synthesis of cationized pullulan

2.2.1. Alkylation with GTMAC

Pullulan was synthetized based on a protocol previously described by San Juan et al. to graft primary and tertiary amine groups into pullulan backbone (San Juan et al., 2007). Briefly, pullulan (500 mg) was dissolved in 5 mL of an aqueous solution of 10 M NaOH. Then, the solution was placed at 4 °C under magnetic stirring until pullulan was completely solubilized. Glycidyltrimethylammonium chloride (GTMAC) was added to polysaccharide solution at different feeding ratios (1 eq = 3.1 mmol; 2 eq = 6.2 mmol, and 3 eq = 9.3 mmol) drop by drop and under high magnetic stirring at 4 °C. The solution was placed under magnetic stirring at 55 °C for 4 h. After cooling down to room temperature, the pH was adjusted to 7 with concentrated hydrochloric acid solution. The mixture was exhaustively dialyzed (MWCO of 20 kDa) for 48 h with ultrapure water and the derivatives were obtained as fluffy white materials after freeze-drying.

2.3. Chemical characterization of modified pullulan

2.3.1. Elemental analysis

Elemental analysis (C, H, N, O) was performed by the Microanalysis service of *Centre National de la Recherche Scientifique* (CNRS) (Gif/

Table 1
Characterization of pullulan and cationic pullulan derivatives.

Amine	Feeding[a]	M_n[b,c] (kDa)	M_w[b,c] (kDa)	PdI[b]	N[d] (%)	DS[e]
No amine (pullulan)	0	113	298	2.6	0	0
QA-pullulan	1	125	186	1.4	1.83 ± 0.25	0.3
	2	240	270	1.1	2.75 ± 0.34	0.4
	3	275	320	1.2	3.27 ± 0.04	0.5

[a] Feeding: $mol_{amine}/mol_{hydroxyl\ groups}$.
[b] Measured by SEC-MALLS.
[c] SD ± 5–10%.
[d] From nitrogen elemental analysis.
[e] Degree of substitution of QA-pullulan calculated per anydroglucose unit.

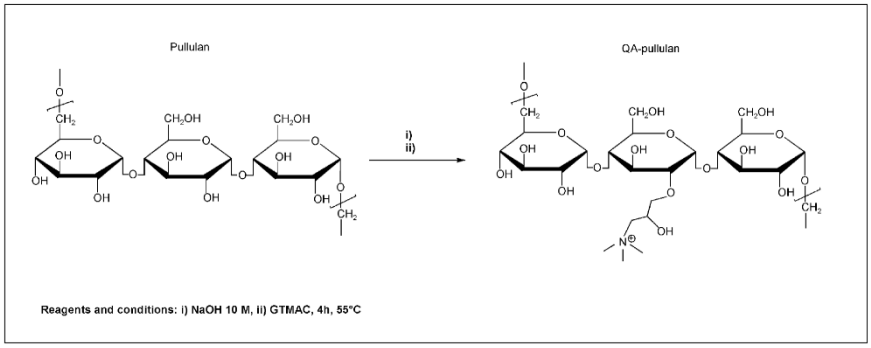

Fig. 1. Schematic representation of synthesis route for alkylation of pullulan using glycidyltrimethylammonium chloride (GTMAC).

Yvette, France) (Table 1 and Table A.1). Degree of substitution was estimated using N content values.

2.3.2. Molecular weight determination

Weight-average molecular weight (Mw) and number-average molecular weight (Mn) were determined by size exclusion chromatography (SEC) coupled to a multiangle laser light scattering (MALLS) detector (DAWN-F, Wyatt Technology, Santa Barbara, CA, USA). The SEC line consisted of a TSK-Gel PWXL Guardcolumn and TSK-Gel GMPWXL in series (Tosoh Bioscience, Stuttgart, Germany). The eluent was 0.2 M $NaNO_3$ containing 0.02% (w/v) NaN_3 at 0.5 mL/min flow rate. The samples were dissolved in the eluent at a concentration of 10 mg/mL. The dn/dc value used for the molecular weight distribution calculations was 0.14. The collected data were analyzed using the software Astra V-6.1.2 (Santa Barbara, CA).

2.3.3. FTIR spectroscopy

FTIR spectroscopy was carried out with KBr pellets on a Thermo-Nicolet-AVATAR 370 FTIR (Thermo Electron Corporation, Waltham, MA). A first pellet with 200 mg of KBr was prepared. Then, pellets were made using 200 mg KBr and 2 mg of polymer. A 32-scan interferogram was collected in transmittance mode. Scans were taken from 400 cm^{-1} to 4000 cm^{-1} at a resolution of 2 cm^{-1}. The spectrum of KBr pellet was used as background.

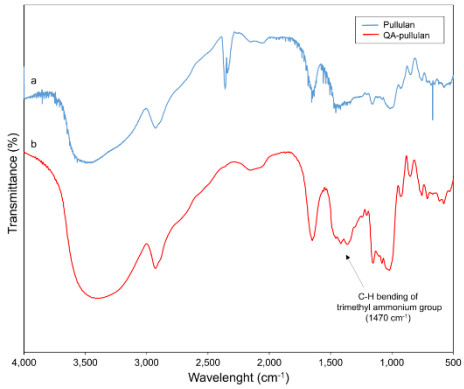

Fig. 2. FTIR spectra of **(a)** non-modified pullulan and **(b)** QA-pullulan.

2.3.4. NMR spectroscopy

^1H NMR spectra was recorded with a Bruker-400 Ultrashield (Bruker, Germany) operating at 400 MHz. Polymers samples were prepared in D_2O at a concentration of 20 mg/mL.

2.4. Synthesis of QA-pullulan/miRNA polyplexes

Briefly, cationic pullulan and anionic miRNA were dissolved in ultrapure water to obtain stock solutions at 0.08 mg/mL and 0.04 mg/mL, respectively. All polysaccharide solutions were filtered before use (0.2 µm). Nanosized polyplexes were produced by dropping 1 mL of miRNA solution over 1 mL of quaternized pullulan solution under high magnetic stirring at room temperature in aqueous solution. Samples were placed at 4 °C during 20 min for stabilization before use.

2.5. Characterization of QA-pullulan/miRNA polyplexes

2.5.1. Size and zeta potential measurements

Particle size and zeta potential of polyplexes were measured by Dynamic Light Scattering (DLS) and Electrophoretic Light Scattering (ELS) using a Zetasizer Nano-ZS (Malvern Instruments, Malvern, UK) respectively. Size and zeta potential measurements were performed at 25 °C using a 173° and 13° scattering angle for size and zeta potential measurements, respectively, equipped with a 4 mW HeNe laser beam with a wavelength of 633 nm. Size and ζ potential values were automatically calculated through the software DTS Nano v.6.30 (Malvern, UK) using the Stokes-Einstein equation and the Henry equation with the Smoluchowski approximation, respectively. Size measurements were performed in water using disposable polystyrene cuvettes and zeta potential measurements were performed in 1 mM KCl solution using a DTS1070-folded capillary cell (ELS, Malvern, UK). Data were acquired in triplicate.

2.5.2. Morphology

The morphology of optimized polyplexes was assessed using a Transmission Electron Microscope (TEM) Tecnai 12 (80 kV; FEI; Hillsboro, OR, USA) with a 1 K × 1 K KeenView camera (OSiS). Nanosized polyplexes were produced as previously described. Then, 3 µL of polyplexes suspension was placed onto a 400 µL mesh copper grid coated with carbon (EMS) without any sample dilution. Uranyl acetate 1% (w/v) was used for negative staining. TEM pictures was performed at the platform ImagoSeine of the Institute Jacques Monod (Paris, France).

2.5.3. miRNA presence into polyplexes

The presence of the miRNA was monitored by agarose gel

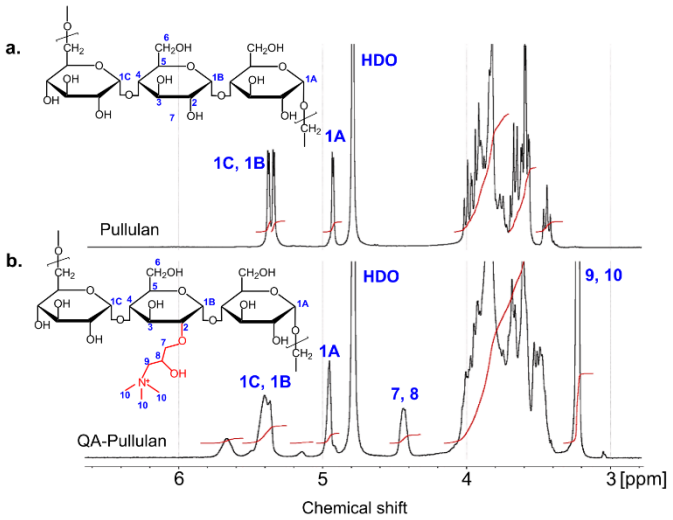

Fig. 3. ^{1}H NMR spectra at 400 Mhz of **(a)** non-modified pullulan and **(b)** QA-pullulan in D_2O. 1A, 1B, 1C signals depicted anomeric H from maltotriose base unit of pullulan. Numbers 2–6 corresponded to H on anydroglucose unit. H from GTMAC **(b)** were depicted with numbers from 7 to 10.

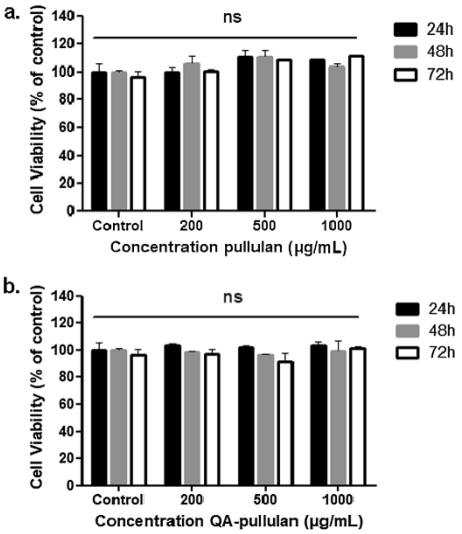

Fig. 4. Cytocompatibility of **(a)** non-modified pullulan and **(b)** QA-pullulan towards HUVECs at 200, 500 and 1000 µg/mL after 24, 48 and 72 h of incubation. Results are shown as mean ± SD from 3 independent experiments with no statistical differences detected using the Wilcoxon matched-pairs signed rank test.

electrophoresis (AGE) and UV spectrophotometry after miRNA desorption. Agarose gel electrophoresis was perfomed using 5% agarose gels containing ethidium bromide in TBE (Tris-Borate-EDTA, Thermo Fisher Scientific, Vilnius, Lithuania) buffer. An Ultra-Low Range GeneRuler DNA Ladder (10–300 bp; Thermo Fisher Scientific, Bleiswijk, Netherlands) was used to monitor miRNA presence. Samples included solution of free polymer (QA-pullulan), plus additional controls from different steps of the miRNA loading: miRNA alone (at the concentration used for loading), QA-pullulan polysaccharide solution and QA-pullulan/miRNA polyplexes. Samples were run by electrophoresis (50 V, 120 min) and detected through a UV transilluminator (Vilber Lourmat smart imaging system, Collegien, France). Additional miRNA quantification was performed by UV spectrophotometry using NanoDrop™ 2000/2000c Spectrophotometer (Thermo Fisher Scientific, Wilmington, DE, USA).

2.5.4. Stability of QA-pullulan/miRNA polyplexes

The stability of complexes was evaluated over time while stored at 4 °C in aqueous media. Size and PdI (Polydispersity Index) evolutions of polyplexes suspensions were monitored by DLS (n = 3) at each time point (0 h, 6 h, 12 h, 18 h, 24 h).

2.5.5. Cytotoxicity of QA-pullulan and QA-pullulan/miRNA polyplexes

Cytotoxicity was evaluated in Human Umbilical Vein Endothelial Cells (HUVECs, ATCC CRL-1730, Manassas, VA, USA) by resazurin conversion assay (Sigma-Aldrich, Saint Louis, MO, USA). Cells were seeded at a concentration of 10,000 cells/well onto 96-well plates in Dulbecco's Modified Eagle Medium (DMEM) (Thermo Fisher Scientific, Carlsbad, CA, USA) supplemented with 10% (v/v) of fetal bovine serum, 1% (v/v) of penicillin and 1% (v/v) of streptomycin in a humidified atmosphere with 5% CO_2 at 37 °C. At a subconfluent to confluent stage, cells were detached with 0.05% trypsin/EDTA (Gibco) and re-seeded until the required number of cells for the subsequent experiments was obtained. Cell metabolic activity was assessed after different culture conditions by resazurin conversion. Cells were incubated with medium containing 10% resazurin for 2 h at 37 °C. Fluorescence intensity (530 nm/590 nm) of the cell culture supernatants was measured with an Infinite® 200 PRO microplate reader (TECAN Group Ltd., Männedorf, Switzerland). A blank control comprising only medium was also included. Bright field images (EVOS™ XL

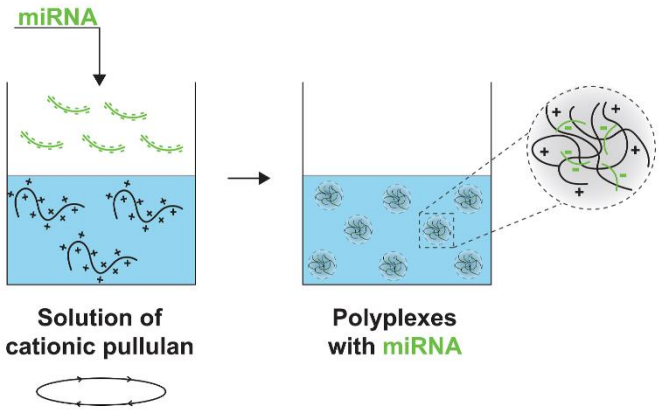

Fig. 5. Schematic representation of preparation of QA-pullulan/miRNA polyplexes by electrostatic interactions.

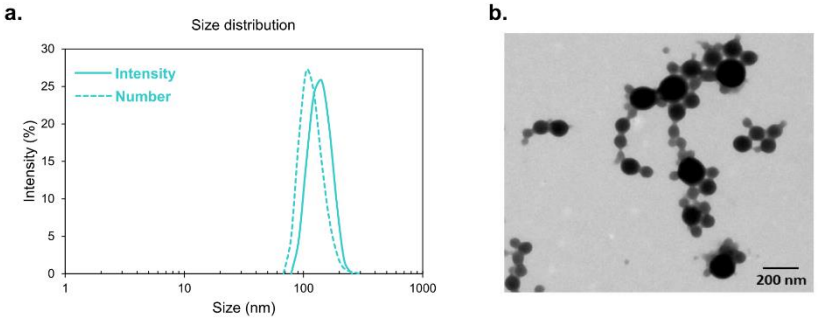

c.

Size (nm)	PdI	Attenuator	Count rate (kcps)	ζ potential (mV)
133 ± 30	0.07 ± 0.04	7	178	-12 ± 5

Fig. 6. Physico-chemical characterization of QA-pullulan/miRNA polyplexes: **(a)** Size distribution from Light Scattering (LS) expressed by intensity and number percentages; **(b)** Morphology of polyplexes obtained by TEM microscopy; **(c)** Size (nm), PdI, attenuator and count rate values measured by LS and zeta potential (mV) measured by Doppler laser electrophoresis. Results are shown as mean ± standard deviation of 3 different samples.

Core Cell Imaging System, Thermo Fisher Scientific, Carlsbad, CA, USA) were taken during culture to monitor cell morphology.

2.5.6. miRNA delivery

Human Umbilical Vein Endothelial Cells (HUVECs, ATCC CRL-1730, Manassas, VA, USA) cells were seeded at a concentration of 8,000 cells/well onto Nunc™ Lab-Tek™ chamber slides (Thermo Fisher Scientific) and grown for 48 h. Polyplexes of QA-pullulan and scramble FAM-miRNA were prepared as previously described on the same day of treatment and incubated for 20 min at 4 °C before adding to the cells. After 30 min of incubation using serum-free supplemented cell culture medium, cells were washed with PBS and fixed with fresh 4% paraformaldehyde. Cell nucleus was stained with 4′,6-DiAmidino-2-PhenylIndole (DAPI) (Sigma Aldrich, St. Louis, MO, USA). Coverslips were mounted using Ibidi Mounting Medium (IMM) for fluorescence microscopy (ibidi GmbH, Germany). Fluorescence images were taken to evaluate miRNA delivery (Axiovert Observer Z1 inverted microscope, Zeiss, Germany).

2.6. Statistical analysis

The data were expressed as mean ± SD (standard deviation). Statistical analysis was performed using GraphPad Prism (version: 5.0a, San Diego, CA, USA). Since data followed a non-parametric distribution, Wilcoxon matched-pairs test was performed to compare each paired group and p smaller than 0.05 was considered to be statistically significant.

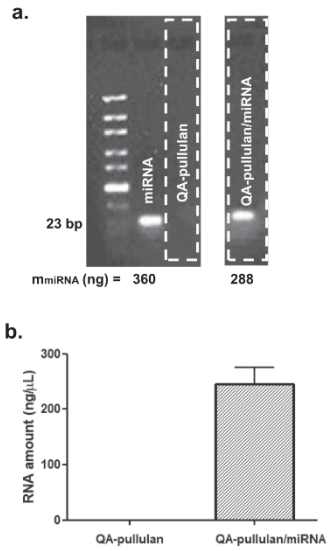

Fig. 7. (a) miRNA presence onto polyplexes after miRNA desorption confirmed by agarose gel electrophoresis using an Ultra-Low Range GeneRuler DNA Ladder (10–300 bp) as control and RNA amount (ng) quantified by the intensity of the band when compared to miRNA alone (0.04 mg/mL, 9 μL) using ImageJ software; **(b)** RNA amount (ng/μL) quantified by UV absorbance (n = 3).

3. Results and discussion

3.1. Chemical modification of pullulan and characterization

Pullulan was grafted with glycidyltrimethylammonium chloride to provide QA-pullulan (Fig. 1) with molar feeding ratios of 1, 2 and 3. Cationic derivatives were characterized to confirm the success of incorporation of trimethylammonium groups into the pullulan backbone. Nitrogen elemental analysis confirmed the substitution reaction with N content ranging from 1.8 to 3.3% (w/w) corresponding to 1.3 to 2.3 mmol of QA groups per g of polymer. SEC-MALLS analysis evidenced monomodal molecular weight distributions (PdI ranging from 1.1 to 1.4) (Table 1 and Table A.1).

The extent of the derivatisation reaction was given by the degree of substitution (DS) defined as the number of substituted hydroxyls groups per AGU (AnhydroGlucose Unit) (Cumpstey, 2013). DS can be calculated using N content from elemental analysis results. Derivatives with a degree of substitution in QA groups around 0.3–0.5 were obtained in one step and in a shorter time (4 h) compared to others conditions used to obtain quaternized polymers with reaction time of 8, 14 and 24 h (Dionísio et al., 2016; Liu et al., 2015; Stefan et al., 2016). Moreover, the protocol of Liu et al. performed in 8 h used a mixture of water and isopropanol as reaction medium, in contrast to our protocol performed only in water without organic solvent (Liu et al., 2015).

IR spectra of pullulan and its cationic derivative presented the general pattern characteristic of polysaccharides (Stuart, 2004). The substitution with QA groups was confirmed by a signal at 1470 cm^{-1} (Fig. 2) due to C-H scissoring in methyl groups (Li et al., 2016; Stefan et al., 2016). This was further confirmed by ^{1}H NMR spectra (Fig. 3) with signals at 3.2 ppm and 4.4 ppm (Dionísio et al., 2016; Stefan et al., 2016).

Highly charged cationic polymers can have non-specific interactions with polyanionic biomolecules in the bloodstream leading to the inhibition of many crucial cellular processes and causing severe inflammatory reactions (Rekha and Sharma, 2009; Shi et al., 2017). When compared to non-modified pullulan, cationic pullulan did not show toxicity up to 72 h of incubation with increasing concentrations of QA-pullulan until 1000 μg/mL (Fig. 4) and supports results of literature that pullulan modified with glycidyltrimethylammonium chloride is a non-toxic polymer (Stefan et al., 2016).

3.2. Synthesis and characterization of QA-pullulan/miRNA polyplexes

Polyplexes were prepared by mixing miRNA and QA-pullulan at different concentrations under strong magnetic stirring (Fig. 5). They were incubated at 4 °C for 20 min for stabilization of complexes before use. Once QA-pullulan modified with only 1.83% of N showed to be able to form complexes with miRNA by electrostatic interactions, this derivative was selected for all further optimizations. To optimize the production of stable polyplexes, a fixed concentration of miRNA of 5 nmol (0.04 mg/mL) was selected based on previous works performed by Antunes et al. 2019 (Antunes et al., 2019). Different N/P ratios (0.5–15) were tested by increasing the concentration of QA-pullulan. All physicochemical characterizations are summarized in Fig. 6. Samples were characterized by DLS/ELS regarding size, PdI and zeta potential values (Fig. 6C). Complexes were formed at an optimized N/P molar ratio of 0.8 producing polyplexes in the nanosized range with a diameter around 130 ± 30 nm and narrow distribution as shown by the polydispersity index (0.07 ± 0.04). More negative zeta potential values of QA-pullulan/miRNA polyplexes (−12 ± 5 mV) as compared to zeta potential of cationic pullulan solution alone (31 ± 6 mV), suggested the presence of additional negative charges at the surface due to miRNA presence in the complex. The morphology of complexes was characterized by TEM (Fig. 6B) evidencing the formation of homogeneous spherical particles. The observed sizes were well-correlated

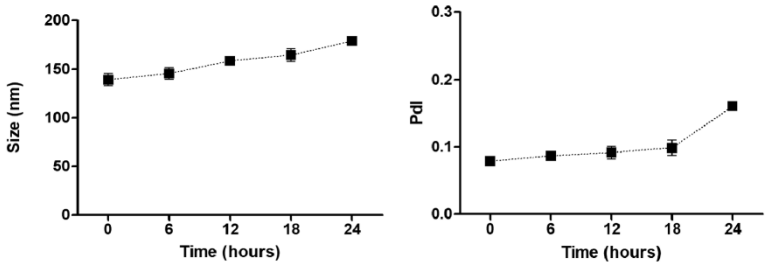

Fig. 8. Stability of QA-pullulan/miRNA polyplexes evaluated by size (left) and PdI (right) measured by Light Scattering as function of time of incubation in water at 4 °C (mean ± SD, n = 3).

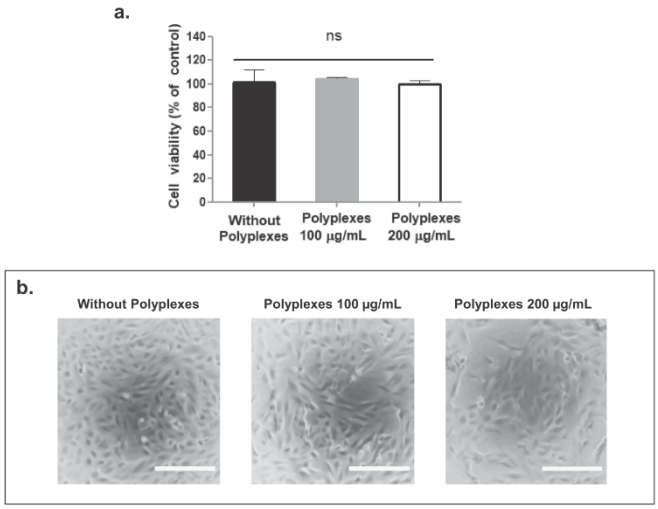

Fig. 9. (a) Cytocompatibility of complexes towards HUVECs exposed to increasing concentrations of QA-pullulan/miRNA polyplexes measured by resazurin conversion after 1 day of incubation. Results are shown as mean ± SD from 3 independent experiments with no statistical differences detected using the Wilcoxon matched-pairs signed rank test. **(b)** Optical images of confluent cells without polyplexes and with 100 µg/mL and 200 µg/mL of polyplexes. Scale bar corresponds to 200 µm.

with those determined by DLS. miRNA presence was confirmed by agarose gel electrophoresis by the presence of a band in the expected region of 23 bp after miRNA desorption from QA-pullulan (Fig. 7A). miRNA was quantified using the software ImageJ by the intensity of the band of polyplexes in the agarose gel normalized by the control naked miRNA and the loading efficiency was around 80%. There was no miRNA degradation or fragmentation after loading as suggested by the absence of smeared bands in AGE indicating that QA-pullulan could effectively protected miRNA. Further miRNA quantification by UV spectrophotometry (Fig. 7B) displayed a similar trend as in AGE results.

The N/P ratio, which corresponds to the ratio between QA groups of pullulan derivatives to the phosphate groups of nucleic acid, plays an important role in the capacity of complexation, particle diameter, stability and cytotoxicity of carriers (Tekie et al., 2015; Vauthier et al., 2013; Zhao et al., 2009). Generally, polyplexes can be formed between polycations and nucleic acids at relatively low N/P ratios (Shao et al., 2014). In our case, this optimum was found at N/P of 0.8. Furthermore, it was described that an increase in the average molecular weight (Mn) of polymer dramatically improved oligonucleotides encapsulation at low N/P ratios (Ahmed and Aljaeid, 2016; de Paula Pansani Oliveira et al., 2013; Vauthier et al., 2013). In a study of Liu and co-workers chitosan with chains having 5 to 10 times the length of siRNA (i.e. with a molecular weight ranging from 65 to 170 kDa) were most suitable to form stable complexes (Liu et al., 2007). Further studies could investigate the effect of the molecular weight of pullulan and its consequence in terms of both physicochemical characteristics of the polyplexes and *in vivo* biodistribution/biodegradation.

Stability of complexes in aqueous media was evaluated here under storage at 4 °C over 1 day without forming aggregates (Fig. 8). In addition, it is noteworthy that our method of complex formation was developed without the use of any chemical crosslinking agent.

The increase of the ionic strength has a significant impact on colloidal stability with aggregate formation, and higher PdI values correlated with the heterogeneity of complexes in this medium. Alameh et al. described that the colloidal instability in 150 mM NaCl increased with the increase of molecular weight when comparing chitosan with low (10 kDa) and high (120 kDa) Mn (Alameh et al., 2018). Keeping a good stability in physiological conditions is one of the major challenges when designing vectors intended for intravenous administration (Ragelle et al., 2014). To achieve this goal, several strategies were thought to overcome this limitation and improve stability in biological fluids (Mao et al., 2010). A classical strategy uses cross-linkers such as sodium tripolyphosphate (TPP) for the preparation of chitosan NPs with nucleic acids (Karimi et al., 2013; Wang et al., 2015). However, TPP is a chemical agent with limited sites of interaction for ionotropic gelation (Avadi et al., 2010). Hence, the colloidal stability of polyplexes nanosystems in physiological conditions was far from being fully addressed in the previous investigations (Wu and Delair, 2015).

To assess if the developed polyplexes could be used in biomedical applications, namely as vectors for gene therapy, the cytocompatibility towards HUVECs was evaluated here through an *in vitro* toxicological assay based on resazurin conversion. *In vitro* tests did not evidence any toxic effect of the QA-pullulan/miRNA complexes after 1 day of incubation up to the maximum tested dose of 200 µg/mL of polyplexes (n = 3) (Fig. 9A). We did not observe any alteration in cell morphology (Fig. 9B). This important result is a key aspect to further investigate the potential use of the new biocompatible systems.

Finally, a comparative study of free miRNA, neutral pullulan/miRNA and polyplexes of QA-pullulan/miRNA, was done using a fluorescently labeled miRNA to evaluate their cellular uptake. As it can be seen from Fig. 10B and 10C, no miRNA could be detected inside cells in case of administration of free miRNA or unmodified pullulan and miRNA indicating that free miRNA could hardly be internalized by cells. miRNA from polyplexes, in contrast, was clearly incorporated by cells (Fig. 10D) by forming complexes with QA-pullulan that is able to promote their internalization usually via endocytic pathways being 150 nm the accepted size limit for cellular uptake by non-specific endocytosis (Ganas et al., 2014; Gary et al., 2007; Goyal et al., 2018).

4. Conclusions

This work demonstrated that nanosized polyplexes are formed and are stable in aqueous medium by simply mixing miRNA with pullulan substituted with quaternized ammonium groups. Such pullulan derivatives have been previously used by André and co-workers to modify the surface of nanoparticles based on sorbitan monooleate (Span® 80) in

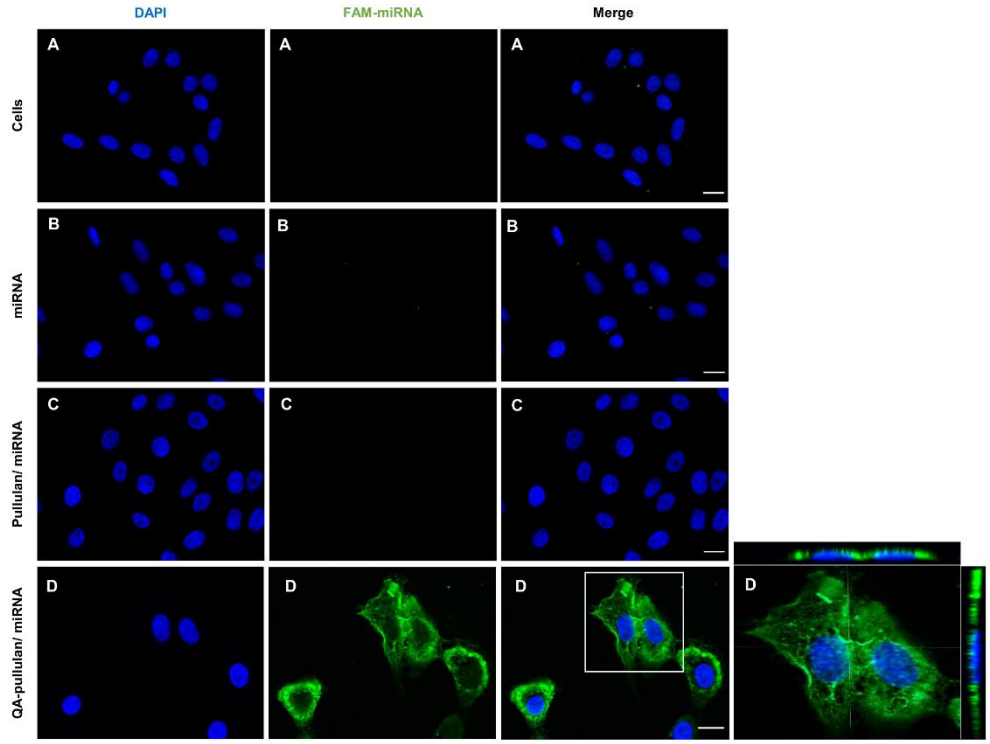

Fig. 10. Fluorescence microscopy images of HUVECs evidencing miRNA delivery. Left column: cells' nuclei stained with DAPI (depicted in blue); middle column: FAM labelled miRNA (depicted in green); right column: merged images. **(A)** Without treatment, **(B)** cells treated with FAM-labelled miRNA, **(C)** cells treated with FAM-labelled miRNA in presence of unmodified pullulan; **(D)** cells treated with polyplexes formed by FAM-labelled miRNA and QA-pullulan including Z-stack-assembled fluorescence images (zoom). Treatments were performed for 30 min at 37 °C. Scale bar: 20 μm. (For interpretation of the references to colour in this figure legend, the reader is referred to the web version of this article.)

order to increase the interaction of this system with siRNA for cellular therapy (André et al., 2016). To the best of our knowledge, cationized pullulan have been used for the first time to build miRNA delivery nanosystems. The obtained nanoparticles proved to be non-cytotoxic on HUVECs cells after 1 day incubation. Neither toxic reagent nor organic solvent were used. With further experiments proving the efficacy of the systems *in vivo*, we expect to contribute for the development of new safe pullulan-based delivery systems for miRNA therapeutics.

Funding

This work was supported by INSERM, Université de Paris and Université Paris 13. The PhD fellowship was funded by CONSELHO NACIONAL DE DESENVOLVIMENTO CIENTÍFICO E TECNOLÓGICO (CNPq) from Brazil grant number 201245/2017-5.

CRediT authorship contribution statement

Fernanda C. Moraes: Conceptualization, Methodology, Validation, Formal analysis, Investigation, Writing - original draft, Writing - review & editing, Visualization. **Joana C. Antunes:** Conceptualization, Investigation, Writing - review & editing, Visualization, Supervision. **Laura Marcela Forero Ramirez:** Conceptualization, Methodology, Investigation. **Paola Aprile:** Methodology, Investigation. **Gregory Franck:** Methodology, Investigation. **Cédric Chauvierre:** Conceptualization, Resources, Writing - review & editing, Visualization, Supervision, Funding acquisition. **Frédéric Chaubet:** Conceptualization, Resources, Writing - review & editing, Visualization, Supervision, Project administration, Funding acquisition. **Didier Letourneur:** Conceptualization, Resources, Writing - review & editing, Visualization, Supervision, Project administration, Funding acquisition.

Declaration of Competing Interest

The authors declare that they have no known competing financial interests or personal relationships that could have appeared to influence the work reported in this paper.

Acknowledgments

The authors are grateful to PhD fellowship for Fernanda C. Moraes from the *Conselho Nacional de Desenvolvimento Científico e Tecnológico* (CNPq) from Brazil grant number 201245/2017-5. Thanks also to Camille Le Guilcher and Soraya Lanouar for assistance in data analysis.

Appendix

See Table A1

Table A1
Elemental analysis of pullulan and cationic pullulan derivatives.

Amine	Feeding[a]	N (%)	C (%)	H (%)	O (%)
No amine (pullulan)	0	Absence	41.92 ± 0.06	6.35 ± 0.01	51.88 ± 011
QA-pullulan	1	1.83 ± 0.25	42.52 ± 0.34	7.09 ± 0.06	46.99 ± 0.55
	2	2.75 ± 0.34	41.88 ± 0.43	7.27 ± 0.19	44.04 ± 0.91
	3	3.27 ± 0.04	43.40 ± 0.14	7.49 ± 0.09	43.26 ± 0.07

[a] Feeding: $mol_{amine}/mol_{hydroxyl\ groups}$.

References

Ahmed, T., Aljaeid, B., 2016. Preparation, characterization, and potential application of chitosan, chitosan derivatives, and chitosan metal nanoparticles in pharmaceutical drug delivery. Drug Des. Devel. Ther. 483. https://doi.org/10.2147/DDDT.S99651.

Alameh, M., Lavertu, M., Tran-Khanh, N., Chang, C.-Y., Lesage, F., Bail, M., Darras, V., Chevrier, A., Buschmann, M.D., 2018. siRNA Delivery with Chitosan: Influence of Chitosan Molecular Weight, Degree of Deacetylation, and Amine to Phosphate Ratio on in Vitro Silencing Efficiency, Hemocompatibility, Biodistribution, and in Vivo Efficacy. Biomacromolecules 19, 112–131. https://doi.org/10.1021/acs.biomac.7b01297.

André, E.M., Pensado, A., Resnier, P., Braz, L., Rosa da Costa, A.M., Passirani, C., Sanchez, A., Montero-Menei, C.N., 2016. Characterization and comparison of two novel nanosystems associated with siRNA for cellular therapy. Int. J. Pharm. 497, 255–267. https://doi.org/10.1016/j.ijpharm.2015.11.020.

Antunes, J.C., Benarroch, L., Moraes, F.C., Juenet, M., Gross, M.-S., Aubart, M., Boileau, C., Caligiuri, G., Nicoletti, A., Ollivier, V., Chaubet, F., Letourneur, D., Chauvierre, C., 2019. Core-shell polymer-based nanoparticles to deliver MiR-155-5p to endothelial cells. Mol. Ther. - Nucleic Acids S2162253119301465. https://doi.org/10.1016/j.omtn.2019.05.016.

Avadi, M.R., Sadeghi, A.M.M., Mohammadpour, N., Abedin, S., Atyabi, F., Dinarvand, R., Rafiee-Tehrani, M., 2010. Preparation and characterization of insulin nanoparticles using chitosan and Arabic gum with ionic gelation method. Nanomedicine Nanotechnol. Biol. Med. 6, 58–63. https://doi.org/10.1016/j.nano.2009.04.007.

Bernardo, B.C., Ooi, J.Y., Lin, R.C., McMullen, J.R., 2015. miRNA therapeutics: a new class of drugs with potential therapeutic applications in the heart. Future Med. Chem. 7, 1771–1792. https://doi.org/10.4155/fmc.15.107.

Candido, S., Lupo, G., Pennisi, M., Basile, M., Anfuso, C., Petralia, M., Gattuso, G., Vivarelli, S., Spandidos, D., Libra, M., Falzone, L., 2019. The analysis of miRNA expression profiling datasets reveals inverse microRNA patterns in glioblastoma and Alzheimer's disease. Oncol. Rep. https://doi.org/10.3892/or.2019.7215.

Cao, Y., Tan, Y.F., Wong, Y.S., Liew, M.W.J., Venkatraman, S., 2019. Recent advances in chitosan-based carriers for gene delivery. Mar. Drugs 17, 381. https://doi.org/10.3390/md17060381.

Chakraborty, C., Sharma, A.R., Sharma, G., Doss, C.G.P., Lee, S.-S., 2017. Therapeutic miRNA and siRNA: moving from bench to clinic as next generation medicine. Mol. Ther. - Nucleic Acids 8, 132–143. https://doi.org/10.1016/j.omtn.2017.06.005.

Cumpstey, I., 2013. Chemical modification of polysaccharides. ISRN Org. Chem. 2013, 1–27. https://doi.org/10.1155/2013/417672.

de Paula Pansani Oliveira, F., Picola, I.P.D., Shi, Q., Barbosa, H.F.G., de Oliveira Tiera, V. A., Fernandes, J.C., Tiera, M.J., 2013. Synthesis and evaluation of diethylethylamine–chitosan for gene delivery: composition effects on the in vitro transfection efficiency. Nanotechnology 24, 055101. https://doi.org/10.1088/0957-4484/24/5/055101.

Devaux, Y., Stammet, P., Friberg, H., Hassager, C., Kuiper, M.A., Wise, M.P., Nielsen, N., for the Biomarker subcommittee of the TTM trial (Target Temperature Management After Cardiac Arrest, NCT01020916), 2015. MicroRNAs: new biomarkers and therapeutic targets after cardiac arrest? Crit. Care 19, 54. https://doi.org/10.1186/s13054-015-0767-2.

Dionísio, M., Braz, L., Corvo, M., Lourenço, J.P., Grenha, A., Rosa da Costa, A.M., 2016. Charged pullulan derivatives for the development of nanocarriers by polyelectrolyte complexation. Int. J. Biol. Macromol. 86, 129–138. https://doi.org/10.1016/j.ijbiomac.2016.01.054.

Falzone, Lupo, Rosa, Crimi, Anfuso, Salemi, Rapisarda, Libra, Candido, 2019. Identification of Novel MicroRNAs and Their Diagnostic and Prognostic Significance in Oral Cancer. Cancers 11, 610. https://doi.org/10.3390/cancers11050610.

Ganas, C., Weiß, A., Nazarenus, M., Rösler, S., Kissel, T., Rivera_Gil, P., Parak, W.J., 2014. Biodegradable capsules as non-viral vectors for in vitro delivery of PEI/siRNA polyplexes for efficient gene silencing. J. Controlled Release 196, 132–138. https://doi.org/10.1016/j.jconrel.2014.10.006.

Gary, D.J., Puri, N., Won, Y.-Y., 2007. Polymer-based siRNA delivery: Perspectives on the fundamental and phenomenological distinctions from polymer-based DNA delivery. J. Controlled Release 121, 64–73. https://doi.org/10.1016/j.jconrel.2007.05.021.

Gaur, S., Wen, Y., Song, J.H., Parikh, N.U., Mangala, L.S., Blessing, A.M., Ivan, C., Wu, S. Y., Varkaris, A., Shi, Y., Lopez-Berestein, G., Frigo, D.E., Sood, A.K., Gallick, G.E., 2015. Chitosan nanoparticle-mediated delivery of miRNA-34a decreases prostate tumor growth in the bone and its expression induces non-canonical autophagy. Oncotarget 6. https://doi.org/10.18632/oncotarget.4971.

Goyal, R., Kapadia, C.H., Melamed, J.R., Riley, R.S., Day, E.S., 2018. Layer-by-layer assembled gold nanoshells for the intracellular delivery of miR-34a. Cell. Mol. Bioeng. 11, 383–396. https://doi.org/10.1007/s12195-018-0535-x.

Hou, W., Tian, Q., Steuerwald, N.M., Schrum, L.W., Bonkovsky, H.L., 2012. The let-7 microRNA enhances heme oxygenase-1 by suppressing Bach1 and attenuates oxidant injury in human hepatocytes. Biochim. Biophys. Acta BBA – Gene Regul. Mech. 1819, 1113–1122. https://doi.org/10.1016/j.bbagrm.2012.06.001.

Karimi, M., Avci, P., Ahi, M., Gazori, T., Hamblin, M.R., Naderi-Manesh, H., 2013. Evaluation of chitosan-tripolyphosphate nanoparticles as a p-shRNA delivery vector: formulation, optimization and cellular uptake study. J. Nanopharmaceutics Drug Deliv. 1, 266–278. https://doi.org/10.1166/jnd.2013.1027.

Sugumaran K.R., Ponnusami V., 2017. Review on production, downstream processing and characterization of microbial pullulan. Carbohydr. Polym. 173, 573–591. https://doi.org/10.1016/j.carbpol.2017.06.022.

Lächelt, U., Wagner, E., 2015. Nucleic acid therapeutics using polyplexes: a journey of 50 years (and Beyond). Chem. Rev. 115, 11043–11078. https://doi.org/10.1021/cr5006793.

Li, Q., Tan, W., Zhang, C., Gu, G., Guo, Z., 2016. Synthesis of water soluble chitosan derivatives with halogeno-1,2,3-triazole and their antifungal activity. Int. J. Biol. Macromol. 91, 623–629. https://doi.org/10.1016/j.ijbiomac.2016.06.006.

Liu, P., Meng, W., Wang, S., Sun, Y., Aqeel Ashraf, M., 2015. Quaternary ammonium salt of chitosan: preparation and antimicrobial property for paper. Open Med. 10. https://doi.org/10.1515/med-2015-0081.

Liu, X., Howard, K.A., Dong, M., Andersen, M.Ø., Rahbek, U.L., Johnsen, M.G., Hansen, O.C., Besenbacher, F., Kjems, J., 2007. The influence of polymeric properties on chitosan/siRNA nanoparticle formulation and gene silencing. Biomaterials 28, 1280–1288. https://doi.org/10.1016/j.biomaterials.2006.11.004.

Lounis, F.M., Chamieh, J., Gonzalez, P., Cottet, H., Leclercq, L., 2016. Prediction of polyelectrolyte complex stoichiometry for highly hydrophilic polyelectrolytes. Macromolecules 49, 3881–3888. https://doi.org/10.1021/acs.macromol.6b00463.

Mao, S., Sun, W., Kissel, T., 2010. Chitosan-based formulations for delivery of DNA and siRNA. Adv. Drug Deliv. Rev. 62, 12–27. https://doi.org/10.1016/j.addr.2009.08.004.

Nuhn, L., Tomcin, S., Miyata, K., Mailänder, V., Landfester, K., Kataoka, K., Zentel, R., 2014. Size-dependent knockdown potential of siRNA-loaded cationic nanohydrogel particles. Biomacromolecules 15, 4111–4121. https://doi.org/10.1021/bm501148y.

Patil, S.D., Rhodes, D.G., Burgess, D.J., 2005. DNA-based therapeutics and DNA delivery systems: a comprehensive review. AAPS J. 7, E61–E77. https://doi.org/10.1208/aapsj070109.

Poddar, S., Kesharwani, D., Datta, M., 2019. miR-449a regulates insulin signalling by targeting the Notch ligand, Jag1 in skeletal muscle cells. Cell Commun. Signal. 17. https://doi.org/10.1186/s12964-019-0394-7.

Prajapati, V.D., Jani, G.K., Khanda, S.M., 2013. Pullulan: An exopolysaccharide and its various applications. Carbohydr. Polym. 95, 540–549. https://doi.org/10.1016/j.carbpol.2013.02.082.

Qiagen, 2018. Guidelines for miRNA mimic and miRNA inhibitor experiments. https://www.qiagen.com/fr/resources/resourcedetail?id=3e1477ad-74a2-4ee6-9c31-54b1997f2941&lang=en.

Ragelle, H., Riva, R., Vandermeulen, G., Naeye, B., Pourcelle, V., Le Duff, C.S., D'Haese, C., Nysten, B., Braeckmans, K., De Smedt, S.C., Jérôme, C., Préat, V., 2014. Chitosan nanoparticles for siRNA delivery: Optimizing formulation to increase stability and efficiency. J. Controlled Release 176, 54–63. https://doi.org/10.1016/j.jconrel.2013.12.026.

Rekha, M.R., Sharma, C.P., 2009. Blood compatibility and in vitro transfection studies on cationically modified pullulan for liver cell targeted gene delivery. Biomaterials 30, 6655–6664. https://doi.org/10.1016/j.biomaterials.2009.08.029.

Rupaimoole, R., Slack, F.J., 2017. MicroRNA therapeutics: towards a new era for the management of cancer and other diseases. Nat. Rev. Drug Discov. 16, 203–222. https://doi.org/10.1038/nrd.2016.246.

San Juan, A., Bala, M., Hlawaty, H., Portes, P., Vranckx, R., Feldman, L.J., Letourneur, D., 2009. Development of a functionalized polymer for stent coating in the arterial delivery of small interfering RNA. Biomacromolecules 10, 3074–3080. https://doi.org/10.1021/bm900740g.

San Juan, A., Ducrocq, G., Hlawaty, H., Bataille, I., Guénin, E., Letourneur, D., Feldman, L.J., 2007. Tubular cationized pullulan hydrogels as local reservoirs for plasmid DNA. J. Biomed. Mater. Res. A 83A, 819–827. https://doi.org/10.1002/jbm.a.31413.
Scholz, C., Wagner, E., 2012. Therapeutic plasmid DNA versus siRNA delivery: common and different tasks for synthetic carriers. J. Controlled Release 161, 554–565. https://doi.org/10.1016/j.jconrel.2011.11.014.
Shao, Z., Xu, T., Wang, S., Liu, W., 2014. Elucidating the role of free polycationic chains in polycation gene carriers by free chains of polyethylenimine or N, N, N-trimethyl chitosan plus a certain polyplex. Int. J. Nanomedicine 3231. https://doi.org/10.2147/IJN.S64308.
Shen, Z., Xia, Y., Yang, Q., Tian, W., Chen, K., Ma, Y., 2017. Polymer-nucleic acid interactions. Top. Curr. Chem. 375, 44. https://doi.org/10.1007/s41061-017-0131-x.
Shi, B., Zheng, M., Tao, W., Chung, R., Jin, D., Ghaffari, D., Farokhzad, O.C., 2017. Challenges in DNA delivery and recent advances in multifunctional polymeric DNA delivery systems. Biomacromolecules 18, 2231–2246. https://doi.org/10.1021/acs.biomac.7b00803.
Stefan, J., Kus, K., Wisniewska, A., Kaminski, K., Szczubialka, K., Jawien, J., Nowakowska, M., Korbut, R., 2016. New cationically modified pullulan attenuates atherogenesis and influences lipid metabolism in apoE-knockout mice. J. Physiol. Pharmacol. 67, 739–749.
Stuart, B.H., 2004. Infrared Spectroscopy: Fundamentals and Applications 208.
Tekie, F.S.M., Atyabi, F., Soleimani, M., Arefian, E., Atashi, A., Kiani, M., Khoshayand, M.R., Amini, M., Dinarvand, R., 2015. Chitosan polyplex nanoparticle vector for miR-145 expression in MCF-7: Optimization by design of experiment. Int. J. Biol. Macromol. 81, 828–837. https://doi.org/10.1016/j.ijbiomac.2015.09.014.
Thanou, M., Florea, B.I., Geldof, M., Junginger, H.E., Borchard, G., 2002. Quaternized chitosan oligomers as novel gene delivery vectors in epithelial cell lines. Biomaterials 23, 153–159. https://doi.org/10.1016/S0142-9612(01)00090-4.
van Rooij, E., Marshall, W.S., Olson, E.N., 2008. Toward MicroRNA–based therapeutics for heart disease: the sense in antisense. Circ. Res. 103, 919–928. https://doi.org/10.1161/CIRCRESAHA.108.183426.
Vauthier, C., Zandanel, C., Ramon, A.L., 2013. Chitosan-based nanoparticles for in vivo delivery of interfering agents including siRNA. Curr. Opin. Colloid Interface Sci. 18, 406–418. https://doi.org/10.1016/j.cocis.2013.06.005.
Wang, S., Cao, M., Deng, X., Xiao, X., Yin, Z., Hu, Q., Zhou, Z., Zhang, F., Zhang, R., Wu, Y., Sheng, W., Zeng, Y., 2015. Degradable Hyaluronic Acid/Protamine Sulfate Interpolyelectrolyte Complexes as miRNA-Delivery Nanocapsules for Triple-Negative Breast Cancer Therapy. Adv. Healthc. Mater. 4, 281–290. https://doi.org/10.1002/adhm.201400222.
Wolff, J.A., Malone, R.W., Williams, P., Chong, W., Acsadi, G., Jani, A., Felgner, P.L., 1990. Direct gene transfer into mouse muscle in vivo. Science 247, 1465–1468.
Wu, D., Delair, T., 2015. Stabilization of chitosan/hyaluronan colloidal polyelectrolyte complexes in physiological conditions. Carbohydr. Polym. 119, 149–158. https://doi.org/10.1016/j.carbpol.2014.11.042.
Xiong, Q., Lee, G.Y., Ding, J., Li, W., Shi, J., 2018. Biomedical applications of mRNA nanomedicine. Nano Res. 11, 5281–5309. https://doi.org/10.1007/s12274-018-2146-1.
Zarghampoor, F., Azarpira, N., Khatami, S.R., Behzad-Behbahani, A., Foroughmand, A.M., 2019. Improved translation efficiency of therapeutic mRNA. Gene 707, 231–238. https://doi.org/10.1016/j.gene.2019.05.008.
Zhao, Q.-Q., Chen, J.-L., Lv, T.-F., He, C.-X., Tang, G.-P., Liang, W.-Q., Tabata, Y., Gao, J.-Q., 2009. N/P Ratio Significantly Influences the Transfection Efficiency and Cytotoxicity of a Polyethylenimine/Chitosan/DNA Complex. Biol. Pharm. Bull. 32, 706–710. https://doi.org/10.1248/bpb.32.706.
Zhu, L., Chen, T., Ye, W., Wang, J.-Y., Zhou, J.-P., Li, Z.-Y., Li, C.-C., 2019. Circulating miR-182-5p and miR-5187-5p as biomarkers for the diagnosis of unprotected left main coronary artery disease. J. Thorac. Dis. 11, 1799–1808. https://doi.org/10.21037/jtd.2019.05.24.

Carbohydrate Polymers 245 (2020) 116457

Contents lists available at ScienceDirect

Carbohydrate Polymers

journal homepage: www.elsevier.com/locate/carbpol

Gd(DOTA)-grafted submicronic polysaccharide-based particles functionalized with fucoidan as potential MR contrast agent able to target human activated platelets

Laura Marcela Forero Ramirez[a,b,c], Elise Gobin[a,b], Rachida Aid-Launais[a,d], Clément Journe[a,d], Fernanda C. Moraes[a,b], Luc Picton[c], Didier Le Cerf[c], Didier Letourneur[a,b], Cédric Chauvierre[a], Frédéric Chaubet[a,b,*]

[a] Laboratory for Vascular Translational Science, UMRS1148, INSERM, Université de Paris, F-75018 Paris, France
[b] Université Sorbonne Paris Nord, F-93430 Villetaneuse, France
[c] Laboratoire Polymères Biopolymères Surfaces, CNRS UMR 6270 & FR3038, Normandie Université, Université de Rouen, INSA de Rouen, F-76821 Mont Saint Aignan, France
[d] UMS34 FRIM, X. Bichat Medical School, Université de Paris, F-75018 Paris, France

ARTICLE INFO

Keywords:
Dextran
fucoidan
MRI
human platelets
crosslinking
submicronic particles

ABSTRACT

Early detection of thrombotic events remains a big medical challenge. Dextran-based submicronic particles bearing Gd(DOTA) groups and functionalized with fucoidan have been produced via a simple and green water-in-oil emulsification/co-crosslinking process. Their capacity to bind to human activated platelets was evidenced *in vitro* as well as their cytocompatibility with human endothelial cells. The presence of Gd(DOTA) moieties was confirmed by elemental analysis and total reflection X-ray fluorescence (TRXF) spectrometry. Detailed characterization of particles was performed in terms of size distribution, morphology, and relaxation rates. In particular, longitudinal and transversal proton relaxivities were respectively 1.7 and 5.0 times higher than those of DOTAREM. This study highlights their potential as an MRI diagnostic platform for atherothrombosis.

1. Introduction

Atherothrombosis remains the leading cause of morbidity and mortality worldwide and represents a major economic burden on health care systems (Lozano et al., 2012;(Herrington, Lacey, Sherliker, Armitage, & Lewington, 2016). Its underlying cause is atherosclerosis, a chronic inflammatory disease characterized by the formation of lipid-rich plaques in the intima of medium and large arteries. While stable plaques remain asymptomatic and relatively harmless, vulnerable plaques may rupture and thrombose causing myocardial infarction, stroke, or sudden death (Schroeder & Falk, 1995;)(Waxman et al., 2006). There is thus a medical need for non-invasive tests allowing to early detect high-risk plaques and thrombus formation in order to prevent major cardiovascular events.

Magnetic resonance imaging (MRI) has been successfully used to characterize plaque composition, detect arterial thrombi and monitor plaque progression and regression in several animal models of atherosclerosis and in humans (Corti & Fuster, 2011; Leiner et al., 2005; Sannino et al., 2014)(Raggi et al., 2016). In routine practice, MRI often requires the use of Gadolinium-based (Gd) contrast agents to enhance relaxation rates of water molecules, which results in better contrast between different biological tissues (Zhou & Lu, 2013)(Caravan et al., 1999)(Yon et al., 2019). Nevertheless, these contrast agents have major limitations including a short circulation time, a low diffusion and affinity with the interstitial space and a lack of tissue specificity. Important doses are thus necessary to improve imaging contrast, exposing patients to potential side effects (Rogosnitzky & Branch, 2016)(Kuo et al., 2007). These limitations can be addressed by combining nanotechnology and molecular imaging strategies. Nanosystems having paramagnetic properties and bearing targeting molecules able to bind specifically to thrombus have gained increased attention as potential imaging probes. Ultra-small particles of iron oxide, micelles, liposomes, and perfluorocarbon nanoparticles have been designed for MRI visualization of several inflammation-related targets, such as macrophages, oxidized low density lipoproteins, endothelial cell expression, plaque neovasculature, apoptosis, and activated platelets (Amirbekian et al., 2007; ; Briley-Saebo et al., 2008; Cai et al., 2010; Li et al., 2010; ; Suzuki et al., 2015; ; van Tilborg et al., 2010)(Barkhausen et al., 2003)(McAteer

* Corresponding author at: Laboratory for Vascular Translational Science, UMRS1148, INSERM, Université de Paris, F-75018 Paris, France.
E-mail address: frederic.chaubet@univ-paris13.fr (F. Chaubet).

https://doi.org/10.1016/j.carbpol.2020.116457
Received 24 January 2020; Received in revised form 12 May 2020; Accepted 13 May 2020
Available online 25 May 2020
0144-8617/ © 2020 Elsevier Ltd. All rights reserved.

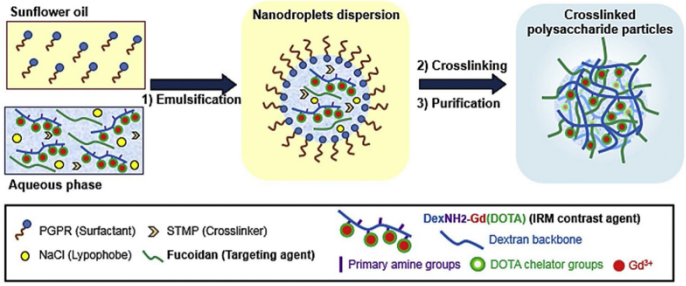

Scheme 1. Preparation of polysaccharide submicron particles via a combined inverse emulsion-crosslinking method.

et al., 2010)(Boekhorst et al., 2012).

P-selectin (140 kDa membrane glycoprotein) is an adhesion molecule overexpressed on the surface of activated platelets and inflamed endothelium of atherothrombotic lesions (Bachelet et al., 2009; Sabourel et al., 2014). P-selectin allows the recruitment of leucocytes through the interaction with its main ligand, PSGL-1 (McEver, 2001). Interestingly, fucoidan is a natural sulfated polysaccharide obtained from brown seaweed extract, which has shown a strong and specific affinity for P-selectin (Bachelet et al., 2009; Chollet et al., 2016; Sabourel et al., 2014). In this context, P-selectin and fucoidan appear as an appropriate target-ligand system for the diagnosis of atherothrombosis. One can therefore hypothesize that the assembly of several molecules of fucoidan with particles containing Gd material will result in MRI contrast probes with increased binding on activated platelets. The aim of the present study was to develop novel and biospecific polysaccharide-based submicronic particles (SPs) functionalized with fucoidan and able to bind to human activated platelets for atherothrombosis imaging by MRI (Scheme 1). Dextran, another polysaccharide widely used in the biomedical field (; Lino Ferreira, 2014;)(Abir et al., 2004)(Naessens et al., 2005), was chosen as polymer carrier for Gd(DOTA) groups as the contrast moieties. The polysaccharide nature of the designed objects was expected to ensure their haemocompatibility and low toxicity. Among all the works dealing with micro/nanoparticles exclusively composed of polysaccharides, very few examples were designed for MRI and almost all of them were developed for cancer diagnostics. Chitosan and hyaluronic acid have been by far the most employed polysaccharides to get Gd-loaded nanoparticles (Na et al., 2016; ; Gheran et al., 2018; ; Nam et al., 2010; Payne et al., 2017; Rigaux et al., 2017;)(Chan et al., 2015)(Huang et al., 2008)(Zhang et al., 2015), but alginate and pullulan-based ones have also been described (; Podgórna et al., 2017)(Kim et al., 2015). They were mainly prepared by self-assembly of amphiphilic polysaccharide derivatives, formation of polyelectrolyte complexes or ionic gelation with sodium tripolyphosphate. To the best of our knowledge, no polysaccharide-based submicronic particle combining fucoidan and Gd-based contrast agent has been developed yet, which contributes to the originality of the present work.

As a first step, a chemical modification of native dextran to introduce Gd(DOTA) groups was performed. Next, SPs were synthesized by co-crosslinking of fucoidan and former dextran macrocomplexes within the droplets of a water-in-oil emulsion. SPs were characterized in terms of morphology, size and zeta potential. *In vitro* assays were performed to evaluate the cytotoxicity, contrast properties and targeting capacity of the obtained objects.

2. Materials and methods

2.1. Materials

Dextran T70 ($\overline{M}_n$ = 55 000 g/mol, Đ = 1.12) was purchased from Pharmacosmos (Holbæk, Denmark), Low molecular weight fucoidan ($\overline{M}_n$ = 4 400 g/mol, Đ = 1.49, 16.8 wt% sulfates) was obtained from Algues & Mer (Ouessant, France) in the framework of a partnership for the pharmaceutical development of a GMP-grade fucoidan for molecular diagnosis of cardiovascular diseases (Chauvierre et al., 2019). 3-chloropropylamine hydrochloride, 1-ethyl-3-(3-dimethylaminopropyl) carbodiimide hydrochloride (EDC.HCl), N-hydroxysuccinimide (NHS), Gadolinium(III) chloride hexahydrate ($GdCl_3.6H_2O$) and Paraformaldehyde (PFA) were purchased from Fisher Scientific (Illkirch, France). 1,4,7,10-Tetraazacyclododecane-1,4,7,10-tetraacetic acid (DOTA) was provided by Leap Labchem (Hangzhou, China). Ethylenediaminetetraacetic acid (EDTA), Trisodium Trimetaphosphate (STMP), Sodium Dodecyl Sulfate (SDS), Triton X-100, 7-hydroxy-10-oxidophenoxazin-10-ium-3-one (resazurin), 3,3′-Dihexyloxacarbocyanine iodide ($DiOC_6$), 4',6-diamidino-2-phenylindole (DAPI) and Phalloidin-TRITC were from Sigma Aldrich (Saint-Quentin-Fallavier, France). Dextran-FITC ($\overline{M}_w$ = 70 000 g/mol) and Dextran-TRITC ($\overline{M}_w$ = 40 000 g/mol) were from TdB Consultancy (Uppsala, Sweden). Polyglycerol polyricinoleate (PGPR 4150) was a gift from Palsgaard SAS (Lyon, France). Sunflower oil (Lesieur, France) is a mixture of saturated fatty acids (palmitic acid ~ 5 wt%- and stearic acid ~ 6 wt%) and unsaturated fatty acids (mainly oleic acid ~ 37 wt% and linoleic acid ~ 51 wt%). Thrombin receptor-activating-peptide (TRAP) was obtained from PolyPeptide laboratories (Strasbourg, France). PE-CyTM5 mouse anti-human CD41a was provided by BD Pharmingen, (Le Pont de-Claix, France), mouse anti-human CD62 P and mouse anti-human CD62P-FITC were obtained from Beckman Coulter (Villepinte, France). Tyrode-Hepes buffer (0.3 wt% BSA, pH 7,24) contained 137 mM NaCl, 2 mM KCl, 12 mM $NaHCO_3$, 0.3 mM Na_2HPO_4, 5.5 mM glucose and 5 mM Hepes. All materials were used without further purification. Dialysis membranes of 10 000 Da were purchased from Spectrum Laboratories (New Brunswick, NJ, USA).

2.2. Preparation of $DexNH_2$-Gd(DOTA) complexes

Dextran derivatives bearing Gd(DOTA) groups were synthesized in three steps (Scheme 2). In the first step, the attachment of primary amine functions (NH_2) onto dextran was performed in aqueous basic media. Typically, 5 g of dextran (31 mmol of anhydroglucopyranose unit (AGU)) were dissolved in 25 mL of water. 25 mL of NaOH (6.2 M) were added and the mixture was stirred during 30 minutes. The reaction flask was then immersed in a thermostated oil bath at 55 °C before the addition of 8 g of 3-chloropropylamine hydrochloride (62 mmol, 2

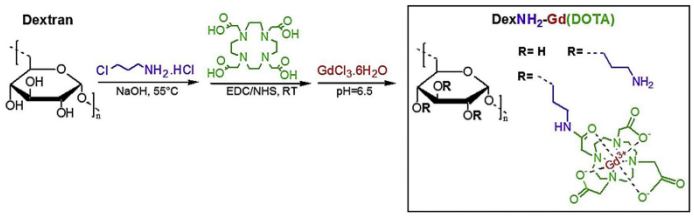

Scheme 2. Synthesis of $DexNH_2$-Gd(DOTA) complexes.

equivalents per AGU) and the mixture was maintained under stirring during different reaction times. After neutralization, the polymer ($DexNH_2$), was extensively dialyzed against ultrapure water (cut-off: 10 000 Da) and finally freeze-dried. Degree of substitution of primary amine groups per 100 AGU (DS_{NH2}) was estimated by elemental analysis of nitrogen.

In the second step, DOTA groups were linked to aminated dextran using classical EDC/NHS reaction. Typically, DOTA (1 equivalent per primary amine group) was dissolved in 10 mL of water and pH was adjusted to 3.5 with diluted HCl (0.5 M). After 30 min of stirring, EDC and NHS were added at a molar ratio DOTA/EDC/NHS of 1/5/1.25. The pH was raised to 7 and $DexNH_2$ previously dissolved in 10 mL of water was added in small amounts for 1 h. The mixture was stirred at room temperature for 2 h. Resulting $DexNH_2$-DOTA derivative was dialyzed against EDTA (0.05 M) to avoid the complexation of contaminating metal ions by DOTA then against water (cut-off: 10 000 Da) before freeze-drying. Degree of substitution of DOTA moieties per 100 AGU (DS_{DOTA}) was estimated from the increase of nitrogen content with respect to the one of $DexNH_2$ precursor.

In the third step, the chelation of Gd^{3+} ions by DOTA groups along the dextran backbone was performed by mixing $GdCl_3.6H_2O$ (1 Gd^{3+} per DOTA group) with $DexNH_2$-DOTA in water as previously described (Nguyen et al., 2017). After adjusting the pH to 6.5 with NaOH, the solution was maintained at room temperature overnight followed by heating at 60 °C for 4 h. Chlorides were removed by dialysis (cut-off: 10 000 Da) and white fluffy products were obtained after freeze-drying. Dextran gadolinium chelates were called $DexNH_2$-Gd(DOTA). Degree of substitution of Gd^{3+} ions per 100 AGU (DS_{Gd}) was determined by total reflection X-ray fluorescence (TRXF) spectrometry (S2 Picofox, Bruker, Germany).

2.3. Polysaccharide submicron particles synthesis

Dextran T70 particles were obtained via a water-in-oil emulsification-crosslinking method inspired from our previous works (Bonnard et al., 2014). Typical experimental conditions were as follows: 1.2 g of dextran and 1.4 g of NaCl were solubilized in 4 mL of water. 1.2 g of this solution were then mixed with 120 µL of NaOH (10 M) and 240 µL of trisodium trimetaphosphate (STMP) (30% (w/v) in water). 300 µL of the mixture were slowly injected into 15 ml of sunflower oil containing 6.0% (w/v) of polyglycerol polyricinoleate (PGPR) as emulsion stabilizer and dispersed with a homogenizer at 30,000 rpm for 4 min (Polytron PT 3100, dispersing aggregate PT-DA 07/2EC-B101, Kinematica, Luzernerstrasse, Switzerland). The resulting emulsion was then transferred to an oven (50 °C) wherein the crosslinking step took place for 20 min. Polysaccharide particles were recovered by ultracentrifugation (15,000 g, 45 min), washed once with PBS 1X, twice with SDS (0.04% (w/v)) and four times with water. The resulting pellets were resuspended in water and stored at 4 °C until use. To prepare Gd-loaded particles (Gd-SPs), dextran was replaced by $DexNH_2$-Gd(DOTA). Fucoidan-functionalized particles (FUCO-Gd-SPs) were prepared with 60 mg of fucoidan and 1.14 g of $DexNH_2$-Gd(DOTA).

2.4. Physico-chemical characterizations

^1H NMR spectra were recorded on a Bruker-400 Ultrashield (Bruker, Germany). Samples were prepared in D_2O at a concentration of 20 mg/mL.

Average molecular weight of dextran derivatives was determined by size exclusion chromatography coupled to a multi-angle laser light scattering detector (SEC-MALLS) in $NaNO_3$/NaN_3 (0.15 M/0.02% (w/v)). Refractive index increment (dn/dc) of 0.146 $mL.g^{-1}$ was used (See Supporting).

The viscosities of sunflower oil and dextran solutions were measured at 25 °C using a rotational rheometer with a concentric cylinder geometry (TA instrument HR2, Delaware, USA).

Nitrogen content was estimated by elemental analysis (Service de Microanalyse du CNRS, ICSN, Gif-sur-Yvette, France). Phosphorus and gadolinium contents were determined by total reflection X-ray fluorescence (TRXF) spectrometry (S2 PICOFOX, Bruker, Germany). Fucoidan content was assessed by colorimetric quantification of sulfates as previously described ()(Sabourel et al., 2014).

Particle size distribution was measured by using Laser Diffraction Particle Size Analyzer (Mastersizer 3000, Malvern Instruments, UK) and number distributions are reported. The obtained size (D50) and span values were an average of at least three consecutive measurements.

Zeta potential of particles was measured in 1 mM KCl at 25 °C using a Zetasizer Nano-ZS (Malvern Instruments, Malvern, UK).

The morphology of particles was investigated by Transmission Electron Microscopy (TEM, Tecnai 12, 80 kV; FEI; Hillsboro, OR, USA), Scanning Electron Microscopy (SEM, Philips XL30 ESEM-FEG, Netherlands) and confocal microscopy (Zeiss LSM 780 with 63× oil objective, Carl Zeiss Microscopy, Oberkochen, Germany). For TEM observation, 3 µL of particles suspension were dropped onto a 400 mesh copper grid and positive stained with uranyl acetate (1% (w/v)) and allowed to air-dry at room temperature. For SEM images, one drop of particles suspension was dropped onto a silicon wafer, then air-dried and coated with a thin layer of gold before observation.

2.5. Cytotoxicity tests

Human Umbilical Vein Endothelial Cells (HUVECs) were grown in DMEM supplemented with 10% (v/v) fetal bovine serum, 4 mM of L-glutamine, 100 U/mL penicillin and 100 µg/mL streptomycin. Cells were cultivated at 37 °C under 5% CO_2 (v/v) in a humidified incubator. HUVECs were seeded at 10,000 cells per well in 96-well plates and incubated for 24 h. After that, culture medium was removed and 100 µL of particle suspensions at different concentrations (200, 500 and 1 000 µg/mL) were added. Cells metabolic activity was determined after 24 h by resazurin assay. Cells were incubated with medium containing 10% resazurin for 2 h at 37 °C and fluorescence intensity ($\lambda ex = 560$ nm; $\lambda em = 590$ nm) was read in an Infinite M200 PRO microplate (TECAN Group Ltd, Switzerland). Metabolic activity in the presence of particles was compared to the control condition.

To assess cells morphology, samples were fixed with PFA and

incubated with TRITC-phalloidin and DAPI to stain for F-actin and nuclei respectively.

2.6. MRI phantoms

DOTAREM, $DexNH_2$-Gd(DOTA) and FUCO-Gd-SPs gel phantoms (Gd concentrations ranging between 0.12 and 1.0 mM) were prepared in 0.5 mL tubes using 2% (w/v) agarose. These tubes were put inside of a larger container, which was itself filled with agarose gel.

Longitudinal relaxation (T_1) and transversal relaxation (T_2) times were acquired on a 7 Tesla animal MR imager (Pharmascan 70/16, Bruker Biospin, Ettlingen, Germany), and analyzed with Bruker software Paravision 6.0.1. In order to calculate T_1 map, a rapid acquisition with relaxation enhancement (RARE) sequence was used, with echo time (TE) of 8.5 ms, variable repetition time (TR, 200, 400, 800, 1500, 3000, 5500 ms), matrix (MTX): 128 × 128, field of view (FOV): 30 x 30 mm and slice thickness of 1 mm. For T_2 map calculation, a multislice multiecho (MSME) sequence was employed with TR of 2200 ms and TE between 6.8 to 170 ms (25 echoes; echo spacing: 6.8 ms). MTX, FOV and slice thickness were as before. The slope of the line obtained by plotting the relaxation rates R_1 and R_2 ($R_1 = 1/T_1$; $R_2 = 1/T_2$) at different concentration, provided the relaxivity r_1 and r_2 respectively.

2.7. Interaction of SPs with human activated platelets

2.7.1. Under static conditions

The interaction between three groups of PE-Cy5 labeled platelets (non-activated platelets (PRP), activated platelets (PRP + TRAP) and P-selectin blocked activated platelets (PRP + TRAP + anti-CD62P)) and FUCO-Gd-SPs was measured by flow cytometry. Protocol was adapted from (Li et al., 2017). Briefly, 5 mL of blood from healthy adult volunteers were collected in sodium citrate 3.8% (w/v). Platelet-rich plasma (PRP) was obtained by centrifugation at 200 g for 15 min (5702RH centrifuge Beckman Coulter, Villepinte, France) and platelet concentration was adjusted to 1×10^8 ml^{-1} with Tyrode-HEPES buffer (0.3 wt% BSA). Platelets were labeled by incubation with PE-CyTM5 mouse anti-human CD41a for 15 min. Conjugate excess was then eliminated by a wash step. Activated PRP was obtained by stimulation of PRP with 20 µM TRAP. In some experiments, activated then P-selectin-blocked PRP were obtained by incubation with a non-labeled anti-human CD62P at high concentration (0.04 mg/mL). Before assessing the interaction with particles, P-selectin expression level at the platelet surface was assessed using an anti-human CD62P-FITC and measuring FITC signal by flow cytometry. To evaluate the binding ability of particles to P-selectin expressed onto platelets, 5 µL of non-activated PRP, activated PRP with TRAP or anti P-selectin-treated activated PRP were incubated for 20 min with 5 µl of FITC-labeled FUCO-Gd-SPs (10 mg/mL). Sample volume was then completed to 100 µL using Tyrode-HEPES buffer (0.3 wt% BSA). Samples were analyzed on a LSRII flow cytometer (BD Biosciences, Le Pont de Claix, France), 10,000 PE-Cy5 positive platelets were collected per sample, and the mean fluorescence intensity (MFI) of FITC channel was measured in these platelets. FITC-labeled Gd-SPs were used as negative control.

2.7.2. Under arterial flow conditions

Binding ability of FUCO-Gd-SPs to P-selectin expressed on activated platelet aggregates was as well evaluated *in vitro* as previously reported (Juenet et al., 2018; Li et al., 2017). Briefly, micro-channels of Vena8 Fluoro + chambers (Cellix Ltd, Dublin, Ireland) were coated overnight with 50 µg/mL of collagen and then washed with NaCl 0.9%. Human whole blood labeled with $DiOC_6$ (a green fluorescent dye) was perfused under arterial flow conditions for 5 min to induce platelet activation and aggregation on the collagen-coated channel. TRITC labeled FUCO-Gd-SPs at 1 mg/mL in NaCl 0.9% were then perfused during 5 min. Their accumulation onto preformed platelet aggregates was monitored in real time by fluorescence microscopy (Axio Observer, Carl Zeiss Microscopy, Oberkochen, Germany). Fluorescence images were taken along each micro-channel after washing with NaCl 0.9%. Gd-SPs were used as negative control.

2.8. Statistical Analysis

Data are presented as mean ± SEM ($n \geq 3$). Flow cytometry results were analyzed statistically with a one-way ANOVA with Bonferroni post-tests to compare data obtained with Gd-SPs and Fuco-Gd-SPs. A difference of $p < 0.05$ was considered significant.

3. Results

3.1. Synthesis of dextran gadolinium chelates

A series of aminated dextran ($DexNH_2$), dextran ligands ($DexNH_2$-DOTA) and their corresponding gadolinium complexes ($DexNH_2$-Gd(DOTA)) were synthesized in three consecutive steps (Scheme 2). All modifications were done in aqueous media. Three sets of reaction conditions were used (Conditions-1, 2, 3), resulting in three final macrocomplexes named Complex-1, 2, 3, respectively. The substitution degrees (DS) of primary amines, DOTA groups and Gd^{3+} ions were expressed as the number of introduced groups per 100 AGU. All physicochemical characterizations are reported in Table 1.

Amination of dextran was performed in basic solution (3.1 M NaOH) by reaction with 3-chloropropylamine leading to $DexNH_2$ derivatives (1st step, Table 1). Successful introduction of amine moieties was confirmed by elemental analysis of nitrogen content (%N) and ^{1}H NMR spectroscopy. The characteristic peaks of methylene protons of propylamine group (-CH_2-CH_2-CH_2-NH_2) were clearly visible at 1.9 ppm and 3.1 ppm (Fig. S1). Substitution degree of amine (DS_{NH2}) could be tuned from 5.6 to 23.9% by increasing reaction time (1.5, 3 and 14 h) at

Table 1
Physicochemical characteristics of $DexNH_2$-Gd(DOTA) complexes.

Reaction set	1st step Amination ($DexNH_2$)			2nd step DOTA attachment ($DexNH_2$-DOTA)			3rd step Gd complexation ($DexNH_2$-Gd(DOTA))		Resultant derivative		
	t (h)	%N[a] (wt)	DS_{NH2}[b] (%)	%N[a] (wt)	DS (%)		%Gd[c] (wt)	DS_{Gd}[d] (%)		$\bar{M}_{n\,exp}$[e] (g/mol)	Đ[e]
					NH_{2r}[b]	DOTA[b]					
Conditions-1	1.5	0.48 ± 0.05	5.6	1.27 ± 0.04	3.0	2.6	2.0 ± 0.1	2.4	Complex-1	67 000	1.5
Conditions-2	3.0	0.65 ± 0.03	7.7	2.12 ± 0.03	2.6	5.1	4.0 ± 0.2	5.0	Complex-2	75 000	1.7
Conditions-3	14	1.90 ± 0.10	23.9	3.54 ± 0.09	17.1	6.8	4.9 ± 0.2	6.7	Complex-3	73 000	1.6

(a) Nitrogen content estimated by elemental analyses. (b) Degree of substitution of initial primary amines (NH_2), residual primary amines (NH_2r, not modified with DOTA groups) and grafted DOTA moieties (DS_{DOTA}) per 100 AGU were calculated from N content (DS_{NH2r} + DS_{DOTA} = DS_{NH2}). (c) Gadolinium content determined by total reflection X-ray fluorescence (TRXF) spectrometry. (d) Degree of substitution of gadolinium ions per 100 AGU estimated from Gd content. (e) Evaluated from SEC-MALLS in $NaNO_3$/NaN_3 (0.15 M/0.02% (w/v)) with dn/dc = 0.146 mL/g.

Table 2
Formulation and physico-chemical characterization of polysaccharide submicronic particles. Crosslinking reaction was performed at 50 °C during 20 min with [Polysaccharide] = 200 g/L [NaOH] = 1 M, [PGPR] = 6% (w/v).

R.	Polysaccharide	$\frac{[STMP]}{[AGU]}$	D(nm)	Span [a]	Zeta potential (mV)	%P [b]	%Gd [b]
1	$DexT_{70}$	0.043	1720 ± 50	0.61 ± 0.01	−18 ± 3	0.6 ± 0.1	-
2	$DexT_{70}$	0.087	1230 ± 45	0.67 ± 0.03	−22 ± 3	0.8 ± 0.1	-
3	$DexT_{70}$	0.170	790 ± 30	0.61 ± 0.01	−30 ± 3	1.1 ± 0.1	-
4	Complex-2	0.170	720 ± 35	0.67 ± 0.03	−28 ± 5	1.0 ± 0.1	2.6 ± 0.2
5	Complex-2/Fuco	0.170	840 ± 45	0.60 ± 0.02	−25 ± 4	1.1 ± 0.1	2.3 ± 0.1

(a) Width of the distribution calculated using $Span = (D(0.9) - D(0.1))/D(0.5)$.D(0.1), D(0.5) and D(0.9) were the particle diameters at 10%, 50% and 90% of the particle number size distribution. (b)Determined by Total Reflection X-ray Fluorescence (TXRF).

constant amine/AGU feeding ratio (2/1). These results are in agreement with those reported by De Nooy et al. for the amination of scleroglucan (De Nooy et al., 2000). Furthermore, no degradation of the dextran backbone under basic conditions (pH ≈ 13) was evidenced at early times and only a slight decrease in molecular weight was observed at 14 h as attested by SEC-MALLS analysis (Table S1).

EDC/NHS chemistry was used to graft DOTA ligands to amine functions of $DexNH_2$. Higher nitrogen content of resultant $DexNH_2$-DOTA derivatives (with respect to the corresponding $DexNH_2$ precursors) confirmed the incorporation of the DOTA tetraazamacrocycle (2nd step, Table 1). Initial quantity of amine functions (DS_{NH2}) was shown to influence both the degree of substitution DS_{DOTA} and the grafting yield. As expected, the number of DOTA groups linked to dextran chains increased with the initial amine content, all other conditions being the same. In all cases, DOTA grafting was incomplete leaving unreacted propylamines along dextran backbone. Coupling yields were in about 50-60% for initial DS_{NH2} values below 8% (Conditions-1 and 2, Table 1) and of less than 30% when DS_{NH2} was equal to 23.9% (Conditions-3). This low yield was likely due to steric hindrance effects.

$DexNH_2$-Gd(DOTA) macrocomplexes were finally produced by reacting former $DexNH_2$-DOTA ligands with gadolinium chloride (3rd step, Table 1). An aminated dextran (without DOTA groups) was used as negative control. The amount of complexed Gd^{3+} was assessed by TXRF. According to X-ray fluorescence emission spectra, Gd was effectively chelated by $DexNH_2$-DOTA ligands while no Gd was detected in the case of aminated dextran (Fig. S2). These results further demonstrated the presence of DOTA moieties covalently linked to the polysaccharide. In addition, DS_{Gd} calculated from Gd content (%Gd) matched well with DS_{DOTA} previously estimated from N content, indicating the presence of one Gd^{3+} ion per DOTA group. Three $DexNH_2$-Gd(DOTA) complexes having 2.4 (Complex-1), 5.0 (Complex-2) and 6.7 (Complex-3) Gd(DOTA) groups per 100 AGU were obtained corresponding to 8, 17 and 23 Gd(DOTA) groups per dextran chain, respectively.

3.2. Preparation of polysaccharide-based submicronic particles

3.2.1. Optimization of crosslinking and emulsion conditions

Polysaccharide-based particles were prepared in one-step using a combined water-in-oil emulsion/co-crosslinking process. This process was solvent-free in both production and purification steps. Sunflower oil was used as continuous phase instead of organic solvents commonly reported in the literature. Furthermore, STMP and PGPR, safe materials with no reported adverse effects on humans (Abed et al., 2011;) (Nikolovski et al., 2016), were used as crosslinking agent and emulsion stabilizer respectively.

Native dextran (Dextran T70) was used as a model polysaccharide to optimize the preparation of particles. Crosslinking reaction was performed at 50 °C at constant 1 M NaOH concentration. SEC/MALLS measurements indicated that no degradation of dextran backbone occurred during 5 h under these conditions (Table S2). The use of sodium chloride (4 M) appeared to increase the reaction rate. NaCl screened phosphate negative charges coming from STMP reaction keeping macromolecular chains closer, thus improving the crosslinking process.

We determined the lower polysaccharide and STMP concentrations required to succesfully crosslinked dextran chains. For a dextran solution at about or below 120 g/L no gelation was noted. This result was expected as the critical overlap concentration (C*) of Dextran T70 in water is reported at about 112 g/L at 40 °C (Antoniou & Tsianou, 2012). Stable 3D networks were obtained for dextran concentrations equal or above 200 g/L since the entanglement density of dextran chains was sufficient in such conditions. Minimal [STMP]/[AGU] molar ratio required for crosslinking was equal to 0.02. Below this value, no reaction occurred.

The viscosity of both dispersed (η_d) and continuous phases (η_c), and more specifically the viscosity ratio (η_d/η_c) play an important role in droplets size, dispersity and stability. Typically, the emulsification process is highly intensified when that ratio tends to 1 and smaller droplets can be obtained ()(Vananroye et al., 2006). On one hand, regarding continuous phase, sunflower oil viscosity was 16 mPa.s at 25 °C and increased slightly to 19 mPa.s with the addition of 6% (w/v) of PGPR. On the other hand, dextran solutions containing 4 M NaCl behaves like Newtonian fluids (i.e. viscosity does not depend on the shear rate) in the concentration range studied (50-500 g/L) (Fig. S3a). As the concentration of solutions increased from 50 to 500 g/L, the relative viscosity increased exponentially from 1.6 to 163 (Fig. S3b). An aqueous phase containing 200 g/L of dextran, giving a viscosity of 12 mPa.s and a viscosity ratio η_d/η_c of ~ 0.6, was finally chosen for the preparation of particles.

3.2.2. Tuning particles size

Table 2 summarizes experimental conditions used in the present study (Runs 1-5), as well as the average size of the particles after purification and resuspension in water. In all formulations, aqueous phase contained 200 g/L of polysaccharide and 1 M NaOH while continuous phase was composed of sunflower oil and PGPR (6% (w/v)). Water to oil phases ratio was kept to 30/150 (v/v). Phosphorus content (%P) in as-obtained particles was used as indicator of the actual amount of phosphoester groups incorporated in the polymer network (i.e. intermolecular, intramolecular and monografted)(Dulong et al., 2011)(Lack et al., 2007)

Particles size was tuned by varying STMP concentration and consequently [STMP]/[AGU] molar ratio (Runs 1-3). Unsurprisingly, the higher the initial [STMP]/[AGU] ratio, the smaller the particle size. This observation can be correlated to the increase of crosslinking as suggested by the rise of P content. More densely packed particles with lesser swelling in water were obtained at higher STMP feeding amount. Because of the anionic charges brought by STMP, all particles exhibited negative zeta potential. Submicronic particles (SPs) of about 790 nm with narrow size distribution can be achieved in a reproducible way by using [STMP]/[AGU] = 0.17 (6.0 % (w/v) STMP, Run 3). Production yield was of about 35%.

3.2.3. Synthesis of Gd-SPs and FUCO-Gd-SPs

The optimized emulsion conditions described above (Run 3) were applied to gadolinium Complex-2 (Table 1) to obtain two types of SPs: non-functionalized/Gd-loaded SPs (Gd-SPs, Run 4) and fucoidan-functionalized/Gd-loaded SPs (FUCO-Gd-SPs, Run 5). For dextran derivatives with higher modification degrees (Complex-3), no gel was obtained. This was likely due to a reduced amount of hydroxyl groups available for crosslinking and to steric hindrance. Complex-2 was chosen over Complex-1 because of its higher Gd content.

Size distribution, zeta potential and %P of Gd-SPs and FUCO-Gd-SPs were roughly like those obtained with model SPs (Run 3). Gd content was similar for both types of SPs (2.3-2.6 wt%) but almost 2-times lower than the one of dextran complex precursor (4.0 wt%). Alkaline crosslinking conditions would led to some hydrolysis of amide bonds linking Gd(DOTA) groups to dextran and to a loss of Gd(DOTA) moieties. This hypothesis was supported by the decrease in nitrogen content (around 1.70 wt% in SPs compared to 2.12 wt% in Complex-2). FUCO-Gd-SPs contained 23 ± 5 μmol S/g which corresponded to a fucoidan content of 1.3 wt% (about 26 wt% of the fucoidan initially dissolved in the aqueous phase).

TEM, SEM and confocal micrographs of FUCO-Gd-SPs are depicted in Fig. 1b–d. All techniques confirmed the production of spherical and homogeneous objects in the submicronic range. Average particles sizes observed by confocal microscopy agreed with those measured by laser diffraction (~ 800 nm) whereas smaller average sizes were detected by TEM (~ 700 nm) and SEM (~ 400 nm). These differences arise from sample preparation (in hydrated or dried states) and observation conditions (vacuum).

The FUCO-Gd-SPs were stable for at least two weeks when stored in aqueous suspension at 4 °C. In addition, the effective protection of particle size during freeze-drying can be ensured with 5% (w/v) sucrose as cryoprotectant since no aggregation was observed after resuspension in aqueous medium. This allowed long-term storage of SPs. As expected, FUCO-Gd-SPs average size was found to be smaller in physiological saline solution (0.9% NaCl) because of the screening of phosphate negative charges (Fig. 1a). The FUCO-Gd-SPs remained stable at room temperature and 37 °C for at least 72 h under such conditions.

3.3. Cytotoxicity

Cytocompatibility of Complex-2 (Table 1) toward HUVECs was checked and compared with the one of free Gd^{3+} ions (concentration ranging from 8 to 80 μg/mL). Cell viability was assessed by measuring metabolic activity of the mitochondria using resazurin reagent. Complex-2 did not affect cell viability after 24 h. In contrast, metabolic activity decreased down to 50% in the presence of free Gd^{3+} (Fig. S4). Mitochondrial dysfunction induced by Gd^{3+} and other lanthanide ions has been already reported (Zhao et al., 2014)(Feng et al., 2010)(Liu et al., 2003). These results further proved the successful chelation of Gd^{3+} by DOTA groups of $DexNH_2$-DOTA derivatives.

FUCO-Gd-SPs also showed excellent cytocompatibility even at concentrations at high as 1 mg/mL (Fig. 2a). No major morphological changes of HUVECs were evidenced when compared to control conditions (Fig. 2b). Furthermore, FUCO-Gd-SPs appeared to be internalized by endocytosis. Particles engulfment by HUVECs was clearly seen by confocal microscopy (Fig. 2c). Further *in vitro* and *in vivo* studies will be required for a complete understanding of the mechanism involved in internalization, as well as the fate of the particles.

3.4. Proton relaxation effects of dextran derivatives and FUCO-Gd-SPs

The efficiency of an MRI contrast agent is correlated to its relaxivity.

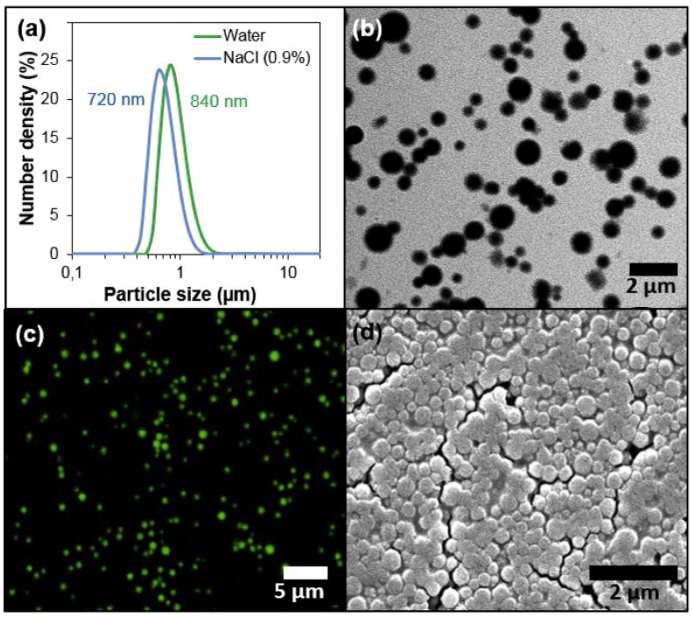

Fig. 1. a) Size distribution in water and NaCl 0.9% and b) TEM c) Confocal microscopy and d) SEM-Micrographs of FUCO-Gd-SPs. In the case of confocal microscopy, sample was analyzed in its hydrated state. For the other techniques (TEM and SEM), SPs were air-dried and submitted to vacuum conditions.

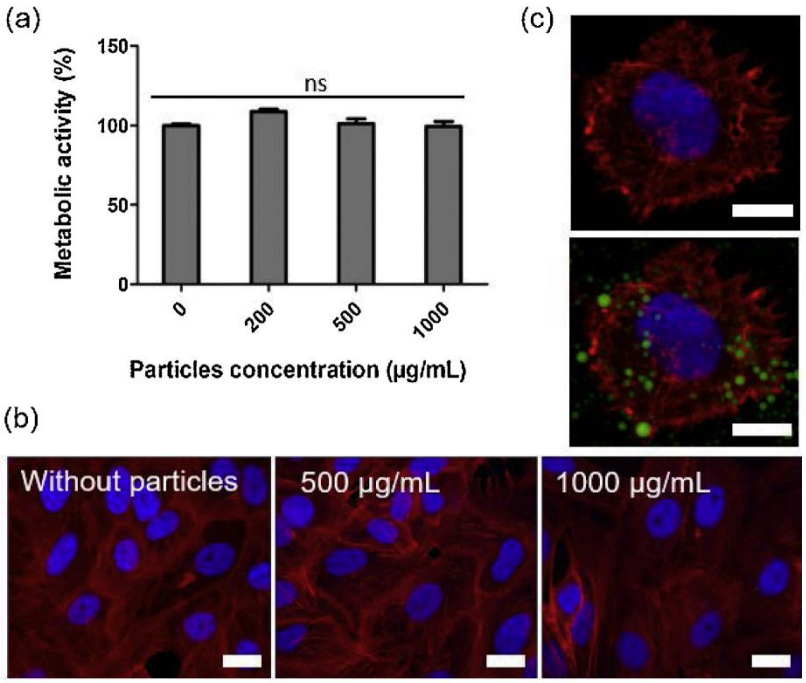

Fig. 2. a) Cytocompatibility of FUCO-Gd-SPs towards HUVECs after 24 h incubation at 37 °C. 100% of mitochondrial metabolic activity (resazurin reduction assay) corresponds to control cells incubated without particles. n = 3. b) Fluorescent images of HUVECs. F-actin is shown in red (TRITC-Phalloidin) and nuclei are shown in blue (DAPI), white scale bar corresponds to 20 µm c) Zoom on an isolated cell evidences the internalization of the fluorescent particles. White scale bar corresponds to 10 µm.

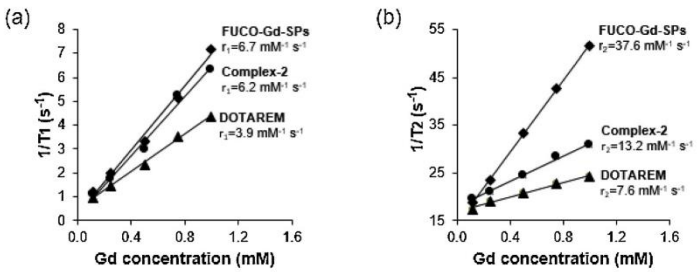

Fig. 3. a) Longitudinal (r_1) and b) transversal (r_2) relaxation rates *vs.* Gd^{3+} concentration for DOTAREM, Complex-2 and FUCO-Gd-SPs at 7 Tesla. The solid lines represent the linear regression of the data. The slopes of the curves corresponding to relaxivity (r_1 or r_2) are indicated. Longitudinal and transversal proton relaxivities of FUCO-Gd-SPs were 1.7 and 5.0 times higher than those of DOTAREM.

That is, its ability to accelerate longitudinal ($1/T_1$) or transversal ($1/T_2$) relaxation rates of the protons of hydrogen atoms from the surrounding water molecules (Jacques et al., 2010). Relaxometric properties of Complex-2 and FUCO-Gd-SPs were assessed *in vitro* on agarose phantoms at 7 Tesla. Commercially available contrast agent DOTAREM (containing free Gd(DOTA) complex) was used for comparison. Relaxation times, T_1 and T_2, were measured at a concentration range of 0.12–1 mM of chelated Gd^{3+}. The relaxivities r_1 and r_2 were then calculated from the linear regression slope of $1/T_1$ and $1/T_2$ *vs.* Gd^{3+} concentration and are depicted in Fig. 3. When Gd(DOTA) complex was attached to the dextran backbone of macromolecular Complex-2 or to the polysaccharide matrix of FUCO-Gd-SPs, both r_1 and r_2 relaxivities were enhanced with respect to DOTAREM. This effect was more pronounced in the case of FUCO-Gd-SPs with about twofold and fivefold increase in r_1 and r_2, respectively. As previously observed for other macromolecular or nanoparticulate contrast agents (Courant et al., 2012; Fransen et al., 2015; Huang et al., 2016), this relaxation rate enhancement can be ascribed to the restriction of the rotational motion of Gd(DOTA) complex inside polysaccharide matrix. In addition, the highly hydrated nature of FUCO-Gd-SPs network, would enhance Gd-water molecule interactions and favor the transfer of magnetic effect to the bulk water (Courant et al., 2012;)(De Sarno et al., 2019).

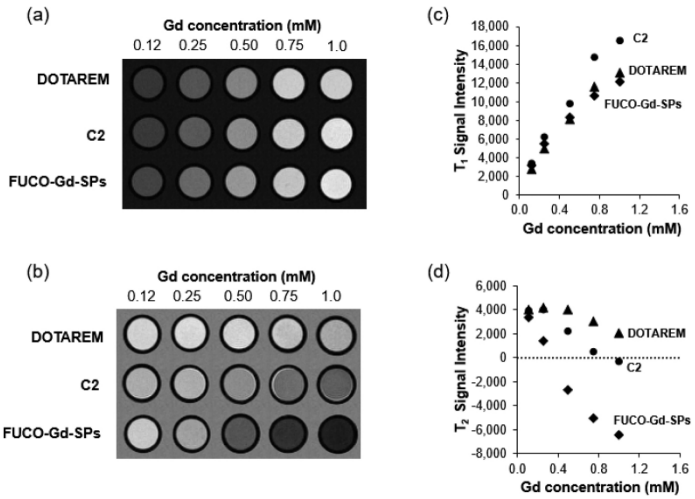

Fig. 4. a) T_1 and b) T_2 weighted MRI acquisitions at 7 Tesla of DOTAREM, Complex-2 and FUCO-Gd-SPs phantoms (agarose 2% (w/v)) used for relaxivity calculations. Background corresponds to control (agarose gel with no Gd). Relative c) T_1 and d) T_2 weighted signal intensities *versus* Gd concentration. FUCO-Gd-SPs showed enhanced negative contrast effect compared to DOTAREM.

In order to check how the relaxometric properties translated in image contrast, the signal intensity of both T_1 and T_2-weighted images (Fig. 4a–b) was as well quantified. While T_1-enhancing agents result in positive/brighter contrast, T_2 ones give predominantly negative/dark contrast. As shown in Fig. 4c, positive contrast properties of FUCO-Gd-SPs were comparable to those of DOTAREM. However, FUCO-Gd-SPs appear to be a better negative contrast agent in agreement with their significant higher r_2 relaxivity (Fig. 4d). Indeed, a signal void was present at high concentrations of Gd^{3+} (Fig. 4b).

3.5. Targeting properties

The binding capacity of Gd-SPs and FUCO-Gd-SPs for P-selectin expressed onto the surface of human activated platelets was assessed by flow cytometry in three conditions: platelet-rich plasma (PRP), PRP with TRAP-activated platelets, and PRP with TRAP-activated platelets after blocking P-selectin with a specific antibody (anti-CD62 P). As shown on Fig. 5a, FITC-labeled FUCO-Gd-SPs strongly bound to activated platelets in absence of the antibody, in agreement with the expression level of P-selectin in each condition (Fig. S5). These results proved both the availability of some fucoidan chains at the surface of the polysaccharide matrix for interacting with P-selectin on activated platelets and the specificity of the interaction between fucoidan-functionalized SPs and P-selectin.

The binding of Gd-SPs and FUCO-Gd-SPs to platelet aggregates under arterial blood flow conditions was evaluated as well (Fig. 5b). Experiments were performed in a flow chamber mimicking arterial blood flow conditions (wall shear stress of 67.5 dyn/cm^2) on activated platelet aggregates. FUCO-Gd-SPs (TRITC labeled) significantly accumulated at the surface of the aggregates whereas Gd-SPs showed almost no binding. Moreover, FUCO-Gd-SPs remained attached even after washing with 0.9% NaCl at arterial shear rate. These results confirmed the targeting ability of fucoidan-functionalized SPs under dynamic physiological conditions.

4. Discussion

The driven idea of the approach presented here was to prepare a new diagnostic platform with the potential for Health agencies approval and human use. That's why we used non-harmful, biocompatible and biodegradable materials as both final particle constituents and preparation process raw materials. STMP was for instance preferred over conventional glutaraldehyde, a crosslinker with documented cytotoxicity (;)(Oryan et al., 2018)(Reddy et al., 2015). Biocompatible vegetable oil was, for its part, chosen as emulsion continuous phase instead of commonly used organic solvents. This choice supposed a challenge for the obtention of smaller particles as a highly viscous polysaccharide aqueous phase needed to be dispersed in a viscous oily phase. Reducing the size of our previous micrometric polysaccharide particles (Bonnard et al., 2014) to submicronic range, required the optimization of several processing parameters including vegetable oil and surfactant type, polysaccharide molecular weight and concentration, and so on. We obtained a final size of about 800 nm far above 100 nm widely admitted as a limit to efficiently avoid a rapid clearance from the reticuloendothelial system (RES). In previous studies we have evidenced *in vivo* interaction of fucoidan-bearing microparticule of 2.5 µm with aneurysmal thrombi (Bonnard et al., 2014; Li et al., 2017). Another key-parameter to limit the risk of quick RES uptake is the nature of the surface (De Jong & Borm, 2008). A polysaccharide coating may provide steric protection against protein adsorption (more particularly opsonins) and early macrophage uptake ()(Lemarchand et al., 2004). Anyway, the biological responses and biodistribution of our submicronic particles remained to be investigated *in vivo*. Additional process optimization could further reduce, if needed, particle size.

Encapsulation of Gd-based contrast agents into polysaccharide nanoparticles have already been approached in three ways: by conjugation with polysaccharide precursor (Huang et al., 2008; Kim et al., 2015; Na et al., 2016; Nam et al., 2010; Payne et al., 2017; Zhang et al., 2015), by ionic trapping during particles preparation (Gheran et al., 2018; Huang et al., 2008; Podgórna et al., 2017; Rigaux et al., 2017), or by post-modification of particles surface (Chan et al., 2015). Nevertheless, Huang et al. demonstrated that Gd^{3+} ionically trapped into chitosan/dextran sulfate polyelectrolytes (PECs) is rapidly released after one day of incubation in PBS at 37 °C. In contrast, no release was detectable from Gd(DTPA)-grafted PECs under the same conditions during at least 6 days. Besides limiting the potential toxicity of free Gd ions, grafting of Gd-chelates to polysaccharide offers also the possibility to adjust Gd-cargo during particles synthesis. Herein, we gave the

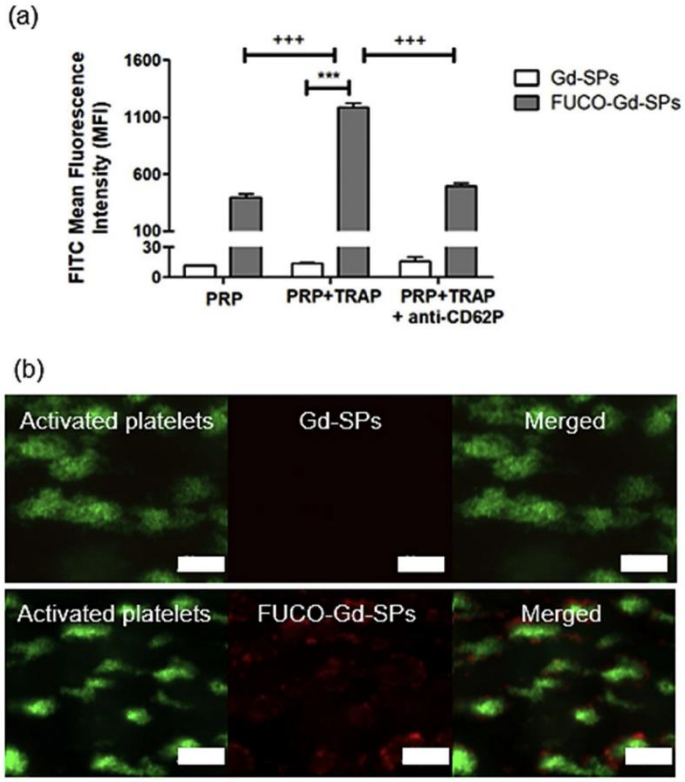

Fig. 5. a) Flow cytometry assessment of interactions of FITC-labeled Gd-SPs and FITC-labeled FUCO-Gd-SPs with either non-activated platelet-rich plasma (PRP), PRP activated with TRAP (PRP + TRAP) and PRP activated with TRAP and blocked with P-selectin antibody (PRP + TRAP + anti-CD62P) (Li et al., 2017). The mean fluorescence intensity (MFI) on the FITC channel was measured for 10,000 events of PE-Cy5 labeled platelets at a particles concentration of 10 mg/mL (n = 3; ***p < 0.001). b) Evaluation of FUCO-Gd-SPs binding on activated platelets under arterial flow conditions (Juenet et al., 2018; Li et al., 2017). Human whole blood labeled with $DiOC_6$ (green) was injected into a collagen-coated microchannel to get platelets aggregates expressing P-selectin (left images). TRITC-labeled particles (red) were then injected during 5 minutes (middle images). Channels were washed with 0.9% NaCl after each step. Particles and platelets aggregates co-localization was evaluated by merged fluorescence microscopy (right images). Gd-SPs (without fucoidan) were used as control. White scale bar corresponds to 50 μm.

priority to the well-known and already clinically approved Gd(DOTA) complex. Gd(DOTA) was conjugated to an aminated dextran via a carbodiimide reaction and the resultant macrocomplexes were employed to synthesize both Gd-SPs and FUCO-Gd-SPs via the optimized emulsion-crosslinking method. By doing so, Gd(DOTA) groups were successfully incorporated to the designed platform conferring it dual positive and enhanced negative contrast properties (r_1 = 6.7 mM^{-1} s^{-1} and r_2 = 37.6 mM^{-1} s^{-1} at 7 T). Similar relaxation rates (r_1 = 5.4 mM^{-1} s^{-1} and r_2 = 36.4 mM^{-1} s^{-1}) were observed under the same magnetic field for self-assembled chitosan nanogels post-modified with Gd (DOTA) moieties (Chan et al., 2015). Increasing Gd cargo per particle would be particularly interesting to eventually improve T_1 relaxometric properties and decrease necessary doses for patients. This would probably require the optimization of the current dextran modification protocol or the implementation of another chemistry route leading to chemical bonds less sensitive to degradation in basic media. It is worth noting that our imaging strategy is not only based on the contrast properties of the resulting SPs but also on their biospecificity. Low molecular weight fucoidan employed here as targeting agent recently passed preclinical evaluation as radiotracer for *in vivo* detection of cardiovascular pathologies (Chauvierre et al., 2019), and early stages of Phase I and Phase II clinical trials for its safety and validation of its ability to detect acute thrombosis in patients with suspected acute deep vein thrombosis are ongoing. Preferential accumulation of fucoidan-functionalized SPs onto thrombosed areas can be expected because of their binding affinity to activated platelets. This should rise the local concentration of contrast agent and increase thrombus imaging sensitivity of the FUCO-Gd-SPs compared to the commercial and non-biospecific DOTAREM at the same Gd dose.

5. Conclusions

Early detection of atherothrombotic lesions remains a big medical challenge. In this work, we developed novel biospecific polysaccharide submicronic particles containing Gd-based MR contrast agent. First, Gd (DOTA) moieties were successfully conjugated to dextran. The resulting macrocomplexes were then used to prepared Gd-loaded and fucoidan-functionalized particles by an emulsion-crosslinking method. This method was solvent-free in both production and purification steps. Particles exhibited good colloidal stability and were cytocompatible with human endothelial cells. The affinity of fucoidan-bearing particles for human activated platelets was evidenced under static and dynamic conditions. The particles exhibited good MR contrast properties with a significant signal enhancement of T_2-weighted images when compared to DOTAREM. These results indicated their high potential as a diagnostic probe for molecular imaging of atherothrombosis by MRI. As a next step, the biospecificity of the particles and their capacity to image atherothrombosis will be checked *in-vivo* in experimental models of the disease.

Credit authorship contribution statement

Laura Marcela Forero Ramirez: Conceptualization, Investigation, Methodology, Formal analysis, Writing - original draft. **Elise Gobin:** Investigation. **Rachida Aid-Launais:** Investigation, Methodology. **Clément Journe:** Investigation, Methodology. **Fernanda C. Moraes:** Investigation, Methodology. **Luc Picton:** Conceptualization, Validation, Writing - review & editing. **Didier Le Cerf:** Conceptualization, Validation, Resources. **Didier Letourneur:** Conceptualization, Validation, Funding acquisition. **Cédric Chauvierre:** Conceptualization, Validation, Resources, Writing - review & editing. **FrédéricChaubet:** Conceptualization, Project administration, Funding acquisition, Supervision, Writing - review & editing.

CRediT authorship contribution statement

Laura Marcela Forero Ramirez: Conceptualization, Investigation, Methodology, Formal analysis, Writing - original draft. **Elise Gobin:** Investigation. **Rachida Aid-Launais:** Investigation, Methodology. **Clément Journe:** Investigation, Methodology. **Fernanda C. Moraes:** Investigation, Methodology. **Luc Picton:** Conceptualization, Validation, Writing - review & editing. **Didier Le Cerf:** Conceptualization, Validation, Resources. **Didier Letourneur:** Conceptualization, Validation, Funding acquisition. **Cédric Chauvierre:** Conceptualization, Validation, Resources, Writing - review & editing. **Frédéric Chaubet:** Conceptualization, Project administration, Funding acquisition, Supervision, Writing - review & editing.

Acknowledgments

The authors express their highest gratitude to Murielle Maire (LVTS, Villetaneuse, France) for fucoidan content determination, to Alina Zenych (LVTS, Paris, France) for some preliminary experiments, to Christine Choqueux (LVTS, Paris, France) and UTC (Compiègne, France) for SEM images, to Samira Benadda and CRI U1149 imaging facilities for confocal imaging training and to Stéphane Loyau and Kevin Guedj (LVTS, Paris, France) for flow cytometry experiment design and data analysis. We also thanks Rémi Le Borgne from the ImagoSeine facility (Jacques Monod Institute Paris, France), and the France BioImaging infrastructure supported by the French National Research Agency (ANR-10-INSB-04, « Investments fit the future ») for their precious help with TEM images.

This work was supported by INSERM, Université de Paris, Université Sorbonne Paris Nord and UMS34 FRIM, and received the financial support of the ANR-16-CE18-0031NANOPACT.

Appendix A. Supplementary data

Supplementary material related to this article can be found, in the online version, at doi:https://doi.org/10.1016/j.carbpol.2020.116457.

REFERENCES

Abed, A., Assoul, N., Ba, M., Derkaoui, S. M., Portes, P., Louedec, L., et al. (2011). Influence of polysaccharide composition on the biocompatibility of pullulan/dextran-based hydrogels. *Journal of Biomedical Materials Research Part A, 96A*(3), 535–542. https://doi.org/10.1002/jbm.a.33007.

Abir, F., Barkhordarian, S., & Sumpio, B. E. (2004). Efficacy of Dextran Solutions in Vascular Surgery. *Vascular and Endovascular Surgery, 38*(6), 483–491. https://doi.org/10.1177/153857440403800601.

Amirbekian, V., Lipinski, M. J., Briley-Saebo, K. C., Amirbekian, S., Aguinaldo, J. G. S., Weinreb, D. B., et al. (2007). Detecting and assessing macrophages in vivo to evaluate atherosclerosis noninvasively using molecular MRI. *Proceedings of the National Academy of Sciences, 104*(3), 961–966. https://doi.org/10.1073/pnas.0606281104.

Antoniou, E., & Tsianou, M. (2012). Solution properties of dextran in water and in formamide. *Journal of Applied Polymer Science, 125*(3), 1681–1692. https://doi.org/10.1002/app.35475.

Bachelet, L., Bertholon, I., Lavigne, D., Vassy, R., Jandrot-Perrus, M., Chaubet, F., et al. (2009). Affinity of low molecular weight fucoidan for P-selectin triggers its binding to activated human platelets. *Biochimica et Biophysica Acta (BBA) - General Subjects, 1790*(2), 141–146. https://doi.org/10.1016/j.bbagen.2008.10.008.

Barkhausen, J., Ebert, W., Heyer, C., Debatin, J. F., & Weinmann, H.-J. (2003). Detection of Atherosclerotic Plaque With Gadofluorine-Enhanced Magnetic Resonance Imaging. *Circulation, 108*(5), 605–609. https://doi.org/10.1161/01.CIR.0000079099.36306.10.

Bonnard, T., Serfaty, J.-M., Journé, C., Ho Tin Noe, B., Arnaud, D., Louedec, L., et al. (2014). Leukocyte mimetic polysaccharide microparticles tracked in vivo on activated endothelium and in abdominal aortic aneurysm. *Acta Biomaterialia, 10*(8), 3535–3545. https://doi.org/10.1016/j.actbio.2014.04.015.

Briley-Saebo, K. C., Shaw, P. X., Mulder, W. J. M., Choi, S.-H., Vucic, E., Aguinaldo, J. G. S., et al. (2008). Targeted Molecular Probes for Imaging Atherosclerotic Lesions With Magnetic Resonance Using Antibodies That Recognize Oxidation-Specific Epitopes. *Circulation, 117*(25), 3206–3215. https://doi.org/10.1161/CIRCULATIONAHA.107.757120.

Cai, K., Caruthers, S. D., Huang, W., Williams, T. A., Zhang, H., Wickline, S. A., et al. (2010). MR Molecular Imaging of Aortic Angiogenesis. *JACC: Cardiovascular Imaging, 3*(8), 824–832. https://doi.org/10.1016/j.jcmg.2010.03.012.

Chan, M., Lux, J., Nishimura, T., Akiyoshi, K., & Almutairi, A. (2015). Long-Lasting and Efficient Tumor Imaging Using a High Relaxivity Polysaccharide Nanogel Magnetic Resonance Imaging Contrast Agent. *Biomacromolecules, 16*(9), 2964–2971. https://doi.org/10.1021/acs.biomac.5b00867.

Caravan, P., Ellison, J. J., McMurry, T. J., & Lauffer, R. B. (1999). Gadolinium(III) Chelates as MRI Contrast Agents: Structure, Dynamics, and Applications. *Chemical Reviews, 99*(9), 2293–2352. https://doi.org/10.1021/cr980440x.

Chauvierre, C., Aid-Launais, R., Aerts, J., Chaubet, F., Maire, M., Chollet, L., et al. (2019). Pharmaceutical Development and Safety Evaluation of a GMP-Grade Fucoidan for Molecular Diagnosis of Cardiovascular Diseases. *Marine Drugs, 17*(12), 699. https://doi.org/10.3390/md17120699.

Chollet, L., Saboural, P., Chauvierre, C., Villemin, J.-N., Letourneur, D., & Chaubet, F. (2016). Fucoidans in Nanomedicine. *Marine Drugs, 14*(8), 145. https://doi.org/10.3390/md14080145.

Corti, R., & Fuster, V. (2011). Imaging of atherosclerosis: magnetic resonance imaging. *European Heart Journal, 32*(14), 1709–1719. https://doi.org/10.1093/eurheartj/ehr068.

Courant, T., Roullin, V. G., Cadiou, C., Callewaert, M., Andry, M. C., Portefaix, C., et al. (2012). Hydrogels Incorporating GdDOTA: Towards Highly Efficient Dual T1/T2 MRI Contrast Agents. *Angewandte Chemie International Edition, 51*(36), 9119–9122. https://doi.org/10.1002/anie.201203190.

De Jong, W. H., & Borm, P. J. A. (2008). Drug delivery and nanoparticles: Applications and hazards. *International Journal of Nanomedicine, 133*. https://doi.org/10.2147/IJN.S596.

De Nooy, A. E. J., Rori, V., Masci, G., Dentini, M., & Crescenzi, V. (2000). Synthesis and preliminary characterisation of charged derivatives and hydrogels from scleroglucan. *Carbohydrate Research, 324*(2), 116–126. https://doi.org/10.1016/S0008-6215(99)00286-4.

De Sarno, F., Ponsiglione, A. M., Grimaldi, A. M., Netti, P. A., & Torino, E. (2019). Effect of crosslinking agent to design nanostructured hyaluronic acid-based hydrogels with improved relaxometric properties. *Carbohydrate Polymers, 222*, 114991. https://doi.org/10.1016/j.carbpol.2019.114991.

Dulong, V., Forbice, R., Condamine, E., Le Cerf, D., & Picton, L. (2011). Pullulan–STMP hydrogels: a way to correlate crosslinking mechanism, structure and physicochemical properties. *Polymer Bulletin, 67*(3), 455–466. https://doi.org/10.1007/s00289-010-0435-2.

Feng, X., Xia, Q., Yuan, L., Yang, X., & Wang, K. (2010). Impaired mitochondrial function and oxidative stress in rat cortical neurons: Implications for gadolinium-induced neurotoxicity. *NeuroToxicology, 31*(4), 391–398. https://doi.org/10.1016/j.neuro.2010.04.003.

Fransen, P., Pulido, D., Simón-Gracia, L., Candiota, A. P., Arús, C., Albericio, F., et al. (2015). r 1 and r 2 Relaxivities of Dendrons Based on a OEG-DTPA Architecture: Effect of Gd^{3+} Placement and Dendron Functionalization. *Journal of Nanotechnology, 2015*, 1–8. https://doi.org/10.1155/2015/848020.

Gheran, C., Rigaux, G., Callewaert, M., Berquand, A., Molinari, M., Chuburu, F., et al. (2018). Biocompatibility of Gd-Loaded Chitosan-Hyaluronic Acid Nanogels as Contrast Agents for Magnetic Resonance Cancer Imaging. *Nanomaterials, 8*(4), 201. https://doi.org/10.3390/nano8040201.

Herrington, W., Lacey, B., Sherliker, P., Armitage, J., & Lewington, S. (2016). Epidemiology of Atherosclerosis and the Potential to Reduce the Global Burden of Atherothrombotic Disease. *Circulation Research, 118*(4), 535–546. https://doi.org/10.1161/CIRCRESAHA.115.307611.

Huang, M., Huang, Z. L., Bilgen, M., & Berkland, C. (2008). Magnetic resonance imaging of contrast-enhanced polyelectrolyte complexes. *Nanomedicine: Nanotechnology, Biology and Medicine, 4*(1), 30–40. https://doi.org/10.1016/j.nano.2007.10.085.

Huang, Y., Cao, J., Zhang, Q., Lu, Z., Hua, M., Zhang, X., et al. (2016). Chitosan oligosaccharide based Gd-DTPA complex as a potential bimodal magnetic resonance imaging contrast agent. *Magnetic Resonance Imaging, 34*(1), 1–7. https://doi.org/10.1016/j.mri.2015.10.006.

Jacques, V., Dumas, S., Sun, W.-C., Troughton, J. S., Greenfield, M. T., & Caravan, P. (2010). High-Relaxivity Magnetic Resonance Imaging Contrast Agents Part 2: Optimization of Inner- and Second-Sphere Relaxivity. *Investigative Radiology, 45*(10), 613–624. https://doi.org/10.1097/RLI.0b013e3181ee6a49.

Juenet, M., Aid-Launais, R., Li, B., Berger, A., Aerts, J., Ollivier, V., et al. (2018). Thrombolytic therapy based on fucoidan-functionalized polymer nanoparticles targeting P-selectin. *Biomaterials, 156*, 204–216. https://doi.org/10.1016/j.biomaterials.2017.11.047.

Kim, K. S., Park, W., & Na, K. (2015). Gadolinium-chelate nanoparticle entrapped human

mesenchymal stem cell via photochemical internalization for cancer diagnosis. *Biomaterials, 36*, 90–97. https://doi.org/10.1016/j.biomaterials.2014.09.014.
Kuo, P. H., Kanal, E., Abu-Alfa, A. K., & Cowper, S. E. (2007). Gadolinium-based MR Contrast Agents and Nephrogenic Systemic Fibrosis. *Radiology, 242*(3), 647–649. https://doi.org/10.1148/radiol.2423061640.
Lack, S., Dulong, V., Picton, L., Cerf, D. L., & Condamine, E. (2007). High-resolution nuclear magnetic resonance spectroscopy studies of polysaccharides crosslinked by sodium trimetaphosphate: a proposal for the reaction mechanism. *Carbohydrate Research, 342*(7), 943–953. https://doi.org/10.1016/j.carres.2007.01.011.
Leiner, T., Gerretsen, S., Botnar, R., Lutgens, E., Cappendijk, V., Kooi, E., et al. (2005). Magnetic resonance imaging of atherosclerosis. *European Radiology, 15*(6), 1087–1099. https://doi.org/10.1007/s00330-005-2646-8.
Lemarchand, C., Gref, R., & Couvreur, P. (2004). Polysaccharide-decorated nanoparticles. *European Journal of Pharmaceutics and Biopharmaceutics, 58*(2), 327–341. https://doi.org/10.1016/j.ejpb.2004.02.016.
Li, B., Juenet, M., Aid-Launais, R., Maire, M., Ollivier, V., Letourneur, D., et al. (2017). Development of Polymer Microcapsules Functionalized with Fucoidan to Target P-Selectin Overexpressed in Cardiovascular Diseases. *Advanced Healthcare Materials, 6*(4), 1601200. https://doi.org/10.1002/adhm.201601200.
Li, D., Patel, A. R., Klibanov, A. L., Kramer, C. M., Ruiz, M., Kang, B.-Y., et al. (2010). Molecular Imaging of Atherosclerotic Plaques Targeted to Oxidized LDL Receptor LOX-1 by SPECT/CT and Magnetic Resonance. *Circulation: Cardiovascular Imaging, 3*(4), 464–472. https://doi.org/10.1161/CIRCIMAGING.109.896654.
Lino Ferreira, J. M. (2014). *Dextran-based materials for biomedical applications, 31-53.* M. H. Gil.
Liu, H., Yuan, L., Yang, X., & Wang, K. (2003).). La^{3+}, Gd^{3+} and Yb^{3+} induced changes in mitochondrial structure, membrane permeability, cytochrome c release and intracellular ROS level. *Chemico-Biological Interactions, 146*(1), 27–37. https://doi.org/10.1016/S0009-2797(03)00072-3.
Lozano, R., Naghavi, M., Foreman, K., Lim, S., Shibuya, K., Aboyans, V., et al. (2012). Global and regional mortality from 235 causes of death for 20 age groups in 1990 and 2010: a systematic analysis for the Global Burden of Disease Study 2010. *The Lancet, 380*(9859), 2095–2128. https://doi.org/10.1016/S0140-6736(12)61728-0.
McAteer, M. A., Akhtar, A. M., von zur Muhlen, C., & Choudhury, R. P. (2010). An approach to molecular imaging of atherosclerosis, thrombosis, and vascular inflammation using microparticles of iron oxide. *Atherosclerosis, 209*(1), 18–27. https://doi.org/10.1016/j.atherosclerosis.2009.10.009.
McEver, R. P. (2001). Adhesive interactions of leukocytes, platelets, and the vessel wall during hemostasis and inflammation. *Thrombosis and Haemostasis, 86*(3), 746–756.
Na, J. H., Lee, S., Koo, H., Han, H., Lee, K. E., Han, S. J., et al. (2016). T_1-Weighted MR imaging of liver tumor by gadolinium-encapsulated glycol chitosan nanoparticles without non-specific toxicity in normal tissues. *Nanoscale, 8*(18), 9736–9745. https://doi.org/10.1039/C5NR06673E.
Naessens, M., Cerdobbel, A., Soetaert, W., & Vandamme, E. J. (2005). Leuconostoc dextransucrase and dextran: production, properties and applications. *Journal of Chemical Technology & Biotechnology, 80*(8), 845–860. https://doi.org/10.1002/jctb.1322.
Nam, T., Park, S., Lee, S.-Y., Park, K., Choi, K., Song, I. C., et al. (2010). Tumor Targeting Chitosan Nanoparticles for Dual-Modality Optical/MR Cancer Imaging. *Bioconjugate Chemistry, 21*(4), 578–582. https://doi.org/10.1021/bc900408z.
Nguyen, T. N., Tinet, E., Ettori, D., Beilvert, A., Pavon-Djavid, G., Maire, M., et al. (2017). Gadolinium/terbium hybrid macromolecular complexes for bimodal imaging of atherothrombosis. *Journal of Biomedical Optics, 22*(7), 76004. https://doi.org/10.1117/1.JBO.22.7.076004.
Nikolovski, B. G., Ilić, J. D., & Sovilj, M. N. (2016). HOW TO FORMULATE A STABLE AND MONODISPERSE WATER-IN-OIL NANOEMULSION CONTAINING PUMPKIN SEED OIL: THE USE OF MULTIOBJECTIVE OPTIMIZATION. *Brazilian Journal of Chemical Engineering, 33*(4), 919–931. https://doi.org/10.1590/0104-6632.20160334s20140140.
Oryan, A., Kamali, A., Moshiri, A., Baharvand, H., & Daemi, H. (2018). Chemical crosslinking of biopolymeric scaffolds: Current knowledge and future directions of crosslinked engineered bone scaffolds. *International Journal of Biological Macromolecules, 107*, 678–688. https://doi.org/10.1016/j.ijbiomac.2017.08.184.
Payne, W. M., Hill, T. K., Svechkarev, D., Holmes, M. B., Sajja, B. R., & Mohs, A. M. (2017). Multimodal Imaging Nanoparticles Derived from Hyaluronic Acid for Integrated Preoperative and Intraoperative Cancer Imaging. *Contrast Media & Molecular Imaging, 2017*, 1–14. https://doi.org/10.1155/2017/9616791.
Podgórna, K., Szczepanowicz, K., Piotrowski, M., Gajdošová, M., Štěpánek, F., & Warszyński, P. (2017). Gadolinium alginate nanogels for theranostic applications. *Colloids and Surfaces B: Biointerfaces, 153*, 183–189. https://doi.org/10.1016/j.colsurfb.2017.02.026.
Raggi, P., Baldassarre, D., Day, S., de Groot, E., & Fayad, Z. A. (2016). Non-invasive imaging of atherosclerosis regression with magnetic resonance to guide drug development. *Atherosclerosis, 251*, 476–482. https://doi.org/10.1016/j.atherosclerosis.2016.06.028.
Reddy, N., Reddy, R., & Jiang, Q. (2015). Crosslinking biopolymers for biomedical applications. *Trends in Biotechnology, 33*(6), 362–369. https://doi.org/10.1016/j.tibtech.2015.03.008.
Rigaux, G., Gheran, C. V., Callewaert, M., Cadiou, C., Voicu, S. N., Dinischiotu, A., et al. (2017). Characterization of Gd loaded chitosan-TPP nanohydrogels by a multi-technique approach combining dynamic light scattering (DLS), asymetrical flow-field-flow-fractionation (AF4) and atomic force microscopy (AFM) and design of positive contrast agents for molecular resonance imaging (MRI). *Nanotechnology, 28*(5), 055705. https://doi.org/10.1088/1361-6528/aa5188.
Rogosnitzky, M., & Branch, S. (2016). Gadolinium-based contrast agent toxicity: a review of known and proposed mechanisms. *BioMetals, 29*(3), 365–376. https://doi.org/10.1007/s10534-016-9931-7.
Saboural, P., Chaubet, F., Rouzet, F., Al-Shoukr, F., Azzouna, R., Bouchemal, N., et al. (2014). Purification of a Low Molecular Weight Fucoidan for SPECT Molecular Imaging of Myocardial Infarction. *Marine Drugs, 12*(9), 4851–4867. https://doi.org/10.3390/md12094851.
Sannino, A., Brevetti, L., Giugliano, G., Scudiero, F., Toscano, E., Mainolfi, C., et al. (2014). Non-invasive vulnerable plaque imaging: how do we know that treatment works? *European Heart Journal - Cardiovascular Imaging, 15*(11), 1194–1202. https://doi.org/10.1093/ehjci/jeu097.
Schroeder, A. P., & Falk, E. (1995). Vulnerable and dangerous coronary plaques. *Atherosclerosis, 118*, S141–S149. https://doi.org/10.1016/0021-9150(95)90081-0.
Suzuki, M., Bachelet-Violette, L., Rouzet, F., Beilvert, A., Autret, G., Maire, M., et al. (2015). Ultrasmall superparamagnetic iron oxide nanoparticles coated with fucoidan for molecular MRI of intraluminal thrombus. *Nanomedicine, 10*(1), 73–87. https://doi.org/10.2217/nnm.14.51.
te Boekhorst, B. C., van Tilborg, G. A., Strijkers, G. J., & Nicolay, K. (2012). Molecular MRI of Inflammation in Atherosclerosis. *Current Cardiovascular Imaging Reports, 5*(1), 60–68. https://doi.org/10.1007/s12410-011-9114-4.
van Tilborg, G. A. F., Vucic, E., Strijkers, G. J., Cormode, D. P., Mani, V., Skajaa, T., et al. (2010). Annexin A5-Functionalized Bimodal Nanoparticles for MRI and Fluorescence Imaging of Atherosclerotic Plaques. *Bioconjugate Chemistry, 21*(10), 1794–1803. https://doi.org/10.1021/bc100091q.
Vananroye, A., Van Puyvelde, P., & Moldenaers, P. (2006). Effect of Confinement on Droplet Breakup in Sheared Emulsions. *Langmuir, 22*, 3972–3974. https://doi.org/10.1021/la060442+.
Waxman, S., Ishibashi, F., & Muller, J. E. (2006). Detection and Treatment of Vulnerable Plaques and Vulnerable Patients: Novel Approaches to Prevention of Coronary Events. *Circulation, 114*(22), 2390–2411. https://doi.org/10.1161/CIRCULATIONAHA.105.540013.
Yon, M., Billotey, C., & Marty, J.-D. (2019). Gadolinium-based contrast agents: From gadolinium complexes to colloidal systems. *International Journal of Pharmaceutics, 569*, 118577. https://doi.org/10.1016/j.ijpharm.2019.118577.
Zhang, L., Liu, T., Xiao, Y., Yu, D., & Zhang, N. (2015). Hyaluronic Acid-Chitosan Nanoparticles to Deliver Gd-DTPA for MR Cancer Imaging. *Nanomaterials, 5*(3), 1379–1396. https://doi.org/10.3390/nano5031379.
Zhao, J., Zhou, Z.-Q., Jin, J.-C., Yuan, L., He, H., Jiang, F.-L., et al. (2014). Mitochondrial dysfunction induced by different concentrations of gadolinium ion. *Chemosphere, 100*, 194–199. https://doi.org/10.1016/j.chemosphere.2013.11.031.
Zhou, Z., & Lu, Z.-R. (2013). Gadolinium-based contrast agents for magnetic resonance cancer imaging: Gadolinium-based CA for MR cancer imaging. *Wiley Interdisciplinary Reviews: Nanomedicine and Nanobiotechnology, 5*(1), 1–18. https://doi.org/10.1002/wnan.1198.

International Journal of Pharmaceutics 597 (2021) 120302

Contents lists available at ScienceDirect

International Journal of Pharmaceutics

journal homepage: www.elsevier.com/locate/ijpharm

P-selectin targeting polysaccharide-based nanogels for miRNA delivery

Fernanda C. Moraes [a,*], Laura Marcelo Forero Ramirez [a], Rachida Aid [a], Samira Benadda [b], Murielle Maire [a], Cédric Chauvierre [a], Joana C. Antunes [c,1], Frédéric Chaubet [a,1], Didier Letourneur [a]

[a] Université de Paris, LVTS, INSERM U1148, Université Sorbonne Paris Nord, F-75018 Paris, France
[b] Université de Paris, Centre de recherche sur l'inflammation, INSERM U1149, CNRS ERL8252, 75018 Paris, France
[c] Universidade do Minho, 2C2T, Campus de Azurém, 4800-058 Guimarães, Portugal

ARTICLE INFO

Keywords:
Pullulan
Fucoidan
Genipin
Nanogels
P-selectin
miRNA

ABSTRACT

Nanogels were prepared in aqueous media without the use of any organic solvent via a simple polyelectrolyte complexation method between aminated pullulan and fucoidan followed by covalent crosslinking with genipin. Homogeneously distributed genipin crosslinked nanogels (G-PECs) were obtained with a mean hydrodynamic diameter of ~155 nm and zeta potential of 0.86 ± 4.35 mV. Their capacity to bind to human activated platelets was evaluated *in vitro*, as well as their cytocompatibility within human endothelial cells after 1 day of incubation up to 1000 μg/mL of G-PECs (94.56 ± 7.82% of viable cells). Additional hemolysis tests support the biocompatible character of the developed nanosystems (hemolysis rate of 2.09 ± 0.06% for 1000 μg/mL of G-PECs). Under acid conditions, the surface charge of G-PECs was tuned to around ~10 mV allowing miRNA incorporation via electrostatic interactions. G-PECs were able to promote miRNA delivery inside cells, as demonstrated by fluorescence microscopy images of labelled miRNA. With further studies to demonstrate the biological activity of delivered miRNA, these nanogels could be an interesting platform for miRNA-based therapeutics in atherothrombotic-related diseases thanks to the possibility to target over-expressed P-selectin.

1. Introduction

In the past few years, small non-coding microRNAs (miRNAs) have emerged as key regulators of gene expression and are some of the most important biopharmaceuticals candidates as future medicines due to their multiple unique features and advantages when compared to conventional plasmid DNA (pDNA)-based therapy (Chakraborty et al., 2017; Xiong et al., 2018). RNA therapeutics do not have the risk of genomic integration, do not need to cross the nucleus membrane to their function, and are expressed instantaneously (Itani and Al Faraj, 2019; Patil et al., 2005; Uchida et al., 2020). They play important roles in many cellular processes and have been investigated as therapeutics and biomarkers for various diseases such as cancer, diabetes, cardiovascular diseases and other pathologies whose etiology is related to aberrant gene expression (Candido et al., 2019; Falzone et al., 2019; Gaur et al., 2015; Hou et al., 2012; Poddar et al., 2019; Zhu et al., 2019). However, unfavorable physicochemical features of miRNAs such as their anionic charge, sensitivity to nuclease degradation, and inefficient cellular uptake are major hindrances for their clinical application. The success of miRNA-based therapies relies on the development of suitable vehicles able to specifically target cells for the efficient delivery of the nucleic acid with minimum toxicity (Chakraborty et al., 2017; Singh et al., 2014).

Recently, nanogels have arised as a class of interesting polymeric

Abbreviations: miRNA, MicroRNA; pDNA, Plasmid DNA; siRNA, small interfering RNA; Mw, Weight average molecular weight; Mn, Number average molecular weight; EA-pullulan, ethylamine-pullulan; PECs, polyelectrolyte complexes; G-PECs, genipin-crosslinked polyelectrolyte complexes; 6-FAM, 6-Fluorescein amidite; RBITC, Rhodamine B isothiocyanate; SEC-MALLS, Size exclusion chromatography- multiangle laser light scattering; FTIR, Fourier-transform infrared spectroscopy; ^{1}H NMR, Proton nuclear magnetic resonance; Dimethyl sulfoxide, DMSO; TBE, Tris-Borate-EDTA; PdI, Polydispersity Index; HUVECs, Human umbilical vein endothelial cells; PBS, Phosphate buffered saline; DS, Degree of substitution; AGU, Anhydroglucose unit; DAPI, 4′,6-Diamidino-2-phenylindole.

* Corresponding author.
E-mail addresses: fernanda.moraes@inserm.fr (F.C. Moraes), lmforeror@gmail.com (L. Marcelo Forero Ramirez), rachida.aid@gmail.com (R. Aid), samira.benadda@inserm.fr (S. Benadda), murielle.maire@univ-paris13.fr (M. Maire), cedric.chauvierre@inserm.fr (C. Chauvierre), joana.antunes@2c2t.uminho.pt (J.C. Antunes), frederic.chaubet@univ-paris13.fr (F. Chaubet), didier.letourneur@inserm.fr (D. Letourneur).

[1] Equivalent work.

https://doi.org/10.1016/j.ijpharm.2021.120302
Received 21 December 2020; Received in revised form 18 January 2021; Accepted 19 January 2021
Available online 1 February 2021
0378-5173/© 2021 Elsevier B.V. All rights reserved.

materials for the delivery of biopharmaceuticals because of their hydrophilic three-dimensional macromolecular networks that allow a high loading capacity for hydrophilic biotherapeutics, protecting the loaded molecules against degradation. Additionally, they possess stimuli-responsive behavior potential and can participate in versatile drug release protocols (D. Li et al., 2017; Shatsberg et al., 2016; Zhang et al., 2018). Nanogels can either be composed of natural or synthetic polymers and may contain more than one type of polymer (Baipaywad et al., 2014). Cationic polymers are widely used in gene therapy applications since they form interpolyelectrolyte complexes with nucleic acids through ionic interactions with their negatively charged phosphate groups (Gao et al., 2015; Gaur et al., 2015; Safari et al., 2011; Zintchenko et al., 2008). Polymers derived from natural sources are preferable because they are naturally biocompatible, biodegradable and nontoxic, and can overcome the cytotoxicity associated with the use of several synthetic polymers, which do not satisfy the requirements for clinical applications.

Pullulan is a natural water-soluble homopolysaccharide produced by the fungus *Aureobasidium pullulans* considered as a promising material for biomedical applications such as drug/gene delivery and tissue engineering because of its inherent non-toxic, non-immunogenic, and biodegradable characters (Prajapati et al., 2013). Charged hydrophilic derivatives of pullulan provide the possibility to formulate nanoparticles via electrostatic interactions with oppositely charged materials of interest (dos Santos and Grenha, 2015). Electrostatic interactions between oppositely charged polymers are becoming an interesting alternative to produce nanogel systems. Since the polyelectrolyte complexation method can be performed in aqueous media, this process is environment-friendly and does not require the use of organic solvents which is interesting for pharmaceutical applications (Bourganis et al., 2017).

Cationic pullulan derivatives grafted with primary or tertiary amine groups were previously demonstrated to be able to form complexes with plasmid DNA as well as siRNA in cationized pullulan-based hydrogels (San Juan et al., 2009; 2007). In previous work from our group, we demonstrated the feasibility of quaternized cationic pullulan (QA-pullulan) nanosized polyelectrolyte complexes (PECs) for *in vitro* miRNA delivery (Moraes et al., 2020). To the best of our knowledge, it was the first time that QA-pullulan was used to build miRNA delivery nanosystems. However, in this study, the colloidal stability of the developed nanosystems in physiological conditions was not addressed. One of the major drawbacks associated with the use of PECs is the lack of stability in physiological conditions due to the presence of electrolytes and changes in pH values responsible for a decrease in the charge density of polyions (Wu and Delair, 2015). Especially with regard to *in vivo* applications, PECs stability becomes an even more important issue, as they face a much harsher environment in the blood circulation than in cell culture media (Fröhlich et al., 2012).

Chemical crosslinking is an effective approach to stabilize PECs upon the formation of permanent networks allowing the free diffusion of water and enhancing the mechanical properties of the nanogels (Berger et al., 2004). However, the majority of crosslinking agents used are synthetic reactants (e.g. glutaraldehyde) that are highly cytotoxic often impairing the biocompatibility of crosslinked products (Sung et al., 1999). Hence, many investigations have focused on finding suitable crosslinking agents for use in biomedical applications. Genipin is an alternative natural crosslinking agent extracted from the fruit of *Gardenia jasminoides* Ellis that is commonly used in herbal medicine and as a food dye (Berger et al., 2004; Hu et al., 2014; Yu et al., 2015). It can spontaneously react with materials containing primary amine groups, such as chitosan and some peptides and polypeptides, to form covalently crosslinked networks. Genipin is described to be 10,000 times less cytotoxic than glutaraldehyde being a great promise for the preparation of biocompatible crosslinked materials (Butler et al., 2003). A few researchers used genipin to crosslink chitosan nanoparticles improving their physical and chemical stability with good biocompatibility profile (Lin et al., 2013; Razi et al., 2018; Yu et al., 2015). To the best of our knowledge, no report of nanogel made from pullulan derivatives crosslinked with genipin exists.

Here we propose a simple drug delivery system based on two polyelectrolytes derived from naturally occurring, biocompatible polysaccharides, pullulan and fucoidan, which instantly and spontaneously self-assembly to form nanosized hydrogels. A cationic pullulan derivative was first obtained by grafting primary amine groups. The addition of genipin produced nanosized hydrogels with high colloidal stability. Then, their functionalization with fucoidan confered them the ability to target P-selectin, an adhesion molecule over-expressed at the surface of activated platelets and endothelial cells in atherothrombotic-related diseases (Bachelet et al., 2009). The capacity of these novel polysaccharide-based PECs to cargo nucleic acids, in particular miRNA, into endothelial cells was investigated.

2. Materials and methods

2.1. Materials

Pullulan (Mw 200 kg/mol) was purchased from Hayashibara Company (Okayama, Japan). 2-chloro-ethylamine hydrochloride (Mw 115.99 g/mol) was purchased from Sigma-Aldrich (St. Louis, MO, USA). Fucoidan low molecular weight (Mw 7 kg/mol) was a gift from Algues & Mer (île d'Ouessant, France). Carboxymethyl-dextran (Mw 10 kg/mol) was purchased from Sigma-Aldrich (St. Louis, MO, USA). Genipin (CAS number 6902-77-8) was purchased from TCI chemicals (Chennai, Tamilnadu, India). Dialysis membranes of 20 kDa was purchased from Spectrum Laboratories (New Brunswick, NJ, USA). Chemically modified, double-stranded RNA oligonucleotides from Qiagen were used to mimic the natural human mature microRNA miR-155-5p (miRNA sequence: 5′-UUA AUG CUA AUC GUG AUA GGG GU-3′). Single-stranded miRNA and 6-Fluorescein AMidite (6-FAM)-miRNA scramble oligonucleotides with 23 bp of length (RNA sequence: 5′-UUA AUG CUA AUC GUG AUA GGG GU-3′) were purchased from Sigma-Aldrich (Saint Quentin Fallavier, France). Sequences were reconstituted in RNase-free water to achieve a final concentration of 20 μM and stock solutions were stored at −20 °C. Ultrapure water was prepared by ion-exchange of running tap water (Millipore, France).

2.2. Synthesis of cationic pullulan derivatives

Pullulan (1 g) was dissolved in 5 mL of distilled water. The solution was placed at 4 °C until complete solubilisation of pullulan. Then, 5 mL of soda (6.2 M NaOH) was added to activate the hydroxyl functions. The solution was kept at 4 °C under magnetic stirring for 20 min followed by the addition of 1.43 g of 2-chloro-ethylamine hydrochloride (2 equivalents per AGU). The solution was placed under magnetic stirring at 55 °C for 3 h. The mixture was placed at room temperature and the pH was adjusted to 7 with 37% hydrochloric acid (HCl) solution. The mixture was dialyzed with a 20 kg/mol membrane and freeze-dried before characterization. Final product was named as ethylamine- pullulan (EA-pullulan).

2.3. Synthesis of fluorescent cationic pullulan

Ethylamine-pullulan (500 mg) was dissolved in anhydrous DMSO. Few drops of pyridine were added, followed by the addition of 500 μL of Rhodamine B isothiocyanate (RBITC) solution (100 mg RBITC dissolved in 1 mL of DMSO) and 10 μL of dibutyltin dilaureate. The reaction was performed for 2 h at 95 °C under inert atmosphere using nitrogen. The grafted polysaccharide was recovered by cooled precipitation (4 °C) in absolute ethanol. Final product was freeze-dryer before use.

2.4. Chemical characterization of modified pullulan

2.4.1. Elemental analysis

The weight percentages of N of pullulan and cationic pullulan derivatives were determined using a combustion method with catharometric detection (CHNS Vario EL III, Elementar Analyzer). Degree of substitution of primary amine groups was estimated by elemental analysis of nitrogen.

2.4.2. Size exclusion chromatography equipped with multi-angle light scattering (SEC-MALS)

Apparent molecular weight-average (M_w) and number-average molecular weight (M_n) were determined by size exclusion chromatography (SEC) coupled online to a multiangle laser light scattering (MALLS) detector. The SEC line consisted of an TSK-Gel PW_{XL} Guardcolumn and TSK-Gel $GMPW_{XL}$ in series (Tosoh Bioscience, Stuttgart, Germany). The eluent was 0.2 M $NaNO_3$ containing 0.02% w/v NaN_3 at 0.5 mL/min flow rate. The samples were dissolved in the eluent at a concentration of 10 mg/mL. The dn/dc used in the molecular weight distribution calculations were 0.14. The collected data were analysed using the software Astra V-4.81.05.

2.4.3. NMR spectroscopy

^{1}H- NMR spectra was recorded with a Bruker-400 Ultrashield operating at 400 MHz. Polymers samples were prepared in D_2O in a concentration of 20 mg/mL.

2.5. Synthesis of polyelectrolyte complexes and crosslinked nanoparticles

Cationic pullulan derivatives containing primary amine groups (EA-pullulan) were dissolved in 1% acetic acid at a final concentration of 1.0 mg/mL and the pH of the solution was adjusted to pH 5 using 10 M NaOH. Low molecular weight fucoidan was dissolved in distillated water at 0.25 mg/mL. Polyelectrolyte complexes (PECs) were produced by dropping 2 mL of fucoidan over 2 mL of EA-pullulan under high magnetic stirring at room temperature. Crosslinked PECs (G-PECs) were produced by adding 1 mL of genipin at 1.25 mg/mL to polyelectrolyte solution. The mixture was placed under moderate magnetic stirring (250 rpm) for 48 h at room temperature. G-PECs were recovered by ultracentrifugation at 15000*g* during 20 min at 21 °C.

2.6. Characterization of crosslinked nanoparticles

2.6.1. Size and zeta potential measurements

Particle size and zeta potential of nanoparticles were measured by Dynamic Light Scattering (DLS) and Electrophoretic Light Scattering (ELS) using a Zetasizer Nano-ZS (Malvern Instruments, Malvern, UK) respectively. Size and zeta potential measurements were performed at 25 °C using a 173° and 13° scattering angle for size and zeta potential measurements, respectively, equipped with a 4 mW HeNe laser beam with a wavelength of 633 nm. Size and ζ potential values were automatically calculated through the software DTS Nano v.6.30 (Malvern, UK) using the Stokes-Einstein equation and the Henry equation with the Smoluchowski approximation, respectively. Size measurements were performed in water using disposable polystyrene cuvettes and zeta potential measurements were performed in 1 mM KCl solution using a DTS1070-folded capillary cell (ELS, Malvern, UK). Data were acquired in triplicate.

2.6.2. Nanoparticles concentration

Nanoparticle concentration was assessed by Tunable Resistive Pulse Sensing (TRPS). TRPS technology measures nanoparticles suspended in electrolytes on a particle-by-particle basis as they pass through a nanopore. To perform TRPS analysis nanoparticles were isolated by ultracentrifugation and redispersed in 0.9% NaCl.

2.6.3. Morphology

Transmission Electron Microscopy and Environmental Scanning Electron Microscopy were employed to assess the morphology of crosslinked PECs.

Transmission Electron Microscope (TEM) was performed in a Tecnai 12 (80 kV; FEI; Hillsboro, OR, USA) with a 1 K × 1 K KeenView camera (OSiS). Samples were prepared by placing 3 μL of G-PECs suspension onto a 400 μL mesh copper grid coated with carbon (EMS). Uranyl acetate 1% (w/v) was used for negative staining.

Environmental Scanning Electron Microscopy (ESEM) was performed using a Philips XL30 ESEM-FEG (Amsterdam, The Netherlands) in aqueous media with no special sample preparation.

2.6.4. Fourier transform infrared spectroscopy (FTIR)

FTIR spectroscopy was carried out with KBr pellets on a Thermo-Nicolet-AVATAR 370 FTIR (Thermo Electron Corporation, Waltham, MA). A first pellet with 200 mg of KBr was prepared. Then, pellets were made using 200 mg KBr and 2 mg of sample. A 32-scan interferogram was collected in transmittance mode. Scans were taken from 400 cm^{-1} to 4000 cm^{-1} at a resolution of 2 cm^{-1}. The spectrum of KBr pellet was used as background.

2.6.5. Swelling behavior

The swelling behavior of nanoparticles was determined by incubating them in either NaCl 0.9%, PBS 1x or distilled water, solutions with different ionic strengths. Their hydrodynamic diameter was measured by DLS.

2.6.6. Stability of nanoparticles

The stability of crosslinked polyelectrolyte complexes was evaluated over time while stored at 4 °C in water or 0.9% NaCl solution. Size, PdI (Polydispersity Index) and surface charge evolutions were monitored by DLS and ELS (n = 3) at each time point up to 28 days of storage.

2.6.7. Freeze-drying nanoparticles

With the aim of developing a pharmaceutically acceptable dry form of the nanoparticle suspensions, nanoparticles were submitted to a freeze-drying study. Samples were freeze-dried in MUT (Cryotec®) in three steps. First, samples were frozen until −20 °C at −0.1 °C/min. Then, the primary drying was performed under 5 Pa and gradually increasing of temperature in two phases until reaches 10 °C (+0.1 °C/min until −5°C during 8 h and +0.2 °C/min until 10 °C during 4 h). Finally, secondary drying was performed at 25 °C and 0.1 Pa for at least 1 h. After the freeze-drying procedure, nanoparticles were resuspended by adding the volume of water corresponding to the initial volume of nanoparticles (1 mL), and their size was assessed by DLS measurements.

2.6.8. Cytotoxicity assays

Cytotoxicity was evaluated on Human Umbilical Vein Endothelial Cells (HUVECs, ATCC CRL-1730, Manassas, VA, USA) passage 17 (P17) by resazurin conversion assay (Sigma-Aldrich, Saint Louis, MO, USA). Cells were seeded at a concentration of 10,000 cells/well onto 96-well plates in Dulbecco's Modified Eagle Medium (DMEM) (Thermo Fisher Scientific, Carlsbad, CA, USA) supplemented with 10% (v/v) of fetal bovine serum, 1% (v/v) of penicillin and 1% (v/v) of streptomycin in a humidified atmosphere with 5% CO_2 at 37 °C. At a subconfluent to confluent stage, cells were detached with 0.05% trypsin/EDTA (Gibco) and re-seeded until the required number of cells for the subsequent experiments was obtained. Cell metabolic activity was assessed after different culture conditions by resazurin conversion. Cells were incubated with medium containing 10% resazurin for 2 h at 37 °C. Fluorescence intensity (530 nm/590 nm) of the cell culture supernatants was measured with an Infinite® 200 PRO microplate reader (TECAN Group Ltd., Männedorf, Switzerland). A blank control comprising only medium was also included. Bright field images (EVOS™ XL Core Cell Imaging System, Thermo Fisher Scientific, Carlsbad, CA, USA) were taken during

culture to monitor cell morphology.

2.6.9. Hemolysis test

The blood compatibility of crosslinked polyelectrolyte complexes was evaluated by hemolysis tests on human red blood cells (RBC). In brief, the anti-coagulated blood was centrifuged at 800g at 4 °C for 10 min. Then, the erythrocytes pellet was incubated with different concentrations of nanogels (250, 500 and 1000 μg/mL). Water and PBS 1x were used as positive and negative controls, respectively. The resulting mixtures were incubated at 37 °C for 2 h and centrifuged at 3000g at 4 °C for 10 min. The absorbance of the supernatant solution of the test sample (Atest), positive control (Apos), and negative control (Aneg) at 540 nm was determined by UV–Vis spectrophotometry. Each set of experiments was carried out three times and the hemolysis (%) was calculated by the formula = [(Atest − Aneg)/(Apos − Aneg)] × 100%.

2.6.10. Cell internalization

HUVECs were seeded at a concentration of 8000 cells/well onto Nunc™ Lab-Tek™ chamber slides (Thermo Fisher Scientific). Fluorescent labelled pullulan derivatives was used to produce crosslinked polyelectrolyte complexes for cell internalization assays. After 24 h of incubation using serum supplemented cell culture medium, cells were washed with PBS and fixed with fresh 4% paraformaldehyde. Cytoplasm was stained with FITC-phalloidin (Invitrogen) (dilution 1/200 on PBS from stock at 1 mg/mL) and cell nucleus was stained with 4′,6-DiAmidino-2-PhenylIndole (DAPI) (dilution 1/50 000 in PBS from stock at 5 mg/mL) (Sigma Aldrich, St. Louis, MO, USA). Coverslips were mounted using Ibidi Mounting Medium (IMM) for fluorescence microscopy (ibidi GmbH, Germany). Confocal images were taken to evaluate nanoparticles internalization (Microscope Confocal Zeiss LSM 780, Germany).

2.6.11. Targeting assays

The interaction of genipin crosslinked NPs with P-selectin was evaluated *in vitro* as previously reported (B. Li et al., 2017). Briefly, micro-channels of Vena8 Fluoro + chambers (Cellix Ltd, Dublin, Ireland) were coated overnight with 50 μg/mL of collagen and then washed with NaCl 0.9%. Human whole blood labeled with DiOC6 (a green fluorescent dye) was perfused under arterial flow conditions for 5 min to induce platelet activation and aggregation on the collagen-coated channel. Rhodamine labeled G-PECs at 1 mg/mL in NaCl 0.9% were then perfused during 5 min. Their accumulation onto preformed platelet aggregates was monitored in real time by fluorescence microscopy (Axio Observer, Carl Zeiss Microscopy, Oberkochen, Germany). Fluorescence images were taken along each micro-channel after washing with NaCl 0.9%. G-PECs formulated with carboxymethyl-dextran were used as negative control.

2.7. miRNA loading and characterization

2.7.1. miRNA loading

Loaded G-PECs nanogels were produced by adding 1 mL of miRNA solution (0.04 mg/mL) to 1 mL of nanoparticle solution at 1 mg/mL (N/P ratio 10) redispersed in 1% acetic acid solution (pH 3) or ultrapure water (pH 7). Nanoparticles were placed at 4 °C during 30 min for stabilization. Then, ultracentrifugation at 15,000 g during 20 min at 4 °C was performed to remove the free or poorly adsorbed miRNA. The entrapment efficiency (EE) of miRNA into G-PECs, was determine by UV spectrophotometry using NanoDrop™ 2000/2000c Spectrophotometer (Thermo Fisher Scientific, Wilmington, DE, USA) by measuring the concentration of free miRNA in the supernatant. The entrapment efficiency was calculated as EE% = (miRNA initially added-miRNA in the supernatant/miRNA initially added) × 100%.

2.7.2. Presence of miRNA within loaded G-PECs

The presence of the miR-155-5p was monitored by agarose gel electrophoresis (AGE). Agarose gel electrophoresis was perfomed using 5% agarose gels containing ethidium bromide in TBE (Tris-Borate-EDTA, Thermo Fisher Scientific, Vilnius, Lithuania) buffer. An Ultra-Low Range GeneRuler DNA Ladder (10–300 bp; Thermo Fisher Scientific, Bleiswijk, Netherlands) was used to monitor miRNA presence. Samples included solution of unloaded G-PECs, plus additional controls from different steps of the miRNA loading: miRNA alone (at the concentration used for loading), loaded G-PECs before ultracentrifugation, loaded G-PECs after ultracentrifugation and the supernatant of loaded G-PECs after ultracentrifugation. Samples were run by electrophoresis (50 V, 120 min) and detected through a UV transilluminator (Vilber Lourmat smart imaging system, Collegien, France).

2.7.3. miRNA release

To assess miRNA release from nanogels, the loaded G-PECs were resuspended in PBS 1x and subjected to strong orbital shaking at 250 rpm at 37 °C. At each time point (15 min, 30 min, 1 h, 3 h and 6 h), G-PECs were centrifuged (15,000g, 20 min, 4 °C) and the supernatant was separate to quantify released miRNA by UV spectrophotometry using NanoDrop™ 2000/2000c Spectrophotometer (Thermo Fisher Scientific, Wilmington, DE, USA).

2.7.4. miRNA delivery

HUVECs were seeded at a concentration of 8000 cells/ well onto Nunc™ Lab-Tek™ chamber slides (Thermo Fisher Scientific) and grown for 48 h. Loaded G-PECs nanogels were prepared as previously described using scramble FAM-miRNA. After 2 h of incubation using serum-free supplemented cell culture medium, cells were washed with PBS and fixed with fresh 4% paraformaldehyde. Cell nucleus was stained with 4′,6-DiAmidino-2- PhenylIndole (DAPI) (Sigma Aldrich, St. Louis, MO, USA). Coverslips were mounted using Ibidi Mounting Medium (IMM) for fluorescence microscopy (ibidi GmbH, Germany). Fluorescence images were taken to evaluate miRNA delivery (Axiovert Observer Z1 inverted microscope, Zeiss, Germany).

2.7.5. Cellular uptake analysis by flow cytometry

HUVECs were seeded on a 24-well plate at a density of 50,000 cells/well and incubated overnight in 500 μL of DMEM containing 10% FBS. Then, the cells were incubated with 500 μL of G-PECs nanogel/miRNA solution at 1 mg/mL containing 5 nmol of scramble fluorescein-labeled miRNA. After incubation for 2 h, the medium was removed and the cells were washed with phosphate buffer saline (PBS). The cells were then trypsinized and collected by centrifugation (1500 rpm, 4 °C, 5 min). Finally, the cells were suspended in 200 μL of PBS. Flow cytometric analysis was carried out using LSRII flow cytometer (BD Biosciences, Le Pont de Claix, France). The mean fluorescence intensity (MFI) of fluorescein was measured for each condition. Naked FAM-miRNA was used as negative control.

2.8. Statistical analysis

The data were expressed as mean ± SD (standard deviation). Statistical analysis was performed using GraphPad Prism (version: 5.0a, San Diego, CA, USA). Since data followed a non-parametric distribution, Wilcoxon matched-pairs test was performed to compare each paired group and p smaller than 0.05 was considered statistically significant.

3. Results and discussion

3.1. Synthesis and characterization of cationic pullulan derivatives

In this work, cationic pullulan/fucoidan nanoparticles were prepared in a two-step procedure based on polyelectrolyte complexation followed by polycationic crosslinking through the addition of genipin which forms bridges between primary amines (Butler et al., 2003). Cationic pullulan derivatives with primary amine groups were prepared by

substitution of hydroxyl groups from pullulan with chloroethylamine in basic aqueous media (Figure S1) (Moraes et al., 2020).

Successful introduction of amine moieties was confirmed by elemental analysis of nitrogen content (%N) and ^{1}H NMR spectroscopy (see Figure S2 and Figure S3 in supplementary data). It was possible to synthetize derivatives with N content of 1.60 ± 0.05% N (1.18 mmol/g) and monomodal molecular weight distributions (PdI of 1.6) in two synthesis steps using a molar feeding ratio of 2 equivalents (mol amine/mol OH) of chloroethylamine (Table 1). San Juan et al. obtained a similar N content of 1 mmol/g for 40 min of reaction at 55 °C to modify pullulan but using a feeding ratio of 8 equivalents of bromoethylamine (San Juan et al., 2007). We found that in order to get higher degree of substitution (DS), the reaction should be performed once more on the substituted derivatives rather than increasing the quantity of ethylamine (see Table S1 and Table S2 in supplementary data).

3.2. Crosslinking of polyelectrolyte complexes nanoparticles

PECs formed merely by electrostatic interactions are known to have limited stability in physiological media. To obtain nanogels with interesting characteristics, the use of covalent crosslinkers is necessary. Crosslinked PECs (G-PECs) were produced by using genipin as crosslinking agent in a two steps process.

First, PECs of EA-pullulan and fucoidan were prepared by simple dropping process and their physicochemical properties were studied without covalent crosslinking. PECs are formed using very diluted solutions and the effect of pH and mass ratio between polyelectrolytes was investigated. As the charge of primary amines (–NH_2) from EA-pullulan derivatives are dependent on the pH (Figure S5), four different pH settings were selected in order to obtain polymer solutions with different charges during the formation of the PECs. As expected, increasing the pH values of polycations solution lead to an increase in the size of polyplexes, PdI values and a decrease in zeta potential due to to the lower number of positively charged groups from EA-pullulan (Table 2).

As it was possible to form PECs in the nanometric range and with nice distribution at pH values up to 5, this value was thus selected. The effect of mass ratio between polyelectrolytes was evaluated by keeping constant the concentration of the polycation. PECs prepared with lower concentrations of fucoidan showed increased size values and PdI, probably due to lower contribution of the polyanion counterpart to form compacted PECs. Interestingly, it should be noted that by varying the polymer ratios, it was possible to modulate zeta potential values of PECs. Decreasing the concentration of fucoidan in PECs formulation led to a decrease in zeta potential values (Table 3).

Then, genipin was added to a solution of EA-pullulan (1.0 mg/mL) and fucoidan (0.25 mg/mL) at pH 5 to get G-PECs. The crosslinking reaction was monitored by the appearance of blue coloration in the reaction mixture. After 48 h of reaction, particles were isolated by ultracentrifugation at 15,000 g for 20 min.

The crosslinking reaction occurs by mean of a complex mechanism, which consists in two reactions involving different sites on the genipin molecule. The first reaction is a nucleophilic attack of the genipin C3 carbon atom from a primary amine group to form an intermediate aldehyde group. The opening of the dihydropyran ring is then followed by attack on the resulting aldehyde group by the secondary amine formed in the first step of the reaction. A heterocyclic compound of genipin crosslinked to the primary amine groups of EA-pullulan is thereby formed (Fig. 1C) (Butler et al., 2003; Mi et al., p. 200, 2005).

Table 1
Characterization of cationic pullulan derivative with primary amine groups.

Amine	Feeding[a]	M_n^b(kDa)	M_w^b(kDa)	PdI[b]	N[c] (%)	DS[d]
No amine (pullulan)	0	113	298	2.6	0	0
EA-pullulan	2	178	298	1.6	1.60 ± 0.05	0.20

[a]Feeding: $mol_{amine}/mol_{hydroxyl\ groups}$; [b]Measured by SEC-MALLS; [c]Calculated from nitrogen elemental analysis; [d]Degree of substitution calculated per anydroglucose unit.

Table 2
Effect of pH on PECs formation by mixing EA-pullulan (0.2 mg/mL) and fucoidan (0.2 mg/mL). Results are expressed as mean ± SD (n = 3).

pH	Size (nm)	PdI	ζ-potential (mV)
pH 2	181 ± 17	0.120 ± 0.00	−2.02 ± 4.93
pH 3	130 ± 29	0.156 ± 0.01	−4.29 ± 3.79
pH 5	205 ± 38	0.123 ± 0.02	−5.49 ± 5.55
pH 6	472 ± 59	0.213 ± 0.01	−8.36 ± 5.28

Table 3
Effect of EA-pullulan/fucoidan mass ratio on PECs formation. Results are expressed as mean ± SD (n = 3).

pH	EA-pullulan (mg/mL)	Fucoidan (mg/mL)	EA-pullulan/fucoidan mass ratio	Size (nm)	PdI	ζ-potential (mV)
pH 5	1.0	0.50	1/2	109 ± 10	0.155 ± 0.08	−3.75 ± 5.82
		0.34	1/3	141 ± 25	0.138 ± 0.12	−2.47 ± 4.33
		0.25	1/4	150 ± 8	0.142 ± 0.03	0.51 ± 2.76
		0.20	1/5	181 ± 14	0.098 ± 0.08	4.25 ± 4.98
		0.10	1/10	251 ± 6	0.215 ± 0.01	4.06 ± 0.53

The crosslinking reaction in function of time and temperature was monitored by UV–Vis spectroscopy by the apparition of a blue color (λ max = 600 nm). Genipin-crosslinked PECs gradually turned from uncolored solution into a light blue colored one within 48 h (Fig. 2). Several studies with chitosan reported that a crosslinking reaction time of 2 h was enough to produce nanoparticles without specifying the temperature (Kumar et al., 2016; Lin et al., 2017; 2013). Razi *et al.* performed the crosslinking reaction with genipin during 24 h at 30 °C to produced chitosan crosslinked nanoparticles (Razi et al., 2018). In the work of Pujana *et al.* the crosslinking reaction was carried out for 4 days at 25 °C using W/O microemulsions to produce chitosan nanogels (Arteche Pujana et al., 2013). Our protocol of 48 h of reaction was performed at room temperature and can be decreased to 6 h by increasing the temperature to 50 °C while keeping nanoparticles characteristics.

Different concentrations of genipin were evaluated (0.125 mg/mL, 0.25 mg/mL, 0.50 mg/mL). Both the low (0.125 mg/mL) and high (0.50 mg/mL) concentration of genipin produced nanoparticles after 48 h treatment, indicating that highly crosslinked PECs could be obtained even from a low genipin concentration (Figure S6). Since the concentration of 0.25 mg/mL allowed the production of nanoparticles with a diameter lower than 200 nm with low PdI this concentration was selected for all further experiments.

Crosslinked PECs were comprehensively characterized by size, surface charge, polydispersity, morphology and swelling properties (Fig. 3). Crosslinked nanoparticles exhibited a size around 155 nm in water with zeta potential value of 0.86 ± 4.35 mV. The presence of fucoidan in G-PECs was confirmed by elemental analysis (7% w/w of the total nanoparticles weight) (Fig. 3C). No notable differences in particle size and

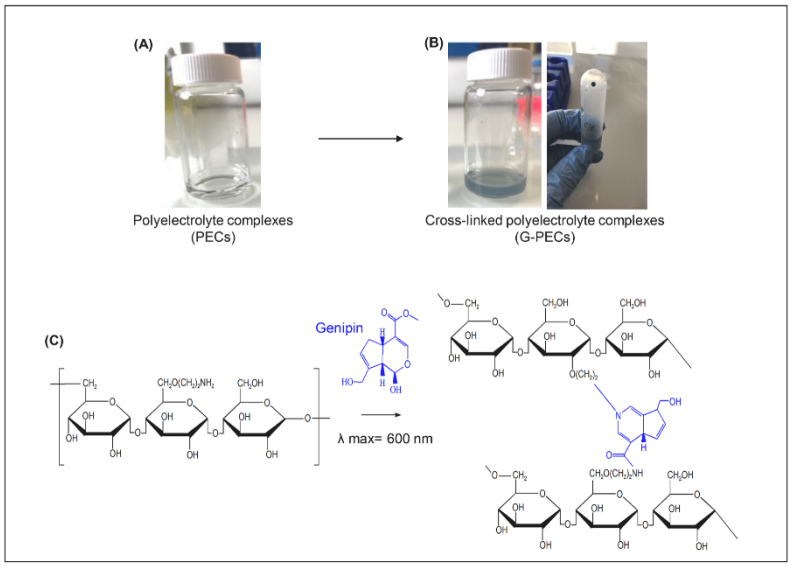

Fig. 1. Polyelectrolyte complexes nanoparticles of EA-pullulan and fucoidan: (A) before crosslinking, (B) after crosslinking with genipin and (C) schematic representation of crosslinking bridges between genipin and primary amine groups of EA-pullulan.

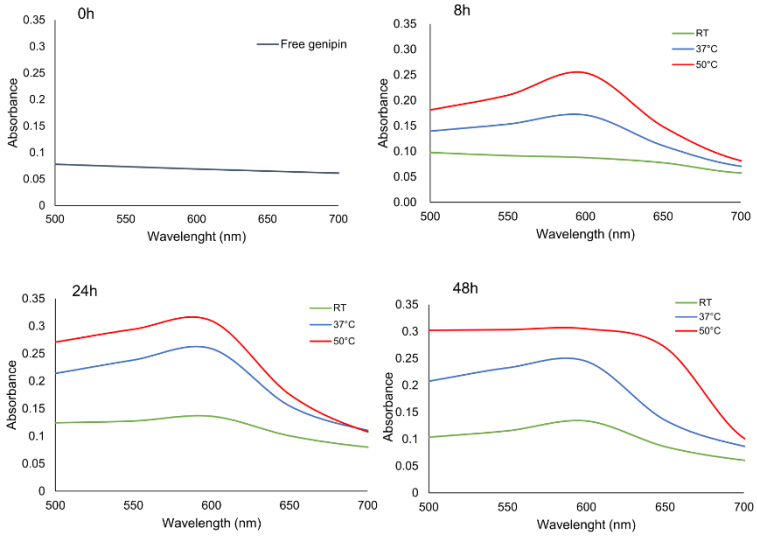

Fig. 2. Absorption spectra of free genipin and genipin crosslinked PECs (G-PECs) at different temperatures (room temperature, 37 °C and 50 °C) over time (0 h, 8 h, 24 h, 48 h).

zeta potential were observed between PECs and G-PECs, suggesting that interpolyelectrolyte structures remained unaffected by the crosslinking process (Figure S7). FTIR spectroscopy was employed to characterize the chemical structure of the prepared sample (Figure S8). TEM and E-SEM images exhibited spherical morphology and uniform particle size distribution of G-PECs (Fig. 3B).

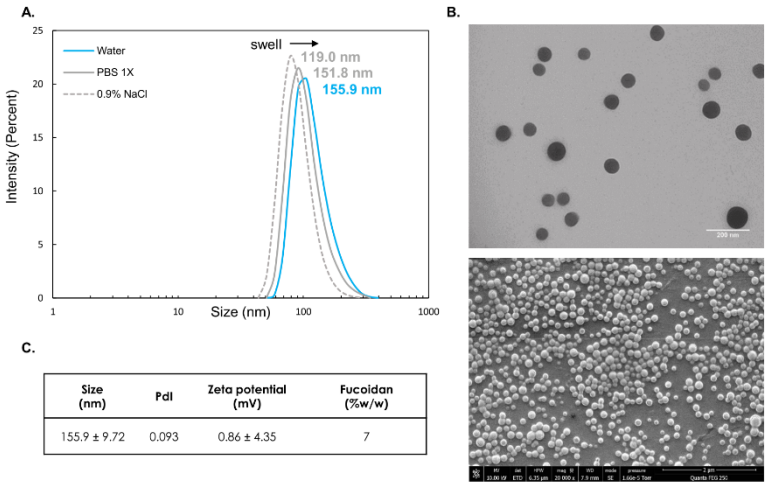

Size (nm)	PdI	Zeta potential (mV)	Fucoidan (%w/w)
155.9 ± 9.72	0.093	0.86 ± 4.35	7

Fig. 3. Physico-chemical characterization of crosslinked nanoparticles: (A) Dynamic diffusion of light measured in intensity. (B) Images obtained by transmission electron microscopy (upper image) and environmental scanning electron microscopy (bottom image). (C) Size (nm), polydispersion index and zeta potential (mV) measured by Zetasizer Nano-ZS. The percent of fucoidan by weight of the total nanoparticle weight was determined by elemental analysis.

When incubated in either PBS 1x or 0.9%NaCl, G-PECs exhibited a swelling behavior (Fig. 3A) that characterize them as nanogels, even if the swelling ability of polymeric networks was reduced due to chemical crosslinking. The polymeric matrix of nanogels whould be able to retain a significant amount of low molecular weight drugs and releasing them in a controlled manner (Lachowicz et al., 2019; Shatsberg et al., 2016).

Long-term stability of G-PECs was evaluated in distilled water and NaCl upon storage of the nanoparticles suspensions at 4 °C. By genipin crosslinking, the colloidal stability of interpolyelectrolyte complexes was improved up to 1 month of incubation in 0.9%NaCl (Fig. 4A, B and C). The formation of PECs, based only in electrostatic interactions, was found to be poor against pH and ionic strength because of repulsive forces and salt-screening effects (Razi et al., 2018). The covalent crosslinking of EA-pullulan with genipin in the presence of fucoidan has led to

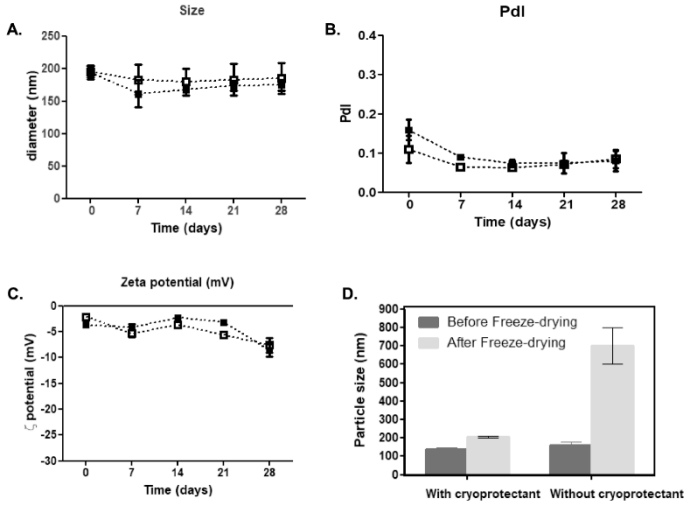

Fig. 4. Stability of G-PECs in water (-□-) and NaCl 0.9% (-■-) after preparation (day 0), and after 1, 7, 14, 21 and 28 days of storage at 4 °C. (A) NP size (nm) and (B) PdI were measured by DLS; (C) ζ potential values (mV) by ELS; (D) Effect of the addition of a cryoprotectant on nanoparticles size before and after freeze-drying. Results are shown as mean ± SD from three independent experiments.

the formation of permanent networks in which fucoidan has been retained by ionic interactions between the sulfate groups and the primary ammoniums. In addition, it was possible to freeze-dry G-PECs while keeping the same size after re-dispersion in 0.9% NaCl, using 5% (w/w) of sucrose as cryoprotectant agent (Fig. 4D). Freeze-dryer process is useful for long-term storage of pharmaceutical formulations and to concentrate PECs nanoparticles prior to use by rehydrating them in reduced volumes.

3.3. Cell viability, hemocompatibility and cellular uptake studies

EA-pullulan showed to be biocompatible up to 200 μg/mL (Figure S4). When increasing the concentration of polycation up to 1000 μg/mL, the cell viability decreased for less than 70% (48.19 ± 3.59%). Lou *et al.* tested the toxicity of different polycations for much lower concentrations ranging from 2 to 100 μg/mL (Lou et al., 2017). Similarly, Huang *et al.* evaluated the toxicity of chitosan derivatives reconstructed with different alkylamines for concentrations only up to 200 μg/mL (Huang et al., 2020). Cationic pullulan derivatives modified with quaternary amine groups have previously showed to be non-cytotoxic (Moraes et al., 2020). It is known that the cytotoxicity of polycations is a function that results from their polyamine nature (i.e., primary, secondary, tertiary, and quaternary amino groups) (Fischer et al., 2003). In comparison to primary amines, higher order amines can induce lower toxicity by reducing the cationic polymer's ability to bind to and disrupt the organization of cell membrane lipid bilayer (Lou et al., 2017; Palermo et al., 2011; Toy et al., 2019). Cytotoxicity assays of G-PECs in endothelial cells showed that no decrease in cell viability was observed up to 1000 μg/mL (Fig. 5A). Results were confirmed by optical (Fig. 5B) and fluorescence (Fig. 5C) images, in which no alteration of cell morphology was observed when compared with control. PECs have been found to be usually less cytotoxic than uncomplexed polycations (Fischer et al., 2003).

For further clinical safety evaluation, we investigated the hemolytic property of G-PECs on human erythrocytes (Fig. 6). Hemolysis assays are generally considered valuable in testing the hemocompatibility of new nanoformulations (Naeye, 2011). All tested concentrations (250 –1000 μg/mL) had a hemolytic value below 5% (hemolysis rate of 0.79 ± 0.04%, 1.45 ± 0.15% and 2.09 ± 0.06% for G-PECs concentrations of 250, 500 and 1000 μg/mL respectively). According to the American Society for Testing and Materials International (ASTM, 2013) materials with less than 5% hemolytic reaction can be considered as non-hemolytic and G-PECs nanogels could be thereby classified as non-hemolytic material (Chatzitaki et al., 2020).

The cellular uptake was evaluated in HUVECs after 24 h of incubation. For this purpose, G-PECs were produced using fluorescent-labelled

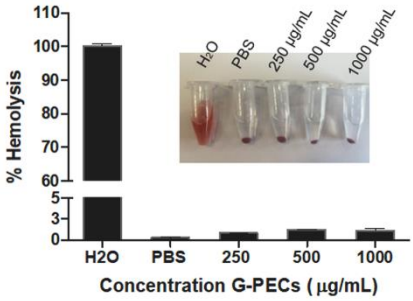

Fig. 6. Blood hemolysis percentage of human blood from healthy donors after incubation with increasing concentrations of 250, 500 and 1000 μg/mL of G-PECs nanogels. Water and PBS were used as positive and negative control, respectively. Results are shown as mean ± SD from three independent experiments.

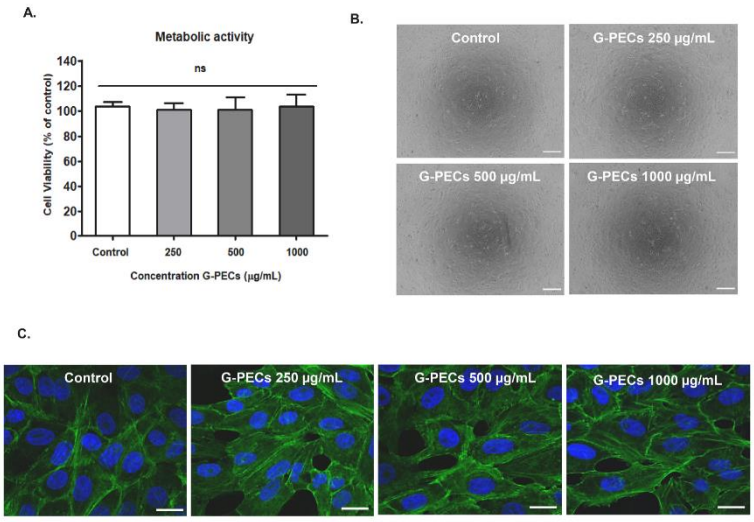

Fig. 5. (A) Cytocompatibility of G-PECs towards HUVECs exposed to increasing concentrations of G-PECs measured by resazurin conversion after 1 day of incubation. Results are shown as mean ± SD from 3 independent experiments with no statistical differences detected using the Wilcoxon matched-pairs signed rank test. (B) Optical and (C) fluorescence images of confluent cells without G-PECs and with 250, 500 and 1000 μg/mL of G-PECs, respectively. Scale bar corresponds to 200 μm (top image) and 20 μm (bottom image).

EA-pullulan with rhodamine-B isothiocyanate. The cells incubated with G-PECs exhibited intense red accumulations in the cytoplasm, indicating an efficient cell internalization (Fig. 7 and Figure S9) probably via non-specific endocytosis due to their relatively small size of less than 200 nm (Goyal et al., 2018).

3.4. Biospecificity of G-PECs

Nanosystems decorated with fucoidan have been previously shown to be able to target P-selectin (Forero Ramirez et al., 2020; Juenet et al., 2018; B. Li et al., 2017; Suzuki et al., 2015). *In vitro* capacity of rhodamine-B labelled G-PECs to target human activated platelets was evaluated via flow adhesion assay. Control fluorescent G-PECs were formulated using carboxymethyl-dextran as polyanion. As evidenced on Fig. 8, G-PECs with fucoidan were able to target P-selectin expressed in activated platelets.

3.5. miRNA loading, release and delivery

Nanogels can be used as highly efficient and biodegradable carriers for the transport of drugs in controlled drug delivery devices. Strongly charged biotherapeutics, such as nucleic acids, are generally post-loaded into oppositely charged nanogels by electrostatic interactions with oppositely charged groups.

In order to evaluate the influence of the surface charge of G-PECs on miRNA interactions, two different pHs (pH 3 and pH 7) were studied for miRNA loading. Under neutral conditions, the primary amine groups chains of G-PECs were deprotonated, thereby leading to nearly neutral surface charge of developed nanogels (0.86 ± 4.35 mV). However, in a more acidic environment, the amount of primary ammonium groups led to G-PECs with a positive zeta potential (9.23 ± 0.81 mV) which could contribute for miRNA loading onto the particle surface through electrostatic interactions.

After miRNA addition, loaded G-PECs were characterized regarding size, polydispersity, surface charge and agarose gel electrophoresis. miRNA loaded as well as unloaded G-PECs showed equivalent diameters around 200 nm, although the PdI increased considerably for the loaded ones indicating a more heterogeneous population (Figure S10). Similary, Raemdonck *et al.* revelead that siRNA-loaded cationic dextran nanogels had nearly the same hydrodynamic size as the nanogels prior to loading with siRNA (Raemdonck et al., 2009). The charge of surface G-PECs slightly decreased indicating the presence of additional negative charges (Fig. 9A). A loading efficiency of 70.23 ± 5.33% at pH 3 was achieved compared to 33.11 ± 6.51% at pH 7 (Fig. 9B). This difference was likely due to the higher affinity the particles had for miRNA as a direct result of polymer protonation in acidic conditions. The agarose gel electrophoresis supports more effectively miRNA retardation from nanogels loaded with miRNA in acidic conditions when compared to miRNA loaded in neutral pH (Figure S11). For all the subsequent experiments, the miRNA was loaded into G-PECs only at pH 3.

These results are in agreement with the literature. Pereira *et al.* performed siRNA loading onto glycol chitosan-based nanogels by simple mixing nanogels supensions in 0.2 M acetate buffer at pH 4.5 with siRNA (Pereira et al., 2013). Its positive charge (25–30 mV) under slightly acidic conditions allowed the electrostatic interaction between glycol chitosan and negatively charged siRNA. Under neutral or alkaline conditions, the siRNA binding was essentially stabilized by hydrogen bonding and hydrophobic interactions of modified chitosan. Pilipenko *et al.*, demonstrated that the ability of chitosan–heparin complexes to encapsulate the siRNA was also depending on pH of the medium due to the pH sensitive behavior of chitosan (Pilipenko et al., 2019). Under acidic conditions, almost 100% of siRNA was entrapped into polyplexes due to the greatest protonation of the amino groups of chitosan in acidic media resulting in maximum binding efficiency. Thus, they determined the optimal pH for oligonucleotide entrapment around pH 6.0 or below. Khaled *et al.* also evaluated the siRNA loading efficiency into hybrid nanogel particles formed by a nanostructured inorganic silica core and an organic pH-responsive hydrogel shell at acidic and physiological pH conditions. They obtained a loading efficiency of 95% of siRNA at pH 6 compared to 70% at pH 7.4 (Khaled et al., 2016).

Further, to evaluate if the miRNA could be released from G-PECs, the release profile was studied in physiological conditions. When placed under strong orbital shaking at 37 °C in PBS, loaded G-PECs released nucleic acids up to 6 h, with a $t_{1/2}$ of 15 min after incubation (Fig. 9C). Antunes *et al.* obtained similar release profiles from core-shell polymer based nanoparticles loaded with miR-155-5p (Antunes et al., 2019).

Finally, a comparative study of naked miRNA and miRNA loaded into G-PECs was done using a fluorescently labeled miRNA to evaluate their cellular uptake. As it can be seen from Fig. 10A, no miRNA could be detected inside cells in case of administration of free miRNA confirming

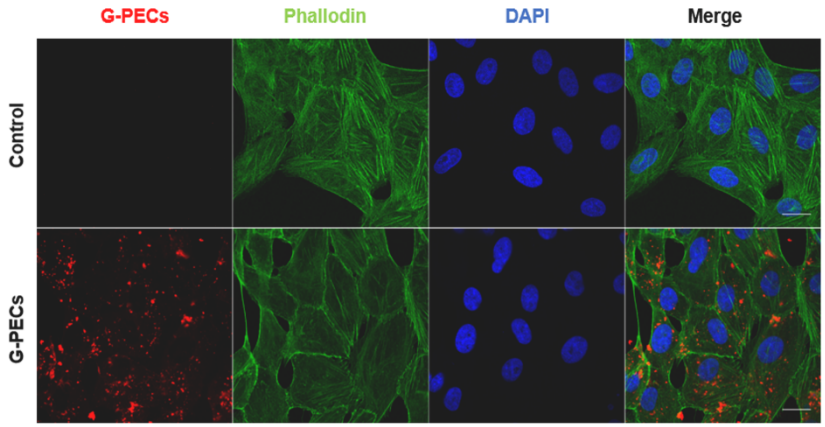

Fig. 7. Confocal microscopy images of HUVECs treated without G-PECs and with G-PECs produced using fluorescent labelled EA-pullulan (RBITC-EA-pullulan). G-PECs were incubated with HUVECs for 24 h at 37C. HUVECs were then washed, fixed, and observed under fluorescence microscopy. Red, G-PECs; green, phalloidin; blue, cell nuclei. Scale bars, 20 μm.

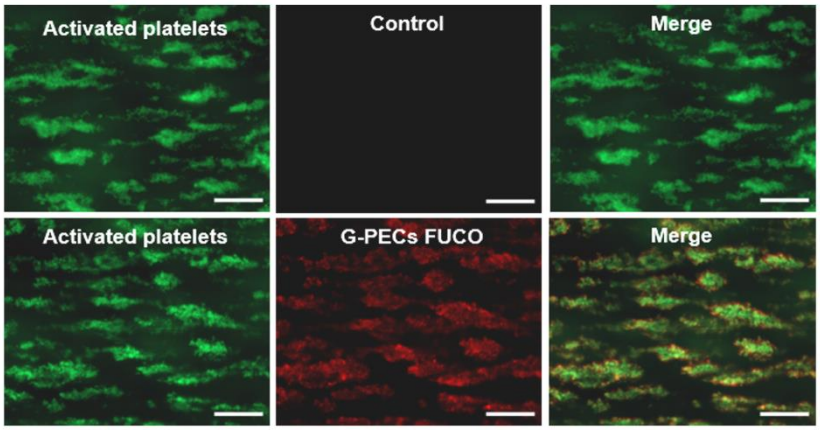

Fig. 8. Evaluation of G-PECs binding on activated platelets under arterial flow conditions. Particles and platelets aggregates co-localization was evaluated by merged fluorescence microscopy images (right). G-PECs without fucoidan were used as control. Scale bars corresponds to 50 μm.

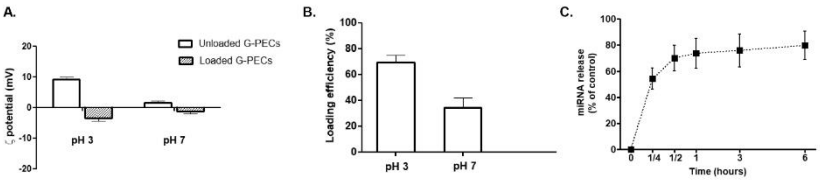

Fig. 9. miRNA loading and release. (A) Zeta potential (mV) measured by the Zetasizer Nano-ZS at pH 3 and pH 7 before and after miRNA loading. (B) Loading efficiency of miRNA at pH 3 and 7 and (C) miRNA release from G-PECs nanogels at 37 °C in PBS. Results are shown as mean ± SD from three independent experiments.

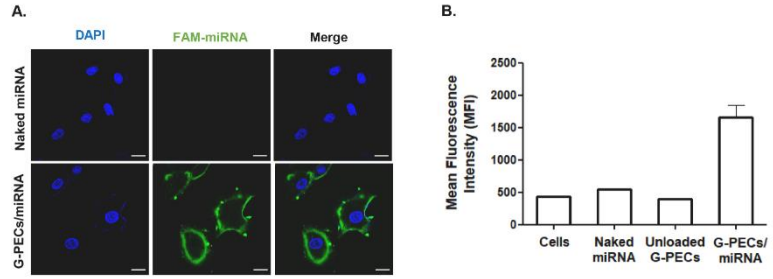

Fig. 10. FAM-miRNA delivery. (A) Fluorescence microscopy images of HUVECs evidencing miRNA delivery. Left column: cells' nuclei stained with DAPI (depicted in blue); middle column: FAM labelled miRNA (depicted in green); right column: merged images for cells treated with naked FAM-labelled miRNA and cells treated with G-PECs nanogels loaded with FAM-labelled miRNA; Treatments were performed for 2 h at 37 °C. Scale bar: 20 μm. (B) Mean fluorescence intensity (MFI) of fluorescein amidite (FAM) measured by flow cytometry analysis. Results are shown as mean ± SD from three experiments.

that free miRNA cannot be internalized by cells. miRNA from G-PECs nanogels, in contrast, was clearly incorporated by cells. The strong and difuse green fluorescence from FAM-miRNA indicated the distribution of the polyplexes in the cytoplasm after 2 h incubation with G-PECs. Flow cytometry analysis confirmed quantitative differences in FAM-miRNA uptake levels upon loading into G-PECs (Fig. 10B).

4. Conclusions

In this work, we demonstrated the development of a simple and versatile drug delivery system based on two polyelectrolytes derived from natural biocompatible polysaccharides, pullulan and fucoidan, which spontaneously interact to form PECs of adjustable size and surface charge for miRNA delivery. The ability of our nanosystems to target P-

selectin make them attractive candidates for the delivery of small sized nucleic acids, while foccused on the cardiovascular field. Future studies about the potency of these systems for gene silencing should clarify if the amount of delivered miRNA is able to induce the desired pharmacological effect.

Funding

This work was supported by INSERM, Université de Paris and Université Sorbonne Paris Nord. The PhD fellowship was funded by CONSELHO NACIONAL DE DESENVOLVIMENTO CIENTÍFICO E TECNOLÓGICO (CNPq) from Brazil, grant number 201245/2017-5.

CRediT authorship contribution statement

Fernanda C. Moraes: Conceptualization, Methodology, Validation, Formal analysis, Investigation, Writing - original draft, Writing - review & editing, Visualization. **Laura Marcelo Forero Ramirez:** Methodology, Investigation. **Rachida Aid:** Methodology, Investigation. **Samira Benadda:** Methodoly, Investigation. **Murielle Maire:** Methodology, Investigation. **Cédric Chauvierre:** Conceptualization, Resources, Visualization, Funding acquisition. **Joana C. Antunes:** Conceptualization, Investigation, Writing - review & editing, Visualization, Supervision. **Frédéric Chaubet:** Conceptualization, Resources, Writing - review & editing, Visualization, Supervision, Project administration, Funding acquisition. **Didier Letourneur:** Conceptualization, Resources, Writing - review & editing, Visualization, Supervision, Project administration, Funding acquisition.

Declaration of Competing Interest

The authors declare that they have no known competing financial interests or personal relationships that could have appeared to influence the work reported in this paper.

Acknowledgments

The authors express their highest gratitude to Kevin Guedj (LVTS, Paris, France) for flow cytometry experiments and data analysis, to Christine Choqueux (LVTS, Paris, France) and UTC (Compiègne, France) for SEM images, to Camille Roesch (Izon Science, France) for nanoparticles concentration analysis and to Camille Le Guilcher for assistance in data analysis. The authors are grateful also to the PhD fellowship for Fernanda C. Moraes from the *Conselho Nacional de Desenvolvimento Científico e Tecnológico* (CNPq). The graphical abstract includes figures made using the software Biorender®.

Appendix A. Supplementary material

Supplementary data to this article can be found online at https://doi.org/10.1016/j.ijpharm.2021.120302.

References

Antunes, J.C., Benarroch, L., Moraes, F.C., Juenet, M., Gross, M.-S., Aubart, M., Boileau, C., Caligiuri, G., Nicoletti, A., Ollivier, V., Chaubet, F., Letourneur, D., Chauvierre, C., 2019. Core-shell polymer-based nanoparticles to deliver MiR-155-5p to endothelial cells. Mol. Ther. Nucleic Acids S2162253119301465. https://doi.org/10.1016/j.omtn.2019.05.016.

Arteche Pujana, M., Pérez-Álvarez, L., Cesteros Iturbe, L.C., Katime, I., 2013. Biodegradable chitosan nanogels crosslinked with genipin. Carbohydr. Polym. 94, 836–842. https://doi.org/10.1016/j.carbpol.2013.01.082.

Bachelet, L., Bertholon, I., Lavigne, D., Vassy, R., Jandrot-Perrus, M., Chaubet, F., Letourneur, D., 2009. Affinity of low molecular weight fucoidan for P-selectin triggers its binding to activated human platelets. Biochimica et Biophysica Acta (BBA) - General Subjects 1790, 141–146. https://doi.org/10.1016/j.bbagen.2008.10.008.

Baipaywad, P., Udomluck, N., Pyo, S.-G., Park, H.H., Park, H., 2014. Fabrication of nanogels for delivery of molecules. J. Nanosci. Nanotechnol. 14, 7363–7373. https://doi.org/10.1166/jnn.2014.9579.

Berger, J., Reist, M., Mayer, J.M., Felt, O., Peppas, N.A., Gurny, R., 2004. Structure and interactions in covalently and ionically crosslinked chitosan hydrogels for biomedical applications. Eur. J. Pharm. Biopharm. 57, 19–34. https://doi.org/10.1016/S0939-6411(03)00161-9.

Bourganis, V., Karamanidou, T., Kammona, O., Kiparissides, C., 2017. Polyelectrolyte complexes as prospective carriers for the oral delivery of protein therapeutics. Eur. J. Pharm. Biopharm. 111, 44–60. https://doi.org/10.1016/j.ejpb.2016.11.005.

Butler, M.F., Ng, Y.-F., Pudney, P.D.A., 2003. Mechanism and kinetics of the crosslinking reaction between biopolymers containing primary amine groups and genipin. J. Polym. Sci. A Polym. Chem. 41, 3941–3953. https://doi.org/10.1002/pola.10960.

Candido, S., Lupo, G., Pennisi, M., Basile, M., Anfuso, C., Petralia, M., Gattuso, G., Vivarelli, S., Spandidos, D., Libra, M., Falzone, L., 2019. The analysis of miRNA expression profiling datasets reveals inverse microRNA patterns in glioblastoma and Alzheimer's disease. Oncol. Rep. https://doi.org/10.3892/or.2019.7215.

Chakraborty, C., Sharma, A.R., Sharma, G., Doss, C.G.P., Lee, S.-S., 2017. Therapeutic miRNA and siRNA: moving from bench to clinic as next generation medicine. Mol. Ther. Nucleic Acids 8, 132–143. https://doi.org/10.1016/j.omtn.2017.06.005.

Chatzitaki, A.-T., Jesus, S., Karavasili, C., Andreadis, D., Fatouros, D.G., Borges, O., 2020. Chitosan-coated PLGA nanoparticles for the nasal delivery of ropinirole hydrochloride: in vitro and ex vivo evaluation of efficacy and safety. Int. J. Pharm. 589, 119776 https://doi.org/10.1016/j.ijpharm.2020.119776.

dos Santos, M.A., Grenha, A., 2015. Polysaccharide Nanoparticles for Protein and Peptide Delivery, in: Advances in Protein Chemistry and Structural Biology. Elsevier, pp. 223–261. https://doi.org/10.1016/bs.apcsb.2014.11.003.

Falzone, Lupo, Rosa, Crimi, Anfuso, Salemi, Rapisarda, Libra, Candido, 2019. Identification of Novel MicroRNAs and Their Diagnostic and Prognostic Significance in Oral Cancer. Cancers 11, 610. https://doi.org/10.3390/cancers11050610.

Fischer, D., Li, Y., Ahlemeyer, B., Krieglstein, J., Kissel, T., 2003. In vitro cytotoxicity testing of polycations: influence of polymer structure on cell viability and hemolysis. Biomaterials 24, 1121–1131. https://doi.org/10.1016/S0142-9612(02)00445-3.

Forero Ramirez, L.M., Gobin, E., Aid-Launais, R., Journe, C., Moraes, F.C., Picton, L., Le Cerf, D., Letourneur, D., Chauvierre, C., Chaubet, F., 2020. Gd(DOTA)-grafted submicronic polysaccharide-based particles functionalized with fucoidan as potential MR contrast agent able to target human activated platelets. Carbohydr. Polym. 245, 116457 https://doi.org/10.1016/j.carbpol.2020.116457.

Fröhlich, T., Edinger, D., Russ, V., Wagner, E., 2012. Stabilization of polyplexes via polymer crosslinking for efficient siRNA delivery. Eur. J. Pharm. Sci. 47, 914–920. https://doi.org/10.1016/j.ejps.2012.09.006.

Gao, S., Tian, H., Guo, Y., Li, Y., Guo, Z., Zhu, X., Chen, X., 2015. miRNA oligonucleotide and sponge for miRNA-21 inhibition mediated by PEI-PLL in breast cancer therapy. Acta Biomater. 25, 184–193. https://doi.org/10.1016/j.actbio.2015.07.020.

Gaur, S., Wen, Y., Song, J.H., Parikh, N.U., Mangala, L.S., Blessing, A.M., Ivan, C., Wu, S. Y., Varkaris, A., Shi, Y., Lopez-Berestein, G., Frigo, D.E., Sood, A.K., Gallick, G.E., 2015. Chitosan nanoparticle-mediated delivery of miRNA-34a decreases prostate tumor growth in the bone and its expression induces non-canonical autophagy. Oncotarget 6.

Goyal, R., Kapadia, C.H., Melamed, J.R., Riley, R.S., Day, E.S., 2018. Layer-by-layer assembled gold nanoshells for the intracellular delivery of miR-34a. Cel. Mol. Bioeng. 11, 383–396. https://doi.org/10.1007/s12195-018-0535-x.

Hou, W., Tian, Q., Steuerwald, N.M., Schrum, L.W., Bonkovsky, H.L., 2012. The let-7 microRNA enhances heme oxygenase-1 by suppressing Bach1 and attenuates oxidant injury in human hepatocytes. Biochimica et Biophysica Acta (BBA) - Gene Regulatory Mechanisms 1819, 1113–1122. https://doi.org/10.1016/j.bbagrm.2012.06.001.

Hu, B., Xie, M., Zhang, C., Zeng, X., 2014. Genipin-structured peptide-polysaccharide nanoparticles with significantly improved resistance to harsh gastrointestinal environments and their potential for oral delivery of polyphenols. J. Agric. Food. Chem. 62, 12443–12452. https://doi.org/10.1021/jf5046766.

Huang, G., Chen, Q., Wu, W., Wang, J., Chu, P.K., Bai, H., Tang, G., 2020. Reconstructed chitosan with alkylamine for enhanced gene delivery by promoting endosomal escape. Carbohydr. Polym. 227, 115339 https://doi.org/10.1016/j.carbpol.2019.115339.

Itani, R., Al Faraj, A., 2019. siRNA conjugated nanoparticles—a next generation strategy to treat lung cancer. IJMS 20, 6088. https://doi.org/10.3390/ijms20236088.

Juenet, M., Aid-Launais, R., Li, B., Berger, A., Aerts, J., Ollivier, V., Nicoletti, A., Letourneur, D., Chauvierre, C., 2018. Thrombolytic therapy based on fucoidan-functionalized polymer nanoparticles targeting P-selectin. Biomaterials 156, 204–216. https://doi.org/10.1016/j.biomaterials.2017.11.047.

Khaled, S.Z., Cevenini, A., Yazdi, I.K., Parodi, A., Evangelopoulos, M., Corbo, C., Scaria, S., Hu, Y., Haddix, S.G., Corradetti, B., Salvatore, F., Tasciotti, E., 2016. One-pot synthesis of pH-responsive hybrid nanogel particles for the intracellular delivery of small interfering RNA. Biomaterials 87, 57–68. https://doi.org/10.1016/j.biomaterials.2016.01.052.

Kumar, G.V., Su, C.-H., Velusamy, P., 2016. Ciprofloxacin loaded genipin cross-linked chitosan/heparin nanoparticles for drug delivery application. Mater. Lett. 180, 119–122. https://doi.org/10.1016/j.matlet.2016.05.108.

Lachowicz, D., Mielczarek, P., Wirecka, R., Berent, K., Karewicz, A., Szuwarzyński, M., Zapotoczny, S., 2019. Nanohydrogels based on self-assembly of cationic pullulan and anionic dextran derivatives for efficient delivery of piroxicam. Pharmaceutics 11, 622. https://doi.org/10.3390/pharmaceutics11120622.

Li, B., Juenet, M., Aid-Launais, R., Maire, M., Ollivier, V., Letourneur, D., Chauvierre, C., 2017a. Development of polymer microcapsules functionalized with fucoidan to

target P-selectin overexpressed in cardiovascular diseases. Adv. Healthcare Mater. 6, 1601200. https://doi.org/10.1002/adhm.201601200.
Li, D., van Nostrum, C.F., Mastrobattista, E., Vermonden, T., Hennink, W.E., 2017b. Nanogels for intracellular delivery of biotherapeutics. J. Control. Release 259, 16–28. https://doi.org/10.1016/j.jconrel.2016.12.020.
Lin, Y.-H., Lu, K.-Y., Tseng, C.-L., Wu, J.-Y., Chen, C.-H., Mi, F.-L., 2017. Development of genipin-crosslinked fucoidan/chitosan- *N* -arginine nanogels for preventing *Helicobacter* infection. Nanomedicine 12, 1491–1510. https://doi.org/10.2217/nnm-2017-0055.
Lin, Y.-H., Tsai, S.-C., Lai, C.-H., Lee, C.-H., He, Z.S., Tseng, G.-C., 2013. Genipin-cross-linked fucose–chitosan/heparin nanoparticles for the eradication of Helicobacter pylori. Biomaterials 34, 4466–4479. https://doi.org/10.1016/j.biomaterials.2013.02.028.
Lou, B., Beztsinna, N., Mountrichas, G., van den Dikkenberg, J.B., Pispas, S., Hennink, W. E., 2017. Small nanosized poly(vinyl benzyl trimethylammonium chloride) based polyplexes for siRNA delivery. Int. J. Pharm. 525, 388–396. https://doi.org/10.1016/j.ijpharm.2017.03.036.
Mi, F.-L., Shyu, S.-S., Peng, C.-K., 2005. Characterization of ring-opening polymerization of genipin and pH-dependent cross-linking reactions between chitosan and genipin. J. Polym. Sci. A Polym. Chem. 43, 1985–2000. https://doi.org/10.1002/pola.20669.
Moraes, F.C., Antunes, J.C., Forero Ramirez, L.M., Aprile, P., Franck, G., Chauvierre, C., Chaubet, F., Letourneur, D., 2020. Synthesis of cationic quaternized pullulan derivatives for miRNA delivery. Int. J. Pharm. 577, 119041 https://doi.org/10.1016/j.ijpharm.2020.119041.
Naeye, B., 2011. Hemocompatibility of siRNA loaded dextran nanogels 8.
Palermo, E.F., Lee, D.-K., Ramamoorthy, A., Kuroda, K., 2011. Role of cationic group structure in membrane binding and disruption by amphiphilic copolymers. J. Phys. Chem. B 115, 366–375. https://doi.org/10.1021/jp1083357.
Patil, S.D., Rhodes, D.G., Burgess, D.J., 2005. DNA-based therapeutics and DNA delivery systems: a comprehensive review. AAPS J 7, E61–E77. https://doi.org/10.1208/aapsj070109.
Pereira, P., Morgado, D., Crepet, A., David, L., Gama, F.M., 2013. Glycol chitosan-based nanogel as a potential targetable carrier for siRNA: glycol chitosan-based carrier of siRNA. Macromol. Biosci. 13, 1369–1378. https://doi.org/10.1002/mabi.201300123.
Pilipenko, I., Korzhikov-Vlakh, V., Sharoyko, V., Zhang, N., Schäfer-Korting, M., Rühl, E., Zoschke, C., Tennikova, T., 2019. pH-Sensitive chitosan-heparin nanoparticles for effective delivery of genetic drugs into epithelial cells. Pharmaceutics 11, 317. https://doi.org/10.3390/pharmaceutics11070317.
Poddar, S., Kesharwani, D., Datta, M., 2019. miR-449a regulates insulin signalling by targeting the Notch ligand, Jag1 in skeletal muscle cells. Cell Communication and Signaling 17. https://doi.org/10.1186/s12964-019-0394-7.
Prajapati, V.D., Jani, G.K., Khanda, S.M., 2013. Pullulan: an exopolysaccharide and its various applications. Carbohydr. Polym. 95, 540–549. https://doi.org/10.1016/j.carbpol.2013.02.082.
Raemdonck, K., Naeye, B., Buyens, K., Vandenbroucke, R.E., Høgset, A., Demeester, J., De Smedt, S.C., 2009. Biodegradable dextran nanogels for RNA interference: focusing on endosomal escape and intracellular siRNA delivery. Adv. Funct. Mater. 19, 1406–1415. https://doi.org/10.1002/adfm.200801795.
Razi, M.A., Wakabayashi, R., Tahara, Y., Goto, M., Kamiya, N., 2018. Genipin-stabilized caseinate-chitosan nanoparticles for enhanced stability and anti-cancer activity of curcumin. Colloids Surf., B 164, 308–315. https://doi.org/10.1016/j.colsurfb.2018.01.041.
Safari, S., Dorkoosh, F.A., Soleimani, M., Zarrintan, M.H., Akbari, H., Larijani, B., Tehrani, M.R., 2011. N-Diethylmethyl chitosan for gene delivery to pancreatic cancer cells and the relation between charge ratio and biologic properties of polyplexes via interpolations polynomial. Int. J. Pharm. 420, 350–357. https://doi.org/10.1016/j.ijpharm.2011.08.050.
San Juan, A., Bala, M., Hlawaty, H., Portes, P., Vranckx, R., Feldman, L.J., Letourneur, D., 2009. Development of a functionalized polymer for stent coating in the arterial delivery of small interfering RNA. Biomacromolecules 10, 3074–3080. https://doi.org/10.1021/bm900740g.
San Juan, A., Ducrocq, G., Hlawaty, H., Bataille, I., Guénin, E., Letourneur, D., Feldman, L.J., 2007. Tubular cationized pullulan hydrogels as local reservoirs for plasmid DNA. J. Biomed. Mater. Res. Part A 83A, 819–827. https://doi.org/10.1002/jbm.a.31413.
Shatsberg, Z., Zhang, X., Ofek, P., Malhotra, S., Krivitsky, A., Scomparin, A., Tiram, G., Calderón, M., Haag, R., Satchi-Fainaro, R., 2016. Functionalized nanogels carrying an anticancer microRNA for glioblastoma therapy. J. Control. Release 239, 159–168. https://doi.org/10.1016/j.jconrel.2016.08.029.
Singh, A., Arora, S., Swaminathan, S.K., Kirtane, A., Srivastava, S., Bhardwaj, A., Singh, S., Panyam, J., 2014. Synthesis, characterization, and evaluation of poly (D, L-lactide-co-glycolide)-based nanoformulation of miRNA-150: potential implications for pancreatic cancer therapy. IJN 2933. https://doi.org/10.2147/IJN.S61949.
Sung, H.-W., Huang, R.-N., Huang, L.L.H., Tsai, C.-C., 1999. In vitro evaluation of cytotoxicity of a naturally occurring cross-linking reagent for biological tissue fixation. J. Biomater. Sci. Polym. Ed. 10, 63–78. https://doi.org/10.1163/156856299X00289.
Suzuki, M., Bachelet-Violette, L., Rouzet, F., Beilvert, A., Autret, G., Maire, M., Menager, C., Louedec, L., Choqueux, C., Sabourel, P., Haddad, O., Chauvierre, C., Chaubet, F., Michel, J.-B., Serfaty, J.-M., Letourneur, D., 2015. Ultrasmall superparamagnetic iron oxide nanoparticles coated with fucoidan for molecular MRI of intraluminal thrombus. Nanomedicine 10, 73–87. https://doi.org/10.2217/nnm.14.51.
Toy, R., Pradhan, P., Ramesh, V., Di Paolo, N.C., Lash, B., Liu, J., Blanchard, E.L., Pinelli, C.J., Santangelo, P.J., Shayakhmetov, D.M., Roy, K., 2019. Modification of primary amines to higher order amines reduces in vivo hematological and immunotoxicity of cationic nanocarriers through TLR4 and complement pathways. Biomaterials 225, 119512. https://doi.org/10.1016/j.biomaterials.2019.119512.
Uchida, S., Perche, F., Pichon, C., Cabral, H., 2020. Nanomedicine-based approaches for mRNA delivery. Mol. Pharmaceutics 17, 3654–3684. https://doi.org/10.1021/acs.molpharmaceut.0c00618.
Wu, D., Delair, T., 2015. Stabilization of chitosan/hyaluronan colloidal polyelectrolyte complexes in physiological conditions. Carbohydr. Polym. 119, 149–158. https://doi.org/10.1016/j.carbpol.2014.11.042.
Xiong, Q., Lee, G.Y., Ding, J., Li, W., Shi, J., 2018. Biomedical applications of mRNA nanomedicine. Nano Res. 11, 5281–5309. https://doi.org/10.1007/s12274-018-2146-1.
Yu, S.-H., Wu, S.-J., Wu, J.-Y., Wen, D.-Y., Mi, F.-L., 2015. Preparation of fucoidan-shelled and genipin-crosslinked chitosan beads for antibacterial application. Carbohydr. Polym. 126, 97–107. https://doi.org/10.1016/j.carbpol.2015.02.068.
Zhang, T., Yang, R., Yang, S., Guan, J., Zhang, D., Ma, Y., Liu, H., 2018. Research progress of self-assembled nanogel and hybrid hydrogel systems based on pullulan derivatives. Drug Delivery 25, 278–292. https://doi.org/10.1080/10717544.2018.1425776.
Zhu, L., Chen, T., Ye, W., Wang, J.-Y., Zhou, J.-P., Li, Z.-Y., Li, C.-C., 2019. Circulating miR-182-5p and miR-5187-5p as biomarkers for the diagnosis of unprotected left main coronary artery disease. Journal of Thoracic Disease 11, 1799–1808. https://doi.org/10.21037/jtd.2019.05.24.
Zintchenko, A., Philipp, A., Dehshahri, A., Wagner, E., 2008. Simple Modifications of Branched PEI Lead to Highly Efficient siRNA Carriers with Low Toxicity. Bioconjugate Chem. 19, 1448–1455. https://doi.org/10.1021/bc800065f.

RÉSUMÉ DE LA THÈSE EN LANGUE FRANÇAISE

Alors que nous développons de nouveaux systèmes de délivrance de médicaments, nous devons nous concentrer sur le choix des maladies qui ont un besoin élevé de nouvelles thérapies. Les maladies du système cardiovasculaire représentent la première cause de morbidité et de mortalité dans le monde, soulignant la nécessité de développer des thérapies innovantes. Parmi les nombreuses stratégies explorées, l'utilisation de microARN (miARN) associé à un vecteur adapté est l'une des plus prometteuses.

Les miARN sont de petits acides nucléiques non codants qui s'expriment instantanément dans le cytoplasme sans risque d'intégration génomique. Les travaux les plus récents ont montré que ces molécules pouvaient remplir des fonctions relativement génériques dans des cellules impliquées dans le contrôle de nombreux processus cellulaires et physiologiques fondamentaux tels que la différenciation cellulaire, le métabolisme, la prolifération, le contrôle du cycle cellulaire, la migration et l'apoptose.

Cependant, afin de faire progresser les miARN vers l´utilisation clinique, leur délivrance reste un défi majeur. Combiner l'utilisation des miARN avec la nanotechnologie est une stratégie prometteuse pour le développement d'options thérapeutiques cliniquement viables.

Dans les différentes classes de biomatériaux utilisés pour les applications biomédicales (polymères, métaux, céramiques et composites), les polymères représentent le plus grand pourcentage. En particulier, l'utilisation de polysaccharides présente un grand intérêt grâce à leur bonne biocompatibilité ainsi qu'à celle de leurs produits de dégradation. Par ailleurs, les polysaccharides peuvent être facilement modifiés avec différents groupes chimiques pour leur conférer, à titre d'exemple, la capacité d'interagir avec des molécules anioniques en introduisant des substituants cationiques. En raison de leurs potentiels uniques, les polysaccharides ont donc reçu une attention considérable pendant longtemps pour construire des systèmes de délivrance de médicaments.

Dans ce travail, nous avons développé une stratégie basée sur la formation de complexes de polyélectrolytes (PEC) entre des dérivés cationiques du pullulane et un miARN capable de déclencher des modifications spécifiques dans des voies cellulaires impliquées dans le développement de maladies vasculaires. Le pullulane, un polysaccharide extrait d'une levure, est largement utilisé par l'industrie pharmaceutique. Bien qu'il n'y ait

toujours pas de nanothérapies à base de pullulane dans l'utilisation clinique actuelle, de nombreux travaux ont déjà mis en évidence ce potentiel.

Finalement, les PEC ont été dotés d'une biospécificité en les combinant avec le fucoïdane, un polysaccharide sulfaté capable de cibler spécifiquement la P-sélectine exprimée sur les plaquettes et cellules endotheliales activées présentes dans la paroi vasculaire pathologique. Avec ce projet, nous espérons contribuer au développement de nouveaux systèmes de délivrance sûrs à base de polysaccharides pour les thérapies à base de miARN, en particulier pour le traitement de l'athérosclérose et de ses complications.

Le manuscrit est divisé en deux parties principales:

La **revue bibliographique** est divisée en trois thèmes principaux. Dans le premier sujet, nous discutons brièvement du mécanisme pathogène de l'athérosclérose qui conduit à l'infarctus du myocarde et de l'intérêt d'utiliser les miARN comme alternative thérapeutique pour traiter les maladies cardiovasculaires. En raison de l'instabilité sérique du miARN, de sa nature hydrophile, de sa charge négative et de son poids moléculaire élevé, la délivrance est un point clé à considérer lors de l'utilisation du miARN en thérapeutique. Le deuxième sujet se concentre sur les systèmes d'administration de médicaments à base de polysaccharides. Dans la troisième partie, nous présentons un aperçu des principaux nanosystèmes (nanoparticules inorganiques, nanoparticules à base de lipides et nanoparticules à base de polymère) qui ont été utilisés pour la livraison de miARN et les défis qui doivent être relevés pour concevoir des systèmes de délivrance de miARN efficaces.

Dans la **partie expérimentale**, les résultats sont présentés sous deux chapitres principaux rédigés sous forme de publication. Chaque chapitre est précédé d'une introduction, qui situe la stratégie développée dans le contexte du projet.

Dans le **1er chapitre**, nous avons développé des nanoparticules à base de pullulane via l'approche de la complexation des polyélectrolytes en utilisant des dérivés cationiques de pullulane et des miARN, qui ont été caractérisés par des techniques physiques et chimiques.

Ces travaux s'inscrivent dans la continuité des travaux d'Antunes *et al.* 2019 initié au laboratoire pour développer des nanoparticules pour la délivrance de miARN dans des maladies cardiovasculaires. Des nanoparticules à base de polymère du type *core-shell*

chargées de miARN ont été préparées par polymérisation en émulsion radicalaire redox pour obtenir des NP *core-shell*, dont le noyau est composé du poly (isobutylcyanoacrylate) synthétique et hydrophobe, et la coquille est constituée de polysaccharides naturels et hydrophiles (10% fucoïdane, 20% DEAE-dextran et 70% dextran). Le miR-155-5p a été chargé dans les NP via des interactions électrostatiques grâce à la présence de DEAE-dextran cationique sur la surface des nanoparticules. Le fucoïdane conférerait aux NP la capacité de cibler la P-sélectine, surexprimée dans les cellules endothéliales activées. Ces nanosystèmes biospécifiques se sont avérés capables d'être internalisés par des cellules endothéliales activées et ont diminué les niveaux du gène cible BACH 1, fournissant une preuve de concept de validation fonctionnelle *in vitro* de la livraison de miR-155-5p. Cependant, la cytotoxicité associée aux NPs à base de cyanoacrylates était le principal obstacle au développement de ces nanosystèmes.

Dans ce contexte, ce projet de thèse a visé à développer des NP 100% polymériques en utilisant des dérivés de pullulane chargés positivement. Le pullulan est un polysaccharide naturel d'intérêt potentiel pour les applications biomédicales en raison de ses propriétés non toxiques, non immunogènes et biodégradables. Des dérivés cationiques de pullulane ont été obtenus par greffage d'amines tertiaires (DEAE-pullulane) et de groupements ammonium quaternaire (QA-pullulane). La capacité de différents dérivés cationiques à former des complexes avec des miARN entraînés par une interaction électrostatique (polyplexes) a été évaluée. Comme pour l'étude précédente, le fucoïdane a été introduit pour conférer une biospécificité aux NP envers les cellules endothéliales activées.

Le première chapitre est divisé en deux parties: la première partie a été publiée dans *International Journal of Pharmaceutics* et la deuxième partie présente des résultats complémentaires.

La première partie a étudié l'utilisation de pullulane quaternisé cationique comme alternative aux polycations classiques pour former des complexes avec miARN et leur transfection dans les cellules vasculaires.

En résumé, des dérivés cationiques de pullulane greffés avec des groupements ammonium quaternaire (QA-pullulane) ont été synthétisés et caractérisés. Le produit s'est révélé cytocompatible avec les cellules endothéliales humaines dans une large gamme de doses. Le QA-pullulan est un polycation prometteur en raison de sa capacité à former des complexes avec le miARN via des interactions électrostatiques dans une large gamme de

pH grâce à des charges positives permanentes, un avantage par rapport au chitosane, un polymère cationique naturel classique utilisé en thérapie génique. Les polyplexes formés entre QA-pullulane et miARN présentaient une taille nanométrique (133 ± 30 nm) et une forme sphérique. La charge de surface négative (-12 ± 5 mV) des polyplexes a suggéré la présence de miARN anionique, qui a été confirmée par électrophorèse sur gel d'agarose. Le QA-pullulan était capable de promouvoir la livraison de miARN dans les cellules par rapport au miARN seul.

Les travaux complémentaires non publiés constituent la deuxième partie du 1er chapitre. Des dérivés de DEAE-pullulane ont été préparés et leur capacité à former des polyplexes avec miARN a été évaluée et comparée à celle de QA-pullulans. La faisabilité d'incorporer le fucoïdane dans la formulation des polyplexes a également été évaluée.

Afin de faciliter la lecture du manuscrit et de permettre une meilleure compréhension des stratégies choisies et de leur évolution, la partie publiée de ce chapitre a été intégrée dans la continuité du texte, l´article original étant présenté en annexe.

Dans le **2ème chapitre** de ce manuscrit, des PEC réticulés associés au fucoïdane sont développés en utilisant un agent de réticulation naturel. Les particules sont produites en utilisant une méthodologie de synthèse verte sans utiliser aucun solvant toxique. Leur capacité à cibler la P-sélectine et à délivrer des miARN est étudiée *in vitro* avec des cellules endothéliales humaines. La stabilité élevée des nanoparticules dans des conditions physiologiques et le potentiel de leur stockage à long terme confère leur potentiel en tant que systèmes de délivrance de miARN. Le travail a été publiée dans *International Journal of Pharmaceutics.*

Dans le premier chapitre, nous avons démontré que les dérivés cationiques de pullulane modifiés avec des groupes amine tertiaire et ammonium quaternaire se sont révélés capables de former des nanoparticules complexées par des polyélectrolytes avec des miARN anioniques via des interactions électrostatiques. Cependant, la stabilité de ces complexes dans des conditions physiologiques limitait largement leur application en tant que petits systèmes de délivrance d'acides nucléiques.

Par conséquent, afin d'augmenter la stabilité des complexes, un agent de réticulation a été ajouté à la formulation. La génipine, un agent de réticulation naturel capable de faire des ponts entre des matériaux contenant des groupes amine primaire a été choisie pour

améliorer la stabilité des complexes dans des conditions physiologiques sans altérer leur cytocompatibilité.

Succinctement, nous avons développé un nouveau protocole de synthèse pour produire des nanogels réticulés à base de pullulane cationique entièrement réalisés en milieu aqueux à l'aide de génipine. A cet effet, des dérivés de pullulane modifiés avec des groupes amine primaire ont été produits et caractérisés. Ensuite, la formation de complexes de polyélectrolytes entre les dérivés cationiques de pullulane portant des amines primaires et le fucoïdane a été optimisée. La génipine a été incorporée à la formulation afin de produire des complexes de polyélectrolytes à base de polysaccharides réticulés. Ils ont été entièrement caractérisés en ce qui concerne leurs propriétés physico-chimiques, leur stabilité et leur cytocompatibilité envers les cellules endothéliales. Leur capacité à viser les plaquettes activées *in vitro* a été démontrée.

Enfin, nous avons présenté les résultats du chargement de miARN dans les nanogels développés. Dans des conditions acides, il était possible de moduler leur charge de surface permettant l´incorporation de miARN via des interactions électrostatiques avec l'ammonium primaire. Bien que ces nanosystèmes aient pu pénétrer dans les cellules endothéliales, d'autres expériences restent à effectuer pour évaluer leur potentiel en tant que nanothérapie, à savoir, si le miARN chargé induit une réponse biologique appropriée une fois à l'intérieur de la cellule.

Une **discussion générale,** comparant les résultats de cette thèse à la littérature et développant quelques perspectives, est suivie d'une **conclusion générale**, qui finalise la présentation de ce travail.

Avec les travaux présentés dans ce manuscrit, nous espérons contribuer au développement de nouveaux systèmes de délivrance sûrs à base de pullulane pour les thérapies à base de miARN. La synthèse facile, la possibilité de synthèse en large échelle (*scale-up*) et la facilité de formulation représentent un excellent potentiel d´utilisation clinique pour une variété d'applications biomédicales. Prouvés sûrs et efficaces, ces composés sont très attendus par les partenaires pharmaceutiques ainsi que par la communauté cardiovasculaire.